SPATIAL-TEMPORAL REGULATION OF EGFR PHOSPORYLATION BY PROTEIN TYROSINE PHOSPHATASES

Dissertation

An der Fakultät für Chemie

Technische Universität, Dortmund

Angefertigt am Max-Planck-Institut

für molekulare Physiologie, Dortmund.

Abteilung Systemische Zellbiologie

Prof. Dr. Bastiaens

21. 07. 2014

Vorgelegt von Dipl. Biol. Sven Fengler

geboren in Leverkusen

Erster Gutachter: Prof. Dr. Philippe Bastiaens

Zweiter Gutachter: Prof. Dr. Hernán Grecco

Eidesstattliche Versicherung

Ich versichere hiermit an Eides statt, dass ich die vorliegende Dissertation selbständig verfasst habe und alle in Anspruch genommenen Quellen und Hilfen in der Dissertation vermerkt wurden.

Dortmund, 21.07.2014 _____

Unterschrift

Erklärung

Hiermit erkläre ich, dass die vorliegende Dissertation in der gegenwärtigen oder in einer anderen Fassung, weder an der Technischen Universität Dortmund noch an einer anderen Hochschule im Zusammenhang mit einer staatlichen oder akademischen Prüfung vorgelegt worden ist.

Dortmund, 21.07.2014 _____

Unterschrift

Results and methodologies presented in this thesis have contributed to the following peer-reviewed publications:

Grecco, H.E., Roda-Navarro, P., **Fengler, S.**, and Bastiaens, P.I.H. (2011). High-throughput quantification of posttranslational modifications in situ by CA-FLIM. Methods in enzymology *500*, 37-58.

Fengler, S., Bastiaens, P.I.H, Grecco, H.E., and Roda-Navarro, P. (2012). Optimizing cell arrays for accurate functional genomics. BMC Res Notes *5*, 358.

Dedicated to my family
and friends

CONTENT

ABBREVIATIONS

°C	Degree Celsius
a.u.	Arbitrary units
BSA	Bovine serum albumin
C-terminus	carboxy terminus
CA	Cell array
Cbl	Casitas B-lineage lymphoma proto-oncogene
CDK	cyclin dependent protein kinase
cDNA	complementary DNA
DMEM	Dulbecco´s modified Eagle´s medium
DNA	deoxyribnucleic acid
dNTPs	deoxyribonucleoside triphosphates
DSP	dual-specific phosphatase
EDTA	ethylenediamininetetraacetic acid
EGF	Epidermal growth factor
EGFR	Epidermal growth factor receptor
ER	endoplasmatic reticulum
FERM	4.1 protein ezrin radixin moesin
FLIM	Fluorecence liftime imaging microscopy
FN	fibronectin
FRET	Förster resonance energy transfer
GFP	green fluorecent protien
HeLA	cervical epithelial cancer cell (Henrietta Lacks)
HEPES	N-2-hydroxyethylpiperanzine-N´-2-ethanesulfonic- acid
Hz	hertz
IF	Immunofluorescence
JM	juxtamembrane
KD	Kinase domain
KIM	kinase-interacting motif
LMPTP	low molecular tyrosine specific PTP
MCF7	Michigan cancer foundation 7
min	minutes
MKP	MAP kinase phosphatases
mTFP	monomeric teal fluorescent protein

MVB	multivesicular bodies
N-terminus	amino terminus
NADP	Nicotinamide adenine dinucleotide phosphate
NLS	nuclear localization sequence
NM	Nuclear membrane
NOX	NADPH oxidase
NRPTP	non-receptor PTP
ns	nanosecond
NT	non-targeting
PAGE	Poly-acrylamide gel electrophoresis
PFA	Paraformaldehyde
PI3K	Phosphatidylinositide 3-kinases
PM	plasma membrane
PTB	phosphotyrosine binding
PTP	protein tyrosine phosphatase
pY	phosphotyrosine
RNA	Ribonucleic acid
ROS	reactive oxygen species
RPTP	receptor-like protein tyrosine phosphatase
RT	room temperature
RTK	receptor tyrosine kinase
SH2	src homology 2
siRNA	small interfering RNA
Src	Proto-oncogene tyrosine-protein kinase Src
TGF- α	transforming growth factor-a
TM	transmembrane
WT	wild type
µl	microliter

ABSTRACT

The activity of the epidermal growth factor receptor (EGFR) and its interactions with protein tyrosine phosphatases (PTPs) is what determines growth factor signaling. Due to its intrinsic autocatalytic properties, EGFR can undergo autonomous ligand independent activation. EGFR in this case, cycles between the plasma membrane (PM) and recycling endosomes where PTPs dephosphorylate the receptor to avoid spurious receptor signals. EGF-induced receptor dimerization results in a robust *trans*-phosphorylation of tyrosine residues that allows stable binding of signaling effectors. The majority of EGFR at the PM is internalized and undergoes degradation in lysosomal compartment. After internalization, the EGFR encounters PTPs at different cellular locations, which thereby regulate the signal duration of the receptor. Moreover, specific dephosphorylation of phosphotyrosines that are required for ubiquitin ligase (Cbl) binding reduces the receptor ubiquitylation and thereby its degradation rate. Due to their dephosphorylation activity, PTPs were thought as negative regulators of RTK signalling, but it has been shown that PTPs also promote receptor phosphorylation by activating cytosolic kinases that in turn phosphorylate RTKs (Julien et al., 2011). To understand the spatial-temporal regulation of EGFR phosphorylation by PTPs, we used CA-FLIM (Grecco et al., 2010). This method allowed us to quantify the phosphorylated fraction of EGFR in cells, upon perturbation of PTP expression by siRNAs or cDNAs. Upon opposing perturbations, we identified several PTPs that have indicated either a negative or positive effect on EGFR phosphorylation. Classification of the temporal phosphorylation profiles of EGFR discovered 5 functional groups of PTPs acting at early and/or late time points after EGF stimulation. PTPs within each group showed differences in their regulatory influence highlighting individual impact in EGF signaling. Predominantly cytosolic PTPs regulated early EGFR phosphorylation, whereas receptor-like PTPs (RPTPs) induced a transient response profile. Analysis of the spatial-temporal phosphorylation profile of EGFR upon PTPRA, PTPN1 or PTPN2 expression showed an almost abolished axial phosphorylation of EGFR that might promote receptor recycling. In contrast, we identified a positive regulatory function of MTM1, DUSP7 and

PTPN21 that was further validated using multi-parametric single cell information. These PTPs induced an early amplification of receptor phosphorylation near the PM. Our results strongly suggest that MTM1 and PTPN21 inhibit the degradation pathway and thereby enhancing the phosphorylated fraction of internalized EGFR. In summary, the presented work provides novel insights about when and where PTPs regulate EGFR phosphorylation and how this could affect cellular responses.

ZUSAMMENFASSUNG - DEUTSCH

Die Aktivität des Epidermalen-Wachstumsfaktor-Rezeptor (EGFR) und dessen Interaktionen mit Protein-Tyrosin-Phosphatasen (PTPasen) bestimmt die Signalweiterleitung verursacht durch Wachstumsfaktoren. Der EGFR besitzt intrinsisch-autokatalytische Eigenschaften welche es ihm ermöglichen auch ohne Ligand aktiviert zu werden, unterliegt jedoch einem Recyclingzyklus und bewegt sich zwischen der Plasmamembran (PM) und Recyclingendosomen wo er durch PTPasen dephosphoryliert wird und so ungewollte Rezeptorsignale verhindern werden. Eine EGF-induzierte Rezeptordimerisierung resultiert in einer robusten *Trans*-phosphorylierung von Tyrosinseitenketten und erlaubt so eine stabile Bindung für Signaleffektoren am Rezeptor. Die Mehrheit der EGFR Moleküle an der PM werden internalisiert und in lysosomalen Kompartimenten abgebaut. Durch die Internalisierung begegnet der EGFR PTPasen mit verschiedensten zellulären Lokalisationen welche die Signaldauer des Rezeptors regulieren. Die spezifische Dephosphorylierung von Phosphotyrosinen die für eine Interaktion mit Ubiquitin-Ligasen (Cbl) benötigt werden verringert außerdem die Ubiquitinierung des Rezeptor und dadurch dessen Abbaurate. Wegen ihrer dephosphorylierenden Eingenschaften wurden PTPasen meist nur als negative Regulatoren von Rezeptor-Tyrosinkinasen (RTKasen) beschrieben. Es konnte jedoch gezeigt werden das PTPasen auch die Rezeptorphosphorylierung fördern können indem sie zum Beispiel, zytosolische Kinasen aktivieren die wiederrum RTKasen phosphorylieren können (Julien et al., 2011). Um die räumliche und zeitliche Regulierung des EGFRs durch PTPasen zu verstehen wurde in dieser Arbeit CA-FLIM verwendet (Grecco et al., 2010). Diese Methode ermöglicht eine Quantifizierung der phosphorylierten Fraktion des EGFRs in Zellen die durch siRNA- oder cDNA- Transfektionen ein verändertes Expressionslevel spezifischer Phosphatasen besitzen. Durch reziproke Modulation des Expressionslevels konnte gezeigt werden, dass mehrere PTPasen einen negativen oder positive Effekt auf die Phosphorylierung des EGFRs haben. Durch eine Klassifikation der zeitlich aufgelösten Phosphorylierungsprofile des EGFRs konnten die untersuchten PTPasen in fünf funktionelle Gruppen eingeteilt werden die entweder früh und/oder spät nach der EGF Stimulierung agieren. Phosphatasen

jeder Gruppe zeigten Unterschiede in ihrem regulatorischen Einfluss was deren individuelle Bedeutung im EGF Signalweg wiederspiegelt. Vorzugsweise regulierten zytosolische Phosphatasen den EGFR früh nach EGF Stimulierung während Rezeptor-PTPasen (RPTPasen) ein transientes Phosphorylierungpofil verursachten. Die Analyse des räumlich-zeitlichen Phosphorylierungsprofiles des EGFRs zeigte das eine erhöhte Expression von PTPRA, PTPN1 oder PTPN2 zu einer stark abgeschwächten axialen Phosphorylierung führte welches Rezeptorrecycling fördern könnte. Im Gegensatz dazu wurde eine positive regulatorische Funktion für MTM1, DUSP7 und PTPN21 identifiziert welche mittels multiparametrischer Einzelzellanalyse weiter verifiziert wurde. Eine erhöhte Expression dieser Phosphatasen verursachte eine frühe Amplifikation der Rezeptorphosphorylierung nahe der PM. Unsere Resultate lassen uns vermuten, das MTM1 und PTPN21 den Rezeptorabbau inhibieren was zu einer erhöhten Phosphorylierungsrate des internalisierten EGFRs führt. Die hier präsentierte Arbeit liefert neue Einblicke darüber wann und wo PTPasen die Phosphorylierung des EGFRs regulieren und wie diese Regulation die zelluläre Antwort beeinflussen könnte.

I INTRODUCTION

1.1 Opposing activities determine cellular responses

Recent advancements in our understanding of signaling molecules and their role in signal transduction have led to an evolution in our conceptualization of how extracellular signals are processed to generate specific and robust cellular responses. The traditional understanding of cellular signaling as linear cascades of biochemical reactions, has been replaced by the notion of an integrated *"signaling network",* which better represents the fundamental nature of signal transduction. Individual cellular pathways cannot be considered in isolation from each other as they often share signaling components in a highly overlapping interconnected manner. Furthermore, cellular signaling is subject to extensive regulation by a variety of mechanisms (e.g. feedback loops to switch off or to trigger the duration of a signal). Following a general principle in nature, cell signaling operates with opposing tendencies favoring one or the other state dependent on the given signaling context (Grecco et al., 2011b). On the molecular level, proteins with opposing activities are essential to keep homeostasis but also allow dynamic systems to react according to a given extracellular stimulus. Among various cellular mechanisms, post-translational modifications, such as phosphorylation, alter enzymatic activities or binding affinities in a dynamic and reversible way, well suited for rapidly transmitting messages and terminating them just as quickly.

The activity of receptor tyrosine kinases (RTKs) and protein tyrosine phosphatases (PTPs) is an excellent example of duality in cellular signaling. Their opposing activities maintain physiological levels of phosphor-proteins and regulate the cell response upon growth factor stimulation by controlling the rate of phosphorylation reactions within the cell. Growth factor binding induces kinase activation, thereby shifting the equilibrium to favor RTK activity. It has been shown that the activation of RTKs is dependent on the balance between the intrinsic autocatalytic RTK activity and competing PTP inhibition, a double negative feedback motif that generates a bistable system (Reynolds et al., 2003; Tischer and Bastiaens, 2003). The inhibition of PTPs is mediated by a ligand-induced production of reactive oxygen species (ROS) locally at the PM that leads

to the reversible oxidation of the catalytic cysteine residue of PTPs (Denu and Tanner, 1998; Meng et al., 2002). As a result, RTKs that are negatively regulated by PTPs will exhibit enhanced phosphorylation due to their intrinsic kinase activity (Ostman and Bohmer, 2001). Such a system represents a threshold-dependent switch that both prevents spurious signals in absence of ligand while amplifying the phosphorylation signal when a certain threshold concentration of ligand is present (Reynolds et al., 2003). This system also explains the observation of lateral phosphorylation propagation, in which a wave of RTK phosphorylation leads to full activation of the receptor population at the PM, even in regions where the cell was not exposed to ligand (Verveer et al., 2000b). Ligand-induced activation of RTKs induces the local production of ROS, which could rapidly diffuse through the cell and could result in the inactivation of PTPs further away, resulting in an increased level of phosphorylated receptors as the signal is propagated (Tischer and Bastiaens, 2003). In this way, the balanced action of RTKs and PTPs is considered a major switch of many signal transduction networks (Tonks, 2006), including the epidermal growth factor receptor (EGFR/ErbB) network. The intrinsic kinase activity of EGFR, is dependent on an allosteric interaction of dimerized kinase domains and does not require specific *trans*-phosphorylation events like other RTKs (Lemmon and Schlessinger, 2010). However, EGFR possesses autocatalytic properties that are dependent on specific phosphorylation events e.g. pY845 that enhances its ability to form active dimers (Shan et al., 2012).

EGF binding and subsequent structural alterations stabilizes the dimer formation allowing activation and *trans*-autophosphorylation of C-terminal tyrosine residues which serve as docking sites for downstream effectors, such as those containing Src homology-2 (SH2) and/or phosphotyrosine-binding (PTB) domains. Like other RTKs, EGFR follows distinct trafficking pathways following growth factor stimulation. In the absence of growth factor, EGFR traffics constitutively between the PM and recycling endosomes (G. Xouri, unpublished data). EGF stimulation induces a robust phosphorylation of EGFR and thereby favors the recruitment of SH2/PTB containing adaptors and enzymes to phosphorylated tyrosine residues of the receptor. These proteins can either

activate signaling networks, such as the mitogen-activated protein kinase (MAPK) network (including Raf, Mek and Erk), or initiate signal termination events such as the ubiquitylation ligase Cbl, which mediates a rapid transport of activated EGFR to degradation compartments (Levkowitz et al., 1999; Umebayashi et al., 2008). Receptor trafficking following ligand activation also transports the active receptor deeper inside the cell. It has been shown that the composition of signaling molecules associated with an active receptor can differ between the PM and endosomal compartments. Some evidence suggests that these endocytic events may in fact be required to activate some downstream networks including the MAPK cascade (Miaczynska et al., 2004; Sigismund et al., 2008).

Several receptor like PTPs (RPTPs) have been identified that regulate the phosphorylation of EGFR including PTPRS, PTPRJ (DEP-1) or PTPRK, which are all localized at the PM like EGFR (Suarez Pestana et al., 1999; Tarcic et al., 2009). Other examples, includes PTPN1 (PTP1B) which is localized at the cytosolic face of the endoplasmic reticulum (ER) (Flint et al., 1997; Liu and Chernoff, 1997). Due to its localization, it has been shown that PTPN1 dephosphorylate EGFR at the interface between ER and endosomal compartments (Haj et al., 2002). Similarly to these examples, all PTPs occupy distinct cellular localizations which can also differ among different growth factors (den Hertog et al., 2008), adding a spatial organization to the interaction between EGFR and PTPs. As mentioned before, EGFR traffics constantly between the PM and recycling endosomes in the absence of ligand. However, due to its intrinsic autocatalytic properties, EGFR has the potential to be activated even in the absence of ligand, but a constant PTP activity maintains tonic suppression that prevents spurious receptor signaling in this case. The interaction of EGFR with PTPs at the basal level thereby determines the required ligand concentration that is needed to generate a downstream signal, although this threshold may differ from ligand to ligand (Reynolds et al., 2003). After EGF binding, however, the availability and composition of phosphorylated docking sites at the C-terminus of EGFR is dependent on the dephosphorylation activity of PTPs that the receptor encounters at the PM and during its trafficking in endosomes. In this way, the

spatial interactions of EGFR with PTPs determine the nature of the signaling properties at the PM and in endosomal compartments. In the same way, PTPs also control the trafficking behavior by dephosphoryation of docking sites required for Cbl-mediated ubiquitylation, which targets the receptor for lysosomal degradation. Specific dephosphorylation of these sites by PTP activity leads to a reduction in EGFR degradation (Tarcic et al., 2009) resulting in a prolonged lifetime of activated receptor. In summary, the spatially coordinated dephosphorylation of EGFR docking sites by PTPs controls signal duration in response to growth factor stimulation. The result of these EGFR-PTP interactions generates distinct spatial-temporal phosphorylation patterns inside the cell (Grecco et al., 2011b).

The downstream signaling of EGFR or other RTKs is organized in a highly conserved core process that integrates a dense array of strongly coupled sub-networks (modules) containing a remarkably small set of core signaling molecules (Citri and Yarden, 2006; Ma and Zeng, 2003). The understanding of how distinct cell responses induced by different external growth factors are generated by shared protein modules remains one of the major challenges in systems biology. Insights into this phenomenon came from studies with PC12 cells, a model for neuronal differentiation (Greene and Tischler, 1976). Whereas, stimulation of PC12 cells with nerve growth factor (NGF) resulted in neurite outgrowth (differentiation), EGF treatment resulted in cell proliferation (Marshall, 1995). While both cell responses are controlled by the mitogen activated protein kinase (MAPK) network that consist of the Raf, Mek and Erk cascade, this study demonstrated notable differences in the duration of Erk activity between different growth factors. Erk activity was sustained when cells were stimulated by NGF, but showed a transient Erk activity upon EGF treatment. The observation that signal duration can determine the response of a cell was later extended to other cellular models and other growth factors (Murphy et al., 2002; Nagashima et al., 2007; Neve et al., 2002; Thottassery et al., 2004). MCF7 cells showed similar signaling input-output relationships: sustained Erk activity induced cellular differentiation, whereas transient Erk activity induces proliferation (Nagashima et al., 2007). Work from Murphy and

colleagues (2002) has provided insight into how transient versus sustained Erk activity can differ in the transcription patterns induced. Whereas both transient and sustained Erk activity induce transcription of immediate early gene (IEG) products such as the transcription-factor c-Fos, only a sustained Erk activity causes phosphorylation and stabilization of such products and thereby results in differential gene expression (Murphy et al., 2002; Nagashima et al., 2007). On the level of transcriptional networks, a structure in which an initial input (active Erk) induces an intermediate signal in form of the c-Fos transcription and both, the initial and the intermediate signal are needed to generate the final output (phosphorylated and stabilized c-Fos), is termed: a coherent feed-forward loop (CFL) (Mangan et al., 2003; Nakakuki et al., 2010). Owing to the time lag between transcription initiation and translation of c-Fos, this CFL structure acts as an "AND-gate" to convert the sustained versus transient Erk temporal profile into an all-or-none response (Alon, 2007; Nakakuki et al., 2010). Erk activity also induces the transcription of dual-specific phosphatases (DSPs) or in particular MAPK-phosphatases (MKPs) (Brondello et al., 1999). Active MAPKs phosphorylate MKPs, which enhances the stability of MKPs analogous to c-Fos (Brondello et al., 1999). In addition to the described CFL structure, the increased level of MKPs induces a negative feedback loop that provides the c-Fos response with robustness to system perturbations (Nakakuki et al., 2010). These examples demonstrate how the signal duration of Erk can be converted into an all-or-none response at the transcriptional level to govern the cellular response. Thus, the question remains how different Erk dynamics are generated from upstream processes. Different mechanisms were postulated to explain the differences in the Erk activation dynamics upon different growth factor stimulations and give insights into how different Erk activations lead to the all or none response (Kao et al., 2001; Santos et al., 2007; Sasagawa et al., 2005). For example, systematic perturbation studies in PC12 cells combined with modular response analysis (Kholodenko et al., 2002) uncovered topological differences within the MAPK network dependent on whether cells were stimulated with NGF or EGF (Santos et al., 2007). Cell stimulation with NGF induced a positive feedback from Erk to the upstream kinase Raf leading to a prolonged activity of Erk. In contrast, Erk activation by EGF inhibits Raf through a negative feedback loop that results in a

transient Erk response (Santos et al., 2007). This study has shown that the distinct growth factors differentially determine the topology of the MAPK network and that these differences in the resultant wiring of the network govern cell fate.

One other mechanism has been postulated to explain the differences in the signaling duration of Erk. It is generally believed that ligand-induced RTK endocytosis down-regulates growth factor signaling by trafficking the active receptor population from the PM to degradation compartments. For example, primary studies with PC12 cells have shown that approximately 80-90% of EGF bound at the PM is subsequently degraded after endocytosis, whereas, only 40-50% of bound NGF (bound by TrkA) was degraded (Chandler and Herschman, 1983). As mentioned before EGF-bound EGFR undergoes Cbl-mediated ubiquitylation, targeting the receptor for degradation in lysosomal compartments, thus reducing the amount of recycling receptor (Chen et al., 2005; Kao et al., 2001). Notably, NGF bound TrkA showed a significantly higher rate of recycling compared to EGFR (Chen et al., 2005). In summary, the ligand induced degradation observed for EGFR would therefore lead to a transient phosphorylation signal that induces cell proliferation, whereas the low degradation rate of NGF-TrkA complexes generates a sustained signaling response that results in cell differentiation (Chen et al., 2005).

Given the fundamental aspects of EGFR regulation by PTPs, including their potential to control both, downstream signaling and receptor trafficking by spatial dephosphorylation events let us hypothesize that the activity of PTPs determines the signaling duration upon growth factor stimulation and thereby the response of the cell. For example, it has been shown that PTPRJ silencing by siRNA results in an enhanced phosphorylation of endosomal EGFR, thereby inducing a higher fraction of receptor internalization combined with accelerated degradation. This resulted in an increased fraction of phosphorylated Erk with a much earlier decay over time compared to control cells (Tarcic et al., 2009). In accordance with the change in the Erk duration that accompanies PTPRJ depletion, cells also showed a significantly higher rate of proliferation. In

contrast, ectopic expression of PTPRJ had reciprocal effects, including decreased EGF-induced EGFR phosphorylation, a lower fraction of internalization and decelerated receptor degradation. Erk activation was also decreased, as well as the Erk-dependent transcription of c-Fos (Tarcic et al., 2009). The authors found out that PTPRJ interacts with EGFR already under basal conditions but was enhanced upon EGF stimulation. The dephosphorylation by PTPRJ diminished the interaction of EGFR with Cbl that thereby affect vesicular trafficking of EGFR (Tarcic et al., 2009).

In addition to a direct interaction between EGFR and PTPs immediately after stimulation, other PTPs can be activated instead by Erk, generating a feedback mechanism that controls the duration of EGFR phosphorylation after activating the downstream MAPK cascade. For example, Prahallad and colleges (2012) identified a negative feedback mechanism involving the dual-specific PTP CDC25C. CDC25C is phosphorylated and activated by Erk upon EGF stimulation resulting in the dephosphorylation of EGFR (Prahallad et al., 2012; Wang et al., 2007). This mechanism was observed in colorectal cancer (CRC) tumor cells bearing the constitutive active mutation of BRaf(V600E) and explains why these cells are resistant to treatment with BRaf inhibitors. BRaf inhibition leads to inhibition of Mek and Erk, which in turn leads to a reduced activation of CDC25C and no dephosphorylation of EGFR. Thus the inhibition of BRaf(V600E) in CRC tumor cells resulted in an enhanced phosphorylation of EGFR, promoting EGFR signaling by an alternative pathway when BRaf is inhibited. A combination treatment of BRaf inhibitor together with an EGFR inhibitor, however, was found to reduce cell proliferation by enhancing the rate of apoptosis (Prahallad et al., 2012).

These examples demonstrated that the regulation of EGFR by PTPs controls the phosphorylation of the receptor as well as its trafficking. Both determine the signal duration of EGFR that in turn affects the activity of downstream proteins that encodes the extracellular signal into a distinct cellular response. Because of their phosphatase activity, PTPs were considered potential tumor suppressors that negatively regulate RTK phosphorylation and thereby

their activity. However, several PTPs have been classified as potential oncogenes because of their ability to promote indirect phosphorylation of RTKs by dephosphorylating the inhibitory phosphotyrosine residues of certain cytosolic tyrosine kinases such as Src family kinases (SFKs), which in turn phosphorylate various RTKs including EGFR (Julien et al., 2011).

Therefore, a detailed study about which PTPs regulate EGFR phosphorylation is required. By considering that PTPs encounter EGFR at different localizations during receptor trafficking, one has to measure the change in the spatial-temporal phosphorylation profile of EGFR upon systematic perturbation of different PTPs inside cells. Such a task requires a quantitative approach with spatial-temporal resolution in which multiple protein perturbations can be applied. In the following thesis, we have combined quantitative microscopy with a cell array (CA) based method (Ziauddin and Sabatini, 2001) that allows to study the regulatory role of PTPs in EGFR phosphorylation. After optimizing this method, the aim was to determine where, when and how different PTPs regulate the phosphorylation dynamics of EGFR.

This thesis will continue with **section 1.2** that contains a general description about the four families of PTPs. In this section we will highlight several mechanisms that control the activity of PTPs. We will also outline how PTPs achieve high substrate specificity, which stands in contrast to the previous belief that PTPs are only passive housekeeping enzymes with a broad specificity. In fact, PTPs show a high diversity in terms of binding domains, which both control the localization of PTPs inside the cell and also play an important role in substrate recognition. Furthermore, **section 1.3** will provide an introduction on the molecular properties of EGFR. EGFR activation is dependent on an allosteric interaction and does not require specific *trans*-phosphorylation events like other RTKs. Moreover, EGFR possesses an intrinsic autocatalytic activity that is regulated by specific phosphorylation events. EGFR enters different trafficking pathways dependent on the presents or absence of ligand stimulation and encounters PTPs under these different conditions. I will give an overview about EGFR trafficking and known interactions with PTPs at the end of **section 1.3.** In

section 1.4, an overview of the underlying biological mechanisms that couple the activity of EGFR and PTPs to generate a specific spatial-temporal phosphorylation pattern in the cell is given. In the last **section 1.5** of the introduction, I provide an outline of the methods used in this work and the rationale for these approaches.

1.2 Protein tyrosine phosphatases

In evolutionary terms, phosphotyrosine signaling governs critical cellular processes in all metazoan species, including proliferation, differentiation, cell survival, metabolism, migration and cell cycle control (Blume-Jensen and Hunter, 2001; Ullrich and Schlessinger, 1990). In particular RTKs are known as connectors between both sides of the plasma membrane that allow rapid cellular responses due to upcoming changes of the extracellular milieu. In contrast to RTKs, it has been long believed that PTPs act as unregulated or constitutive active housekeeping enzymes with a broad specificity, associated with the maintenance of the basal cellular state. It was generally assumed that the regulation of cellular signaling is dominated by the activity of protein kinases alone. This has put an emphasis on the study of kinases in the signal transduction community, and has led to a somewhat secondary attitude to phosphatases in the past. Recent research, however, indicates that this view of PTPs needs to be revised, because PTPs regulate the duration of RTK signaling upon growth factor stimulation and therefore the overall growth factor response of the cell.

The first subsection will contain an overview from the current knowledge about the diverse family of PTPs and how they are classified. PTPs are described as having an "*exquisite substrate specificity*" *in vivo* (Tonks, 2013). Furthermore, PTPs are spatially organized in the cell and their activity is regulated by distinct mechanisms, which frequently involves the activity of RTKs.

1.2.1 The four families of PTPs

Based on the sequence of their catalytic domains and their substrate specificity, the 107 currently identified PTPs can be classified into 4 main families **(Figure 1.2)**. The first family includes the class I cysteine-based PTPs, which are divided into the classical PTPs the VH1-like dual-specific PTPs (DSPs). The classical PTPs are strictly tyrosine specific and can be divided into transmembrane receptor-like (RPTPs), and intracellular non-receptor PTPs (NRPTPs) (Andersen et al.,

2004). The DSPs contain the MAP kinase phosphatases (MKPs) and the atypical-DSPs that are both tyrosine/threonine specific. Furthermore, the Slingshots and phosphatases of regenerating liver (termed as PRLs) are included in this group, which are serine and tyrosine specific, receptively. CDC14s are involved in the dephosphorylation of serine and threonine sites and are known to regulate cyclin dependent kinases (Cdks) (Visintin et al., 1998). The last two DSP groups include PTENs and myotubularins, which represent lipid specific phosphatases (Wishart and Dixon, 2002). Because Slingshots, CDC14, PTENs and myotubularins do not show particular phospotyrosine specificity the classification as "PTPs" might be misleading. However, for simplicity, we will use the term "PTP" in the following work also for the members of this subgroup. The next family contains the cysteine-based class II PTPs including the low molecular weight tyrosine-specific phosphatase (LMW-PTP), which is represented by only one member in humans, with an unknown function. The last cysteine-based family is the class III family and its members are structurally related to bacterial rhodanase-like enzymes having a dual tyrosine/threonine specific phosphatase activity. For example, rhodanese-derived PTPs (CDC25) play a significant role in the cell cycle by dephosphorylation and activation of Cdks. All three of the described cysteine-based classes are characterized by the presence of a conserved signature motif with an invariant Cys and Arg residue essential for catalysis. The fourth class currently consists of 4 PTPs, which employ a different catalytic mechanism that is dependent on an enzymatic aspartic acid. These Asp-based PTPs have a tyrosine or dual serine/tyrosine specific activity, but there is very little known about their functions. After this first overview, we next discuss how PTPs bind to their substrates. PTPs have a high substrate specificity conferred by their modular domain structure. The variation in domains targets PTPs to defined cellular compartments where they can interact with their specific substrates, such as RTKs.

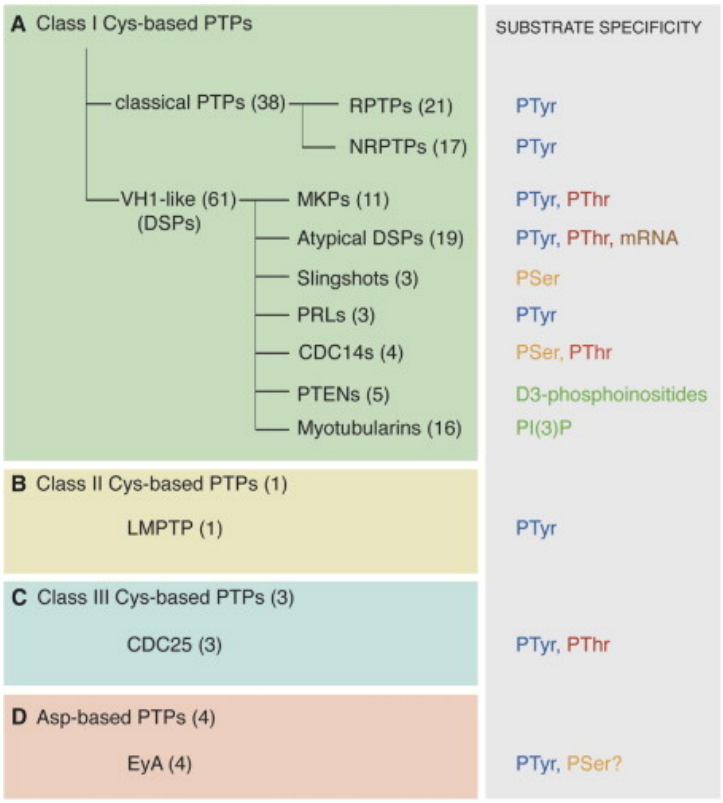

Figure 1.2 Classification and substrate specificity of PTPs. The PTP families are color coded: class I Cys-based PTPs (green), class II Cys-based PTPs (pale yellow), class III Cys-based PTPs (pale blue), and Asp-based PTPs (red). The substrate specificity of each group or class of PTPs is listed (Alonso et al., 2004).

1.2.2 Substrate specificity and modular structure of PTPs

Studies have shown that cytosolic PTPs have a high degree of sequence identity but distinct specificity (Andersen et al., 2001). The substrate specificity of PTPs is controlled by the intrinsic sequence specificity of their catalytic domains (Myers et al., 2001; Ren et al., 2011; Salmeen et al., 2000). In particular, interactions between residues flanking the pY in the primary sequence of the substrate and the residues surrounding the PTP active site contribute to their affinity for substrates. For example, the ER localized PTP1B showed a 70-fold higher affinity for tandem pY containing peptides compared to mono pY substrates (Salmeen et al., 2000). Such a finely tuned regulation allows the PTP activity to be adjusted according to the given amount of phosphotyrosine residues. More recent work shows that each PTP has a different degree of sequence specificity and unique substrate specificity profiles that can range from stringent sequence dependency to a more broad specificity (Ren et al., 2011). Furthermore, additional binding domains or sequences that flank the PTP

domain can also bind to potential substrates or mediate the recruitment to distinct cellular regions to bring the PTP domain in close proximity to its targets (Tonks and Neel, 2001).

In summary, the substrate specificity of PTPs is dependent on the primary sequence specificity of the catalytic domain, but is also dictated by secondary interactions with substrates. Secondary substrate interactions or distinct cellular localizations of PTPs are determined by the modular domain structure of PTPs. Most PTPs consists of at least one additional motif or non-catalytic domain beside their catalytic phosphatase domain **(Figure 1.3)**. In a classical example and as described for SH2/PTB adaptor proteins, the presence of a SH2 domain facilitates direct binding of a PTP to phosphorylated tyrosine signaling proteins, including active RTKs (Neel et al., 2003; Pao et al., 2007). PTPs also contain several phospholipid-binding motifs that target PTPs to different cellular membranes including endosomes or the PM where they can contribute to the assembly of RTK-activated downstream effectors. Some PTPs contain a nuclear localization sequence (NLS) and shuttle between the nucleus and the cytoplasm. Moreover, growth factor stimuli can induce a shift in the nuclear and cytosolic fractions of a PTP, which could have important consequences for their accessibility to substrates (He et al., 2005; Tiganis et al., 1998). In summary, binding domains or sequence motifs function as a "*zip-code*" to direct PTPs to their defined cellular address (Mauro and Dixon, 1994) **(Figure 1.4)**. Beside the broad group of cytosolic PTPs, RPTPs contain a membrane spanning α-helix and are located predominantly at the PM, where they are exposed to the extracellular milieu in a receptor-like fashion. Most RPTPs contain a tandem of PTP-domains that is uncommon for cytosolic PTPs **(Figure 1.3)**.

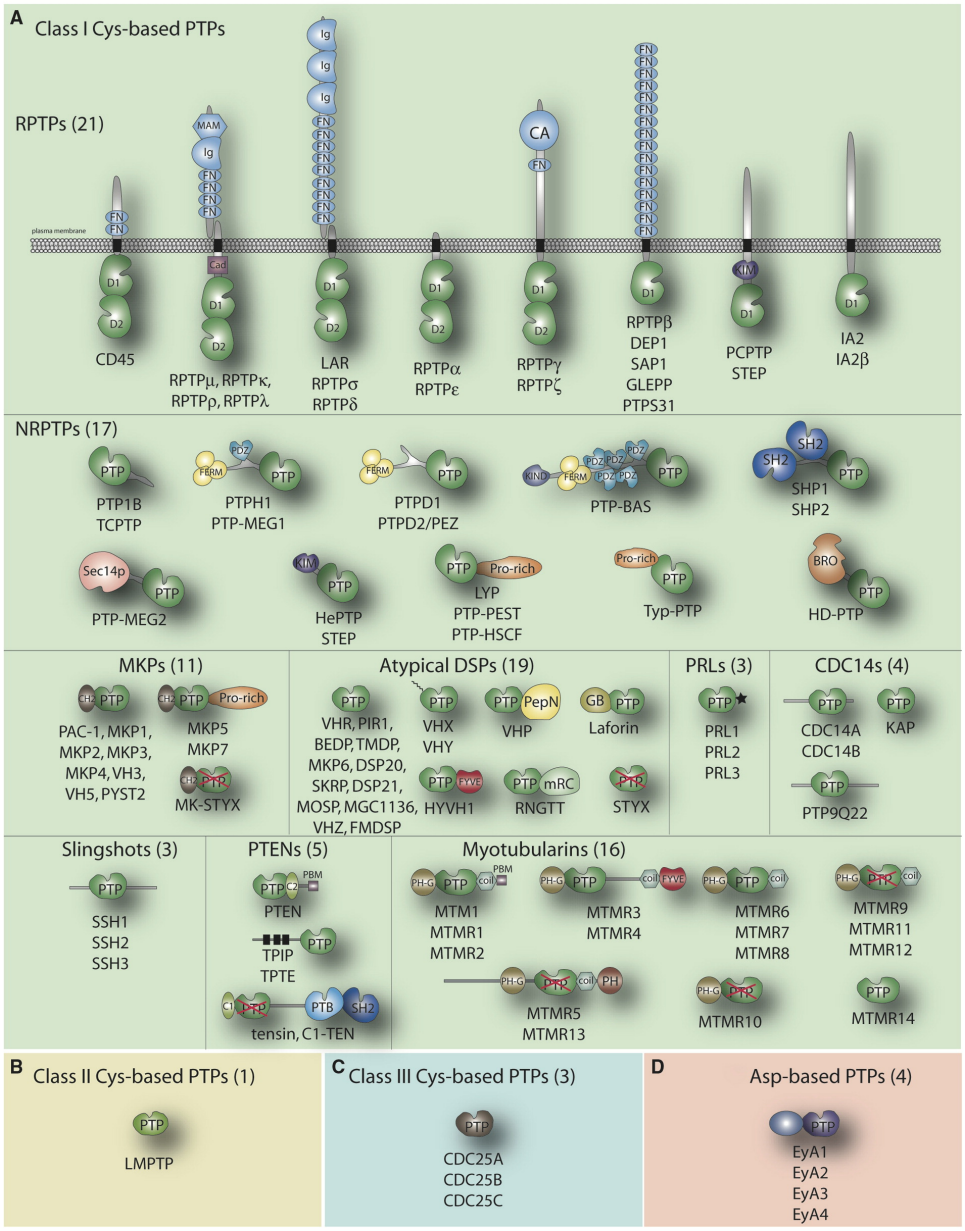

Figure 1.3 Domain structure of all PTPs. Schematic view of the domain composition of all members of the four PTP families. Abbreviations: BRO, baculovirus BRO homology; C1, protein kinase C conserved region 1; C2, protein kinase C conserved region 2; CA, carbonic anhydrase-like; CAAX box, farnesylation signal; CH2, cdc25 homology region 2; CRAL/TRIO, cellular retinaldehyde binding protein/trio homology (Sec14p homology); FERM, band 4.1/ezrin/radixin/moesin homology; FN, fibronectin-like; FYVE, Fab1/Yotb/Vac1p/early endosomal antigen-1 homology; Ig, immunoglobulin-like; KIM, kinase interaction motif; KIND, kinase N lobe-like domain; MAM, meprin, A2, RPTPμ homology; PBM, PDZ binding motif; PDZ, postsynaptic density-95/discs large/ZO1 homology; PH, pleckstrin homology (including GRAM domains); PTB, phosphotyrosine-binding domain; SH2, src homology 2; SH3B, src homology 3 domain binding motif; SH4, src homology 4 (myristylation signal); coil, coiled-coil domain; GB, glycogen binding; mRC, mRNA capping; PBM, PDZ binding motif; pepN, N-terminal peptidase-like; PH-G, pleckstrin homology-"GRAM" domain; Pro-rich, proline-rich; Sec14, Sec14p homology (or CRAL/TRIO). In addition, a small black box signifies transmembrane stretch and a red cross over a PTP domain signifies catalytically inactive domain. (Alonso et al., 2004).

In contrast to the discussed PTPs that are targeted to several intracellular locations PM localization is an important feature of the RPTPs because they share the same compartment where RTKs become activated upon growth factor binding. In summary, research from the last few years has demonstrated that PTPs are a very diverse family with much higher substrate specificity than assumed in the past. The distinct localization and specific substrate recognition of PTPs suggests that there is a spatial dependency that tightly controls RTK phosphorylation. In the next subsection we will describe different mechanisms that ensure that PTPs are regulated enzymes which are integrated in RTK signaling.

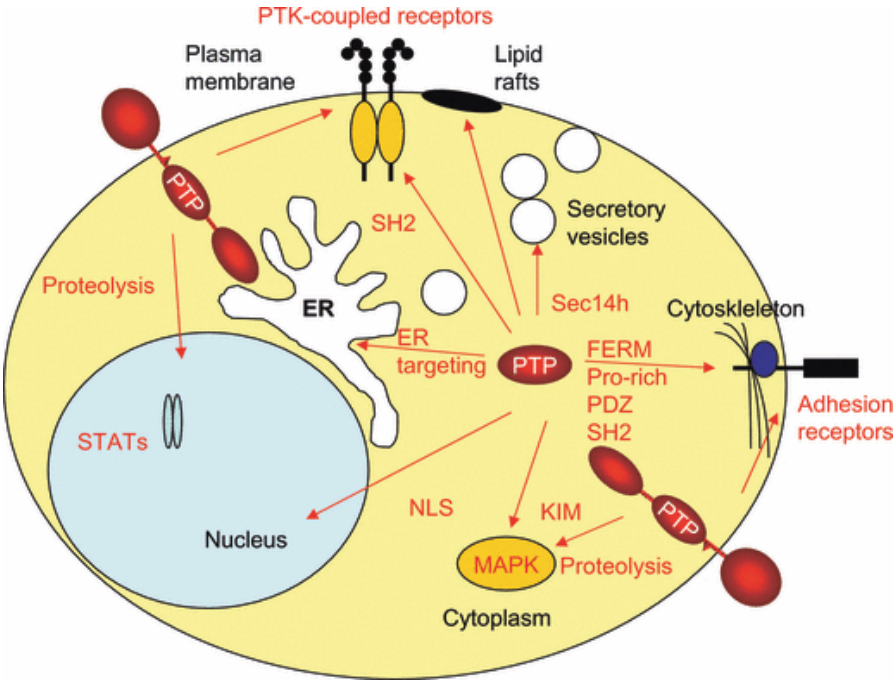

Figure 1.4 Subcellular localization of PTPs. Cytoplasmic PTPs are recruited to activated cell-surface receptors by SH2, proline-rich FERM (band 4.1, ezrin, radixin, moesin homology) and PDZ (postsynaptic density protein 95, discs large, Zonula occludens) domains. RPTPs are also engaged in these complexes. Nuclear localization signals (NLS) and ER targeting domains direct PTPs to these compartments. A Sec14-homology domain (Sec14h) mediates functional association with secretory vesicles. Cytoplasmic PTPs are recruited into lipid rafts by different domains. The kinase-interacting motif (KIM) in PTPs mediates binding to MAPK. Proteolysis releases the catalytic domain of (R)PTPs into the cytoplasm and possibly also into the nucleus (den Hertog et al., 2008).

1.2.3 Regulation of PTP activity

Multiple mechanisms regulate the activity of PTPs. For example, PTP activity can be dependent on alternative splicing or proteolysis. On the other hand, PTPs can be activated by direct recruitment to RTKs or inhibited by growth factor-mediated production of reactive oxygen species (ROS). The latter two mechanisms highlight that the activity of many PTPs is directly coupled to the activity of RTKs.

1.2.3.1 Regulation of PTPs by splicing and proteolysis

To explain the regulation by splicing or protein proteolysis we will start with example based on PTPN1 (PTP1B) and PTPN2 (TCPTP, TC48). Both PTPs are targeted to the cytoplasmic site of the endoplasmatic reticulum (ER) via a C-terminal hydrophobic sequence (Cool et al., 1989; Frangioni et al., 1992). Alternative splicing of TCPTP generates two additional isoforms, a 45 kDa (TC45) and a 41 kDA (termed TC41 in this work), which differ in their C-termini. In contrast to the full length 48 kDA form (TC48) that is targeted to the ER, TC45 lacks the hydrophobic segment exposing a N-terminally located NLS targeting TC45 to the nucleus (Lam et al., 2001). TC41 lacks the NLS and is therefore present in both the nucleus and the cytosol. Similarly to the regulation of TC45 by splicing, PTP1B contains a site for proteolytic cleavage by calpain, which generates a truncated, soluble PTP1B with enhanced activity (Frangioni et al., 1993). This demonstrates the importance of targeting motifs in PTP regulation. The examples of PTP1B and TCPTP illustrate that the subcellular localization is directly coupled to PTP activity. In the following part we discuss a general regulatory mechanism based on RTK-mediated activation of PTPs.

1.2.3.2 PTP activation by RTKs

PTPs can be activated following recruitment to phosphorylated RTKs. For example, crystal structures of the SH2 tandem containing PTP, PTPN11 (SHP2) have shown that its catalytic site is occluded by an interaction with residues of

its own N-terminal SH2 domain keeping the enzyme in a low activity state (Neel et al., 2003). Binding of the N-terminal SH2 domain to phosphorylated RTK sites induces a conformational change that releases this auto-inhibitory interaction leading to the open active conformation (Hof et al., 1998). The recruitment-coupled activation of PTPN11 to auto-phosphorylated RTKs or their phosphorylated adaptor proteins is an important mechanism of how active RTKs are directly regulated by PTPs. Moreover, the C-terminal tail of SHP2 contains two tyrosine phosphorylation sites (Tyr542 and Tyr580) and the phosphorylation of these sites leads to an increase in the catalytic activity. A similar regulation was reported for PTPN6 (SHP1) that is tyrosine phosphorylated once bound to an RTK, leading to an increase in its activity (Uchida et al., 1994). One other example includes the previously mentioned PTPN1 that binds to RTKs at the ER-PM interface. PTPN1 becomes tyrosine phosphorylated at pY66, leading to a 3-fold increase in its catalytic activity, which in turn promotes the dephosphorylation of the RTK (Liu and Chernoff, 1997). The sequence around pY66 fits the consensus sequence (YXNX) for binding of the SH2 adapter protein GRB2, but it is uncertain whether these complexes would serve to activate or to inhibit signaling (Liu and Chernoff, 1997). The recruitment-coupled or phosphorylation-dependent activation of PTPs are classical examples of feedback mechanisms that control the duration of RTK signaling. Both mechanisms will induce a locally enhanced PTP activity in regions where the RTK is active and/or provide phosphorylated docking sites. Specific recruitment, phosphorylation, proteolysis and alternative splicing are general mechanisms of how cytosolic PTPs are regulated. In the next paragraph we describe how the PM localized receptor-like PTPs (RPTPs) are regulated.

1.2.3.3 Regulation of RPTPs

Most RPTPs have cytosolic regions containing tandem PTP domains in which the membrane proximal domain (D1) provides the catalytic activity (Tonks, 2006), while the distal domain (D2) contributes a regulatory function. Recent work has indicated that dimerization of membrane proximal D1 domains might inhibit RPTPs. In particular, the formation of a D1-D1 dimer was inhibited by a helix-

turn-helix wedge motif that inserts from one domain into the catalytic cleft of the partner domain and vice versa, thereby occluding access to substrates (Bilwes et al., 1996). Similarly to ligand-induced dimerization of RTKs, an RPTP ligand could induce dimerization and inhibition or a ligand could initiate a dimer disruption, which would result in two active monomers. For example, the soluble cytokine pleiotropin functions as ligand for PTPRZ and induces receptor inhibition (Meng et al., 2000). In addition, binding to the transmembrane protein syndecan promotes activation of PTPRF, whereas binding of the membrane anchored Dallylike suppresses its function (Tonks, 2006). However, it is so far unclear whether these ligands inhibit or favor RPTP dimerization and thereby regulate phosphatase activity. Moreover, it has been shown that intracellular phosphorylation can be a mechanism of RPTPs to overcome the inhibitory dimer structures (den Hertog et al., 1995). Crystal structures of PTPRM (RPTPμ), PTPRC (CD45) and PTPRF (LAR) have shown an important role of the D2 domain to overcome the wedge dependent D1-D1 dimerization by an intramolecular stabilizing D1-D2 domain interface.

In summary, all of these regulatory mechanisms of PTPs are based on protein-protein interactions. In addition, recent research has demonstrated that oxidation by reactive oxygen species (ROS) plays a major role in PTP regulation (Tonks, 2006). It has been shown that ROS production is induced by RTK activation, which leads to local inactivation of PTPs around activated RTKs (Bae et al., 1997; Reynolds et al., 2003).

1.2.3.4 PTP inhibition by RTK-coupled ROS production

The catalytic domains of the three classes of cysteine-based PTPs are strikingly similar, underlying their classification shown in **subsection 1.2.1**. The shared structural and catalytic features of cysteine-based PTPs is a H-Cys$(X)_5$-R sequence motif (where X is any amino acid) that is termed the PTP loop (Salmeen and Barford, 2005). The dephosphorylation reaction involves the formation of a cysteinyl-phosphate intermediate, followed by water-mediated hydrolysis to release the phosphate. The cysteine residue is characterized by an

extremely low pKα and is present as the thiolate ion (Cys-S^-) at neutral pH that promotes its function as a nucleophile **(Figure 1.5)**. In addition, this nucleophilic cysteine is highly susceptible to reactions with ROS and to a lesser degree with reactive nitrogen species. Oxidation or nitrosylation of the catalytic cysteine renders it unable to act as a nucleophile and the PTP loses its phosphatase activity (Salmeen and Barford, 2005). Dependent on the extent of oxidation, the thiolate anion (Cys-S^-) can be readily oxidized to sulfenic acid (Cys-SOH) under mild oxidative conditions leading to reversible oxidation of the protein activity. The Cys-SOH however, is highly reactive and susceptible to rapid oxidation to the terminally oxidized sulfinic (SHO_2) and sulfonic (SHO_3) acid. Biochemical and crystallographic studies indicate that Cys-based PTPs have evolved a variety of mechanisms to avoid higher irreversible oxidation by stabilizing a reversibly oxidized state.

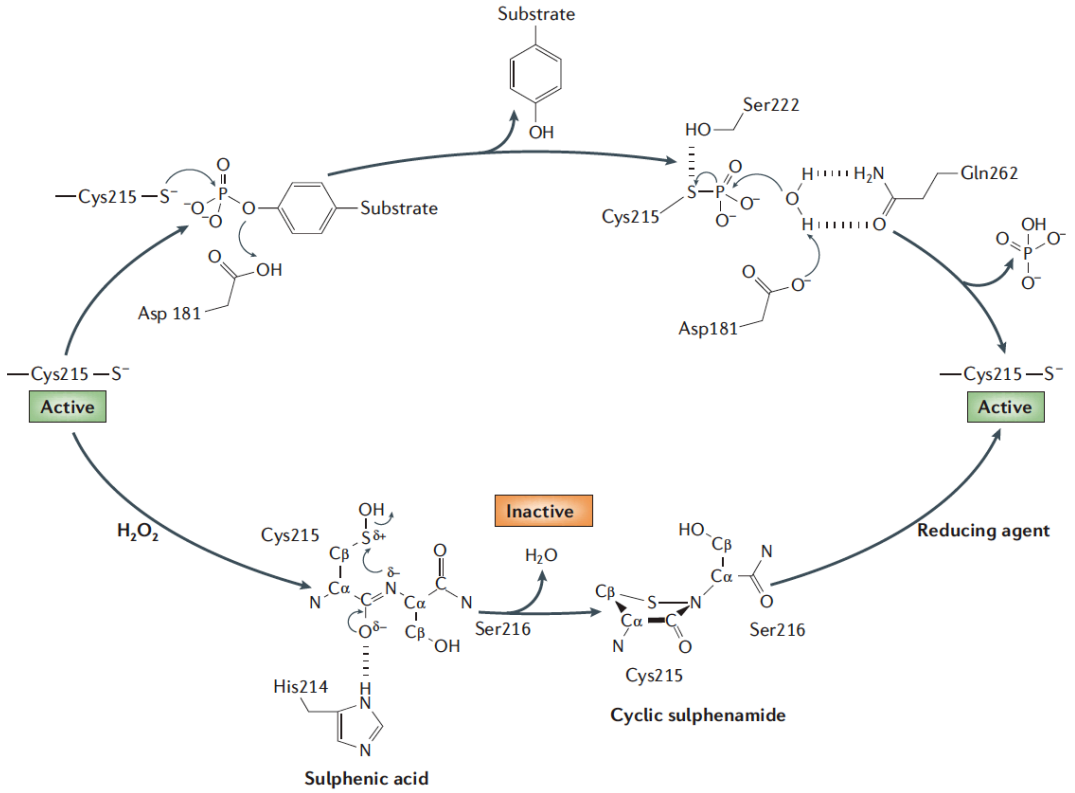

Figure 1.5 Reversible oxidation of PTPs. All members of the protein tyrosine phosphatase (PTP) family use the same basic catalytic mechanism. The $HC(X)_5R$ signature motif contains the essential nucleophilic cysteinyl residue, forms the base of the active-site cleft and recognizes the phosphate of the target substrate. Catalysis proceeds through a two-step mechanism that involves the production of a cysteinyl-phosphate intermediate. In the first step, there is nucleophilic attack on the phosphate by the sulphur atom of the thiolate ion of the essential cysteine residue (Cys215 in PTP1B). This is coupled with protonation of the tyrosyl leaving group of the substrate by the conserved aspartic acid residue (Asp181 in PTP1B). The second

step involves the hydrolysis of the phosphoenzyme intermediate, mediated by a glutamine residue (Gln262 in PTP1B), which coordinates a water molecule, and Asp181, which now functions as a general base, culminating in the release of phosphate. Oxidation of the active site cysteine residue abrogates its nucleophilic function, thereby inhibiting PTP activity. As shown for PTP1B, and presumably reflective of the classical PTPs in general, oxidation is reversible due to the rapid conversion of the sulphenic acid form of the oxidised cysteine to a novel 5-atom-ring structure, a cyclic sulphenamide, which is promoted by the environment of the catalytic site. In particular, the juxtaposition of His214 with Cys215 polarizes the amide bond, promoting nucleophilic attack by the amide nitrogen of Ser216 on the sulphur atom of the Cys215 sulphenic acid, leading to condensation and formation of a covalent bond between the sulphur and nitrogen atoms. The cyclic sulphenamide can be readily reduced to the active, thiolate form of the active site cysteine residue (Tonks, 2006).

For classical PTPs, as shown for PTPN1 (PTP1B), the oxidation is reversible due to a rapid conversion to a cyclic sulpenamide species (Tonks, 2006). This cyclic sulphenamide can be readily reduced to the active, thiolate form of the active-site cysteine residue **(Figure 1.5)**. In contrast, dual-specific phosphatases have evolved a different mechanism. These PTPs contain a second cysteine residue within the active site. Upon oxidation of the catalytic cysteine, a disulfide bond with the neighboring cysteine protects the enzyme from forming an irreversible oxidized states (Salmeen and Barford, 2005). Moreover, inactivation by intermolecular disulfide bridges was observed for RPTPs. In particular, oxidation triggers the formation of an intermolecular S-S bond between both active site cysteine residues of the D2 domains of each receptor (van der Wijk et al., 2004). In the last years, studies have shown that the ROS-dependent inhibition of PTPs is a major mechanism involved in RTK signaling. A large number of RTK ligands including hormones, growth factors and cytokines induce an increase intracellular ROS (Bae et al., 1997; Krieger-Brauer et al., 1997; Sattler et al., 1999; Sundaresan et al., 1995) and treatments with H_2O_2 induce hyperphosphorylation of RTKs (Koshio et al., 1988; Sundaresan et al., 1995). After RTK activation, ROS production is induced by PI3K- and Rac-dependent activation of the NADPH-oxidase complex (Bae et al., 1997). The multicomponent protein complex including the catalytic subunit NADPH oxidases (NOX) is assembled at the PM by the coordinated phosphorylation of regulatory subunits, inositol phospholipid binding and GTPase activity of Rac (Finkel, 2006; Lambeth, 2004). NOX enzymes produce superoxide by transferring an electron from the NADPH complex to molecular oxygen. The

superoxide is generated on the outer leaflet of the PM, after which it dismutates to hydrogen peroxide and from where it can diffuse back into the cell (Rhee, 2006). However, the understanding of the specificity involved in this type of novel signaling is only in its infancy. One aspect that has already emerged is the intrinsic differences between PTP domains with regard to susceptibility to oxidation (Groen et al., 2005; Persson et al., 2004). It is also likely that PTPs that are closer to ROS production will be preferentially oxidized, pointing to the fact that the spatial distribution of ROS sources and PTPs play an obvious role. Clear is that the oxidation of PTPs reveal an additional level of complexity in the regulation of RTK signaling in normal and malignant cells (Karisch et al., 2011).

In summary, we have seen that PTPs are spatially organized and underlie specific regulatory mechanisms for activation. Moreover, PTPs are activated by recruitment to phosphorylated RTKs, exemplifying a major negative feedback mechanism. On the other hand, RTK-coupled ROS production induces local PTP inhibition and amplifies RTK phosphorylation. The interactions between RTKs and PTPs are temporal and spatially organized in the cell, which regulates the signal duration and thereby the cellular response upon growth factor stimulation. In this thesis, we addressed the regulation of EGFR by PTPs. Therefore, an introduction about the molecular properties of EGFR is provided in the next **section 1.3**.

1.3 The epidermal growth factor receptor (EGFR)

EGFR is a member of the ErbB family containing EGFR (ErbB1, HER1), ErbB2 (HER2), ErbB3 (HER3) and ErbB4 (HER4) (Landau and Ben-Tal, 2008; Schlessinger, 2002; Yarden and Sliwkowski, 2001). The EGFR can be activated by a large set of ligands including epidermal growth factor (EGF) and transforming growth factor-α (TGF- α) (Groenen et al., 1994; Harris et al., 2003).

1.3.1 Ligand binding to EGFR

In the absence of ligand, EGFR exists predominantly as monomer at the PM. These monomers are at equilibrium with a small population of transient dimers. Such short-lived dimers are potentially primed for ligand binding but the complete mechanism is not understood in detail (Chung et al., 2010). However, ligand binding to the extracellular region of EGFR enhances the formation of receptor dimers by increasing the stability compared to un-ligated dimers (Low-Nam et al., 2011). Intramolecular interactions stabilize a tethered conformation of monomers that autoinhibits receptor dimerization in the absence of a ligand (Burgess et al., 2003; Ferguson et al., 2003). Ligand binding promotes a substantial rearrangement in the extracellular domain that transforms the "intra"-molecular tether to an extending configuration that permits dimerization of two receptor molecules (Lemmon and Schlessinger, 2010). When bound by two ligands, the conformation of this dimer is entirely receptor-mediated (Garrett et al., 2002; Ogiso et al., 2002).

1.3.2 An allosteric mechanism leads to EGFR activation

In general, the tyrosine kinase domain of RTKs underlies a unique *cis*-autoinhibition by a set of receptor-specific intramolecular interactions that stabilize its inactive form. Ligand-induced receptor dimerization releases this

cis-autoinhibition, leading to a conformation with low but sufficient kinase activity to provide *trans*-phosphorylation. Stepwise *trans*-phosphorylation at distinct phosphorylation sites in the activation loop, the juxtamembrane region and/or the C-terminal tail disrupt these auto-inhibitory interactions and allows the kinase domain to relax to the activated state.

The EGFR/ErbB family is a clear exception of this general mechanism because they do not require *trans*-phosphorylation for activation (Gotoh et al., 1992; Knowles et al., 2006; Zhang et al., 2006). An isolated kinase domain of EGFR possesses low intrinsic catalytic activity. This catalytic activity dramatically increases when the local concentration of the kinase domains are increased by attaching them to the surface of lipid vesicles (Zhang et al., 2006). This points to the fact that the kinase domain of EGFR requires an intermolecular allosteric interaction to overcome its intrinsic autoinhibition. Activation of EGFR is controlled primary by an allosteric interaction between the two protein kinase domains in an asymmetric dimer that is favored upon ligand-induced extracellular dimerization. In this asymmetric dimer, the kinase domain of one receptor molecule resembles that of a cyclin when bound to its Cdk, which is analogous to the kinase domain of the second receptor (Zhang et al., 2006). As in the Cdk/cyclin interaction, the core of the asymmetric EGFR kinase domain dimer is dominated by hydrophobic interactions (hydrophobic patch) involving several residues of the N-lobe of the activated kinase ("receiver") and the C-lobe of the cyclin-like kinase domain ("activator"). A key element of this interaction is the engagement of the helix αC of the "receiver" kinase domain. As a result, the "receiver" kinase domain adopts the characteristic active configuration without phosphorylation of its activation loop **(Figure 1.6)**. Other parts like the juxtamembrane (JM) region of the EGFR contribute to its activity as shown for other RTKs, but notably without the requirement of phosphorylation. For example, the C-terminal half of the JM segment of the receiver kinase latches to the activator kinase. This latch stabilizes the asymmetric dimer formation and is crucial for receptor activation (Jura et al., 2009). The remaining N-terminal half of the receiver JM further has the potential to dimerize with the N-terminal half of activator JM in an antiparallel helix-helix structure that engages the

transmambrane helices of the activated receptor (Jura et al., 2009). Receptor activation requires also an interaction between the two involved transmembrane helices to facilitate the antiparallel interaction between the JM segments in the dimer (Arkhipov et al., 2013; Endres et al., 2013). This configuration is also needed to release further inhibitory interactions at plasma membrane contact points (Endres et al., 2013).

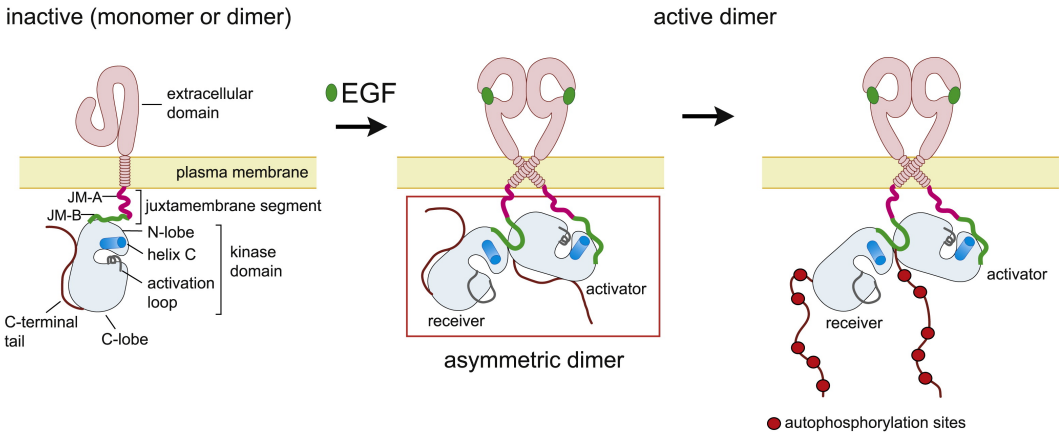

Figure 1.6 Activation of EGFR by EGF results in the formation of an asymmetric kinase domain dimer. The asymmetric dimer results in the activation of the "receiver" kinase domain and *trans*-autophosphorylation of the activator (Jura et al., 2009). It can be assumed that kinase domains change their activator/receiver function leading to trans-phosphorylation of both involved C-terminal domains as indicated.

The fact that the activity of an isolated kinase domain correlates with its local concentration in membrane vesicles suggested the involvement of an allosteric mechanism, but it also rises the question whether EGFR can form active dimers without a bound ligand at increased receptor densities at the PM. EGFR family members are prone to ligand-independent dimerization and activation at high expression levels (Nagy et al., 2010). EGFR exists predominantly as monomer together with small population of dimers under moderate expression levels (e.g. 5 x 10^4 receptors/cell) (Burgess et al., 2003; Ferguson et al., 2003). This ligand-independent dimer showed a different and inhibited configuration compared to the described active ligand bound dimer. In absence of ligand, however EGFR is able to overcomes its auto-inhibition at high

densities (e.g. 2 x 10^6 receptors/cell), probably through the formation of an asymmetric dimer (Arkhipov et al., 2013; Endres et al., 2013).

1.3.3 Intrinsic autocatalytic activity of EGFR

It has been shown that a local stimulation of EGFR with EGF coated beads leads to a lateral phosphorylation wave of EGFR in the whole PM within a few minutes (Sawano et al., 2002; Verveer et al., 2000b). The mechanism of lateral propagation is the result of the intrinsic autocatalytic properties of EGFR. The autocatalytic activity is a general feature of all RTKs that is given by *trans*-autophosphorylation of regulatory receptor sites, for example within the kinase activation loop. Such activating *trans*-autophosphorylation events can trigger an activation wave in a RTK population at the PM. As discussed previously, however, EGFR activation is dependent on its specific asymmetric dimer formation and not on *trans*-phosphorylation of regulatory sites. Recent work have shown that the N-lobe dimerization interface of the EGFR kinase domain is intrinsically disordered but becomes ordered upon dimerization (Shan et al., 2012). Oncogenic mutations, particularly the widespread L834R in the kinase activation loop, promote EGFR dimerization by suppressing this local disorder. Moreover, phosphorylation of the Y845 within the activation loop does not directly activate EGFR in contrast to other RTKs, but may facilitate here a higher affinity for dimerization. As described previously in **subsection 1.3.2**, ligand binding favors the formation of an active asymmetric dimer. Moreover, the phosphorylation of Y845 might also promote the formation of the active asymmetric dimer. Shan and colleagues (2012) proposed that EGFR activation and Tyr845 phosphorylation could explain the mechanism of lateral propagation **(Figure 1.7)**. In this mechanism, local ligand binding initially leads to activation of a subset of EGFR molecules (ligand-induced dimer formation). Other EGFRs may then be phosphorylated at Y845, primed for a higher affinity to dimerize and consequently full activation (phosphorylation-induced dimerization). The phosphorylation of Y845 can be mediated by EGFR (Qiu et al., 2009) and therefore explains the intrinsic autocatalytic activity of EGFR. Alternatively, Y845

is phosphorylated by Src suggesting that this kinase influences the activity of EGFR (Biscardi et al., 1999).

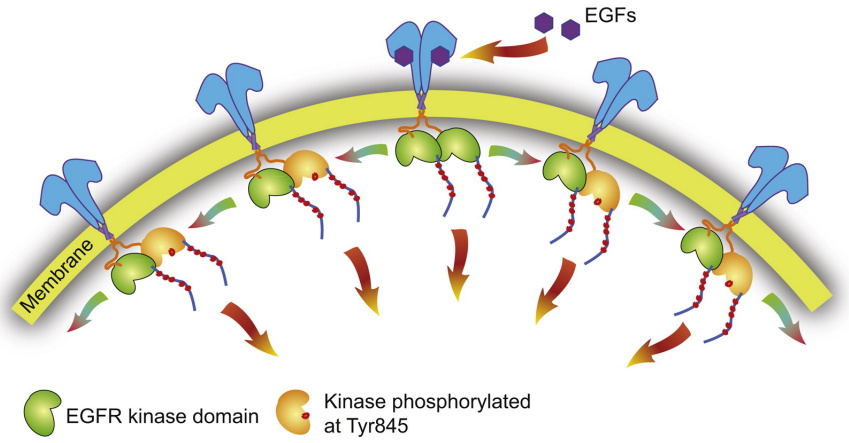

Figure 1.7 A model for EGFR lateral signal propagation. Lateral propagation based on Y845 phosphorylation. A small population of EGFR (center) is activated by ligand-induced asymmetric dimer formation. Besides the phosphorylation of the C-terminal tails, additional phosphorylation of Y845 in the kinase domain occurs. In addition, phosphorylation at Y845 might induce asymmetric dimerization and ligand independent activation of involved kinase domains (Shan et al., 2012).

In particular, it has been shown that few PTPs directly dephosphorylate EGFR at pY845 (see **Table 1.1** in the next **subsection 1.3.4**). It can be assumed that these PTPs influence the lateral propagation of EGFR and thereby the switch-like response upon EGF binding. Next, we give an overview about the phosphotyrosine docking sites on EGFR and which PTPs are known to dephosphorylate such sites in particular.

1.3.4 Phosphorylation docking sites of EGFR

The formation of an active asymmetric dimer, either by ligand binding or promoted by a high receptor density, results in *trans*-autophosphorylation of the C-terminal regions of both involved receptors. These phosphorylation events create docking sites for downstream proteins, thereby generating an initiator complex including SH2 and PTB domain mediated association of downstream

proteins at the intracellular region of the receptor. Most of the *trans*-autophosphorylation sides including Y845, Y992, Y1045, Y1068, Y1086, Y1148 and Y1173 are rapidly phosphorylated within the first 1-5 minutes after receptor stimulation (Helin and Beguinot, 1991; Hsuan et al., 1989; Margolis et al., 1989; Schulze et al., 2005; Walton et al., 1990). The interactions of transduction mediators and adaptor proteins transmit the activation signal of the receptor to different subnetworks (modules) that constitute the conserved core process downstream of EGFR **(Figure 1.8)**. With multiple phosphor-tyrosine sites at the EGFR and the involvement of numerous SH2/PTB docking proteins such as Shc, Grb2 and Grb1, the activated EGFR recruits and influences a large number of different signaling molecules. SH2 and PTB domain containing proteins bind only to receptors in which tyrosines are phosphorylated (with a few exceptions) and subsequently link the EGFR autophosphorylation to the initiation of different downstream events in the signaling network (Pawson, 2004; Schlessinger and Lemmon, 2003). Beside such direct receptor interactions (by e.g. SH2 and PTB), further interactions at the receptor are spatially and temporal determined. In summary, the activated EGFR can be thought of as a key node in a complex signaling network that transmits information from the exterior to the interior of the cell (Lemmon and Schlessinger, 2010). However, the composition and availability of downstream docking sites is dependent on the interactions with PTPs. Like the spatial and temporal interaction with downstream mediators, the interactions with PTPs are similarly organized in space and time. It has been shown that several PTPs dephosphorylate the EGFR either at basal conditions or after activation **(Table 1.1)**.

Through a combination of stimulatory or inhibitory signals, several positive feedback loops and negative feedback loops emerge in the network and regulate the composition of phosphorylated docking sites on EGFR (Lemmon and Schlessinger, 2010). As already discussed in this introduction, PTPs play a key role in such mechanisms. The activation of PI3K and Rac for example mediates growth factor induced ROS production via the activation of NOX that in turn

Gene	Protein	Dephos. of EGFR [basal conditions]	Dephos. of EGFR [after EGF]	PTP localization	Ref.
PTPN1	*PTP1B*	pY*	pY*	ER	Lammers et al. 1993
PTPN2	*TCPTP*	pY*	pY845, pY992, pY1068	Nu or ER [Isoform depend.]	Lammers et al. 1993, Tiganis et al. 1998, Mattila et al. 2005
PTPN6	*SHP1*	pY*	pY*	Nu, Cy	Vogel et al. 1993, Keilhack et al. 1998
PTPN9	*PTP-Meg2*		pY845, pY998, pY1068	Cy	Yuan et al. 2010
PTPN11	*SHP2*		pY992	Nu, Cy	Agazie et al. 2003
PTPN12	*PTP-PEST*	pY1148		Cy	Sun et al. 2011
PTPRC	*CD45*	pY*	pY*	PM	Lammers et al. 1993
PTPRF	*LAR*		pY*	PM	Kulas et al. 1996
PTPRJ	*DEP-1*		pY845, pY1068, pY1173	PM	Tarcic et al. 2009
PTPRK	*RPTPκ*	pY*	pY1068, pY1173	PM	Xu et al. 2005
PTPRM	*RPTPμ*	pY992, pY1068	pY845, pY992, pY1045, pY1068, pY1086, pY1173	PM	Hyun et al. 2011
PTPRS	*RPTPσ*	pY*	pY*	PM	Suarez-Pestana et al. 1999
CDC25A			pY*	Nu, Cy	Wang et al. 2002
CDC25C			pY1068	Nu, Cy	Prahallad et al. 2012
DUSP3	*VHR*	pY992	pY845, pY992, pY1173	Nu, Cy	Wang et al. 2011
ACP1	*LMW-PTP*		pY*	Cy	Ramponi et al. 1989

Table 1.1 PTPs that dephosphorylate EGFR under basal conditions and after EGF induced activation. In most studies a generic anti-phosphotyrosine antibody has been used and a general decrease of phosphorylation was observed, indicated as (pY*). Additionally information from specific EGFR phosphorylation sites are shown when information was available (e.g. pY845, pY1045 etc.). Localization of PTPs is indicated, source Uniprot and LOCATE database.

leads to the reversible inhibition of local PTPs (Bae et al., 1997; Reynolds et al., 2003) resulting in a positive feedback that enhances the phosphorylation level of EGFR **(subsection 1.2.3.4)**. One other classical example contains SH2 containing PTPs e.g. PTPN6 and PTPN11. SH2 mediated binding of such PTPs to phosphorylated sites on EGFR or adaptor proteins induces phosphatase activation and results in dephosphorylation of the receptor that exemplifies a negative feedback (Agazie and Hayman, 2003a; Keilhack et al., 1998) **(subsection 1.2.3.2)**. However, dephosphorylation of RTKs is not always associated with termination of the downstream signal. For example, SHP2 is

known as an essential promoter of EGFR downstream signaling. It has been shown that SHP2 dephosphorylates EGFR at pY992 (Agazie and Hayman, 2003b), which is an important recruiting site for the Ras GTP-activating protein (RasGAP) **(Figure 1.8)**. The inhibition of RasGAP translocation leads to an increased half-life of activated Ras (GTP-Ras) that induces the activation of the MAPK cascade. The example of SHP2 in particular shows that the activity of PTP is important to generate an appropriate downstream signal.

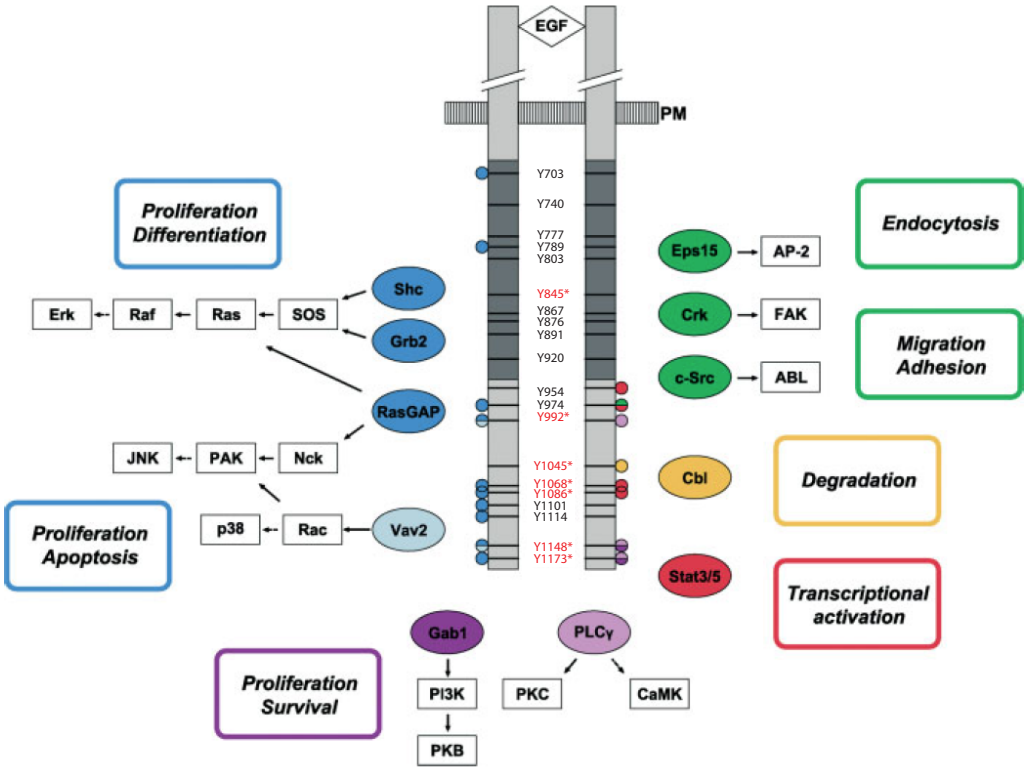

Figure 1.8 Simplified overview about the major pathways initiated by EGFR. Tyrosine phosphorylation sites (Y) of EGFR are indicated in the center. Autophosphorylation sites shown in red. Known binding sites for downstream proteins are labeled with colored circles, corresponding colors indicate direct interaction partners and their associated biological functions. The receptor kinase domain is shown in dark gray. Some residues are targeted by the intrinsic tyrosine kinase activity of EGFR and by Src (Y845, Y992, Y1068 and Y1086), while other tyrosine residues (Y891, Y920 and Y1101 were identified as unique Src sites (Lombardo et al., 1995; Stover et al., 1995; Wu et al., 2002). Figure adapted from (Morandell et al., 2008).

1.3.5 PTPs support EGFR phosphorylation

Cancer is often linked with an increase in the general phosphotyrosine content of the cell, associated with enhanced RTK and PTK activities (Hennipman et al., 1989) and because of the dephosphorylating activity it is generally believed that PTPs negatively regulate the phosphorylation of EGFR C-terminal docking sites. However, several studies have shown an overall increase in total PTP activity suggesting that PTPs could indirectly support the phosphotyrosine level in cancer cells (Julien et al., 2011; Ostman et al., 2006). In this context, PTPs act not only as tumor suppressors but also as oncogenes. Beside autophosphorylation, EGFR phosphorylation can be mediated by other PTKs including non-receptor Src-familiy kinases (SFKs). As previously discussed for Y845 **(subsection 1.3.3),** EGFR *trans*-autophosphorylation sites can be phosphorylated by recruited cytosolic Src that in turn promotes EGFR phosphorylation **(Figure 1.8 and 1.9 a)**. A direct interaction between phosphorylated EGFR and the SH2 domain of Src has been described (Biscardi et al., 1999). Activation of Src requires dephosphorylation of its inhibitory Y527 sites. Dephosphorylation of this site promotes the displacement of the SH2 domain from this residue and subsequent autophosphorylation of residue Y416 within the activation loop of Src **(Figure 1.9 b)** (Abram and Courtneidge, 2000; Sato et al., 2002). It has been shown that several PTPs including PTPN1 (PTPB1), PTPN6 (SHP1), PTPN11 (SHP2), PTPN21 (PTPD1), PTPRA (RPTPα), PTPRC (CD45), PTPRE (RPTPε), PTPRK (RPTPκ), PTPRU (RPTPλ), and ACP1 (LMW-PTP) induce dephosphorylation of the inhibitory phosphotyrosine of Src (pY527) resulting in Src activation (Bjorge et al., 2000; Cardone et al., 2004; Fang et al., 1994; Roskoski, 2005; Somani et al., 1997; Wang et al., 2005; Zambuzzi et al., 2008; Zheng et al., 1992). Notably, beside the promoting function described for several PTPs, it has been shown also that PTPs dephosphorylate the activation site of Src (pY416) leading to kinase inhibition. This function has been shown for PTPN2 (TCPTP), for example (Nunes-Xavier et al., 2013). Furthermore and as already introduced in **section 1.1**, the presence of particular phosphorylation sites of EGFR recruits ubiquitin ligase Cbl that targets the receptor for degradation by ubiquitylation **(Figure**

1.8). Next, we discuss in the following subsection how the interaction of PTPs with EGFR regulates the trafficking behavior of the receptor.

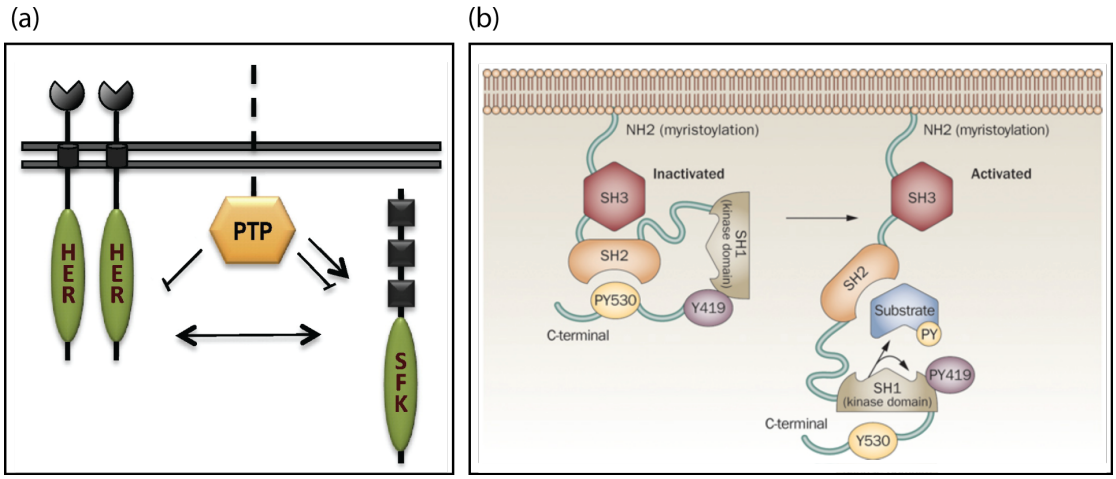

Figure 1.9 Schematic representation of the involvement of Src family kinases (SFKs) and PTPs in the regulation of EGFR (HER) phosphorylation. (a) PTPs can inhibit or activate SFKs by direct dephosphorylation (Arrow-lines indicate activation and blunt-lines inhibition). (b) Structure and activation of Src. When Y530 (Y527) is phosphorylated, the C-terminus binds to the SH2 domain and inhibits Src activity holding the protein in its inactive state. Dephosphorylation of Y530 (Y527) by PTPs allows Src to become open and fully active including autophosphorylation of Y419 (Y416). The free SH2 domain allows the recognition of phosphorylated substrates. Figure adapted and modified from (Kim et al., 2009; Nunes-Xavier et al., 2013)

1.3.6 Regulation of EGFR trafficking by PTPs

Under basal conditions, the majority of EGFR is located at the PM, but receptors are constantly internalized into recycling endosomes (Wiley, 2003). The recycling rate is several times higher than the constitutive internalization rate which results in a predominant localization of EGFR at the PM and a small endosomal receptor pool (Sorkin and Goh, 2008). As discussed in **subsection 1.3.2,** EGFR activation is dependent on an allosteric mechanism and on the basis of its intrinsic molecular properties, EGFR activation is possible even without a ligand. Under these conditions the constant PTP activity at the PM maintains a low phosphorylation level of EGFR. This activity prevents spurious signals in absence of ligand. It has been shown that several PTPs reduce the basal level of EGFR, including receptor-like PTP that are present at the PM, but also cytosolic PTPs **(Table 1.1)**. The recycling pathway transports EGFR constantly trough the

cytoplasm that might allow additional interactions with PTPs in the cytosol or at the ER that were spatially distinguished before.

EGFR appears to alter its trafficking pattern in response to ligand induced phosphorylation. This altered pattern is characterized by accelerating internalization, enhanced lysosomal degradation and a decrease in the fraction that recycles (Wiley et al., 1991). Dependent on the cellular context, activated EGFR at the PM can undergo clathrin-dependent endocytosis that is more rapid (Bonifacino and Lippincott-Schwartz, 2003; Kirchhausen, 2000) and/or clathrin-independent endocytosis that is facilitated by extensive PM ruffling and formation of micro- and macropinocytic vesicles (Chinkers et al., 1979; Haigler et al., 1979). Studies on clathrin-dependent endocytosis have shown that the internalization of EGFR requires its intrinsic kinase activity and its phosphorylation at specific binding sites because mutations of the Y1068 and Y1086 phosphorylation sites at the C-terminus resulted in a decrease of internalization (Jiang et al., 2003b). These sites are recognized by the SH2 domain-containing adaptor Grb2, which is necessary for EGFR recruitment into coated pits. Besides minor binding to pY1086, pY1068 seems to be the major binding site for Grb2 (Batzer et al., 1994). Depletion of Grb2 caused a substantial (60-80%) decrease in EGFR internalization (Sorkin and Goh, 2008), which strongly suggested that the Grb2-dependent pathway plays a major role in clathrin dependent endocytosis. Grb2 recruits Cbl that is a RING finger containing E3 ubiquitin ligases that mediate ubiquitylation of several lysine residues in the kinase domain of EGFR via recruitment of E2 ubiquitin conjugated enzymes (Levkowitz et al., 1999; Umebayashi et al., 2008). There are three members of the Cbl family c-Cbl, Cbl-b and Cbl-3. The first two are able to bind to the SH3 domain of Grb2 (Thien and Langdon, 2005). In addition to the indirect binding via Grb2, all three Cbl proteins can bind directly via a tyrosine kinase binding (TKB) domain to the phosphorylated Y1045 site of EGFR (Levkowitz et al., 1999). Direct binding appears to play the minor role in clathrin-dependent endocytosis of EGFR. However, it has been shown that ubiquitylation is not essential for receptor internalization but may function as a sorting signal, targeting for lysosomal degradation (Huang et al., 2007; Huang et

al., 2006). In **section 1.1** we introduced PTPRJ (DEP-1) as an example PTP that dephosphorylates pY1068 and thereby reduces the degradation of EGFR (Tarcic et al., 2009). However, it has been shown that several other PTPs also target these sites **(Table 1.1)** and it can be assumed that such interactions at the PM collectively regulate the degradation rate of EGFR. Most PTPs including PTPRJ dephosphorylate not only phosphor sites required for degradation they also dephosphorylate pY845 that potentially promotes dimerization and activation of EGFR. Overexpression of PTPs like PTPRJ can reduce dramatically the phosphorylation and degradation of EGFR after ligand binding. In consequence the strongly dephosphorylated EGFR might favor the recycling pathway in contrast to accelerated internalization. However, endocytosis is not only a degradation system, it actively transports the activated EGFR deeper inside the cell and allows additionally interactions. The predominant internalization of EGFR leads to additional interactions with cytosolic PTPs as mentioned before for basal conditions. Such interactions at endosomal compartments regulate the availability of phosphor binding sites including those required for Cbl and degradation. In other words, the collective activity of PTPs at the PM and the cytosol regulates the final rate of EGFR degradation vs recycling.

The endosomal maturation process involves fusion of early endosomes and a change in their biochemical composition and morphology that leads to the formation of multivesicular bodies (MVB) (Sorkin and Goh, 2008). Ubiquitylated EGFR is though to interact with the endosomal sorting complexes required for transport (ESCRTs), containing HRS and TSG101 (Le Roy and Wrana, 2005). This interactions guide the EGFR into intraluminal vesicles of MVBs. MVBs are formed approximately 15-20 min after EGF induced endocytosis and it has been shown that the majority of the internalized EGFR undergoes lysosomal degradation (Carpentier et al., 1987; Dunn and Hubbard, 1984; McKanna et al., 1979; Miller et al., 1986). However, during the endosomal maturation, a rapid recycling path from early endosomes, a slow recycling pathway from the tubular extensions of MVB and a recycling from late recycling endosomes are possible to escape receptor degradation. (Sorkin et al., 1991). After enclosing into intraluminal MVBs, EGFRs looses the ability to be recycled back to the PM and fusion of MVBs

with primary lysosomal vesicles that carry proteolytic enzymes leads to rapid proteolysis of intraluminal components of the MVBs containing EGFR (Miller et al., 1986).

In addition to direct dephosphorylation of Cbl recruiting phosphor-sites on EGFR, it has been shown that several PTPs regulate the trafficking of EGFR by alternative mechanisms. For example, it has been shown that MTM1 (myotubularin 1) is recruited to late endosomes after EGF stimulation by phosphoinositide binding. Overexpression of MTM1 inhibits EGFR trafficking from late endosomes to lysosomes and induces large endosomal vacuoles resulting in an increased EGFR stability (Tsujita et al., 2004). Similarly to MTM1, it has been shown that PTPN21 (PTPD1) is rapidly recruited to endocytotic vesicles containing EGFR (Carlucci et al., 2010). In particular, endosomal localization of PTPN21 is mediated by interaction with KIF16B, an endosomal kinesin that modulates receptor recycling at the PM. Silencing of PTPN21 promotes degradation of EGFR and inhibits downstream ERK signaling. This implies that PTPN21 promotes recycling of internalized EGFR through the endocytic pathway. In summary, the collective interactions of EGFR with PTPs at the PM determines whether a given ligand concentration induces robust receptor phosphorylation and enhanced degradation or not. In the latter case, the population of receptor remains in the inactive state favoring the recycling pathway. In case of a robust phosphorylation, the internalization is enhanced and the rate of degradation is dependent on the sum of all spatial-temporal interaction with PTPs that EGFR encounters in the cytosol.

I have discussed in the **subsection 1.2.3.4** that ligand induced ROS production leads to transient inhibition of PTPs. Furthermore, I have discussed that EGFR is activated by an allosteric mechanism and possesses an intrinsic autocatalytic activity. Considering these features of the system, I want to exemplify how the interaction of RTKs and PTPs generates distinct spatial-temporal phosphorylation patterns inside cells, which are dependent on the local topology of these opposing enzymes.

1.4 EGFR activation coupled to PTP inhibition generates spatial phosphorylation pattern

Due to the intrinsic autocatalytic activity of EGFR, even a local EGF stimulation can lead to an overall wave of receptor phosphorylation, also at regions where no ligand is present. On the other hand, RTK activation is coupled to ROS production that leads to local PTP inhibition. The coupling of RTK activation with PTP inhibition via ROS production can be described in a double negative feedback loop (in sum a positive feedback) that leads to the amplification of the phosphorylation signal **(Figure 1.10a)**. By considering the autocatalytic kinase activity of EGFR the system can be described as bistable **(Figure 1.10b)** (Reynolds et al., 2003; Tischer and Bastiaens, 2003).

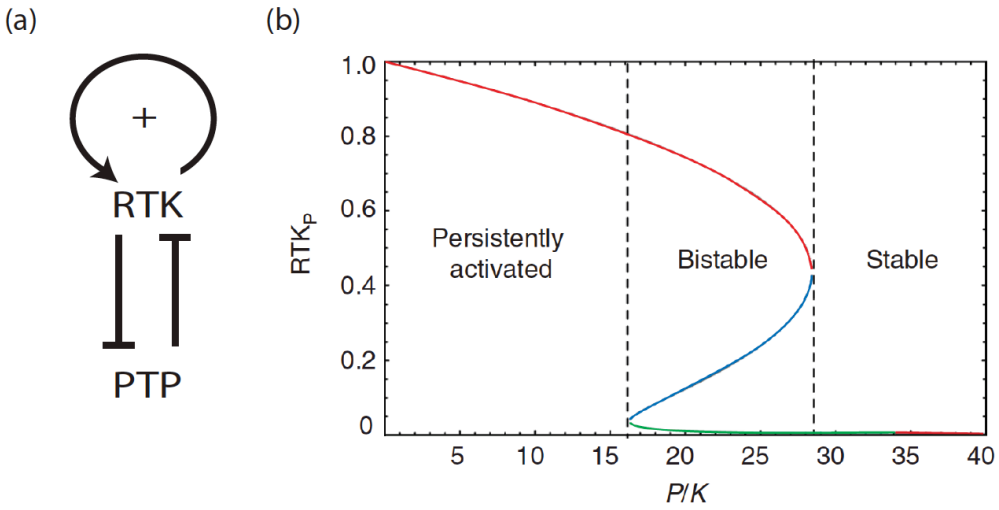

Figure 1.10 (a) Schematic representation of the RTK – PTP network topology exemplifies a double negative feedback loop. Together with the autocatalytic activity of RTKs the system is bistable. (b) Representation of the resulting bistable system. The fraction of phosphorylated RTK (RTKp) at steady state as function of the relative maximal PTP/RTK activity (P/K). Green and read lines, stable steady states (resting and activated, respectively), blue lines, unstable saddle point. Where the red and green lines coincide, the system is bistable. Figure adapted from (Reynolds et al., 2003).

This amplification allows the system to respond in a switch-like manner in which the signal initiation is dependent on a certain threshold concentration of the ligand (Reynolds et al., 2003). In this way, a sufficient local EGF stimulation

results in the activation of a small EGFR population at the PM, which is amplified by a locally mediated ROS production that overcomes PTP activity at the PM. By considering the dynamic distribution of EGFR and the diffusion of ROS at the PM, a local system activation creates a spatial phosphorylation pattern that includes regions where the PM is not exposed to ligand. Notably, ROS are chemically high reactive and randomly oxidize other cellular molecules e.g. amino acids of proteins fatty acids in lipids. Due to the high reactivity, ROS have a relatively short half-time and is spatially constrained to their sources. Cells degrade ROS by antioxidant enzymes such as catalases to prevent severe damage that also limits the range of ROS. However, local production of ROS (induced by an active and phosphorylated population of EGFR) can still inhibit PTPs in a distinct range and lowers down the excitation threshold of neighboring, inactive EGFRs. This triggers a domino like rapid propagation of activity along the PM, whereby the RTK/PTP/H_2O_2 system acts as an excitable medium (Grecco et al., 2011b; Reynolds et al., 2003). *Trans*-phosphorylation events that enhance the dimerization affinity, and thereby the receptor activation are favored under higher receptor densities and become the key to trigger the lateral propagation. The involvement of RTK and PTP activity in the signal initiation exemplifies how the system can avoid spurious signaling and how a proper phosphorylation signal can be initiated after reaching a given reaction threshold. The constant tyrosine cycling between phosphorylated and dephosphorylated forms at the PM influences directly the receptor sensitivity to changes in ligand concentration (Qian and Beard, 2006), and sensitivity to changes in PTP and receptor concentrations (Goldbeter and Koshland, 1981). Moreover, the local RTK-PTP topology in the system has direct consequences on the spatial-temporal phosphorylation pattern of the receptor. In the case of the double negative feedback, the rapid self-amplifying phosphorylation wave propagates through the cell as discussed. In contrast to this, a RTK coupled activation of PTPs that is achieved by PTP recruitment, as described in **subsection 1.2.3.2,** changes the spatial-temporal pattern to phosphorylation hot spots (Grecco et al., 2011b). I will next discuss how the phosphorylation pattern of EGFR propagates within the cytosol to affect downstream signaling.

1.4.1 Axial propagation of EGFR

The downstream or axial signal propagation of EGFR needs to be tightly controlled because the catalytic activity of PTPs is up to three orders of magnitude higher than the activity of the tyrosine kinases (Fischer et al., 1991). Such a PTP activity would terminate any tyrosine phosphorylation signal in the cytosol. On the other hand, the absence of PTPs near the PM would allow spurious transmitted signals as shown in PTP inhibition experiments. The system is able to overcome this problem by the present spatial inhibition of PTPs by growth factor induced ROS production as discussed for lateral propagation. The lateral EGFR activation mediates local ROS production at the whole PM. But ROS diffuses also inside the cell and because of its short half-life, a gradient of ROS is formed in the cytosol. This in turn generates as well a gradient of PTP activity in which PTPs near the PM are more inhibited. Thus, signal penetration via tyrosine phosphorylation is ultimately a self-referencing system in which tyrosine phosphorylation depends on the magnitude of the ROS gradient, which in turn depends on the balance between RTK and PTP activities (Grecco et al., 2011b). As discussed already in **subsection 1.3.6,** activated RTKs undergo endocytosis and this process is necessary in order to remove the activated population of receptor from the PM and to terminate the signal. Moreover, the endocytotic machinery guides the source of the ROS gradient packed in vesicles deeper inside the cytosol (Birtwistle and Kholodenko, 2009). RAC-mediated ROS production has been described in the endosmoal lumen (Li et al., 2006) that could induce an efficient negative regulation of cytosolic PTPs by the diffusion of ROS out of the endosome. In addition, the reduced size and closed surface of endosomes provides a relatively high density of EGFR that could support a sustained activity (Grecco et al., 2011b).

Taking together, the interplay of RTKs and PTPs in space and time allows a tight control of signaling initiation and progression. The high PTP activity at the PM in the absence of a ligand avoids spurious signaling of EGFR that recycles constantly at the PM. On the other hand, the EGFR autocatalytic activity coupled with ROS mediated PTP inhibition facilitates lateral and axial signal propagation,

thus generating a distinct spatial and temporal EGFR phosphorylation pattern, while the majority of receptor is internalized by endocytosis. Such a fine tuned phosphorylation pattern in space and time explains how the external signal is encoded to generate a unique cellular response.

Thus, the picture of how global phosphorylation pattern are generated by the interplay of EGFR and PTP activity needs to be complemented with the information where, when and how strong each individual PTP regulates EGFR phosphorylation. In order to address these questions, we have used FRET measured by FLIM as an effective strategy to quantify the phosphorylated state of EGFR in its cellular environment with the required spatial resolution (Verveer and Bastiaens, 2008). Moreover, to study the effect of multiple PTPs, a method that combines assay miniaturization and automated sample acquisition is required. In this thesis, we used cell array (CA) technology combined with FRET-FLIM (Grecco et al., 2010) that allows us to determine the functional role of PTPs in EGFR signaling. In the following **section 1.5** we introduce the reader to the general principles of FRET-FLIM and CA.

1.5 FRET-FLIM and CA technology

1.5.1 Förster resonance energy transfer (FRET)

Fluorescence is the emission of a photon when an electron relaxes back from its excited singlet (S_1) to its ground state (S_0). In the excited singlet state, the electron in the excited orbital is paired (by opposing spin) to the second electron in the ground state (Lakowicz, 2008). Consequently, relaxation to the ground state is spin allowed and occurs rapidly by emission of a photon. The electronic states of a molecule and the transitions between them can be described using the Jablonski diagram **(Figure 1.11)**. The lifetime (τ) that describes the average time between the excitation and the return to the ground state is typically in the range of nanoseconds. Upon light absorption, the electron in S_0 is usually excited to some higher electronic state, either S_1 or S_2. At each of these states the fluorophores can exist in a number of vibrational energy levels. With a few exceptions, molecules relax rapidly by internal conversion to the lowest vibrational level of S_1 before emission occurs. In consequence, the same fluorescent emission spectrum is generally observed irrespective of the excitation wavelength. Additionally, loss of energy occurs when an emitting fluorophore decays to higher vibrational levels within the S_0 state, and then relaxes to the lowest S_0 level by internal conversion. The energy loss between excitation and emission due to internal conversion is a universal feature of fluorescent molecules and is implicated in the Stokes shift between the excitation and the energy lowered emission spectrum (Lakowicz, 2008). Beside the rapid fluorescence emission, molecules in the S_1 state can also undergo a non-radiative decay by internal conversion (k_{ic}) or a spin conversion to the first triplet state T_1 termed intersystem crossing (k_{isc}). The transition from T_1 is forbidden and results in phosphorescence, which is several orders of magnitude slower then the rapid fluorescence emission.

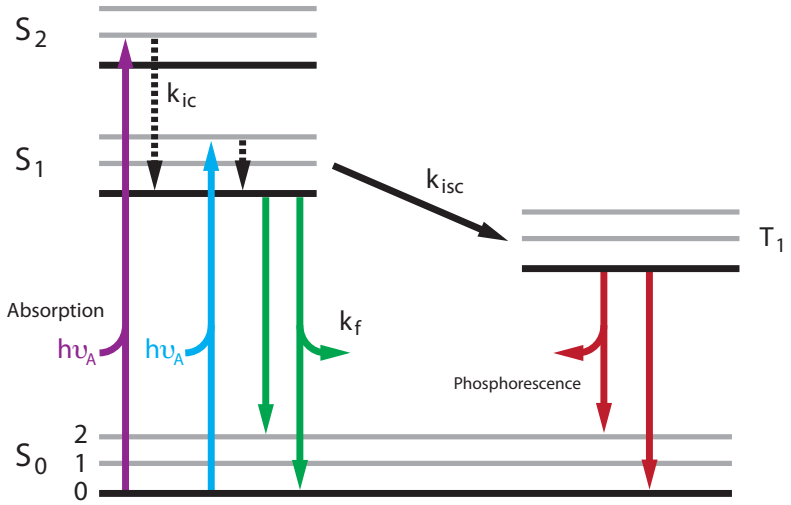

Figure 1.11 Jablonski diagram. After light absorption (magenta and blue arrows), electrons from the singlet ground state (S_0) can be excited to some higher vibrational level of the first two excited singlet states (S_1 and S_2). Molecules relax rapidly to the lowest level of S1 by internal conversion (k_{ic}) or can undergo a spin conversion to the triplet state (T_1) by intersystem crossing (k_{isc}). Electrons loose their energy and returning to the ground state by radiative or non-radiative decays. Radiative decays from the S_1 are termed as fluorescence (green arrow) and decays from the T_1 are termed as phosphorescence (red arrow).

Two important quantities to characterize the fluorescence of a molecule are the fluorescence lifetime (τ) and the quantum yield (Q), defined as the ratio of the number of emitted to the number of absorbed photons. Both quantities depend on the rate of fluorescence emission (k_f) and the rates of the nonradiative decays k_{ic} and k_{isc}.

$$\tau = \frac{1}{k_f + k_{ic} + k_{isc}} \quad (1)$$

$$Q = \frac{k_f}{k_f + k_{ic} + k_{isc}} \quad (2)$$

Another important process that can occur in the exited state is Förster resonance energy transfer (FRET) (Förster, 1948). This process occurs when the emission spectrum of a fluorophore termed donor (D) overlaps with the excitation spectrum of another molecule termed acceptor (A). Importantly, FRET is not a photon emitted by the donor that is absorbed by an acceptor. Instead, the donor

and the acceptor are coupled by a dipole-dipole interaction. The rate of energy transfer (k_{FRET}) is dependent on the distance (r) between the donor and the acceptor, the donor lifetime (τ_D) and the Förster distance (R_0), that is defined as the distance at which 50 % energy transfer takes place.

$$k_{FRET} = \frac{1}{\tau_D}\left(\frac{R_0}{r}\right)^6 \quad (3)$$

R_0 is defined by the relative orientation of the transition dipoles of the fluorophores (κ^2), the overlap integral ($J(\lambda)$; $cm^6\ mol^{-1}$) dependent on the overlap of the donor emission and the acceptor absorption spectra, the refractive index of the intervening medium (n) and the quantum yield (Q) of the donor.

$$R_0 = [\kappa^2 \times J(\lambda) \times n^{-4} \times Q]^{\frac{1}{6}} \times 9.7 \times 10^2 \quad (4)$$

The efficiency of the energy transfer (E) for a given single donor-acceptor pair at a fixed distance is defined by:

$$E = \frac{R_0^6}{R_0^6 + r^6} \quad (5)$$

The typical value of R_0 lies between 2 and 6 nm, which is in the order of magnitude of protein dimensions. For this reason energy transfer has been used as molecular ruler to measure protein interactions. The short range of FRET guarantees that the signal will be highly specific for this interaction yielding a very low false positive rate. FRET reduces the excited state lifetime of the fluorophore as shown in **equation (1)** by providing an additional pathway for depopulating the excited state leading to the following dependency:

$$\tau = \frac{1}{k_f + k_{ic} + k_{isc} + k_{FRET}} \quad (6)$$

In the same way, the quantum yield is reduced, leading to an overall reduced emission intensity. The FRET efficiency (E) can be directly derived from intensity (I) or lifetime (τ) based measurements. E can be calculated by monitoring the donor intensity (I_D) and the donor intensity in presence of the acceptor (I_F) (quenched intensity). Similarly, E can be derived from the donor lifetime (τ_D) and the in donor lifetime in presence of acceptor (τ_F).

$$E = 1 - \frac{I_F}{I_D} = 1 - \frac{\tau_F}{\tau_D} \quad (7)$$

In contrast to intensity based methods, lifetime measurements are independent of fluorophore concentration, less error prone from changes in intensity and allows precise quantification of the donor fraction in complex with the acceptor.
FRET measured by fluorescence lifetime imaging microscopy (FLIM) goes beyond intensity based readouts as it provides a map of the absolute fraction of the donor in complex with the acceptor. We will next give a background about the FLIM measurement by frequency domain and how information can be extracted from lifetime data by global analysis.

1.5.2 Frequency domain FLIM

The fluorescence lifetime (τ) of a donor fluorophore can be measured by time-domain or frequency domain FLIM. In time domain FLIM, τ is directly calculated from the fluorescence decay after a short excitation pulse, where the pulse is ideally much shorter than τ (Bastiaens and Squire, 1999). For a sample comprising a single fluorescence species, the decay follows a single exponential and τ is given by the time over which the fluorescence intensity drops to about 37 % of its initial value. In frequency domain FLIM, the excitation light is modulated at high frequencies. The excitation intensity is typically sinusoidally modulated at frequencies in the range of 10 MHz – 100 MHz by an acousto-optic modulator (AOM). When the excitation intensity is modulated, the emission follows the same frequency, but shows a decreased modulation amplitude and a

shift in phase that dependents on the delay in time generated by the fluorescence emission lifetime **(Figure 1.12)**.

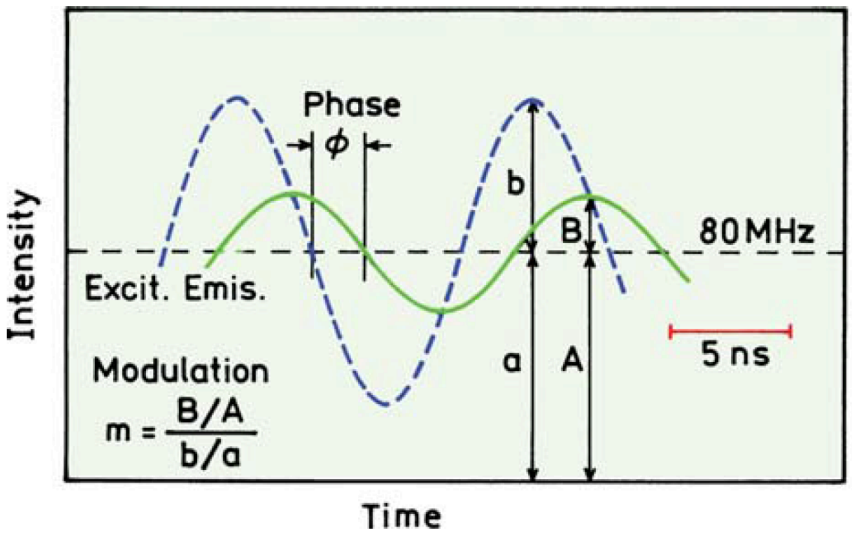

Figure 1.12 Definitions of the phase angle and modulation of emission. The assumed decay time is 5 ns and the light modulation frequency is 80 MHz. (J. Lakowicz, Principles of Fluorescence Spectroscopy, Third Edition 2006)

Therefore, the shift in phase Δϕ and the change of the relative modulation depth M between excitation and emission is a direct measurement of the fluorescence lifetime (Lakowicz, 2008). Δϕ and M can be used to calculate the apparent frequency-dependent fluorescence phase (τ_ϕ) and modulation (τ_M) lifetime.

$$\tau_\phi = \omega^{-1} \, tan(\Delta\phi) \tag{8}$$

$$\tau_M = \omega^{-1} \sqrt{(M)^{-2} - 1} \tag{9}$$

These apparent frequency-dependent fluorescence lifetimes are only equal to each other when the fluorescence decay is characterized by a single exponential. The resulting phase shift and the modulation of the emission are dependent on the relative lifetime but also on the light modulated frequency (Lakowicz, 2008). The optimal frequency f for measuring a fluorescence lifetime is chosen so that $2\pi f\tau \sim 1$. The current inability to acquire images at GHz frame rate makes it

impossible to directly measure the dephase and demodulation of the fluorescence emission using a CCD camera. Therefore, most wide field homodyne FD-FLIM systems recover the phase τ_ϕ and modulation τ_M lifetime from multiple sample excitations generating a stack of images (FLIM stack). A microchannel plate (MCP) intensifier is placed in front of the camera to modulate the gain at the same frequency as the modulated excitation but the frequency of the intensifier is slightly shifted in phase (Gadella, 1993). The resulting FLIM-stack contains intensity images taken at different phase shifts ϕ_k over 2π **(Figure 1.13)**. The phase shift ϕ and the demodulation M at each pixel or alternatively their complex representation $R = Me^{i\phi}$ can be obtained using singular value decomposition.

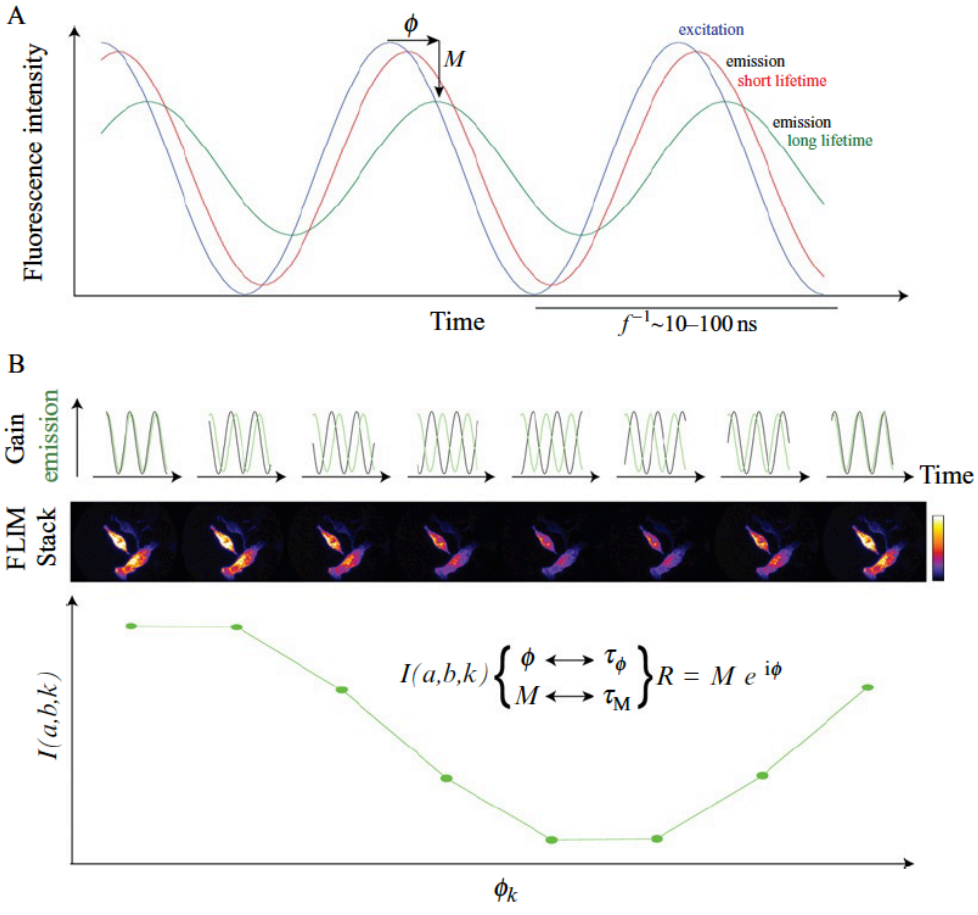

Figure 1.13 FD-FLIM. (A) Sinusoidally modulated excitation and emission of two fluorophores with two different lifetimes (short and long). The phase shift, demodulation, and the period of the wave are indicated. (B) Acquisition of the FLIM stack by homodyne detection. Upper panels show the modulated emission along with the different phases of the modulated gain of the intensifier. Middle panel shows the different phases of the acquired FLIM stack. Plot in the lower panel shows the change in I(i, j, k) in the different phases of the FLIM stack. Figure adapted from (Grecco et al., 2011a)

1.5.3 Global analysis of FRET–FLIM data

The phase and modulation parameterization of the fluorescence decay profile can be superseded by a parameterization in terms of three biophysically relevant quantities. The first two are the fluorescence lifetime of the donor (τ_D) alone and the donor in complex with the acceptor (τ_F), which together define the FRET efficiency (E) **(equation 7)**. The third parameter is the fraction of the donor in complex with the acceptor (α). When assessing interactions, the fluorescence lifetimes are only dependent on the photophysical properties of the donor alone and in complex. Therefore, for a given FRET pair, these values can be considered as spatially invariant and globally linked across all datasets. In contrast, the biologically relevant parameter $\alpha(i,j)$ quantifies in each pixel the fraction of interacting protein. In the complex plane representation of the data (Grecco et al., 2009; Verveer and Bastiaens, 2003; Verveer et al., 2000a), points corresponding to a monoexponential fluorescence decay lay in a semicircle with radius and center 0.5 **(Figure 1.14)**.

$$R_\tau = \frac{1}{1-i\omega\tau} \tag{10}$$

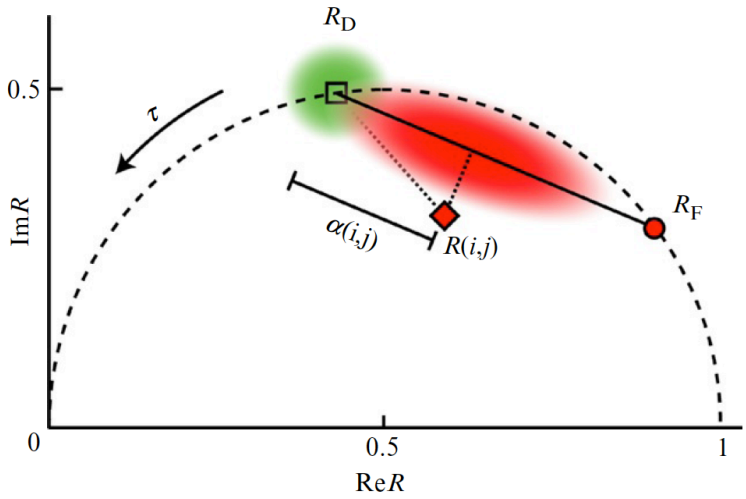

Figure 1.14 Global analysis in the complex plane. Complex plane schematic representation of phase shift and modulation data before (green cloud) and after the addition of the FRET acceptor (red cloud). The dashed semicircle described by equation (10) represents all possible monoexponential fluorescence lifetimes (τ). R_D and R_F are the Fourier coefficients corresponding to the global lifetime of the donor alone and the global lifetime of the donor in present of the acceptor. A mixture will be a linear combination of those. The fraction of donor in complex with the acceptor (α) is the length of the projection of R - R_D onto the vector R_F - R_D. Figure adapted from (Grecco et al., 2011a)

A bi-exponential decay (τ_D *and* τ_F) is just the linear combination of the complex quantities for each component and the prefactors are the relative fractions of each component.

$$R(i,j)=(1-\alpha(i,j))R_D+\alpha(i,j)R_F \quad (11)$$

If there is enough dispersion in the α values, a straight line can be fitted to the cloud of $R(i,j)$. The intersection points with the "monoexponential semicircle" are R_D and R_F from which the corresponding lifetimes can be derived. The value of $\alpha(i,j)$ can be obtained by projecting the vector $R(i,j)$ - R_D into the vector R_F - R_D (**Figure 1.14).** The fact that recovering these parameters constitutes a linear problem is of special interest in screening applications because of saving computation time, so that a large number of datasets can be analyzed together and compared (Clayton et al., 2004).

1.5.4 Cell array (CA) technology provides systematic perturbation of PTPs

In order to address, the spatial-temporal regulation of EGFR by PTPs a method that combines assay miniaturization and quantitative microscopy is required. High throughput microscopy-based protein screenings require an addressable array of genomic material (plasmid DNA or siRNA) on imaging compatible cell culture chamber. Transfection in multi-well plates provides strict separation between samples but hinders the application of homogeneous treatment to all cells. In contrast, reverse transfection of immobilized genetic material arrayed in a single culture chamber allows spatially restricted perturbation of cell colonies without the use of wells **(Figure 1.15)**. As all cells are grown in the same cell culture chamber, applied treatments are ineluctably homogeneous except for the unique transfection in each spot. In addition, all the experimental error generated due to well-to-well variation is avoided. By using these so called cell arrays (CA) the function of many proteins can be analyzed in a short time in a slide with up to 10 spots / mm^2 (spot size 120-150 μm in diameter).

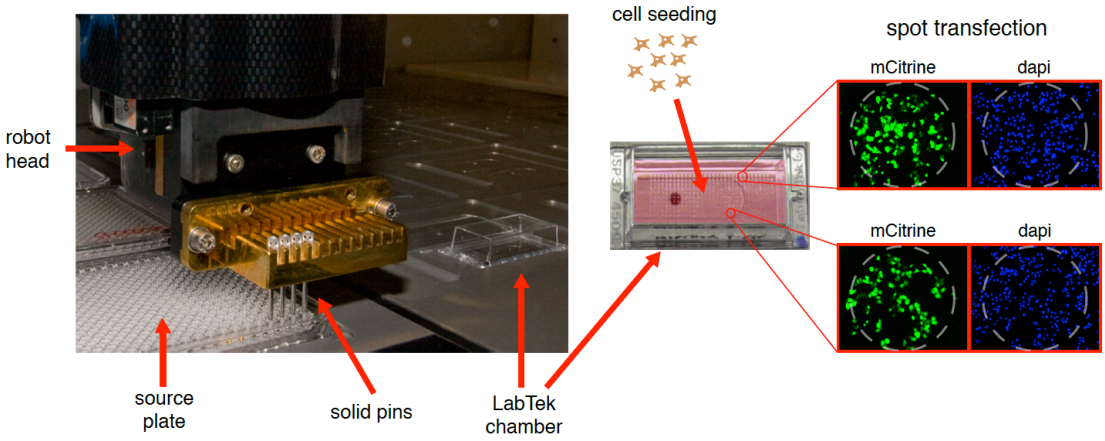

Figure 1.15 Schematic representation of CA production. Arrays are produced by spotting transfection material such as plasmid DNA loaded in 384 well plates on LabTek chambered cover glasses (left). Arrays with 384 individual spots were seeded with human culture cells and incubated for reverse transfection on spots. Reverse transfection of cells on spots loaded with mCitrine expression plasmids are shown together with nucleus dapi staining (right).

Thus, CA have emerged as new devices for automated high-throughput quantitative microscopy providing spatial resolution (Grecco et al., 2010; Kumar et al., 2003; Mousses et al., 2003; Ziauddin and Sabatini, 2001). CA is flexible to study a high variation of biological questions because of its variability in terms of readout and spotted material. CA have been used in several loss- or gain- of function screenings by using siRNA or plasmid cDNA arrays. Beyond cell-based phenotypic readouts, CA has been successfully combined with FRET-FLIM to generate quantitative data about the phosphorylated state of signaling proteins (Grecco et al., 2010). Moreover, CA-FLIM also allows systematic perturbation of multiple PTPs, as well as the possibility to quantify the phosphorylated state of EGFR. In this way, CA-FLIM is suitable to study the regulatory function of PTPs in EGFR phosphorylation signaling.

II SCOPE

The intrinsic autocatalytic activity of EGFR and its interactions with PTPs determines the phosphorylation of the receptor and its trafficking. Both features control the signaling duration of downstream effectors and thereby govern the cellular response. PTPs underlie specific activation mechanisms and occupy distinct cellular locations, thus shaping the spatial-temporal phosphorylation profile of EGFR during trafficking **(Figure 2.1)**. Differences in the coupling of EGFR and PTP activities have direct consequences on the global phosphorylation profile. For example, a double negative (positive) feedback between EGFR and a particular PTP would result in a rapid self-amplifying phosphorylation wave that propagates through the cell. In contrast, a negative feedback loop induces phosphorylation hot spots when EGFR supports PTP activity (Grecco et al., 2011b). Despite their inhibitory function, it has been proposed that several PTPs might also promote EGFR phosphorylation (Julien et al., 2011). Thus, the picture of how global phosphorylation patterns are generated by the opposing activities of EGFR and PTP needs to be complemented with the information where, when and how strong each individual PTP regulates EGFR phosphorylation. The following questions were therefore addressed in this thesis:

1. The functional role of many PTPs in RTK signaling remains uncharacterized. Therefore, we first aimed at identifying which PTPs reduce or enhance the tyrosine phosphorylation level of EGFR upon EGF stimulation, or in particular, which PTPs can be classified as **negative or positive regulators**.

2. PTPs encounter EGFR with a defined temporal hierarchy at distinct cellular regions after ligand stimulation. Our second question was: How is the **temporal phosphorylation profile** of EGFR regulated by PTPs? Can we classify different PTPs by their regulatory function?

3. What is the **relative influence** of PTPs in EGFR phosphorylation over time? Can we rank PTPs according their impact in EGFR regulation? Does the **localization** contribute to the regulatory function?

4. How is the **spatial-temporal phosphorylation profile** of EGFR regulated by PTPs? Is EGFR trafficking affected by PTPs?

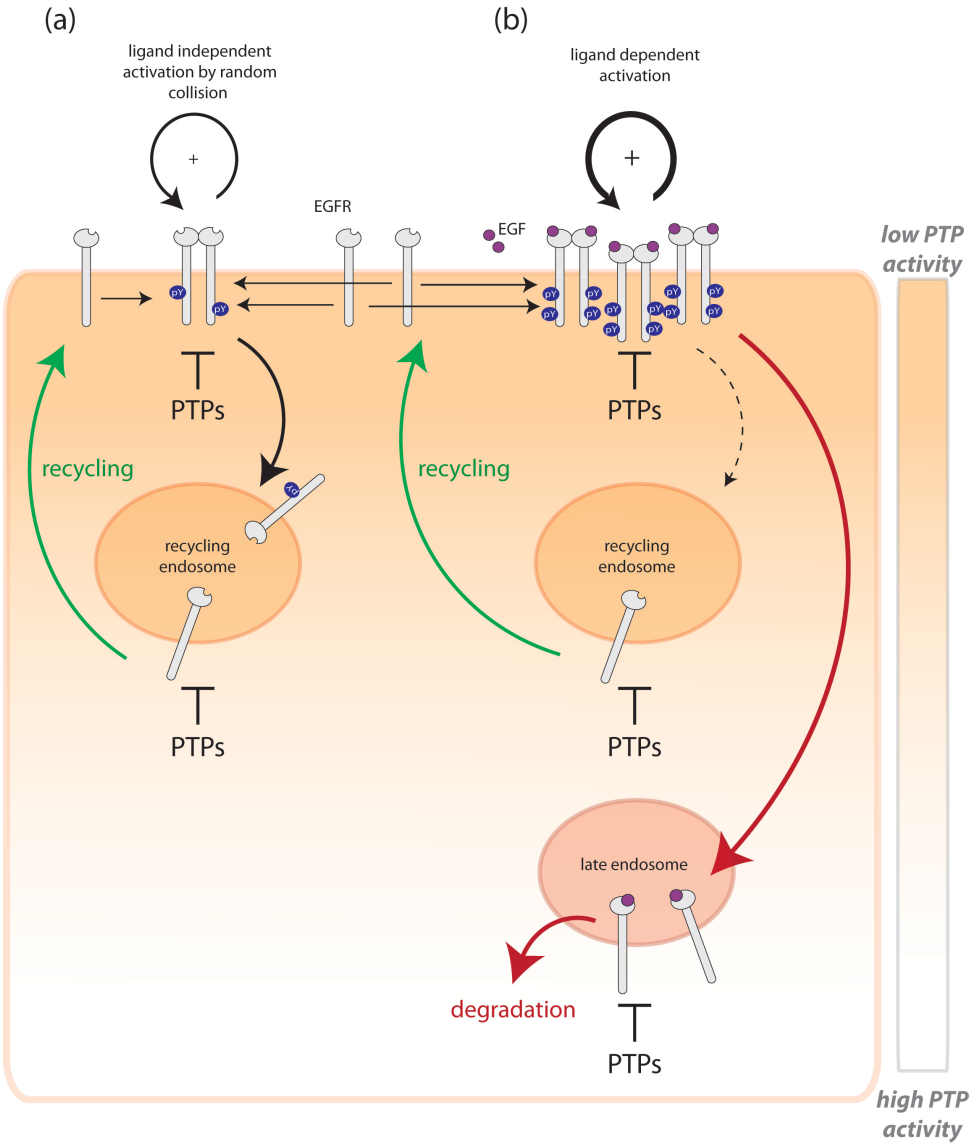

Figure 2.1 Schematic presentation of the spatial distribution of EGFR. **(a)** Due to its intrinsic autocatalytic properties, EGFR can undergo *trans*-autophosphorylation events by random collusions at the PM in absence of EGF ligands. EGFRs cycle between the PM and recycling endosomes where they interact with PTPs. Under these conditions, a constant PTP activity prevents spurious phosphorylation signals and degradation of EGFR. The activity of PTPs is up to three orders of magnitude higher than the activity of tyrosine kinases (Fischer et al., 1991) that would terminate any tyrosine phosphorylation signal. The system is able to overcome this problem by the present spatial inhibition of PTPs by growth factor induced ROS production at

the PM. EGFR recycling into areas where PTPs have a higher activity compared to the PM might favor a low basal phosphorylation level of EGFR in absence of ligand. **(b)** Upon growth factor binding, EGFR dimerization is favored leading to enhanced *trans*-phosphorylation of the receptor population that is coupled with PTP inhibition by ROS production. The EGFR provides sufficient phosphorylated tyrosines at pY1045, pY1068 and pY1086 to interact with the ubiquitin ligase Cbl, which targets the receptor for degradation. In contrast to recycling, the majority of EGFRs is internalized and undergoes degradation in lysosomes. The spatial-temporal tyrosine phosphorylation pattern of EGFR inside the cell is than dependent on the regulatory function and the distinct localization of certain PTPs.

III EXPERIMENTAL PROCEDURE

3.1 cDNA library generation by high-throughput cloning

We have cloned a library of mCitrine fusion proteins in cooperation with our in-house cloning facility, Dortmund Protein Facility (DPF). For cloning, the DPF uses a combination of "*in-vivo-cloning*" and "*SLIC" (Li and Elledge, 2007; Oliner et al., 1993)*. The method facilitates the "capture" of PCR products directly into expression vectors independent of internal or flanking restriction sites or the use of ligases (Dortmund Protein Facility, Germany). For the generation of N- and C-terminal Citrine fusion proteins, the expression vectors p2297-OPIN(n)Citrine-His_6 and p2150-OPIN(c)Citrine-His_6 (pTriEx-2) were selected from the DPF as initial destination backbones (Berrow et al., 2007). We have modified both Citrine vectors by mutagenesis PCR to create monomeric- (m)Citrine (A207K) without a His_6-Tag. The modification by classical cloning is described in **section 3.1.1.** The final p2297-OPIN(n)mCitrine and p2150-OPIN(c)mCitrine were then used as backbones to generate a library of fusion proteins with ORFs coding for PTPs **(Figure 3.1)**. ORFs provided by Genescript or isolated by reverse transcription of mRNA from human cell lines were used as PCR templates in SLIC. Positive clones were sequenced and later on pufified using a high content PureYield plasmid Midiprep System (Promega), following the instruction manual. A list of generated PTP-mCitrine plasmids and the primer information is provided in **Appendix 6.3.**

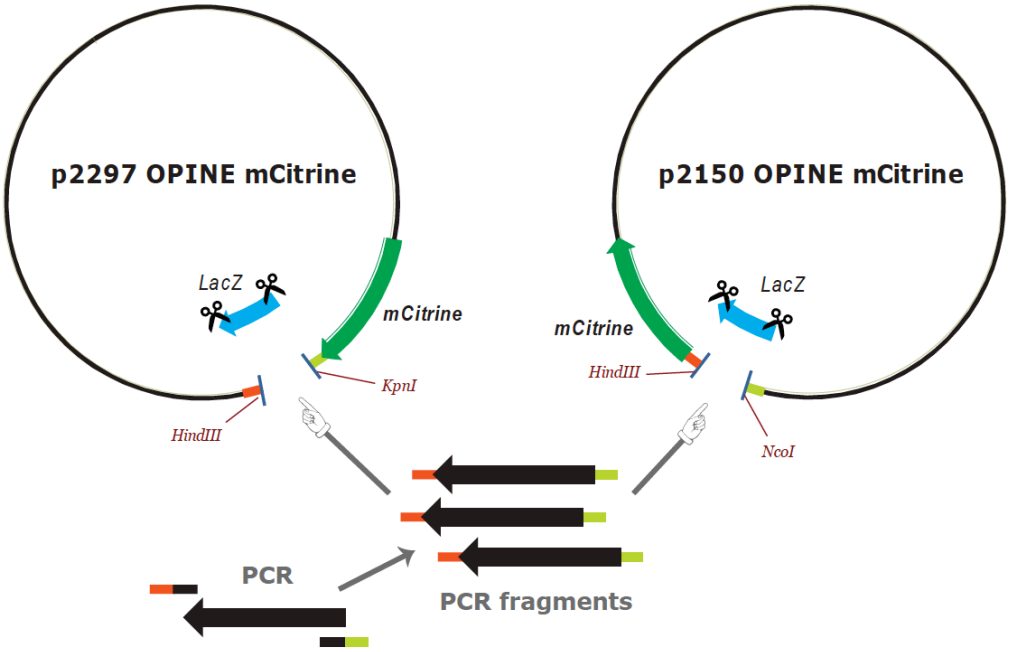

Figure 3.1 Schematic of SLIC based cloning. PCR frequents of PTP cDNA are generated with specific sequence overhangs (orange and light green) by primer design to allow homologous recombination with linear destination backbones. p2297-OPIN(n)mCitrine and p2150-OPIN(c)mCitrine backbones were used to create either N-terminal (with p2150) or C-terminal (with p2297) mCitrine fusion proteins. Plasmids were linearized by either KpnI/HindIII or NcoI/HinIII, as indicated. LacZ was used as selection marker to determine the digestion efficiency.

3.1.1 Modification of Citrine pOPIN backbones

We have modified the initial p2297-OPIN(n)Citrine-His_6 and p2150-OPIN(c) Citrine-His_6 sequence (DPF, Dortmund, Germany) as follows. The His_6 in p2297-OPIN(n)Citrine-His_6 was excluded by a primer pair flanking the His_6 segment at both sites (primer pair 1). The resulting blunt-ends of the linear plasmid were joined by ligation with the 5' phosphate group provided by the reverse primer. In case of the p2150-OPIN(c) Citrine-His_6, a stop codon was introduced in front of the His_6 by mutagenesis PCR (primer pair 2 and 3). Modified plasmids from mutagenesis PCRs or blunt-end ligation were transformed and single clones were selected for sequencing. Positive clones of p2279 were digested with NcoI/KpnI, or in case of the p2150 with HindIII/ClaI, and subcloned back into the original vector. In particular, the cleavage by ClaI is methylation sensitive and p2150 plasmids were prepared in Dam/Dcm methylase deficient SCS110

cells. After excluding the His_6 from the reading fame in p2150 and p2297, both plasmids were modified in the Citrine sequence. Two mutations (S24N and A207K) were introduced in each Citrine sequences to generate the monomeric- (m)Citrine (Griesbeck et al., 2001). The Citrine mutations were introduced by two individual mutagenesis PCRs (primer pair 4 and 5). Successful modified clones of p2279 were digested with NcoI/KpnI or in case of p2150 with HindIII/SphI and subcloned into the original vector. A schematic of both resulting p2297-OPIN(n)mCitrine and p2150-OPIN(c)mCitrine plasmids are shown in **(Figure 3.2)**. A detailed description about the protocols and used primer pairs is provided in the following subsections.

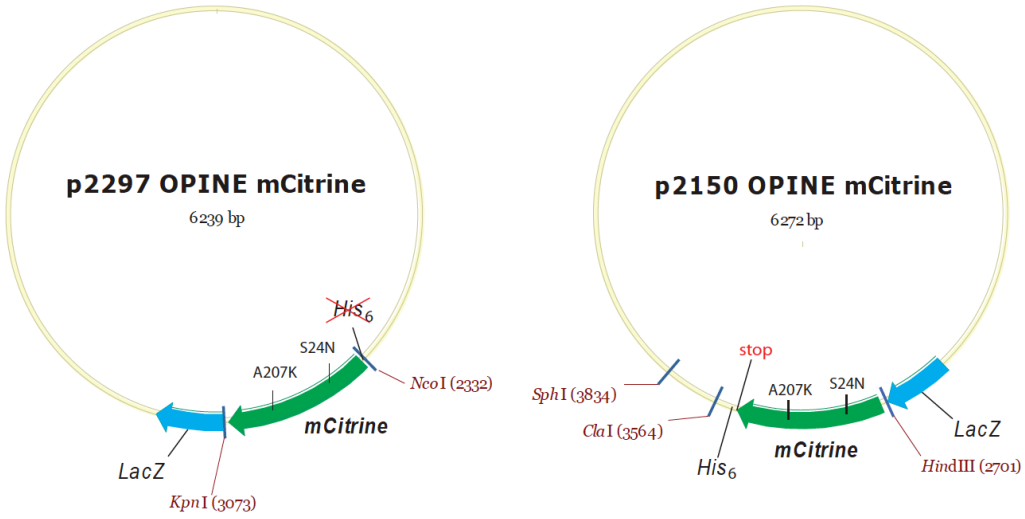

Figure 3.2 Schematic of introduced modifications in p2297-OPIN(n)Citrine and p2150-OPIN(c)Citrine. In p2297 the His_6 was excluded by blunt-end ligation. In p2150 a stop codon was introduced in front of the His_6 to exclude it from the reading frame. A207K and S24N mutations were introduced in the Citrine sequence to generate an monomeric- (m)Citrine in p2297 and p2150. Restriction sites used for sub-cloning are indicated for both plasmids.

Blunt-end PCR and ligation

PCRs were performed with the Pfu-Ultra-HF (Stratagen) polymerase. Each reaction mix contained 5 µl 10x PfuBuffer, 20 µl dNTPs (10 mM), 1 µl of each primer, 1.5 µl Pfu-Ultra-HF polymerase (2.5 U/µl), 650 ng template in a volume of 50 µl. The PCR was established on a PCR cycler (Eppendorf) by using the following protocol:

(1)	95°C	2 min	
(2)	95°C	30 sec	 16x
(3)	55°C	30 sec	
(4)	72°C	6.45 min	
(5)	go back to step (2)		
(6)	72°C	8 min	
(7)	end/hold 4 °C		

DpnI (Stratagen) was added and incubated 1 hr at 37°C to remove the template plasmid from the PCR reaction. The PCR reaction was incubated with Quick-Ligase (New England Bioscience) and transformed.

Primer pair 1: Oligonucleotides to exclude the His_6 from the p2297 by blunt-end ligation. Targeting sequence containing the His_6 indicated in blue. The primer pair flanks the His_6 region at both sites. The 5'-primer contains a phosphorylated end (PHOS-5').

Targeting sequence p2297:

5'-**cattttatttacaatcaaaggagatataccatg**gcacaccatcaccaccatcacagcagcggt**gtgagcaaggggaggagc**-3'

delHtagN-citrine–F	5'- gtgagcaagggcgaggagc-3'
delHtagN-citrine–R$^{PHOS-5'}$	5'-^{PHOS}catggtatatctcctttgattgtaaataaaatg-3'

Mutagenesis PCR

Mutagenesis PCR was performed using a mutagenesis kit (Stratagene, QuikChange XL Site-Directed Mutagenesis kit) and following the manufactures protocol. Every mutation was introduced by a separate PCR. For each reaction: 5 µl 10x reaction buffer, 10 ng plasmid DNA, 125 ng of each primer, 1 µl dNTPs (2 mM), 3 µ Quicksolution and 1 µl Turbo Pfu polymerase (2.5 U/µl) were mixed together and filled up to a total volume of 50 µl with H_2O. The PCR was established on a PCR cycler (Eppendorf) by using the following protocol:

(1)	95°C	1 min	
(2)	95°C	50 sec	 18x
(3)	60°C	50 sec	
(4)	68°C	6.45 min	
(5)	go back to step (2)		
(6)	68°C	7 min	
(7)	end/hold 4 °C		

PCR products were digested by DpnI (Stratagen) for 1 hr at 37°C to remove the template plasmid.

Primer pair 2: Oligonucleotides to insert a stop-codon in front of the His_6 in the p2150-OPIN. His_6 underlined, targeting triplet in blue and new stop codon triplet in red.

Targeting sequence p2150:	5'-**gcatggacgagctgtacaagcagtttaaacatcaccatcaccatcactaa**-3'
c43t_t45g F	5'-tggacgagctgtacaagcagtttaaatagcaccatcaccatca-3'
c43t_t45g R	5'-tgatggtgatggtgctatttaaactgcttgtacagctcgtcca-3'

Primer pair 3: Oligonucleotides to shift the stop-codon in the p2150-OPIN backbone. Present stop codons in grey, His_6 underlined, targeting triplet in blue and new stop codon triplet in red.

Targeting sequence p2150:	5'-**cgagctgtacaagcagtttaaatagcaccatcaccatcactaa**-3'
p2150_Gln/stop F	5'-cgagctgtacaagtagtttaaatagca-3'
p2150_Gln/stop R	5'-ggtgctatttaaactacttgtacagct-3'

Primer pair 4: Oligonucleotides for Citrine correction used in both pOPIN backbones at S24N. Targeting triplet at the Citrine sequence in blue. Mutated triplet at the primer sequences is indicated in red.

Targeting citrine sequence:	5'-**gctggacggcgacgtaagcggccacaa**-3'
primer S24N F	5'-gctggacggcgacgtaaacggccacaa-3'
primer S24N R	5'-ttgtggccgtttacgtcgccgtccagc-3'

Primer pair 5: Oligonucleotides for Citrine correction used in both pOPIN backbones at A207K. Targeting triplet at the Citrine sequence in blue. Mutated triplet at the primer sequences is indicated in red.

Targeting citrine sequence:	5'-**tacctgagctaccagtccgccctgagcaaagaccccaac**-3'
primer A207K-F	5'-tacctgagctaccagtccaagctgagcaaagaccccaac-3'
primer A207-R	5'-gttggggtctttgctcagcttggactggtagctcaggta-3'

Transformation

Aliquots of 45 µl XL10-Gold (Stratagen) or SCS-110 Stratagen) chemical-competent cells were thaw on ice and mixed with 2 µl β-Mercapto-ethanol (SERVA Electrophoresis GmbH). The mixture was incubated for 10 min on ice. After incubation, 2 µl DpnI digested PCR product was added and cells were incubated for 30 min on ice. Cells were heat-shocked at 42°C for 30 sec and placed back on ice for 2 min. 500 µl SOC medium was added cells were incubate for 1 hr under moving at 37°C. Cells were shortly centrifuged down and most of the medium removed. Cells were resuspended in the remaining medium and plated on an agarose/LB plate containing Ampicillin. Plates were incubated over

night at 37°C. On the next day, single colonies were selected and incubated in 5 ml LB containing 100 µg/ml Amp. Single clone cultures were incubated over night at 37 °C under moving.

Mini-plasmid purification

Plasmid purification was established by using Qiagen plasmid purification kit (QIAprep® Spin Miniprep kit) by following the manufactures protocol. Selected single clones of bacteria cells after transformation were cultured in 5ml LB or TB containing the appropriate antibiotic for selection (Kanamycin 50 µg/ml (GERBU Biotechnik GmbH) or Ampicillin 100 µg/ml (SERVA Electrophoresis GmbH)). Bacteria cultures were pelleted at 4200 rpm at 4 °C and 10 min. Each pellet was resuspend in 250 µl P1 buffer. Next, 250 µl P2 buffer was added and the culture was inverted for six times. Afterwards, 350 µl N3 buffer was added and the sample was inverted six times again. The lysate was centrifuged for 10 min at 13.000 rpm and the supernatant was transferred into a QIAprep® Spin column (Qiagen)with collection tube. The column was centrifuged (always the same speed like before) for 1 min and the flow through discarded. The column was washed with 500 µl PB buffer followed by 1 min centrifugation and than with 750 µl PE buffer followed 1 min centrifugation. The column was placed in a new tube and the plasmid DNA was eluted by adding 50 µl EB buffer and centrifugation. The plasmid concentration was measured by Nano-drop system (Peqlab Biotechnologie GmbH).

Sequencing PCR

Plasmid DNA was sequenced by terminator nucleotide PCR BigDye® Terminator v3.1 Cycle Sequencing kit (Life Technologies). Each PCR contains 300 ng plasmid DNA, 10 µM oligonucleotides, 4 µl reaction mix, big dye 2 µl big dye buffer and was filled up to a total volume of 20 µl with H_2O. The PCR was established on a PCR cycler (Eppendorf) by using the following protocol:

(1)	96 °C	1 min	
(2)	96°C	10 sec	
(3)	50 °C	5 sec	32x
(4)	60°C	4 min	
(5)	go to step (2)		
(6)	end/hold 4°C		

After the PCR, remaining terminator nucleotides were removed by DyeEX® 2.0 Spin kit (Qiagen) by following the manufactures protocol. The purified PCR was lyophilized by vacuum centrifugation and given to the in-house sequencing facility.

Primer 6: Sequencing primer aligning in the GFP/Citrine sequence.

GFP 133 F	5'-ctgaagttcatctgcaccac-3'
GFP 393 R	5'-gaagtcgatgcccttcagctc-3'
GFP 378 F	5'-gagctgaagggcatcgacttc-3'

Sub-cloning - digestion and gel extraction

After successful mutagenesis or blunt-end PCR, modified pOPIN plasmids were digested as indicated above and re-ligated with its original appropriate backbone. For each digestion the following protocol was used: 2 µl plasmid DNA**,** 1 µl enzyme A**,** 1 µl enzyme B**,** 2 µl 10x buffer and 2 µl 10x BSA as recommended from the manufactures protocol (New England Bioscience). The reaction mix was filled up to 20 µl with H_20 and incubated for 1 hr at 37°C. Digested inserts and backbones were separated from each other by gel electrophoreses and were extracted with a scalpel from gel. The digestion products were purified by Zymoclean Gel DNA recovery kit (Zymoresearch). 3 volumes of ADB buffer was added to every 100 mg extracted gel and incubated for 10 min at 50°C. After dissolving the agarose, the solution was transferred into a zymo-spin1 column with collection tube, centrifuged for 30 sec at 10.000 rpm, and the flow-trough was discarded. The column was washed two times with 200 µl wash buffer by centrifugation (always with same time and speed). Afterwards, DNA was eluted by adding 10 µl TE buffer to the column followed by centrifugation.

Ligation

Digested inserts/backbones of interest were extracted from agerose gel and purified. For ligation, an estimated ratio of 1:5, backbone to insert was combined. The reaction was performed with 1 µl Quickligase (New England Biolabs), 10 µl 2x buffer in a total volume of 20 µl. The ligation mix was incubated for 10 min at RT. The complete ligation mix was transformed into chemical competent cells and single colonies were used for plasmid purification and sequencing.

Midi plasmid purification

Selected single clones of bacteria cells after transformation were cultured in 100-300 ml LB or TB containing the appropriate antibiotic for selection (Kanamycin 50 µg/ml or Ampicillin 100 µg/ml). Bacteria cultures were pelleted at 4500 rpm at 4 °C and 20 min and used for high- or low-copy plasmid purification with the Nucleo-Bond® Xtra Midi Plus EF® kit + Nucleo-Bound® Finalizer (Machery-Nagel) by following the manufactures protocol. The concentration of purified plasmid DNA was measured with a Nanodrop (Peqlab Biotechnologie GmbH) system.

3.2 Cell culture techniques

3.2.1 Human cell lines

HeLa, MCF7 (ATCC), MCF7-EGFR-GFP (stable expressing EGFR-GFP, provided from EMBO Heidelberg, Germany) and A431D (kindly provided by Prof. Alpha Yap, Institute for Molecular Bioscience, University of Queensland, Australia) were cultured in DMEM (PAN Biotech GmbH) supplemented with 10 % heat-inactivated fetal calf serum (FCS) (Invitrogen), 2 mM L-glutamine (PAN Biotech GmbH), non-essential amino acids (PAN Biotech GmbH) and 100 U/ml penicillin and 100 μg/ml streptomycin (Gibco) and 37 °C and 5 % CO_2 growing conditions. Cells were grown in 75 cm^2 culture flasks (BD Falcon). For seeding, cells were washed with DPBS (PAN Biotech GmbH) and treated for 5 min at 37 °C with Trypsin (PAN Biotech GmbH). Cell solutions were counted using a cell counter system (Beckman Coulter, Vi-Cell-XR).

3.2.2 Liquid phase transient transfection of plasmid cDNA

For microscopy, MCF7 cells were seeded in 8 well chambers (Nalge Nunc International) (25.000/well) and incubated for 24 hours. Transfection mixtures per well containing 25 ul DMEM, 0.75 µl FuGENE® (Promega) were incubated for 5 min. Total amount of 0.25 µg plasmid was added, mixed and incubated for 20 min. For co-transfections with two plasmids, 0.125 µg per plasmid was used. During incubation fresh serum containing DMEM was supplied to the cell and the transfection mix was added. Cells were incubated for 24 hours. For western blot lysates, MCF7 or HeLa cells were seeded in 6 well plates (Nalge Nunc International) (250.000/well). In this case, transfection-mixtures for each well contained 80 µl DMEM, 4 µl FuGENE® and 1.6 µg plasmid cDNA.

3.2.3 Liquid phase transfection of siRNA

For western blot lysates, MCF7 cells were seeded in 6 well plates (Nalge Nunc International) (250.000/well) and transfected with 50 or 100 nM siRNA smart-pools® (Dharmacon) using HiPerFect (Qiagen) or DharmaFECT (Thermo Scientific) following the manufacturer instructions. Cells were incubated for 48 hours to allow protein down-modulation.

3.3 Biochemistry techniques

3.3.1 SDS-PAGE and western blot

Dependent on the experiment, cDNA or siRNA transfected cells growing in 6 well plates were starved for 6 hours (DMEM 0 % FCS) and stimulated with EGF or as indicated in every experiment. Cells were lysed by 30 min incubation in ice cold RIPA-buffer: 20 mM Tris-HCl (J.T.Baker), pH 7.5, 150 mM NaCl (Fluka Analytical), 5 mM EGTA (Sigma-Adrich), 5 mM EDTA (Fluka Analytical), 1 % IGEPAL CA-630 (Sigma-Aldrich), 1 % Sodium deoxycholate (Sigma-Alrich), 2.5 mM Na-pyrophosphate (Sigma-Aldrich), 1 mM beta-Glycerophosphate (Sigma-Aldrich), EDTA free protease inhibitor tap (Roche), 0.01 % Phosphatase inhibitor cocktail 2 and 3 (Sigma-Aldrich), 0.1% SDS (SERVA Electrophoresis GmbH) and 10 mM PMSF (in isopropanol) (Sigma-Aldrich). After centrifugation with 20.000 xg and 4°C for 30 min to remove the non-soluble fraction, protein concentrations were measured by Bradford assay (Sigma-Aldrich). Protein samples were supplemented with 2x Laemmli buffer: 4 % SDS (SERVA Electrophoresis GmbH), 10 % β-Mercapto-ethanol (SERVA Electrophoresis GmbH), 20% Glycerol (GERBU Biotechnik GmbH), 0.004% Bromophenolblue (Sigma-Aldrich), 0.125 M Tris HCl (J.T. Baker), pH 6.8) and loaded on a 7.5 % SDS-PAGE. Gel chamber was filled with running buffer: 25 mM Tris base (Carl Roth GmbH), 190 mM Glycine, 0.1% SDS, 8.3 pH). Proteins were transferred to a PVDF membrane (Millipore) by using a semi-dry blotting system (Bio Rad). Membranes were probed with primary antibodies specific for GFP (Rockland), phosphotyrosines (pY) (invivo bioscience), PTPD1 (Stratagen #B50270), PTP1B (Calbiochem, FG6-1G), LAR (R&DSystems #AF3004), SHP2 (Cell Signaling #2752), GAPDH (Cell Signaling #2118) and alpha-Tubulin (Cell Signaling #2144), as indicated in every experiment. Fluorescent IRDye 800 and IRDye 680 conjugated secondary antibodies (LICOR Biosciences, USA) were used for detection. Membranes were scanned with an Odyssey Infrared Imager (LICOR Biosciences). Images of both channels were used for quantification with ImageJ software (Wayne Rasband, National Institutes of Health, USA).

3.3.2 Antibody labeling

Mouse monoclonal anti-phosphotyrosine antibody (InVivo BioTech Services GmbH, clone P172.1) was labeled with fluorescent Cy3 or Cy3.5 dye (GE Healthcare). The antibody was concentrated to 20 µM in a total volume of 100 µl PBS. 1 M Bicine (Sigma-Aldrich) (adjusted to pH 9) was added to reach a final concentration of 0.1 M. Lyophilized Cy dye was solved in 10 µl dry-DMF (SERVA Electrophoresis GmbH) and the concentration was determined. A 10x fold molar excess of dye was added to the antibody solution. The labeling reaction was incubated for 20 min at RT. Adding Tris buffer to reach a final concentration of 10 mM terminates the labeling reaction. Unbound dye was removed by gel filtration column (Thermo scientific, # 89849 desalting spin column). After filtration, the absorption at 280 nm and 581 nm (Cy 3.5) was measured. The dye/protein ratio (D/P) and the antibody concentration (C) was determined with the following two equations:

$$D/P = (A_{581} * 170\,000) \,/\, [(A_{280} - 0.24 * A_{581}) * 150\,000] \qquad (12)$$

$$C\ (mol/l) = (A_{280} - 0.24 * A_{581}) / 170\,000 \qquad (13)$$

The molar extinction coefficient of Cy3.5 dye at 581 nm = 150 000 M^{-1} cm^{-1} and the molar extinction coefficient of proteins at 280 nm = 170 000 M^{-1} cm^{-1} was used. The calculation is corrected for the absorbance of the dye at 280 nm (approximately 24 % of the absorbance at 581 nm). This calculation is an example for calculating the (D/P) ratio for Cy3.5. For labeling Cy3 the equations were modified according the instruction manual (GE Healthcare).

For FRET-FLIM experiments, labeling ratios between 3–5 were used and labeled antibodies were stored at 4°C.

3.4. Immunofluorescence

Antibody accessibility in fixed cells was tested by immunofluorescence (IF) microscopy. MCF7 cells were transfected with EGFR-mCitrine **(subsection 3.2.2)** in 8 well chambers (Nalge Nunc International). Cells were starved (DMEM 0 % FCS) for 6 hours, stimulated for 5 min with 100 ng/ml human EGF (Sigma-Aldrich) and fixed with different 2-4 % PFA/PBS (Sigma-Aldrich) concentrations as indicated in the experiment. Cells were washed 3x with TBS and permeabilized for antibody staining with 0.1 % Triton-X/TBS (SERVA Electrophoresis GmbH) for 10 min. Cells were incubated for 20 min with 0.2 % BSA/TBS for blocking and then 1 hr with anti-EGFR antibody (anti-C-terminal, (D28B1) rabbit #4267, Cell-Signaling) in blocking solution. After washing with TBS, cells were incubated for 45 min with a fluorescent secondary antibody (chicken anti-rabbit Alexa647, Invitrogen #A21443) in TBS. Images were acquired on Olympus CellR by using a GFP filter set (Ex 460-480, U-MGFPHQ (DM485), Em 495-540) and a Cy5 filter set (Ex 620/60, U-N41024 (DM660), Em 600.5/75) set to avoid bleed through. Images were acquired by keeping a constant exposure time in both channels. The intensity in each pixel from both channels was correlated and plotted with python software (Python Software Foundation).

3.5 Cell array (CA) production

3.5.1 Functionalization of chambered cover glasses

LabTek chambered cover glasses (Nalge Nunc International) were treated with 1M NaOH (J.T. Baker) for 15 min and washed three times with H_2O afterwards.

3.5.2 Preparation of transfection mix plate

The array production was based on the work of (Erfle et al., 2007). The production of transfection mixtures were handled using an automated MICROLAB STAR Line robot system (Hamilton Robotics GmbH). For each spot mixture assembled on a 384 well plate, 3 µl Sucrose/OptiMEM (Sigma-Aldrich / GIBCO) was mixed with 3.5 µl Lipofectamine 2000 (Invitrogen). For cDNA arrays, we used 1 µg plasmid cDNA per spot mixture for single reverse transfections or 2x 0.5 µg for co-transfections with two plasmids. 1 µg plasmid cDNA was filled up with H_2O to reach a 5 µl total volume (0.20 µg/µl) and used for a spot mixture. For siRNA arrays, lyophilized siRNA (4nmol) were solved in 200 µl siRNA (1x) buffer (Thermo Scientific) to generate a 20 µM concentration. For each spot mixture, we used 2.5 µM siRNA in 5 µl volume. The 5 µl siRNA/cDNA solutions were mixed with the Sucrose/Lipofectamine on the 384 well plate and incubated for 20 min. 7.25 µl of 0.2 % Gelantin/H_2O (Sigma-Aldrich) supplemented with 0.01 % bovine fibronectin (Sigma-Aldrich) was added to each well after incubation. On cDNA spots we have used a final concentration of 0.05 % fibronectin what had increased the reverse transfection efficiency.

3.5.3 Contact spotting routine

Contact spotting was performed with a QArray2 robot (Genetix). The 384 well source plate and functionalized LabTek chambers were placed on the spotter table and immobilized by the vacuum system. The humidity and temperature was set to 60 % and 20 °C during the spotting performance, respectively. Four solid microarray steel pins with a tip diameter of 500 µm (Array-it corporation) were placed in horizontal position in the spotter head (front row, first four positions from left) **(Figure 3.3 a)**. The source order was set to columns. The slide design was set to print grids of 32 rows and 12 columns with a 1125 µm square unit cell (distance between the center of neighboring spots). This yields 384 samples per LabTek chamber. Number of stamps per ink and spot was set to 3. The inking time (time that the pins stays in the 384 well plate) and the stamp time (time that the pin is in contact with the glass of the LabTek chamber) was set to 110 ms. The print depth was set to 180 µm. The multi-stamp timing was adjusted to immediate (the stamps will be done consecutively). After every spot stamping a washing step with the following protocol was performed: Wash 3 sec. with H_2O, wash 3 sec. with EtOH, wash 1 sec. with H_2O and dry 5 sec. by air flow. A csv sheet was prepared containing all positions of wells on the source plate and name of the siRNA/cDNA samples that each of them contains. The file was imported into the QSoft Data Tracking software (Qaray2 system) to generate a galfile that was used for the automated microscopy system. The routine was set to "normal run" to print the array by using all wells of the 384 well source plate.

3.5.4 Spotting of reference points

After finishing the 384 spot routine, 6 ink spots were spotted on top of the generated array. These ink spots are used later as given coordinates of the distinct array grid to define the positions of all other spots on the array. To keep the same array grid, the vacuum system to immobilize array chambers was not interrupted when changing to the ink spotting routine. Approx. 15 µl super-stay24color® #450 fire garnet (Maybelline New York) was placed on position A1

on a new source 384 well plate. We found out that this trademark was not toxic to cells when present on array surfaces and was highly water-proof, thereby providing optimal conditions. The four 500 µm diameter pins were removed and one 300 µm diameter pin was placed on the robot head (front row, fourth position from left). The slide design was set to print grids of 32 rows and 12 columns like described previously, but only the first position of every 4x4 block was set for spotting. The routine was set to "test run" what means that the inking position on the source 384 well plate is always A1. By spotting with one pin, six distinct ink spots on array position 1A, 5A, 9A, 13A, 17A and 21A were printed. Number of stamps per ink and spot was changed to 1. The inking time and the stamp time was set to 10 ms. The washing step was inactivated and the pin was cleaned with acetone by hand after every eighth arrays. After spotting, arrays were dried for 12 hours (or stored longer) in a box containing silica Gel Orange pearls (Carl Roth GmbH). Reference spot are shown in **(Figure 3.3 a).**

3.5.5 Reverse transfection on CA

Spotted arrays were warmed for 10 min at 37 °C in the cell culture incubator before cell seeding. Cultured HeLa, A431, MCF7 or stable transfected EGFR-GFP MCF7 cells were washed with DPBS (PAN Biotech GmbH), trypsinized (PAN Biotech GmbH) and counted by using a cell counter system (Beckman). 2.50.000 cells per array for siRNA CA or 300.000 cells per array for cDNA CA were supplemented in 4 ml DMEM (PAN Biotech GmbH) complete (+P/S) and seeded. In case of HeLa cells, arrays were washed three times with DMEM after 20 min after seeding. Arrays were incubated for 24 hours for reverse transfection of cDNAs or 48 hours for reverse transfection of siRNAs. Cells were incubated at 37 °C and 5 % CO_2.

3.6 Probing and optimization of CA accuracy

3.6.1 CA design

Transfection mixtures containing mCherry (pmCherry-N1, Clontech) or mCitrine (pmCitrine-N1, A206K version of Citrine (Griesbeck et al., 2001) expression plasmids were prepared following the protocols previously described **(subsection 3.5.2)**, and arranged in a low volume 384 well source plate to generate a chequered pattern on the spotted CA. Arrays containing 4 spotted areas **(Figure 4.1 in Results)** of 4 rows and 12 columns with 1125 μm distance between centers of every two neighboring spots, and 2 empty unspotted areas were developed. Corner spots were labeled with a permanent marker for teaching their position to the microscope.

3.6.2 Automated fluorescence microscopy to determine CA accuracy

After 24 or 48 hours incubation, cells were fixed in 4 % paraformaldehyde/PBS (Sigma-Aldrich) and washed with TBS (Tris.HCl 20 mM, NaCl 150 mM, pH 7.5, J.T.Baker / Fluka Analytical). Cell nuclei were stained with 0.5 ng/ml Hoechst (Sigma-Aldrich) in PBS after permeabilization with 0.1 % Triton-X-100/TBS (SERVA Electrophoresis GmbH). All arrays were automatically imaged using a fully motorized microscope (IX81, Olympus) with custom software (Grecco et al., 2010). Briefly, the microscope moved sequentially from spot to spot, following the predefined pattern printed by the spotter robot. A teaching step in which three spots are found in the microscope was performed before imaging to correlate the coordinate system of the robot and the microscope. At each spot on the array, Hoechst nuclear-staining was used for auto-focusing, and images of Hoechst, mCitrine and mCherry channels were acquired and saved asynchronously. Filter sets for mCherry (U-MRFPHQ, Olympus), for mCitrine (U-MYFPHQ, Olympus) and for Hoechst (U-MNUA2, Olympus) were used.

3.6.3 Image processing to determine CA accuracy

Image processing and quantitative analysis was carried out using CellProfiler software (Kamentsky et al., 2011). The threshold for mCitrine was calculated by a two class Otsu-Global method. Threshold values of 24 images of mCitrine cDNA-containing spots were calculated according to this method. The average of resulting thresholds was subtracted by its standard deviation and applied to all acquired images. Images of the nuclear staining (Hoechst) were used to identify primary objects (total number of cells) by applying a two-class Otsu per Object threshold. Identified objects (nuclei) were used to identify secondary objects by propagation in the mCitrine or mCherry channel. In this way, the total number of cells, the number of mCitrine and mCherry expressing cells were obtained for each spot. These values were first grouped according to the plasmid spotted (mCitrine, mCherry or untransfected). The mean value and standard deviation were then calculated for each group using bootstrap resampling (Efron, 1981) with 1000 repetitions using a built-in function in MatLab (Mathworks, USA). Fractional values were obtained by normalizing the number of transfected cells by the total number of cells. In the second part, the center area (672 by 512 pixels) of each image (1344 by 1024 pixels) was cropped for analysis to simulate a higher magnification of 20 x. Cropped images of all three channels were analyzed like described before.

3.6.4 Live cell imaging on chequered CA

HeLa, MCF7 and A431D cells were seeded according to the standard procedure, without applying any wash and incubated for 24 hours (HeLa and MCF7) or 5 hours (A431D). Cells were then imaged in DMEM without phenol red containing 25 mM HEPES (PAN Biotech GmbH) and 10 % FCS at 37 °C and 5 % CO_2. Time-lapse microscopy of single spots was performed with a confocal laser scanning microscope (FluoView 1000 Spectral, Olympus). A transmission image in conjunction with a fluorescence image of mCitrine and mCherry were obtained every 30 minutes for 15 hours (MCF7 and HeLa cells) and 7 hours (A431D). To

image mCitrine and mCherry the sample was sequentially excited at 488 nm and 561 nm through a 488/561/633 dichroic. The emitted fluorescence was split using a dichroic mirror, spectrally filtered 515-560 (for mCitrine) or 580-610 (for mCherry) and detected with the internal PMTs set to analogue mode.

3.7 CA-FLIM screening

3.7.1 siRNA-CA design

Transfection mixtures of 92 siRNAs targeting for specify PTPs (OTP siARRAY smart-pools, Dharmacon RNA Technologies) were arranged on a 384 well plate, and spotted on LabTek chambered cover glasses following the protocols previously described **(subsection 3.5.2)**. 4 spot replicates of the same siRNA were spotted on the same array. Up to 32 array- replicates were spotted by using the same 384 well source plate. A complete list of siRNAs sequences is provided in **Appendix 6.2.** Arrays were seeded with stable transfected EGFR-GFP MCF7 cells (250.000 cells/CA) and incubated for 48 hours.

3.7.2 cDNA-CA design

Transfection mixtures of 55 cDNA plasmids were arranged on 384 well plates and spotted on LabTek chambered cover glasses following the protocols previously described **(section 3.5)**. 11 spot replicates of each cDNA were spotted on the same array. Up to 32 array replicates were spotted by using the same 384 source-plate. A complete list of the fluorescent PTPs versions is provided in **Appendix 6.3.** 300.000 MCF7 cells were seeded on each CA and incubated for 24 hours.

3.7.3 CA preparation for CA-FLIM

Cells incubated on arrays were starved for 4-6 hours (DMEM, 0 % FCS (PAN Biotech GmbH) and stimulated with 100 or 200 ng/ml EGF (Sigma-Aldrich). For stimulations for 30 or 120 min, the EGF was replaced by starving medium after the first 5 min of incubation. After stimulation for indicated time points, cells

were fixed with 4 % PFA/PBS and washed 3 x with TBS. Afterwards cells were permeabilized with 0.1 % Triton-X/PBS (SERVA Electrophoresis GmbH) for 10 min and stained with 0.5 µg/ml Hoechst/PBS (Sigma-Aldrich). Cells on CA were covered with PBS during imaging.

3.7.4 CA-FLIM system

Homodyne frequency domain FLIM was performed on a fully motorized fluorescence microscope (IX-81; Olympus). We use an argon laser (Coherent, Innova 305) as a light source, as it provides enough power (> 100 mW) in the lines (457.0 and 488.0), which are used to excite commonly used fluorescent proteins (TFP, GFP, and mCitrine). The desired excitation wavelength and power is selected with an acousto-optic tunable filter (AOTF, AA, AOTFnC-VIS-TN). The excitation was always modulated at 80 MHz. The laser is coupled into a vibrationally isolated inverted microscope (Olympus, IX81) using a multimode fiber (Schäfter & Kirchhoff GmbH, #46688-03). The spatial coherence of the laser is disrupted by vibrating the fiber using a rotating eccentric wheel attached to the fiber and by vibrating at acoustic frequencies by a loudspeaker. This results in a randomly moving speckle pattern, which averages out during detection. Homogeneous (Koehler) illumination at the sample plane is achieved by imaging the fiber core in the backfocal plane of the objective (UPLSAPO-20x and -40x, Olympus). The fluorescence was collected through a dichroic and emission filters: for mTFP (DC 457 and 482/25), for GFP (DC 485 and 495-540) and for mCitrine (DC 505 and 535/30). We used an intensified charge-coupled device (CCD; Picostar HR12; LaVision) for detection. The intensifier photocathode was modulated at the same frequency as the excitation light with a controlled phase shift. The raw data to derive fluorescence lifetime maps consisted of a background image and 12 images at different phase shift uniformly distributed over 2π acquired in pseudorandom order (van Munster and Gadella, 2004). The electric signals used to drive the AOM and the intensifier where generated using two synchronized signal generators (PXI 5404, National Instruments). We sequentially imaged the CA spots by moving the cell array placed on the

computer-controlled stage (SCAN IM 120 × 100; Märzhäuser Wetzlar). Our microscope system was equipped with a 4x, 10x, 20x and 40x objective (UPSAPO -4X, -10X, -20X, -40X, Olympus). The control of the different devices in the screening workflow was done using software written in LabView 8.5 (National Instruments).

3.7.5 System calibration

The microscopy screening workflow started by calibrating the lifetime measurement. A FLIM stack ($I_{\text{foil}}(i, j, k)$ of a scattering sample (null fluorescence lifetime) in the sample plane was acquired using a filter cube with a 20/80 beam splitter in place of the dichroic. A periodic recalibration is needed to account for the drift in environmental and alignment conditions, but replacing the sample by a reflective one is impractical in screening applications. A more convenient method is to register periodically a reference FLIM stack of a mirror located in a filter cube $I_{\text{ref}}(i, j, k)$, which can be traced to the sample plane with a single measurement of $I_{\text{foil}}(i, j, k)$. In this way a calibration phase (ϕ_{cal}) and modulation (M_{cal}) are obtained at startup of the system and the reference values ϕ_{ref} and M_{ref} are measured periodically during the screening.

3.7.6 Sample positioning

CA covered with PBS were placed on a metal stage holder and fixed with superglue. As a first step, the coordinates as given by the spotter have to be transformed to the coordinated system of the stage. For this purpose, the reference spots are imaged with a low magnification objective (4x). The process is semi-automated as such, that one of the spots has to be selected manually and the others are then located automatically. From those x,y,z – coordinates, the rotation–translation transformation from the spotter coordinate system to the stage coordinate system was then calculated by minimizing the sum of the

distances between the transformed reference points to the measured positions on the stage.

3.7.7 Subpositioning at CA spots

In our cDNA screenings we have used an additional method to guarantee the optimal co-transfected position inside every single CA spot. We performed a pre-screen with a low magnification (10x) objective to acquire mTFP (-EGFR) and mCitrine (-PTPx) fluorescence at each spot. Every spot was autofocused in the Hoechst channel before imaging. From these images we try to estimate which region of interest (ROI) would be best to measure with a higher magnification objective by calculating a score for each possible image shift. The score biases for higher number of bright pixels in the centre of the ROI. The optimal position on the image was saved and translated back as position on the microscope stage. By correcting every spot in this way a new individual positioning for all 384 spot-positions of the array was generated. These corrected positions were then used for the following FLIM-screen with a 40x objective.

3.7.8 Automated acquiring at every CA spot

After CA positioning, every spot was acquired by moving the stage in meandered order from spot to spot. At every spot, the Hoechst staining was used to focus the sample plane. (The autofocussing takes a number of images in different z-planes and calculates the sharpness of each image by evaluating the higher frequency content. The z-coordinates of the image with the highest sharpness is selected as the sample plane. Fluorescent images of Hoechst, mTFP, GFP and mCitrine were taken before acquiring the FLIM-stack. FLIM-stacks were taken first without the antibody in order to have a robust in situ measurement of the variance of donor lifetime. After all the spots in the chamber had been acquired, the PBS on all CA was removed carefully and the FRET acceptor was added. The conjugated anti-pY-Cy3 (or Cy3.5) was added in a concentration of 30 µg/ml diluted in PBS. The

antibody was incubated for 4 hours on CA and replaced afterwards by PBS. The measurement was repeated by keeping the same fluorescent channels at each spot. An additional channel (Cy-dye) to acquire the bound acceptor was introduced in the channel list. By incubating the acceptor on the microscope stage without removing the sample holder, the same set of cells could be analyzed before and after the addition of the acceptor. A schematic overview is presented in **(Figure 3.3).** FLIM sequences were saved together with metadata such as acquisition parameters, modulation frequency and reference information. The description about how the lifetime is calculated from the acquired FLIM-stacks is provided in the FLIM analysis **subsection 3.9.1**.

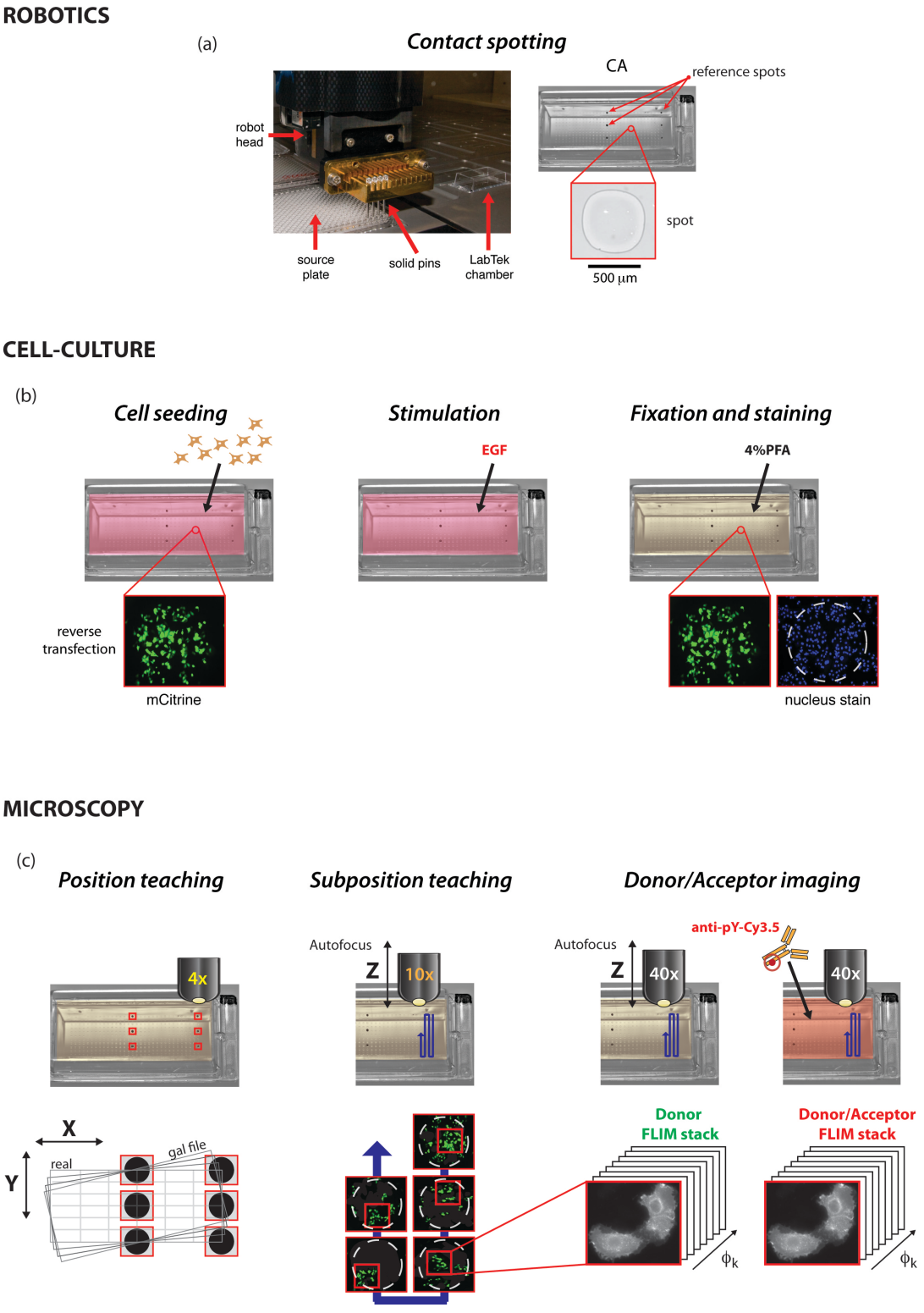

Figure 3.3 CA-FLIM visual workflow. (a) Arrays are spotted on LabTek chambered cover glasses by a QArray2 (Genetix) contact spotter robot. siRNA or cDNA spotting material was prepared in low volume 384 well plates indicated as source plate. Arrays in a pattern of 384 spots were generated by 4 solid pins with a 500 mm head diameter (ArrayIt). 6 distinct reference spots are spotted within the 384 spot pattern. (b) Cells were seeded on CA and incubated for reverse transfection. An image of reverse transfected cells on a mCitrine plasmid containing spot is depicted. Cells were starved, stimulated with EGF and fixed. Fixed cells were stained with

Hoechst and used for microscopy. (c) CA was positioned in x/y by using the 6 reference spots. Fluorescence images with a 10x objective were taken in a first imaging-round and used to calculate the optimal sub-position of each spot. The sub-position was used for the FLIM imaging-round in absences of the acceptor. The acceptor, pY72-Cy3.5 was added to the CA at the microscopy stage and incubated for 4 hours. The FLIM imaging at each spot sub-position was repeated to generate data in presence of the acceptor.

3.8 Automated FLIM in 8 well chambers

MCF7 cells seeded in 8 well chambers were transfected **(subsection 3.2.2)** according to each experiment. Cells were starved for 6 hours (DMEM 0 % FCS) and stimulated with 200 ng/ml EGF for indicated times according to the experiment. The stimulus was removed after the first 5 min and replaced by starving medium. This washing step was only performed when cells were stimulated longer than 5 min in total. To terminate the stimulation, cells were fixed with 4 % PFA/PBS (Sigma-Aldrich) for 20min. Cells were washed 3x with TBS and 10 min permeabilized with 0.1 % Triton-X/PBS (SERVA Electrophoresis GmbH). Afterwards, cells were stained for 10 min with 0.5 ng/ml Hoechst (Molecular Probes). 8 well chambers were placed on metal stage holders and fixed with superglue. Chambers were imaged on the same microscopic system described previously **(subsection 3.7.4)**. After calibrating the system, every centre position of each well was focused and saved (8 positions per chamber). A grid of 5x5 subpositions around the given center was then subsequentially acquired automatically. At every subposition, the sample plane was auto-focused in the Hoechst channel. Fluorescent images and FLIM-stacks were acquired at each subposition before and after addition of the FRET acceptor (anti-pY-Cy3.5). The FLIM analysis was performed as described in the following **(subsection 3.9.1)**.

3.9 Data analysis

3.9.1 Analysis of frequency domain FLIM data

For all acquired FLIM stacks (sample or reference), we calculated the maximum projection intensity image and segment it into foreground and background by using a manual threshold (300-4000). Saturated pixels were excluded from the stack. After masking, the mean intensity of the background image taken before every phase-stack was calculated and subtracted from every image of the phase-stack. Intensity (amplitude values) of every pixel series ($I_{1\text{-}12}$), which were not excluded by masking were used to calculate the phase and the modulation of the excitation wave. We calculated for each pixel (i, j) the mean value (DC) of the FLIM stack and the real ($\mathbb{R}\mathrm{e}R$) and imaginary part ($\mathbb{I}mR$) of the Fourier coefficients R using single value decomposition to fit:

$$I(i,j,k) = \mathrm{DC}(i,j) + \mathbb{R}\mathrm{e}R(i,j)\frac{\cos(\phi_k-\phi_{ref}-\phi_{cal})}{M_{ref}M_{cal}} + \mathbb{I}mR(i,j)\frac{\sin(\phi_k-\phi_{ref}-\phi_{cal})}{M_{ref}M_{cal}} \quad (14)$$

where k is the image series, ϕ_k the phase of the sample, ϕ_{ref} the phase of the reverence, ϕ_{cal} the phase of the calibration mirror, M_{ref} the modulation of the reference and M_{cal} the modulation of the calibration mirror

Finally we calculate the apparent frequency-dependent fluorescence lifetime images (phase and modulation liftime), analogue to **equation (8)** and **(9)** as described in **section 1.5.2**.

$$\tau_\phi(i,j) = \frac{1}{\omega}\frac{\mathbb{I}\mathrm{m}R(i,j)}{\mathbb{R}\mathrm{e}R(i,j)} \quad (15)$$

$$\tau_M(i,j) = \frac{1}{\omega}\sqrt{\frac{1}{\mathbb{R}\mathrm{e}R(i,j)^2+\mathbb{I}\mathrm{m}R(i,j)^2}-1} \quad (16)$$

3.9.2 Global analysis

We have pooled the data coming from different experiment with the same donor molecule to perform a linear fit with their single pixels **equation (17)** to find R_D and R_F, the intersection points of the line within the "monoexponential semicircle" **(Figure 1.14)** and described with **equation (10)** in **section 1.5.2**.

$$\mathbb{I}\mathrm{m}R(i,j) = u + v\mathbb{R}\mathrm{e}R(i,j) \tag{17}$$

where *u* is the offset and *v* the slope

From these intersection points (R_D and R_F) that represents the Fourier coefficients corresponding to the global lifetimes, we calculated the lifetime of the donor τ_D and donor in complex with the acceptor τ_F by using **equation (15)**. By combining these two steps we can obtain the fluorescence lifetimes (τ_D, τ_F) from the slope *v* and the offset *u* of the linear fit described in **equation (17)**.

$$\tau_D, \tau_F = \frac{1 \pm \sqrt{1-4u(u+v)}}{2\omega u} \tag{18}$$

where $\omega = 2\pi f$

By using $\mathbb{I}\mathrm{m}R(i,j)$, $\mathbb{R}\mathrm{e}R(i,j)$, τ_D and τ_F, we finally calculated the fraction of donor in complex with acceptor (α) by projecting the *R* value of each pixel onto the straight line, see **(Figure 1.14)** in **section 1.5.2**.

$$\alpha(i,j) = \frac{\omega(\tau_F+\tau_D)\mathbb{R}\mathrm{e}R(i,j)+(\omega^2\tau_F\tau_D-1)\mathbb{I}\mathrm{m}R(i,j)-\omega\tau_F}{\omega(\tau_D-\tau_F)} \tag{19}$$

3.9.3 Single cell segmentation

In cDNA CA-FLIM screenings, fluorescent images of EGFR-mTPF, PTPx-mCitrine were acquired beside the FLIM-stacks. We used Cell Profiler software (Kamentsky et al., 2011) for single cell segmentation to obtain average intensities per cell from the fluorescent channels of TFP and mCitrine. We used Otsu Global thresholding to identify PTPx-mCitrine expressing cells (primary mCitrine Objects). The primary mCitrine objects were used together wit the EGFR-mTFP image to find mCitrine/mTFP co-transfected cells (secondary objects) with an Otsu per object threshold method. The intensity value of EGFR-mTFP was used to distinguish between clumpy objects. The average intensity of mCitrne and mTFP was calculated for each cell (object). Intensity values per cell were background subtracted. In addition, we used the a-image derived from the FLIM analysis to calculate the phosphorylated fraction of EGFR per cell from the same secondary objects. Single cell values of a, mTFP and mCitrine were exported to a spread sheet (comma separated format or excel sheet) and used for single cell correlations or clustering methods.

3.9.4 Response-based classification of EGFR phosphorylation

The clustering approach that we term “response-based” clustering approach is based on the principle of ordinary patterns (Hempel et al., 2011). The method and the computational task were provided by A. Koseska. The approach is defined as follows:

1) Given a certain number δ of time points, a vector P containing all possible permutations of the ranking (of the time points) is generated, and a symbol (order pattern π_k) is assigned to each of them:

$$(\alpha_k, \alpha_{k-l1}, \ldots, \alpha_{k-l\delta-1}) \rightarrow \pi_k \qquad (21)$$

where l denotes the time lag.

2) Next, a symbol sequence $S^{(i)}$ is defined for each temporal EGFR profile $\alpha^{(i)}$, composed of the order patterns that characterize each k-th group of time points:

$$S^{(i)} = (\pi^{(i)}_{k1}, .., \pi^{(i)}_{kT}) \quad (22)$$

The length of the symbol sequence T depends on the length of the order pattern δ as

$$T = \frac{n!}{\delta!(n-\delta)!} \quad (23)$$

Thus, δ is chosen in such a way to maximize T.

3) To evaluate which EGFR temporal profiles build a "response-based" cluster, the pattern overlap between every pair of symbol sequences $S^{(i)}$ and $S^{(j)}$ is counted using the *symbol sequence similarity*:

$$SySim = \sum_{k=1}^{\delta!} \frac{\sum_{t=1}^{T}\left(S_t^{(i)}=P_k S_t^{(j)}=P_k\right)}{T} \quad (24)$$

where P denotes the vector of all possible patterns of length δ.

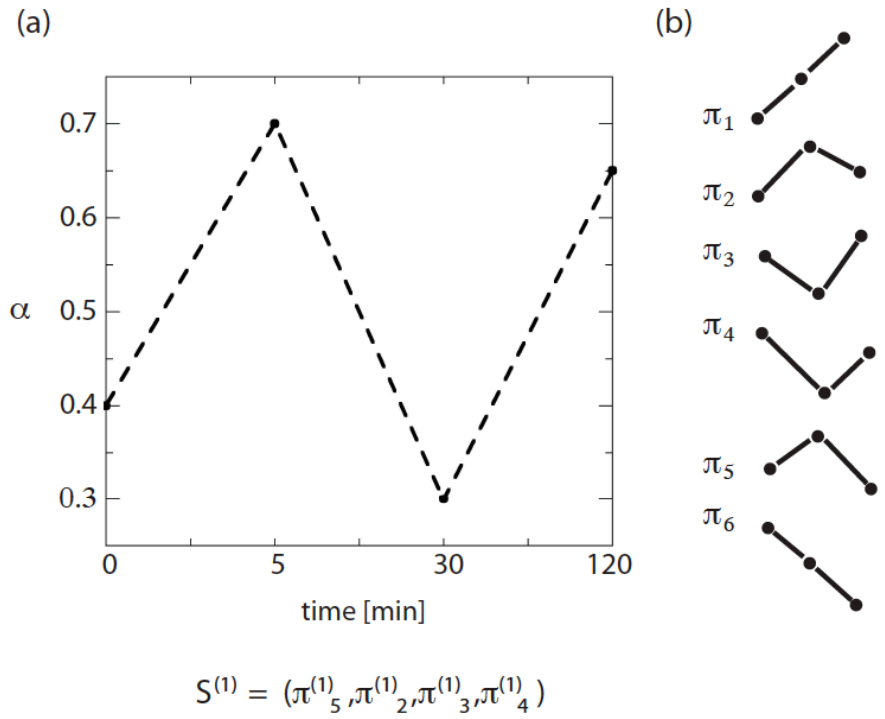

Figure 3.4 (a) An illustration of a temporal EGFR phosphorylation profile as obtained from experiments. (b) Representation of all possible order patterns π_i between three time points (δ=3). Using the defined "response-based" clustering approach, the shape of the EGFR phosphorylation profile is mapped to the symbol sequence $S^{(1)} = (\pi^{(1)}_5, \pi^{(1)}_2, \pi^{(1)}_3, \pi^{(1)}_4)$, where $\pi^{(1)}_5$ marks the relationship between time points 1, 2 and 3, $\pi^{(1)}_2 \rightarrow$ (1,2,4), $\pi^{(1)}_3 \rightarrow$ (1,3,4) and $\pi^{(1)}_4$ corresponds to the relationship between (2,3,4).

3.9.5 Affinity propagation

To distinguish how strong each phosphatase regulates EGFR phosphorylation, we use amplitude-based clustering in order to classify the phosphatases within each identified group **(Figure 4.14)**. The method and the computational task were provided by A. Koseska (unpublished). For the amplitude-based clustering, we used the affinity propagation algorithm (Frey and Dueck, 2007) which takes as an input the set of real-valued similarities calculated between all pairs of EGFR temporal profiles that are obtained after corresponding PTP perturbation. These similarities s(i,k) indicate how well a temporal profile is suited to be center of a given cluster (so-called exemplar). Considering that the goal is to

minimize the squared error, each similarity is set to a negative Euclidean distance:

$$s(i,k) = -\|x_i - x_k\|^2 \quad (25)$$

where x_i and x_k are vector representations of the temporal EGFR phosphorylation profiles upon perturbation of 2 different phosphatases i and k. An advantage of the affinity propagation algorithm is that the number of clusters do not need to be pre-specified, but on the contrary, the algorithm takes as input a real number s(k,k) for each data vector k, so that the vectors with larger values of s(k,k) are more likely to be chosen as exemplars. After a given data vector is chosen as an exemplar, the max-sum algorithm is derived, by sending messages from variables to functions and from functions to variables in a recursive fashion. This allows to estimate whether a given vector is a good exemplar for the chosen members of the cluster, and vice versa, whether a given member of a specific cluster belongs to the corresponding exemplar. The procedure is repeated a fixed number of iterations until changes in the number of exemplars and members in specific clusters fall below a threshold, or until the local changes remain constant for certain number of iterations. Thus, in each of the five previously identified classes, the phosphatases are further separated in amplitude-clusters, where each cluster is composed of phosphatases which have the same strength of regulation on EGFR phosphorylation.

3.9.6 Calculation of the hypergeometric distribution

We investigate whether the clustering of PTPs into functional classes (I-V) is related to their cellular localization. For this purpose, we calculate what is the probability that a number of PTPs with a distinct localization (i.e. nucleus, cytosol or PM) belong to the same functional class.

In probability theory and statistics, this is given by the hypergeometric distribution, which is a discrete probability distribution that describes the

probability of k successes in n draws without replacement from a finite population of size N containing exactly K successes:

$$P(X = k) = \frac{\binom{K}{k}\binom{N-K}{n-k}}{\binom{N}{n}} \quad (26)$$

In this case, N is the total number of phosphatases, K – the total number of phosphatases with a specific cellular localization (i.e. cytosol), n – number of phosphatase that belong to a specific temporal class C ($C \in [1,5]$) and k – number of phosphatases in C_i that have the same cellular localization.

3.9.7 Calculation of the Fano-factor

To identify which of the selected phosphatases act as positive/negative regulator of EGFR phosphorylation, we look in the α-variability when the selected PTP is perturbed. As an appropriate measure of the relative size of the variance we use here the Fano-factor (Becskei and Serrano, 2000; Fano, 1947), which is defined as the ratio of the variance and the mean value:

$$F = \frac{\sigma_\alpha^2}{\mu_\alpha} \quad (27)$$

3.9.8 Generation of spatial-temporal phosphorylation profiles

The method to generate spatial-temporal phosphorylation profiles from imaging data and the computational task were provided by H. Grecco (unpublished). Single cells were identified by Cell profiler software as described in **subsection 3.9.3**. We used the EGFR-mTFP fluorescence and the Hoechst staining to define a mask of the cytoplasm and the nuclear area of each cell. We excluded cells from

the analysis that were not masked properly into cytoplasm and nucleus. A cell has to fulfill the following rules:

(1) The total cellular area has to be double in size compared to the nucleus alone

$$\frac{N_{nucleus}}{N_{cell}} > 2 \tag{28}$$

N = number of pixels

(2) The pixel number of a cell has to be higher than the median - pixel number calculated from the whole cell population:

$$N_{cell} > (N_{cell})_{med} \tag{29}$$

After excluding cells by the described rules, we calculated the center of each cell by using the well-defined nuclear staining. Every pixel within the cell-mask with the coordinates (x,y) were transformed into polar coordinates (angle, ϑ and radius, r), with respect to the center of the nucleus. The contour of the plasma membrane ($r(\vartheta)_{PM}$) and the nuclear membrane ($r(\vartheta)_{NM}$) was defined for every ϑ and normalized to 1 and 0.5, respectively. Thereby, the area of the nucleus and the cytoplasm can be defined with the relative radius:

$$r_{Nuc} \in [0, 0.5]$$
$$r_{Cy} \in [0.5, 1]$$

The relative radius of the nucleus was divided into 3 and the relative radius of the cytoplasm into 10 segments. After cell segmentation, the intensity- (I) and the α- image of EGFR were used to calculate the normalized amount of phosphorylated EGFR (EGFRp) in each segment:

$$EGFRp = \frac{\sum_{i=1}^{n} \alpha_i I_i}{\sum_{i=1}^{N} I_i} * \frac{N}{n} \tag{30}$$

N = total pixels per cell, n = total pixels in the corresponding segment

IV RESULTS

In order to accomplish our aim, we combined automated FRET-FLIM acquisition with cell arrays (CA). The combination of both technologies allows multiple perturbations of different PTPs and the quantification of EGFR phosphorylation with spatial resolution in cells. CAs can contain multiple spots with genetic material including siRNA and/or plasmid cDNA to decrease or increase the level of specific PTPs by local cell transfection. CA has the advantage that the function of around 384 proteins can be addressed on a miniaturized device with a size of 10^2 cm. Furthermore, cells transfected on array spots can be homogenously treated by growth factors without separating walls between cell samples to minimize experimental error and increase the sensitivity of the approach. However, in contrast to multi-well plates, cell colonies transfected with different genetic material are only separated by few microns while they are growing in the same CA. Thus, CA is susceptible to contamination among neighboring spots, which could hinder accurate quantification in cell-based screening experiments. Thus, before combining CA with FLIM, we developed and carried out quality control experiments to quantify the plasmid cDNA transfection efficiency and to minimize contamination between CA spots. The optimization of CA is presented in the following **section 4.1.** Furthermore, to guarantee optimal conditions for down-modulation screenings, the transfection efficiency of siRNA was measured. The quantification of EGFR phosphorylation is based on the interaction of a fluorescent protein-tagged EGFR serving as FRET-donor with a generic anti-phosphotyrosine antibody conjugated to a FRET-acceptor fluorophore. In parallel to the CA optimizations, we improved the antibody binding and tested its accessibility to the EGFR epitope to guarantee robust FRET-FLIM measurements. The improvement of the antibody staining for FRET-FLIM is presented in **section 4.2**. After these two methodological sections regarding CA-FLIM optimizations, **section 4.3** will address the first question of our aims: “Which PTPs are involved in EGFR regulation after EGF stimulation?”

4.1 Optimization of CA

CA technology allows studying multiple gene products on microscope slides via reverse transfection of cells growing on spotted genetic material. Improved protocols for achieving optimal reverse transfection efficiencies and an optimal spot shape have recently been developed (Baghdoyan et al., 2004; Erfle et al., 2007; Fjeldbo et al., 2008; Mannherz et al., 2006; Yoshikawa et al., 2004). The major challenge is to obtain a low rate of contamination between the genetic perturbations in adjacent spots.

4.1.1 Cell type specific optimization and determination of CA accuracy

First we evaluated the accuracy of CA with breast cancer-derived MCF7 cells and compared it with HeLa cells, the most frequently used cell line in microscopy based CA-systems (Erfle et al., 2007; Grecco et al., 2010). For both cell types, we generated checkered arrays by printing mCitrine and mCherry expression plasmids in an alternate spot pattern. The expression of these fluorescent proteins after reverse transfection allowed us to monitor the transfection efficiency and the fraction of contaminating cells in each spot. In addition, part of the array was left unspotted to investigate the presence of transfected cells in those areas **(Figure 4.1a)**. We initially seeded HeLa cells under standard conditions **(Methods 3.5.5)**. After cell seeding, we incubated cells for 24 and 48 hours, as is commonly used for ectopic protein expression after plasmid transfection and protein down-modulation after siRNA transfection, respectively. After 24 hours of incubation, mCitrine- and mCherry-expressing HeLa cells were distributed over the complete culture chamber, including empty areas where no spots were printed. After 48 hours, spots were poorly defined leading to undefined array grids **(Figure 4.1b)**. This data showed that the accuracy of HeLa cell arrays in the standard seeding conditions was very low.

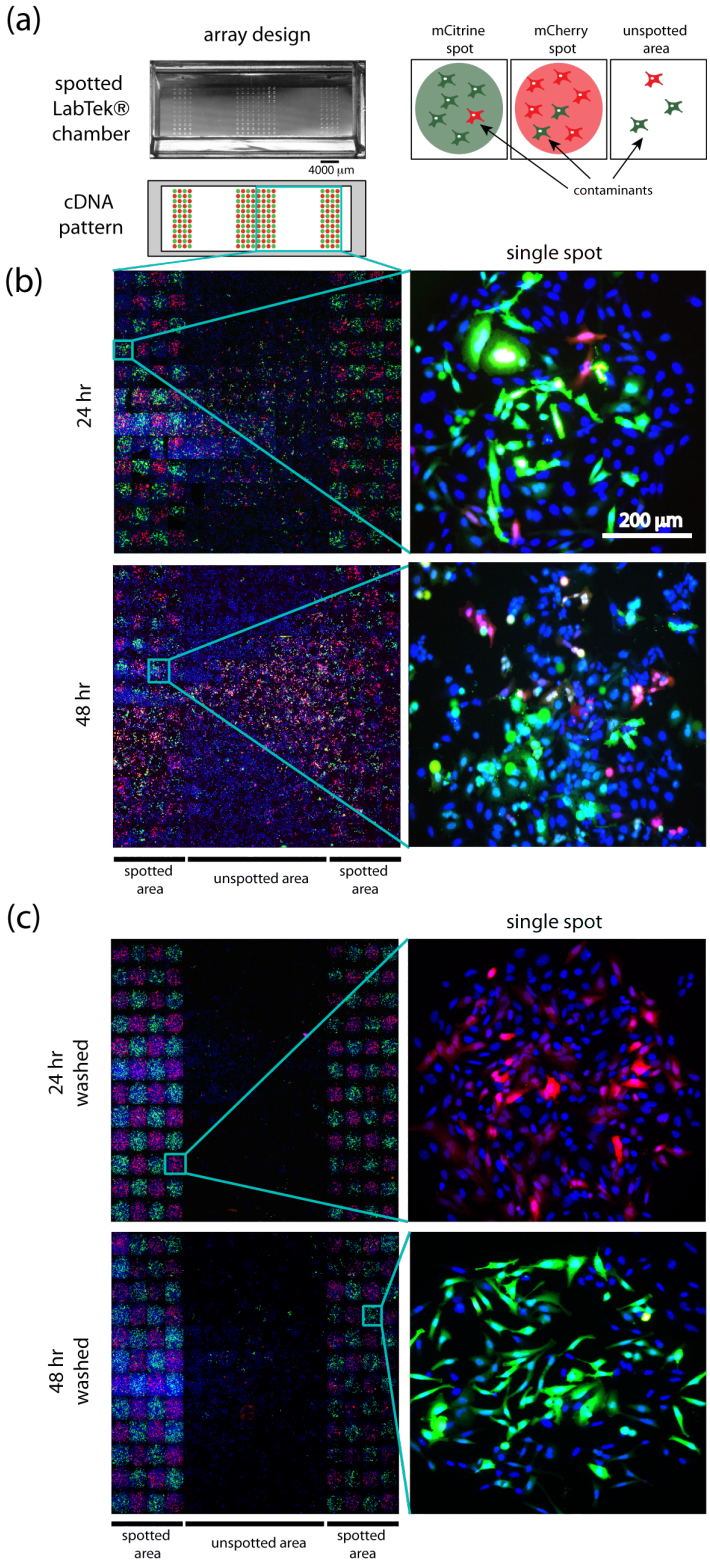

Figure 4.1 Reduction of inter-spot contamination in HeLa cell arrays. (a) Picture of a spotted LabTek chamber. Schematic of locations of plasmids encoding for mCitrine and mCherry (green and red spots), and unspotted (empty) areas are shown in the lower panel. Contaminants expressing the opposite fluorescent protein in mCitrine/mCherry spots or in unspotted areas are shown in the right schematic. (b) and (c) Montage of fields (spots or empty areas) of half arrays containing mCitrine/mCherry-expressing HeLa cells. 20 min after cell seeding a wash step was included in (c) but not in (b). Reverse transfection time is indicated. Right panels show magnifications of representative spots. Figure adapted from (Fengler et al., 2012).

It was previously shown that the presence of fibronectin in the printing solution increases cell adherence (Erfle et al., 2004). We found that HeLa cells adhered faster on fibronectin containing spots, with attachment occurring 10-20 minutes after seeding, than on a glass surface, on which it takes at least 40 minutes. This result prompted us to apply a washing step 20 minutes after cell seeding. In this way, most non-adhered cells on the glass surface were washed away, while cells adhered on spots remained attached **(Supplementary Figure 4.S1)**. To assess the effect of the washing step on cell array accuracy, we included a washing step after cell seeding. This modification of the protocol resulted in an improved expression pattern. Cells on arrays were mainly located on spots while empty unspotted areas were mostly free of cells after 24 and 48 hours of reverse transfection **(Figure 4.1c)**. The distribution of cells after 48 hours in washed arrays indicated that cells do not migrate outside the spot during the reverse transfection time after cell attachment. Thus, the data suggested that non-specific transfection of HeLa cells during the seeding process caused spot contamination. In order to quantify spot contamination, we segmented acquired images into single cells and measured the transfection efficiency and the percentage of contaminating cells in spots and empty areas **(Figure 4.2a, b)**. After 24 hours of incubation, 3% of HeLa cells were found to be contaminating spotted areas. Similar values of contaminating cells were observed in images acquired from empty areas. After 48 hours the percentage of contaminating cells in spots and empty areas increased to 7% and 9%, respectively. In contrast, a clear-cut reduction in the percentage of contaminating cells was found after washing steps were introduced, reducing the percentage of contaminating cells to 3% after 48 hours of incubation. Thus, washing steps notably increased the accuracy of cell arrays, which showed the desired fluorescent protein patterns as dictated by spot organization. On the other hand, MCF7 cell arrays prepared using the standard protocol showed a percentage of contaminating cells in spots and empty areas under 2% for both incubation times. In comparison with HeLa cells, this cell line was found to produce accurate cell arrays without the need of a washing step. This demonstrated that characterization and optimization of protocols for generating accurate CA with low contamination rates must be done independently for each cell line. To further investigate how the contaminating

cells are distributed, we cropped the center of acquired microscopy fields, where the spot is primarily located, and measured the percentage of transfected cells. The size of the cropped field simulated the magnification of a 20x objective **(Figure 4.2c)**. These data showed a general increase in transfection efficiency, which was doubled in MCF7 arrays, consistent with the fact that mainly non-transfected cells were located at the periphery of the spot. In contrast, the percentage of contamination showed no differences with respect to the un-cropped data, demonstrating that contaminating cells were not preferentially located at the spot periphery. As expected, transfection rate in empty areas did not show any change when cropped areas were analyzed. These data indicate that cell migration between spots is not the main cause of contamination, which would render contaminant cells preferentially located at the spot periphery.

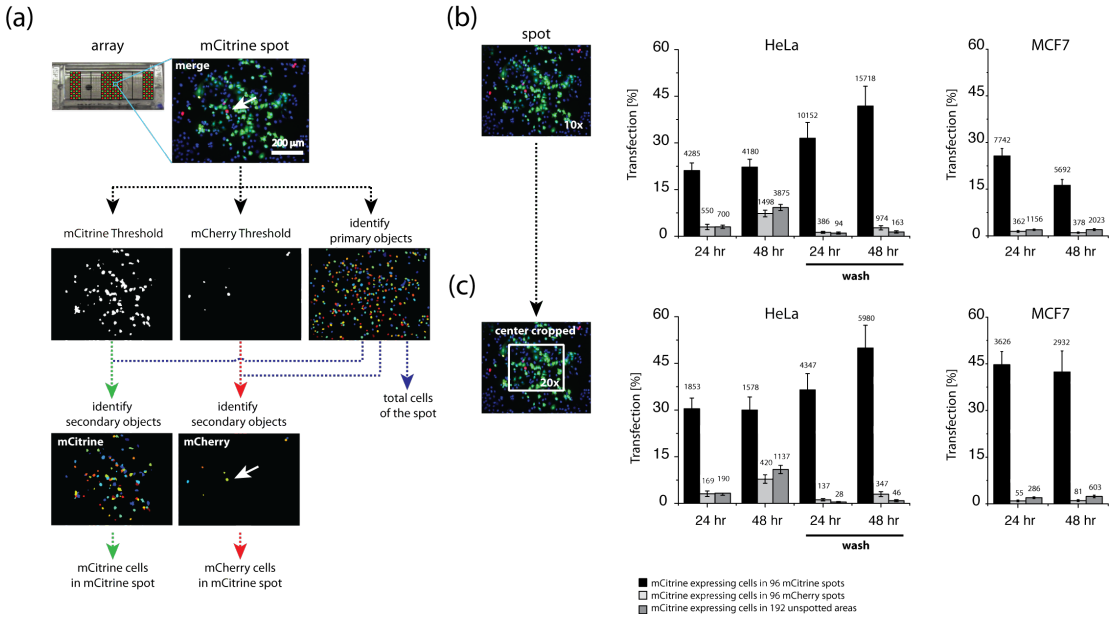

Figure 4.2 Quantitative analysis of array accuracy. (a) Schematic representation of automated image analysis. Schematic of the module built pipeline created with Cell Profiler software to calculate the numbers of mCitrine and mCherry expressing cells in mCitrine spots. Thresholds for mCitrine and mCherry channels were applied as described in methods. The total number of cells was calculated by identifying primary objects by using a nuclei staining. The threshold images of mCitrine or mCherry were used with the primary objects to identify mCitrine and mCherry expressing cells (secondary objects). The white arrow shows one of the interspot contaminating cells. (b) and (c) The percentage of mCitrine expressing cells was calculated for each mCitrine cDNA-containing spot (transfection efficiency, back bars) or for mCherry cDNA-containing spots (interspot contamination, light-gray bars). Dark-grey bars represent the % of mCitrine-expressing cells in empty areas. Results obtained with the protocol that includes the washing step are shown. An example of cropped areas used for 20x objective simulation is shown (left panels). The number of mCitrine cells and the standard deviation are indicated. Figure adapted from (Fengler et al., 2012)

4.1.2 Cell dynamics inside spots

In an attempt to further prove that cell migration among neighboring spots was not the main source of contamination in CAs, live HeLa and MCF7 cells were seeded without a washing step, incubated for 24 hours and tracked in time-lapse microscopy experiments for 15 hours. We found that neither HeLa nor MCF7 cells migrated from spots during long incubation times **(Figure 4.3a, b)**. Moreover, experiments were performed to track the appearance of fluorescence after chromophore expression and maturation. A431D cells tracked 5 hours after seeding captured the first detectable expression of mCherry in non-migrating cells located in mCitrine spots **(Figure 4.3c)**. This experiment indicated an early acquisition of the mCherry plasmid by these cells, before the final adhesion to the mCitrine spot where they were attached before fluorescence emission was detectable.

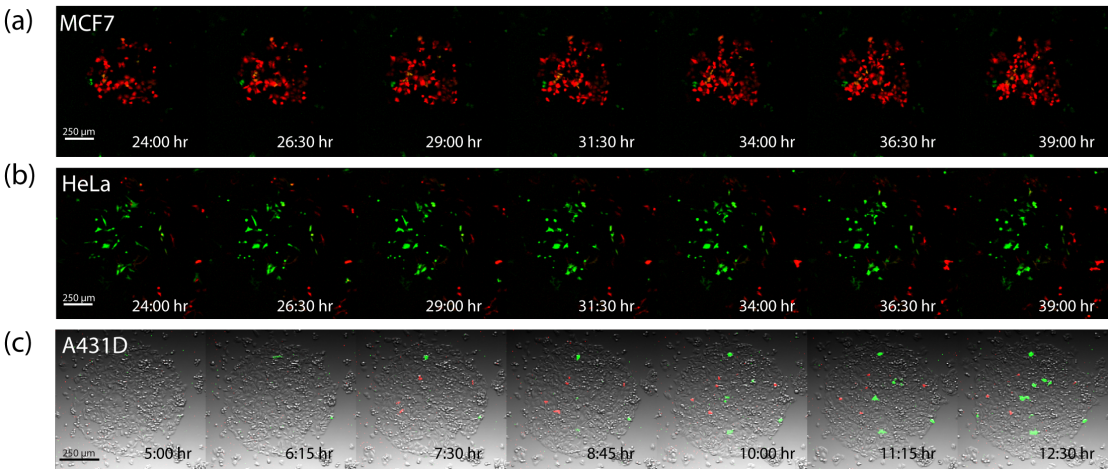

Figure 4.3 Cell dynamics in spots. MCF7 (a) or HeLa (b) cells seeded according to the standard protocol without washing step and incubated for 39 hours. After the first 24 hours of incubation cells were tracked in time lapse live cell imaging for 15 hours under growing conditions. The merged image (mCitrine in green and mCherry in red) of representative frames acquired every 2:30 hours are shown. (c) A431D cells were incubated for 5 hours after cell seeding and monitored for 7 hours. Merged images of the transmission, mCitrine (green) and mCherry (red) channel are shown. Cells were every 75 min exposed. Figure adapted from (Fengler et al., 2012).

The presented data strongly support the hypothesis that cell migration is not the dominant cause of contamination on CAs. We therefore propose that contamination generally originates early after cell seeding. It is possible for

example, that cells touch different spots during seeding and become transfected before their eventual adherence at a final array address. Consistent with this hypothesis, the source of contamination can be notably reduced by applying a washing step early after seeding. In order to avoid interspot contamination it was previously suggested that the spot-to-spot distance could be increased (Erfle et al., 2007). The drawback of this strategy is that the total capacity of the array is reduced and a lower number of samples can be studied. In our study, we show that an increased spot-to-spot distance is not sufficient to reduce the contamination in the case of HeLa cells since fluorescent cells distribute to unspotted areas **(Figure 4.1)**. Moreover, protocols that include a washing step after seeding have been proven to be able to produce high density CAs with short spot-to-spot distances, good transfection efficiencies and spot shapes (Rantala et al., 2011). By using mCitrine and mCherry in an alternate spot pattern, we now show that such protocols not only produce CAs with better spot shape but also with negligible contamination. Therefore, we proposed that the application of a washing step is a convenient way to reduce this phenomenon. In contrast to the results observed with HeLa cells, MCF7 cells showed a 7-fold lower percentage of contaminating cells in cell arrays developed without washing steps after cell seeding. This demonstrates that contamination is not a universal problem and thus, specific adhesion properties and transfection potentials of cell lines may differentially affect the quality of cell arrays developed under standard protocols.

In summary, we have shown that the existence of contaminating cells in spots is a major caveat for certain cell lines which needs to be properly controlled. But by following cell type-specific seeding protocols and quantitative analysis we can guarantee a high accuracy of CA containing either MCF7 or HeLa cells. Our presented method can be used as a general quality control to measure the suitability of cell lines to be used for CAs.

4.1.3 siRNA reverse transfection on CA

To determine the CA accuracy we have used reverse transfection of plasmid cDNAs with a robust transfection efficiency. A major advantage of CA is that it is also suitable for siRNA reverse transfections (Kumar et al., 2003; Mousses et al., 2003). Thus, we next assessed the previously described protocol for reverse transfection of siRNA in CAs. To prove the efficiency of siRNA transfection of cells growing on CA spots, we have used dye labeled non-targeting siRNA (siGLO). Stable EGFR-GFP expressing MCF7 cells were seeded on CAs containing spots with siGLO. Images of CA spots were then acquired 48 hours after cell seeding. Fluorescent siGLO particles were observed which accumulate inside cells growing on CA spots **(Figure 4.4).** We next calculated the occupied pixel area in the GFP channel and correlated it with the number of fluorescent-particles. Because of the stable transfection, the area is a direct measurement of the cell number at each spot. The number of accumulating fluorescent-particles increases linearly with the number of cells indicating a robust transfection at different spots. These results therefore demonstrate that MCF7 cells are sufficiently transfected with siRNA using our standard CA protocol.

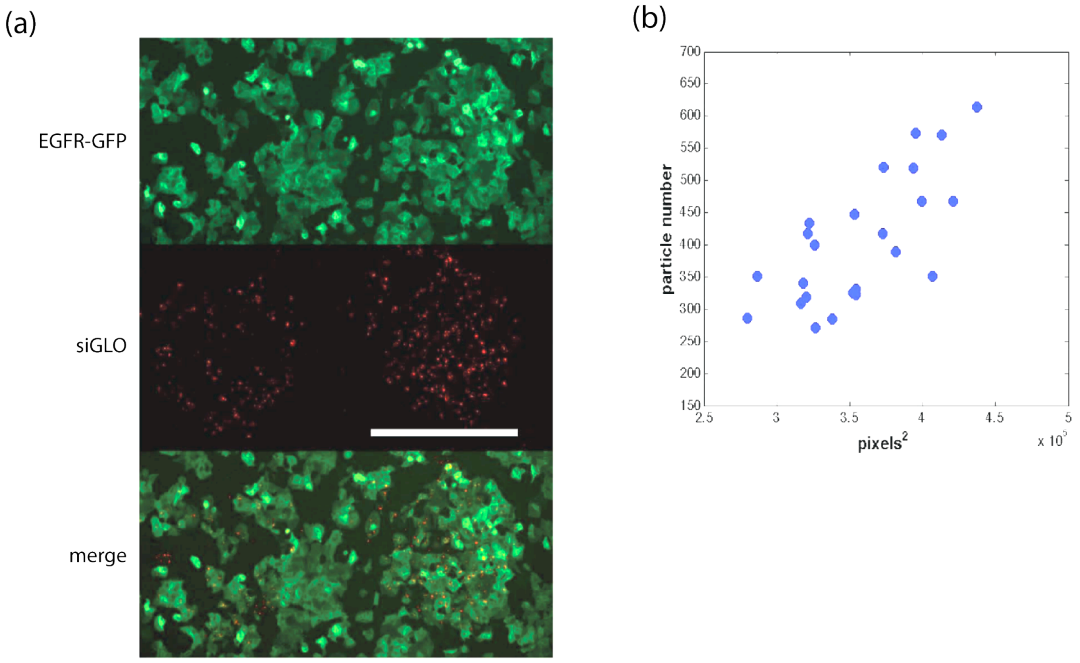

Figure 4.4 (a) Stable EGFR-GFP expressing MCF7 cells were seeded on array spots containing fluorescently labeled non-targeting siRNA (siGLO). After 48 hours of incubation images of complete spots were acquired in both channels. EGFR-GFP (green) and siGLO particles (red) are shown for two different CA spots. Scale bar indicates a spot size of 500 mm. (b) The number of siGLO-particles and the area of GFP (pixels^2) were determined for 25 spots and correlated with each other. Data presented in this figure were kindly provided by P. Roda-Navarro.

4.2 Improvement of the quantification of EGFR phosphorylation by FRET-FLIM

By coupling CA with FLIM (CA-FLIM), we aimed to quantify the phosphorylated fraction of EGFR in perturbed cells with spatial resolution. The FLIM method is based on an EGFR molecule that is C-terminally fused to a FRET-donor (e.g. mCitrine or mTFP). The fluorescence donor lifetime is measured in presence of a generic anti-phosphotyrosine (pY) antibody that is conjugated to a FRET-acceptor (Cy3.5 dye) (Verveer et al., 2000b) **(Figure 4.5a)**. After EGFR activation and *trans*-phosphorylation, for example, the antibody binds specifically to phosphotyrosines and the phosphorylation of EGFR can be quantified by a decrease in the fluorescence donor lifetime. This method provides a highly specific due to the molecular proximity necessary between the donor and its acceptor. Using global analysis **(Methods 3.9.1 and 3.9.2)** the fraction of phosphorylated EGFR (α) can be determined for each pixel (α-image) **(Figure 4.5b)**. In this thesis, we used three different donor-acceptor pairs, GFP-Cy3, mCitrine-Cy3.5 and mTFP-Cy3.5.

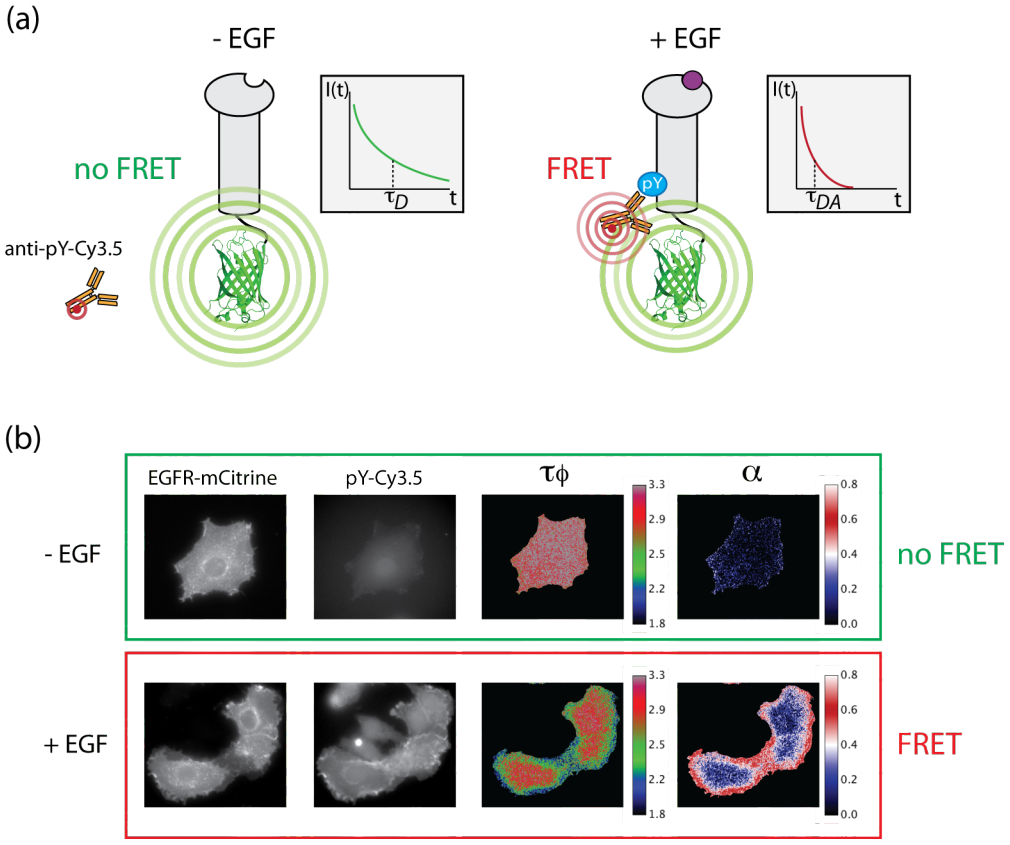

Figure 4.5 Schematic view about the quantification of EGFR tyrosine phosphorylation by FRET-FLIM. (a) EGFR is fused to a fluorescent FRET donor. Receptor phosphorylation is detected by binding of a generic anti-phosphotyrosine antibody labeled with a FRET acceptor (Cy-dye). The acceptor labeled antibody binds to tyrosine phosphorylated residues of EGFR when the receptor was activated. This interaction is detected by FRET that is measured as a drop in donor lifetime. The short range of FRET (~6 nm) guarantees a high specificity for the interaction between donor and acceptor, yielding a very low false positive rate. (b) Images of unstimulated (-EGF) and stimulated (+EGF) EGFR-mCitrine expressing cells. Cells were stained with anti-pY antibody labeled with Cy3.5. Lifetime- and α-images are shown for both cases.

4.2.1 Accessibility of the FRET acceptor in situ

To verify that the expressed fluorescent fusion proteins of EGFR are accessible for antibodies inside fixed cells we tested different immunofluorescence protocols. EGFR-mCitrine transfected MCF7 cells were fixed with a range of PFA concentrations and stained with a total anti-EGFR antibody **(Figure 4.6a)**. Cells were stimulated with EGF before fixation to examine the accessibility of internalized EGFR. Color-merge images of expressed EGFR-mCitrine and EGFR fluorescent staining showed a high overlap in all four fixation protocols. Single pixel correlations of these images show a linear correlation of EGFR-GFP and EGFR stain indicating sufficient accessibility of the antibody. According to our result, we decided to use the usual 4 % PFA/PBS fixation in all further experiments.

Quantification of the donor-based FRET measurements is highly dependent on the acceptor concentration. The optimal conditions for such a measurement is given when saturating amounts of the acceptor are present, which guarantees that the Cy3.5 labeled pY antibodies (anti-pY-Cy3.5) occupy virtually all phosphotyrosine residues at the EGFR. Therefore, we next examined the incubation time of the pY antibody labeled with Cy3.5 to reach binding saturation on the EGFR in stimulated cells. To achieve this, MCF7 cells were transfected with EGFR-mCitrine, stimulated with EGF and then fixed. Cy3.5 labeled pY antibody was then added to cells and the co-localization with EGFR was recorded over a period of 4 hours **(Figure 4.6b)**.

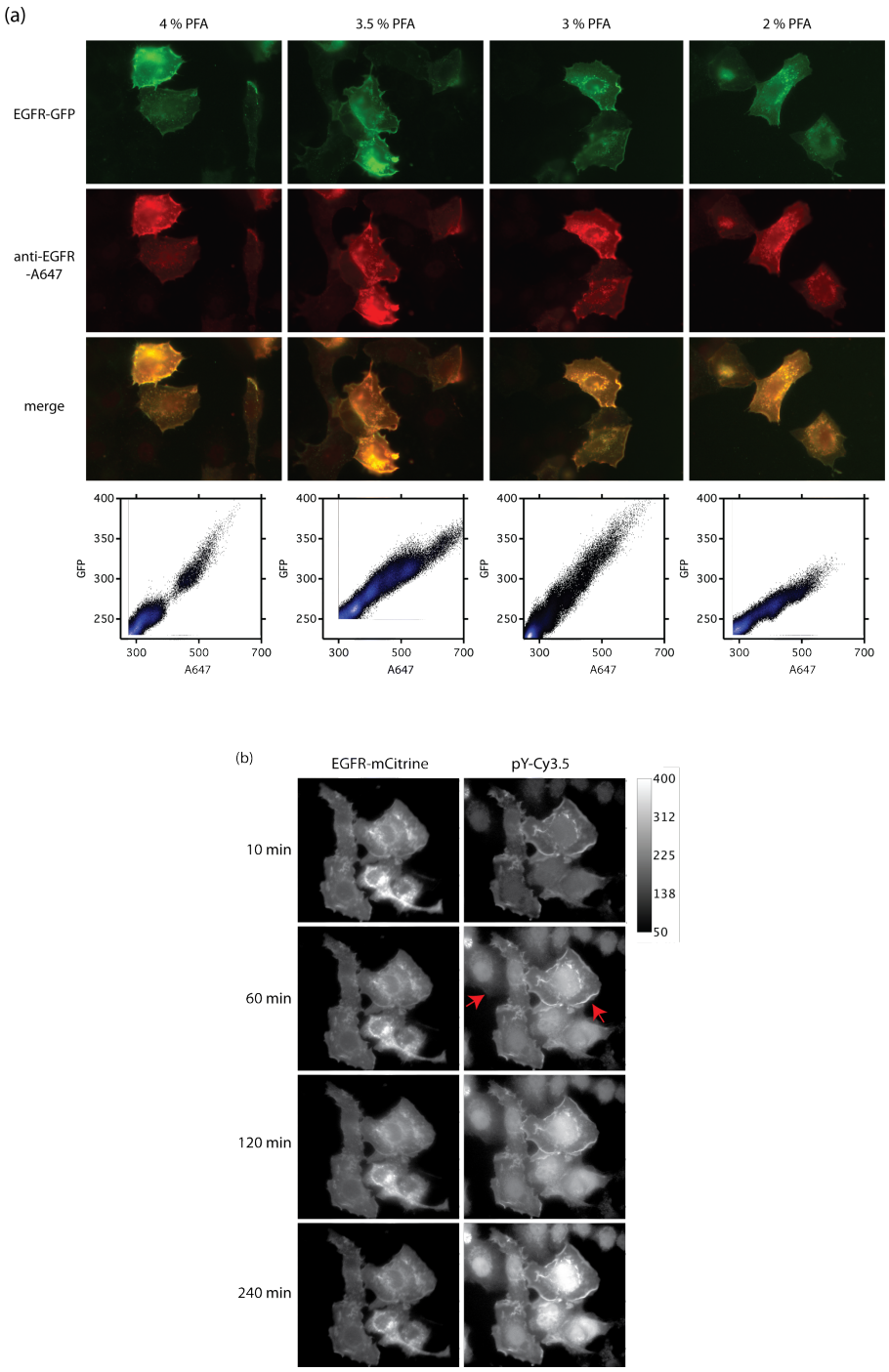

Figure 4.6 Verification of antibody accessibility and FRET acceptor saturation. (a) EGFR-mCitrine transfected MCF7 cells were stimulated for 5 min with 100 ng/ml EGF and fixed with different concentrations of PFA/PBS as indicated. After incubation with total EGFR antibody, that detects the C-terminal region of EGFR, cells were stained with a far-red Alexa647 labeled secondary antibody to avoid bleedtrough. Images and single pixel correlations are shown for all conditions. (b) EGFR-mCitrine expressing MCF7 cells were stimulated with 100 ng/ml EGF and fixed. 30 µg/ml anti-pY antibody conjugated to Cy3.5 (pY-Cy3.5) was added and antibody binding was recorded over a period of 4 hours. Red arrowheads indicate PM regions of a cell transfected with EGFR-mCitrine compared to a cell that is untransfected.

The pY-Cy3.5 antibody co-localized after 10 min incubation with EGFR-mCitrine at the PM and internal structures. After incubation times of over 2-4 hours, only the overall phosphotyrosine background staining increases in intensity while regions of EGFR localization were nearly saturated at shorter incubation times. We decided to incubate cells for 4 hours for FRET measurements to ensure almost saturating conditions. After incubation, the remaining antibody was washed from the cells to standardize the protocol and to avoid errors when different experiments are compared.

Our result indicates that using our developed protocol, the EGFR is completely accessible to immunofluorescent staining in all regions of the cell. In addition, we found that the generic anti-pY antibody showed a saturated staining at sites at the PM after 4 hours of incubation providing sufficient FRET-acceptor staining. These conditions of the antibody are required for accurate quantification of the phosphorylated fraction of EGFR by FRET-FLIM.

4.3 Identification of PTPs that regulate EGFR phosphorylation by CA-FLIM

Our optimization experiments in **section 4.1** demonstrated that our protocol has a low rate of cross-contamination and a sufficient transfection efficiency for both cDNAs and siRNAs. These initial conditions allowed us to perform reciprocal perturbations on CAs. The detection of opposing effects after ectopic PTP expression or siRNA silencing would provide strong evidence to address which PTPs regulate the phosphorylation of EGFR after EGF stimulation. For these experiments, we have produced CAs by spotting a commonly available On-Target-Plus-pool siRNA library (Dharmacon) to down-modulate the expression of 92 different PTPs in MCF7 cells. In parallel, we produced CAs with our in-house cDNA library of 51 fluorescent PTPs to ectopically express specific PTPs. A detailed description of the high-throughput cloning of our cDNA library of fluorescent PTPs can be found in **(Methods 3.1)**. Together with a PTP-specific siRNA or a PTP-coding cDNA, all cells on CA spots were additionally co-transfected with EGFR fused to a fluorescent protein serving as the FRET donor, which, in combination with the FRET acceptor conjugated anti-pY antibody, will be used to quantify its phosphorylated fraction in perturbed cells **(Figure 4.7)**. The result of the siRNA and cDNA screens to identify EGFR regulators is presented in the following **subsections 4.3.1** and **4.3.2**, respectively. In the following study, we used breast cancer derived MCF7 cells, which share genomic and transcriptional features with primary tumor cells (Neve et al., 2006).

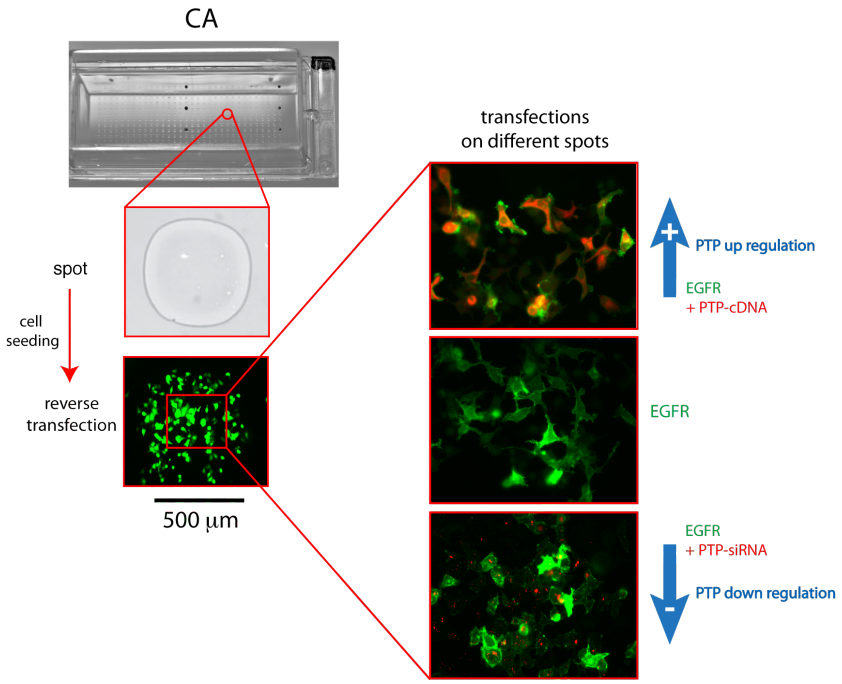

Figure 4.7 Perturbation of culture cells by reverse transfection on CA spots. CA spot mixtures for reverse transfection can contain siRNA and/or cDNA. Cell seeding generates local transfected cell groups on the CA. Spot size is 500 µm. EGFR fused to a fluorescent FRET donor is co-transfected with either expression plasmids of fluorescent PTP versions for protein up-regulation or with siRNAs targeting PTPs for protein down-regulation. Different spot transfection of EGFR with PTPN1 (on the top), EGFR alone as unperturbed control (middle) and EGFR combined with labeled siRNA (on the bottom) is shown with a higher magnification on the right.

4.3.1 Identification of EGFR regulators by down modulation screening

Before we used the whole siRNA library in CA screenings, we have tested the functionality of a small subset of siRNAs. Therefore, MCF7 cells were transfected with siRNA targeting a specific PTP or non-targeting (NT) siRNA and incubated for 48 hours. Lysates were used for western blot analysis with PTP-specific antibodies **(Supplementary Figure 4.S2)**. Sufficient protein down regulation of PTPN1 (PTP1B), PTPN11 (SHP2), PTPN21 (PTPD1) and PTPRF (LAR) were observed upon specific siRNA transfection.

After testing the functionality of single siRNAs, we produced CAs containing the entire library of 92 siRNAs to down-modulate the endogenous

expression of PTPs in MCF7 cells. The total spot number was set to 384 resulting in 4 replicates per PTP (see **Methods 3.5** for a detailed protocol of CA production). Non-targeting siRNA was included as control. The co-expression of EGFR-GFP (FRET-donor) was established by seeding stably expressing EGFR-GFP MCF7 cells directly on the spotted array. Cells were incubated for 48 hours on CAs suitable for siRNA reverse transfection. Cells were starved and stimulated for 5 min with EGF. CA spot positions were determined by using defined reference positions within the spot grid. After positioning, automated image acquisition including FLIM-stacks of EGFR-GFP at every spot, was performed before and after addition of a Cy3 conjugated anti-pY antibody serving as FRET-acceptor. The frequency-dependent apparent phase ($\tau\phi$) and modulation (τ_m) fluorescent lifetime image at every spot was calculated. Furthermore, the phosphorylated fraction (α) at every pixel was derived from the $\tau\phi$ and τ_m measured before and after acceptor addition using global analysis **(Methods 3.9.1 and 3.9.2)**. Specific siRNA transfections may induce an increase or a decrease in the phosphorylated fraction (α) of EGFR compared to non-targeting (NT) siRNA spots **(Figure 4.8)**. We calculated the change of EGFR α upon subsequent PTP perturbation with respect to the α under control (NT) conditions. All PTPs were arranged in an ascending order according to their induced changes in EGFR phosphorylation (score) **(Figure 4.8b)**. We next determined whether the induced scores of particular PTP-siRNAs were significant. In comparison to previous performed PTP screens (Sacco et al., 2012; Tarcic et al., 2009; Yuan et al., 2010), the combination of CA with FRET-FLIM allowed us to quantify EGFR phosphorylation in single cells (Grecco et al., 2010). Single cell analysis has the advantage that observed changes in EGFR phosphorylation can be tested for significance, which is not possible in studies where the variance within the analyzed cell population is not accessible. Therefore, we compared the similarity of different α-distributions derived from single cells transfected with the same siRNA against the α-distribution of cells transfected with non-targeting siRNA (NT) using a two-tailed Kolmogorov-Smirnov-test **(Supplementary Figure 4.S3)**.

From the total of 92 tested siRNAs, we identified 26 PTPs which induce a significant (p-value < 0.2) increase in EGFR phosphorylation with a score > 1.06 compared to control cells (NT), indicating a negative regulatory function of these PTPs. The identified candidates in this group were highly diverse and also contained a few phosphatases that do not possess a reported phosphotyrosine-specificity **(subsection 1.2.1)**. In this group we found 6 RPTPs, 5 NRPTPs, 3, MKPs, 6 atypical DSPs, 1 Slingshot, 1 PRL, 1 PTEN and 3 MTMRs. We identified several PTPs that were described previously to dephosphorylate EGFR after 5 min EGF stimulation **(Figure 4.8,** indicated in red**)**. For example, we identified the 3 NRPTPs, PTPN1 (PTP1B), PTPN2 (TCPTP) and PTPN6 (SHP1), in our screen. PTPN1 is located at the cytoplasmic surface of the ER and it has been shown that it dephosphorylates EGFR after internalization at endosomal compartments (Eden et al., 2010; Haj et al., 2002; Lammers et al., 1993). Studies have shown that EGFR interacts with and is dephosphorylated by PTPN2 (Tiganis et al., 1998). A 48 kDa isoform (TC48) is localized at the ER similar to PTPN1 and dephosphorylates EGFR after endocytosis, while a shorter isoform with 45 kDA (TC45) is localized in the nucleus and accumulates in the cytoplasm after EGF stimulation, where it can dephosphorylate the receptor. In addition, PTPN6 is activated by binding to the phosphorylated EGFR via its SH2 domains that in turn, induces dephosphorylation of the receptor (Keilhack et al., 1998). It has been shown that several receptor-like PTPs dephosphorylate EGFR such as PTPRF**.** Notably, we identified 5 additional RPTPs including PTPRA (RPTPα), PTPRG (RPTPγ), PTPRN (IA-2), PTPRR (PCPTP) and PTPRZ1 (RPTPζ) as potential negative regulator. Moreover, from the analyzed dual-specific phosphatases (DSPs) we found predominately atypical DSPs that where identified as possible negative regulators of EGFR phosphorylation. Excluding the previously described DUSP3, all other 5 candidates had not been associated with EGFR regulation before.

Notably, 36 of the 92 tested siRNAs have induced a significant decrease (p-value < 0.2) of EGFR phosphorylation (score < 0.95) compared to control cells, indicating a positive regulatory function of these PTPs. Similar to what was observed for negative regulators, the group of potentially positive regulators of

EGFR was highly diverse and contained 7 RPTPs, 9 NRPTPs, 6 MKPs, 6 atypical DSPs, 1 Slingshot, 1 PRL, 1 CDC14, 1 PTEN, 4 MTMRs and 1 CDC25. In **subsection 1.3.4** we discussed that several PTPs have the potential to regulate EGFR phosphorylation by dephosphorylation of inhibitory tyrosine residues of cytosolic kinases such as (pY527) of Src. It has been shown that PTPN21 (PTPD1) activates Src tyrosine kinase and increases the magnitude and duration of EGFR phosphorylation (Cardone et al., 2004). An alternative mechanism to activate Src has been proposed in which RPTPs are involved. It has been shown that tyrosine phosphorylation of C-terminal regions of RPTPs promotes the binding of these enzymes to the SH2 domain of Src, resulting in disruption of the closed confirmation formed by interaction between the SH2 domain and phosphorylated pY527 at the C-terminus of Src (Gil-Henn and Elson, 2003; Mori et al., 2010; Pallen, 2003). Such a mechanism could explain how RPTPs support indirectly, by Src activation, EGFR phosphorylation (Matozaki et al., 2010).

Interestingly, we found several phospholipid specific phosphatases including PTENs and MTMRs that either enhance or reduce phosphorylation of EGFR after siRNA knockdown, leading us speculate that several PTPs might regulate the trafficking behavior of EGFR by interacting and modifying internal membrane compartments. For example, MTM1 down modulation led to a significantly lower phosphorylation ratio indicating a positive regulatory function in EGFR phosphorylation. It has been shown that MTM1 inhibits the trafficking of EGFR from late endosomes to lysosomes (Tsujita et al., 2004). The knockdown of MTM1 might, for example, induce a rapid internalization and degradation of all ligand bound phosphorylated EGFR in the cell.

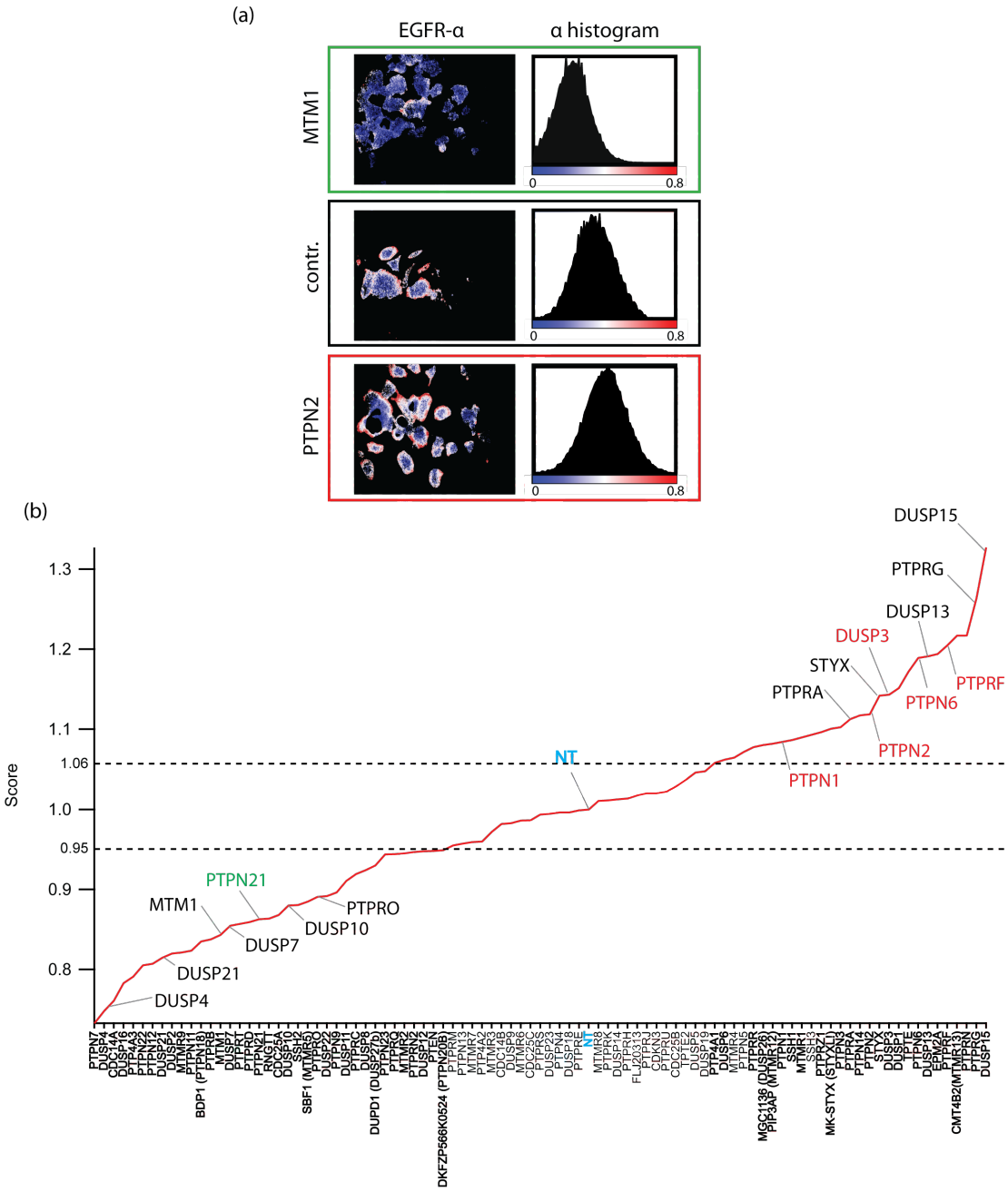

Figure 4.8 Identification of potential regulators of EGFR phosphorylation by siRNA CA-FLIM after 5 min EGF. Stable transfected EGFR-GFP MCF7 cells were seeded on CA containing 92 different siRNA spots for reverse transfection. The phosphorylated fraction of EGFR-GFP (FRET-donor) was measured by FRET-FLIM by using a Cy3 conjugated anti-pY antibody (FRET-acceptor). Cells on CAs were stimulated with 100 ng/ml EGF (a) Representative EGFR-α images from single spots containing cells reverse transfected with MTM1, non-targeting (NT) or PTPN2 (TCPTP) siRNAs. Corresponding α-histograms are shown on the right. Images were acquired with a 20x objective that guaranties a robust number of 5-20 cells per CA spot. (b) PTP targeting siRNAs ordered according their induced EGFR phosphorylation. The average <α> from 4 spot replicats was calculated for each PTP and the non-targeting siRNA (NT). The phosphorylation score of EGFR (PTP<α> 5 min/NT<α> 5 min) was calculated for each PTP siRNA and arranged in an ascending order. PTPs in bold letters at the x-axis have been identified to have a p-value < 0.2. Significant candidates induced at minimum a change of <0.95 (PTPN20B) or > 1.06 (PTP4A1) in score (as indicated by the black dotted lines). PTPs in these two areas highlighted in green or red indicate candidates, which are known as positive or negative regulators of EGFR phosphorylation. The data shown in this figure was kindly provided by P. Roda-Navarro.

4.3.2 Identification of EGFR regulators by expression screening

Next, we employed ectopic expression of PTPs to examine possible reciprocal effects to those obtained in siRNA-transfected cells. We used our in-house mCitrine-PTP library to increase the expression of specific PTPs growing on array spots and confirmed the expression and the correct localization of all chosen fluorescent PTP versions by transfection in MCF7 cells (data not shown). To avoid mislocalization of PTPs by the mCitrine fusion, we selected either the C-terminal or N-terminal fusion depending on existing localization sequences. The observed localization of each PTP was compared with the known localization provided by Universal Protein Resource (UniProt) database and LOCATE – subcellular localization database. The complete list of chosen fluorescent PTPs and their localization is provided in **(Appendix 6.3)**. To take into account the subcellular localization of expressed fluorescent PTPs, a higher resolution 40x objective was used in the following cDNA CA-FLIM experiments. We also increased the number of spot replicates per PTP from the previous 4 to 11 spots/array to guarantee a sufficient cell number to increase our statistical confidence. Therefore, we divided 51 chosen PTPs into two individual CA experiments. Screening experiments were performed with an EGFR-mTFP as FRET-donor together with a Cy3.5 labeled anti-pY antibody as FRET-acceptor. The PTP-mCitrine collection of cDNA plasmids was spotted together with EGFR-mTFP for co-transfection on CA spots. MCF7 cells were seeded on CA replicates and incubated for 24 hours for reverse transfection. Cells growing on arrays were stimulated for 5 min EGF and then fixed. To improve the number of imaged cells expressing EGFR and PTP we performed a subpositioning at every CA spot. After setting the spot grid by reference positions, a fast acquisition of the TFP and Citrine channel was performed at every spot by a 10x objective. Pixel binned scores were used to calculate the optimal position on the image overlay where both channels showed the optimal collective brightness **(Methods 3.7.7)**. The difference in x and y coordinates between the spot center and the optimal position was calculated for every spot. In this way, every spot center was shifted according to (x,y) coordinates, resulting in an optimal intensity-corrected CA spot grid. After spot subpositioning, automated FLIM-stacks of EGFR-mTFP and

fluorescence images of Citrine were acquired with a 40x objective. The phosphorylated fraction of EGFR-mTFP derived from the measured $\tau\phi$ and τ_m was calculated by global analysis. We observed a change in the fraction of phosphorylation of EGFR after 5 min EGF stimulation when specific PTPs were expressed in MCF7 cells **(Figure 4.9a).** As done for the siRNA screen, α scores of upon specific PTP expression were calculated with respect to unperturbed cells. PTPs are presented in an ascending order according to their induced change in phosphorylation **(Figure 4.9b)**. To determine which PTPs induce significant changes in EGFR phosphorylation a two-tailed Kolmogorov-Smirnov-test was performed as described for the siRNA screen **(Supplementary Figure 4.S4)**. We could identify 17 PTPs out of 51 that showed either a significant (p value < 0.2) reduction with a score < 0.95 or a significant enhancement with a score > 1.06 **(Figure 4.9b)**. For example, we identified a significant reduction of EGFR phosphorylation upon ectopic expression of PTPN1 or PTPN2 (TC45) indicating a negative effect of these enzymes. Furthermore, we observed a stronger reduction of EGFR phosphorylation when the third isoform of PTPN2 (TC41) was expressed, which is the version lacking the NLS. On the other hand, we measured a significant increase of EGFR phosphorylation when, for example, MTM1 was ectopically expressed.

We next combined the results from cDNA and siRNA experiments to identify reciprocal effects. From a total of 41 PTPs that were measured in both experiments, we found 12 PTPs with reciprocal effects **(Figure 4.10)**. Beside established negative regulators of EGFR such as PTPN1 (PTP1B), PTPN2 (TCPTP), PTPN6 (SHP1) and DUSP3 (VHR) **(Table 1.1)**, we observed a previously unrecognized negative regulatory function for PTPRA (RPTPα), PTPRG (RPTPγ), PTP4A1 (PRL-1) and STYX by comparing the results of opposing perturbations. This approach also led to the identification of 4 PTPs that potentially promote EGFR phosphorylation, including MTM1, PTPN7 (HePTP), PTPRO (GLEPP1) and DUSP7 (MKP-X).

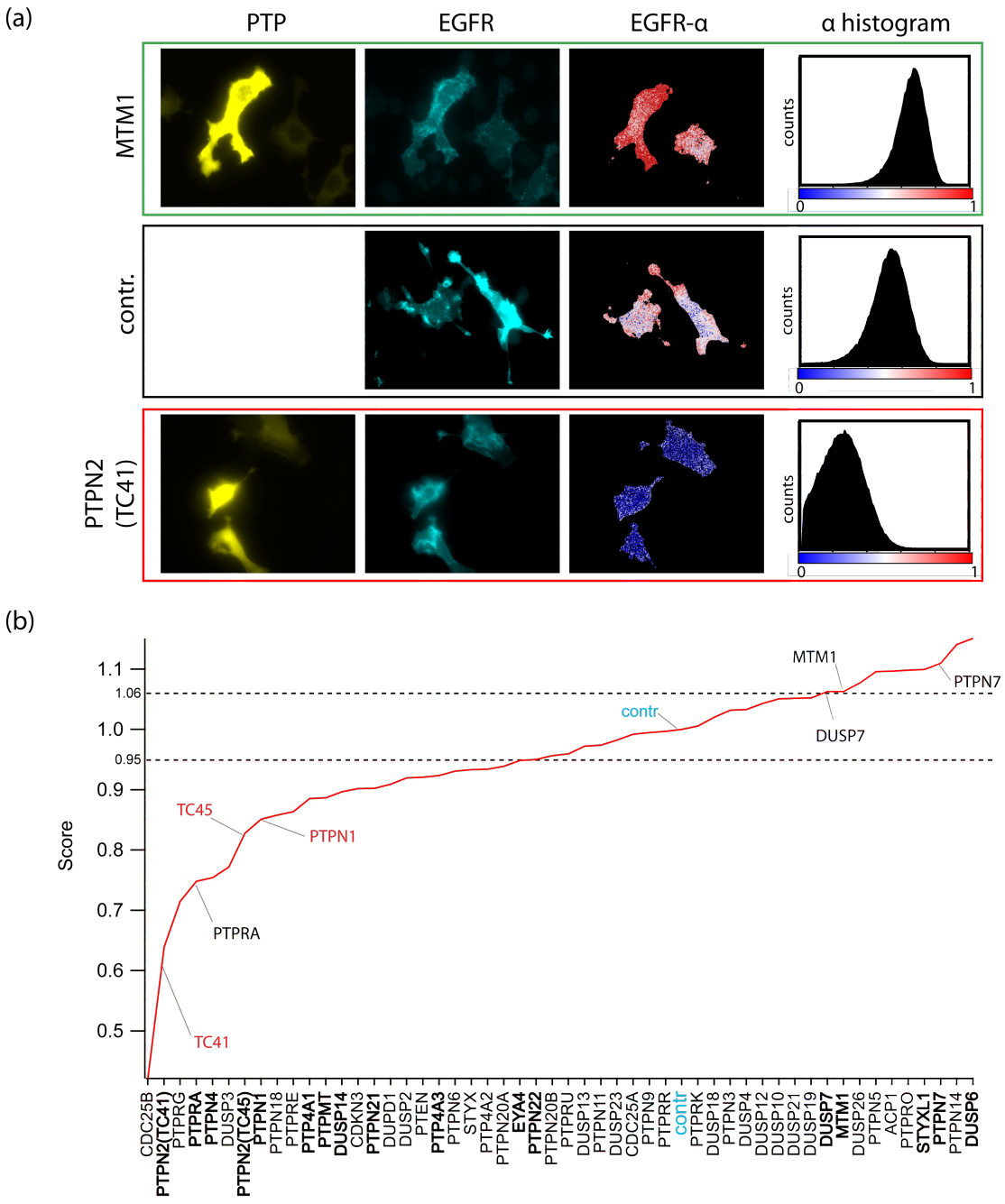

Figure 4.9 Identification of regulators of EGFR phosphorylation by cDNA CA-FLIM after 5 min of EGF. (a) Representative images from CA spots containing cells expressing MTM1-mCitrine or PTPN2–mCitrine together with EGFR-mTFP. Images of EGFR-α and the corresponding α-histograms are shown on the right. (b) The average <α> of EGFR upon the expression of a specific PTP from 11 spot replicats was calculated. The phosphorylation score of EGFR (PTP<α> 5 min/contr<α> 5 min) upon PTP expression was calculated and arranged in ascending order. PTPs in bold letters at the x-axis have been identified to have a p-value < 0.2. Significant candidates induced either a change of <0.95 (PTPN22) or >1.06 (DUSP7). Borders are indicated by the black dotted lines. PTPs highlighted in red indicate known negative regulators of EGFR phosphorylation in this area.

To statistically validate the reciprocal effect of these 14 identified PTPs, we tested which candidates induce a significant change (p value < 0.1) in both the cDNA and the siRNA experiment using the previously described two-tailed KS test. In addition to PTPN1 and PTPN2, we also statistically validated 3 previously uncharacterized regulators of EGFR phosphorylation, the negative regulator PTPRA, and two positive regulators MTM1 and DUSP7.

First evidence that PTPRA might play a role in EGFR regulation has been shown by the work from *Tran* and colleagues (2003). They observed that ligand induced autophosphorylation of EGFR is reduced in near senescent fibroblasts, which was associated with a global increase in PTP activity (Tran et al., 2003). The authors observed a higher expression level of PTPN1, PTPN6 and PTPRA in these cells suggesting a negative regulatory function for PTPRA, similar to PTPN1 and PTPN6. PTPRA activity is regulated by phosphorylation of two serine residues (S180 and S204) by PKC (Tracy et al., 1995) and it can be assumed that EGFR-mediated activation of PKC enhances the activity of PTPRA after EGF stimulation. On the other hand, PTPRA has been associated as RTK supporter because of its function as Src activator. The associated of Src with PTPRA leads to a destabilization of the internal Src-pY527 interaction that might promote kinase activity but also exposes pY527 to be dephosphorylated by activated PTPRA (Pallen, 2003). However, a PTPRA/Src mediated increase of EGFR phosphorylation has not been observed so far. PTPRA is involved in insulin signaling and dephosphorylates the activated insulin receptor (INSR), supporting instead a negative regulatory function (Lacasa et al., 2005; Lammers et al., 1997). One report has shown that PTPRA is able to dephosphorylate a small phosphopeptide *in vitro* containing the EGFR pY1068 site in an *in vitro* substrate screen (Barr et al., 2009). Consistent with our results, we suggest that PTPRA might interact and dephosphorylate EGFR immediately after EGF stimulation.

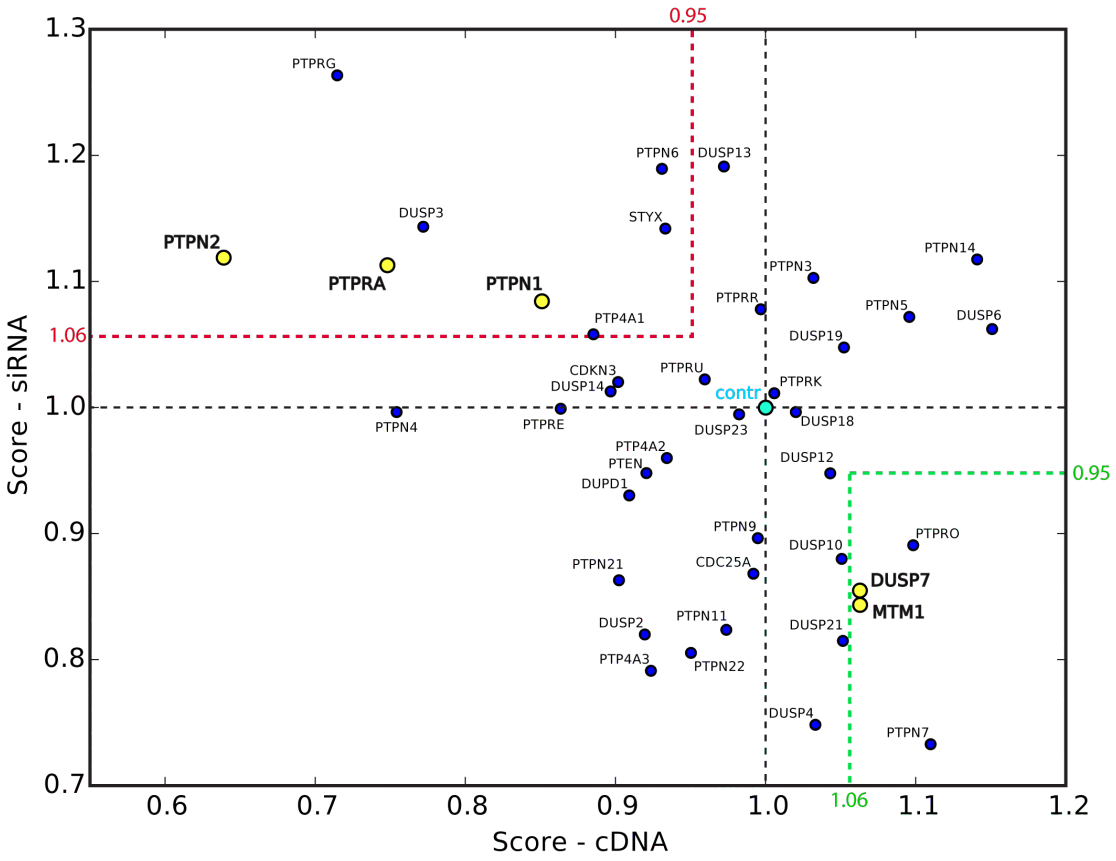

Figure 4.10 Reciprocal effects of PTPs in EGFR phosphorylation. Phosphorylation scores of EGFR (PTP<α> 5 min/contr<α> 5 min) derived from siRNA (and cDNA screens were combined. Red and green lines indicate the areas in which significant changes (p value < 0.2) in score were obtained as indicated in Figure 4.8 and 4.9. PTPs that induced a significant change (p value < 0.1) in both siRNA and cDNA screenings are highlighted with a yellow dots.

Different studies have demonstrated that MTM1 functions in intracellular membrane trafficking and vesicular transport because of its specificity towards PtdIns3P and PtdIns(3,5)P_2. (Backer, 2000; Michell et al., 2006). MTM1 is recruited to early endosomes (Cao et al., 2007) and local loss of PtdIns3P at endosomal compartments disturbs the maturation process resulting in microtubule-dependent tubularization of the endosomal network (Fili et al., 2006). It has been shown that MTM1 recruitment to late endosomes inhibits the transport of EGFR to lysosomal compartments, which increases the stability of EGFR (Tsujita et al., 2004). Consistent with this result a delayed EGF-degradation in cells with a tubularized network has been reported (Fili et al., 2006). Our result shows that MTM1 expression increases the fraction of EGFR phosphorylation after 5 min EGF stimulation, which was not described

previously. By inspecting the EGF-induced translocation of MTM1, we observed that MTM1 transiently co-localizes with EGFR at membrane structures after 5 min EGF stimulation **(Supplementary Figure 4.S5)**. We assume that the ectopic expression of MTM1, might induce an accumulation of EGF-EGFR complexes in early endosome structures by inhibiting the maturation towards lysosomal degradation. The increased receptor density in such endosomes could induce the overall higher phosphorylated fraction of EGFR. On the other hand, silencing of MTM1 resulted in a decreased level of EGFR phosphorylation. MTM1 silencing might induce an accelerated degradation of ligand bound EGFR, which could explain the early loss of phosphorylated receptor. However, first MVBs/lysosomal complexes are formed 15-20 min after internalization (Sorkin and Goh, 2008) and the early reduction of EGFR phosphorylation cannot be explained by receptor degradation alone. In contrast to MTM1 expression, rather assume that MTM1 silencing reduces the EGF-EGFR density in early endosomes by accelerating the vesicular maturation that might induce the lower phosphorylation.

DUSP7 (MKP-X, PYST2) belongs to the group of MAPK-phosphatases (MKPs) that act as negative regulators of MAPK activity (Keyse, 2008) and a positive regulatory function in EGFR signaling has not been described so far for this enzymes. MKPs share a specific N-terminal targeting motif (CH2) that is required for substrate interactions with MAPKs including Erk, Jnk and p38 (Owens and Keyse, 2007). In particular, DUSP7 showed a predominantly substrate specificity for Erk and only lower specificity for other MAPKs (Dowd et al., 1998). Interaction of DUSP7 with Erk has induced DUSP activation and dephosphorylation of Erk. DUSP7 belongs to the cytosolic MKPs and regulates Erk in the cytosol (Dowd et al., 1998). It is unclear how DUSP7 supports the phosphorylation of EGFR after ligand-induced activation but it can be assumed that this phosphatase regulates a negative feedback from Erk to EGFR (Prahallad et al., 2012). As previously described **in section 1.1**, Erk activates CDC25C that in turn dephosphorylates EGFR after EGF stimulation (Prahallad et al., 2012). We assume that DUSP7 could reduce the activity of Erk and thereby enhance EGFR phosphorylation. Notably, we observed similar tendencies for DUSP6 and

DUSP10 that are direct relatives of DUSP7 according to sequence similarities (Theodosiou and Ashworth, 2002). We observed that DUSP10 showed in both siRNA/cDNA screens a positive effect on EGFR phosphorylation, but the changes were not significant **(Figure 4.10)**. In addition, ectopic DUSP6 expression resulted in a significant enhancement of EGFR phosphorylation. But we could not observe opposing effects by DUSP6 silencing.

In summary, by applying opposing perturbations, we identified 3 novel regulators of EGFR that showed significant reciprocal effects in our study. However, several PTPs like DUSP6 did not induce symmetrical effects when ectopically expressed or silenced, which may be the result of technical reasons such as: (i) The applied siRNA transfection might not have sufficiently down modulated the targeted phosphatase; or (ii) cDNA transfections are visible by fluorophore expression, but the mCitrine fusion might hinder phosphatase function or binding domains. Asymmetrical effects could also result from biological reasons; for example, the endogeneous expression of a targeted phosphatase could be low and siRNA transfection might not induce significant changes in EGFR phosphorylation. Similarly, PTPs could have a high endogenous level and additional ectopic expression might not induce detectible changes in EGFR phosphorylation.

4.4 EGFR follows a sustained activation profile

The first siRNA and cDNA screens provided insight into the regulation of EGFR by PTPs after 5 min EGF stimulation. During the first 5 min, EGFR is activated at the PM and the first endosomal complexes are formed (Verveer et al., 2000b). However, our observations are limited to a very small time window and can provide only a snapshot of which PTPs regulate the EGFR phosphorylation. We have discussed in **section 1.2.2** that PTPs occupy distinct cellular locations and several PTPs might not encounter the EGFR at the PM or early endosomes during the first 5 min after EGF treatment. To understand how PTPs regulate the signal duration of EGFR, it is necessary to measure EGFR phosphorylation also at later time points to capture the range of influence of spatially distributed PTPs that the receptors encounter during trafficking. The complete internalization and degradation process occurs over a timescale much longer than 5 minutes (Wiley, 2003) and, as discussed in **section 1.3.6**, some PTPs might influence the trafficking of EGFR, resulting in different phosphorylation dynamics of the receptor.

Therefore, we next measured the temporal phosphorylation profile of EGFR at 0, 5, 30, and 120 min EGF upon PTP perturbation to address when specific PTPs regulate receptor phosphorylation. However, to study EGFR phosphorylation dynamics in perturbed cells, the unperturbed phosphorylation profile must first be defined. In the following two subsections we show how we have determined the phosphorylation profile of EGFR by western blot analysis and FRET-FLIM.

4.4.1 Determination of the temporal phosphorylation profile of EGFR

In order to determine the temporal EGFR phosphorylation profile, EGFR transfected MCF7 cells were stimulated over a period of 2 hours and receptor phosphorylation was determined by western blots **(Figure 4.11a)**. The stimulus was washed out after 5 min to avoid delayed activation of single cells within the cell population, which could confound the determination of the temporal response profile. Such short EGF stimulation resulted in a sustained receptor phosphorylation over the complete period of time. To determine the concentration of EGF required for maximal stimulation of the entire cell population, we stimulated EGFR transfected MCF7 cells with a range of EGF concentrations and performed western blot analysis **(Supplementary Figure 4.S6).** In order to ensure that most of the cells within the population are activated following stimulation, we determined that a dose of 200 ng/ml is required for future screening experiments. To validate the observed sustained phosphorylation profile of EGFR in MCF7 cells we performed the same experiments with HeLa cells **(Figure 4.11b)**. EGFR transfected HeLa and MCF7 cells showed both a sustained profile over the duration of 2 hours, which is consistent with previous reports (Hsu et al., 2011; Wouters and Bastiaens, 1999). In summary, ectopic expression of fluorescent EGFR fusion proteins mimics the EGF-induced sustained phosphorylation of EGFR observed in epithelial cancer cells that endogenously express high levels of the receptor (Hyatt and Ceresa, 2008; Sturani et al., 1988). In addition, our result shows that EGFR expression remains elevated for at least 2 hours after stimulation, indicating that the receptor does not undergo rapid degradation.

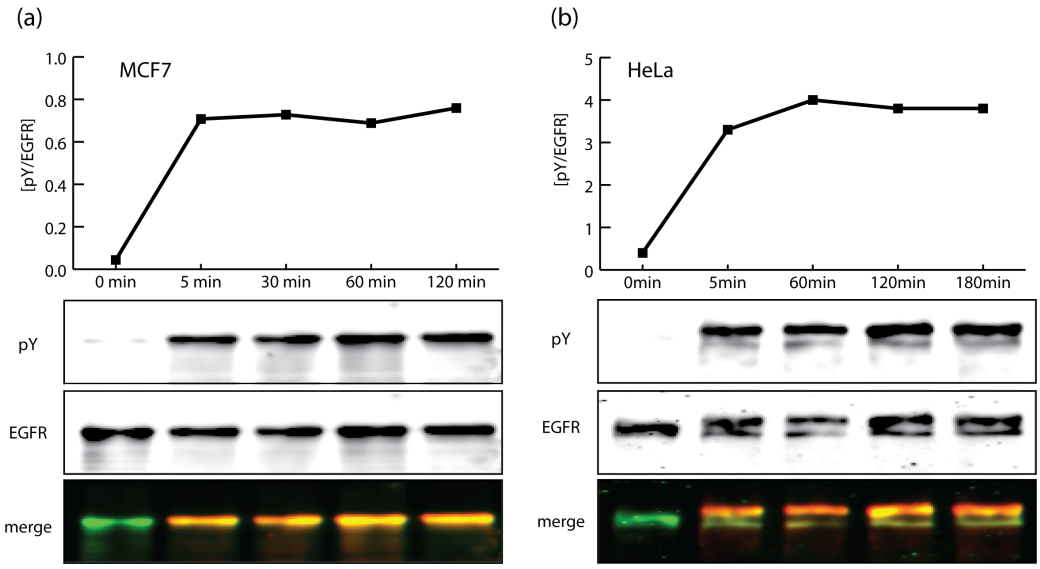

Figure 4.11 Phosphorylation profile of EGFR determined by western blot. EGFR transfected MCF7 (a) or HeLa (b) cells were transfected with EGFR and stimulated with 200 ng/ml for indicated time points. The stimulus was always removed after the first 5 min by replacing it with starving medium. Intensity based ratios show the phosphorylated fraction at each time point (on top).

4.4.2 EGFR phosphorylation dynamics measured by FLIM

Next we compared the EGFR phosphorylation profile as determined by western blot analysis with the spatial EGFR phosphorylation profile obtained by FRET-FLIM **(Figure 4.12a)**. Compared to the basal phosphorylation level under starved conditions, 2 min EGF of stimulation induces an immediate phosphorylation of EGFR at the PM. After 5 min, the phosphorylated receptor becomes internalized and propagates inside the cell. Moreover, the number of endosomes increases over time and the phosphorylated receptor is trafficked deeper into the cytosol. The average α for each time point in a population of cells showed a sustained phosphorylation profile of EGFR over 2 hours **(Figure 4.12b).** This experiment confirms our result obtained by biochemical methods shown previously in **subsection 4.4.1**.

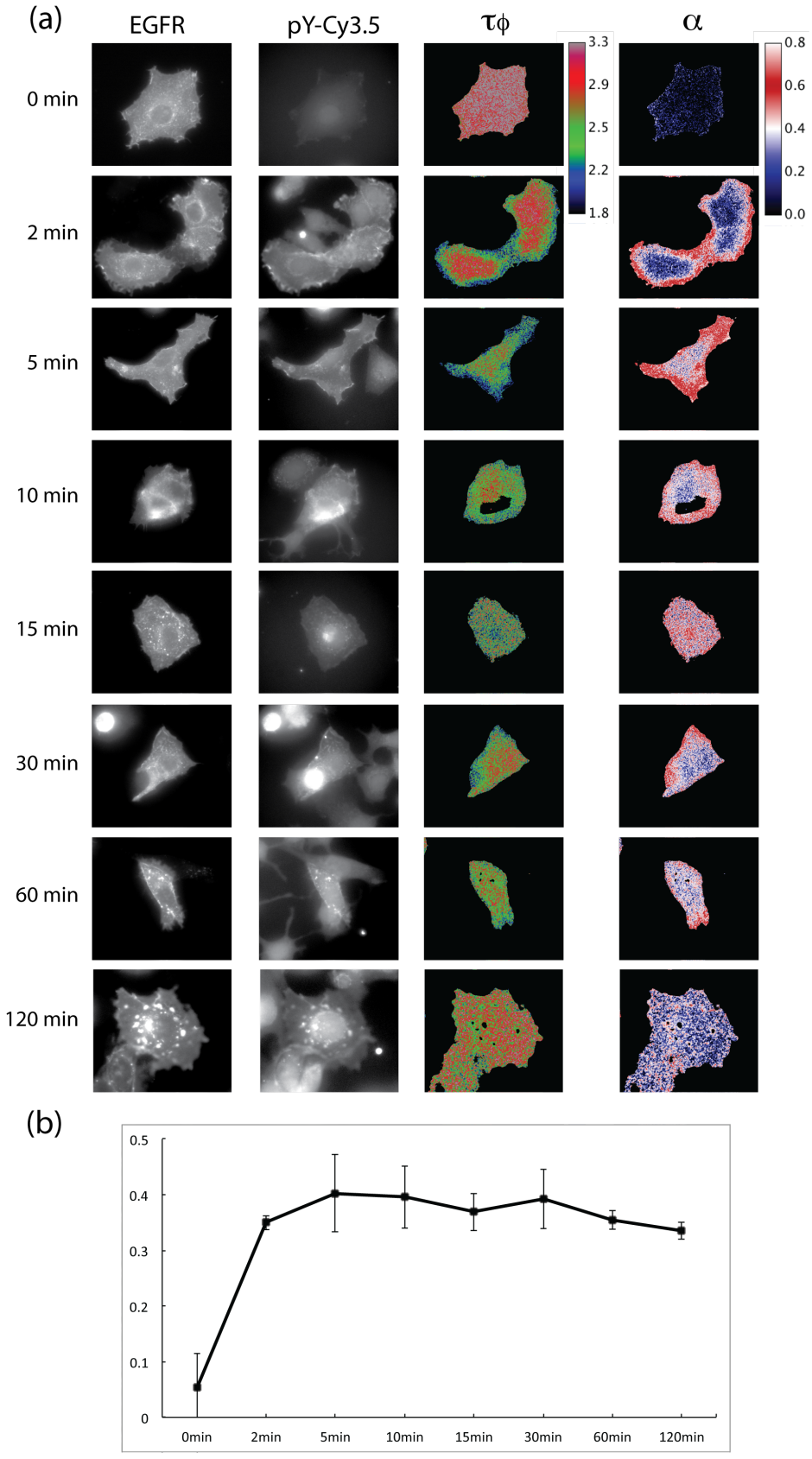

Figure 4.12 Quantification of the EGFR phosphorylation profile with FRET-FLIM. (a) EGFR-mCitrine transfected MCF7 cells were stimulated with 200 ng/ml EGF and fixed at different time points as indicated. The stimulus was washed out after 5 min incubation at all condition (except for 2 min). A representative image of EGFR-mCitrine with the FRET-acceptor staining (pY-Cy3.5),

the apparent phase lifetime ($\tau\phi$) and the corresponding α-image is shown for each time point. (b) The average $<\alpha>$ of each time point was calculated from a set of 5 images per time point. Error bars indicate the standard deviation.

4.5 PTPs can be classified according to their functional role in EGFR signaling

In the following section we want to address the question how PTPs regulate the duration of ligand-induced EGFR phosphorylation. However, a limiting factor of siRNA CA-screenings is that it is difficult to determine the extent of protein down modulation in individual cells or spots. In previous studies, immunofluorescent (IF) staining has been used to detect down modulation of proteins growing on siRNA loaded spots (Mousses et al., 2003). The problem with this technique is that such tests are limited to the quality and availability of antibodies against the target proteins. An antibody stain would only detect the down-modulation of one particular PTP on the CA that is not practical for multiple siRNAs. We have tested the overall transfection efficiency on siRNA spots by using a fluorescently labeled siRNA **(Figure 4.4)**. These control spots indicated a high reverse-transfection efficiency with MCF7 cells with our used CA protocol. While this control experiment provides no indication of the efficiency of individual siRNAs to down-modulate their target protein, but it does provide evidence that the majority of cells should be transfected by siRNA on spots.

For our overexpression screen, on the other hand, the perturbation of cells can easily be confirmed by monitoring the fluorescence of the heterologous expression of mCitrine-fused PTPs. Furthermore, cells without PTP-mCitrine expression can be excluded from the data analysis. One other advantage of cDNA screenings is that the localization of each PTP can be directly compared with the spatial distribution of EGFR. We therefore decided to perform our time resolved experiments in our expression CAs. The collection was again divided into two individual screens with 2 x 384 spots to guaranty at minimum 11 spot replicates

for each PTP. The FRET-donor, EGFR-mTFP was co-transfected together with different PTP-mCitrine fusion proteins on CA spots, as described previously. For each screen, MCF7 cells were seeded on 4 CA replicates to stimulate them individually with EGF for 0, 5, 30 and 120 min. After setting the spot grid by reference positions, a fast acquisition of the TFP and Citrine intensity was used for spot subpositioning to optimize the number of co-transfected cells. FLIM-stacks of EGFR-mTFP and fluorescence images of mCitrine were automatically acquired on every spot position in all 4 CAs mounted at the microscope stage. FLIM-stacks were acquired in absence and in presence of the FRET-acceptor (anti-pY-Cy3.5). The α-image of EGFR-mTFP was calculated for each CA position and time point using global analysis. The images were then segmented into single cells using EGFR intensity, and the average-α per cell was calculated **(Methods 3.9.3)**. Cells without mCitrine expression, which serves as an indicator of PTP perturbation were excluded from the analysis. The corresponding EGFR phosphorylation profile when a given PTP is perturbed is shown in **(Figure 4.13).** Averages of α were calculated from cells expressing a certain PTP and divided with the average-α from unperturbed cells at the corresponding time point. This procedure was done for both cDNA screens and the data were combined. The temporal profiles obtained indicate that several PTPs induced a change of EGFR phosphorylation over the entire experimental duration, including known negative regulators of EGFR such as PTPN1 (PTP1B) and the two isoforms of PTPN2 (TC41 and TC45). Furthermore, we observed a similar negative regulatory function for the full duration for PTPRA, a PTP identified already as early regulator in our first siRNA/cDNA screen. Other PTPs however, change the EGFR profile only at distinct time points. For example PTPN6 (SHP1) decreases the phosphorylation of EGFR only at 5 min. Furthermore, several PTPs also induced changes of EGFR phosphorylation prior to the addition of EGF. By expanding our observation to additional time points several PTPs previously described in the literature as negative regulators were identified to modulate EGFR phosphorylation (e.g. PTPN9 and PTPRK) **(Table 1.1)**.

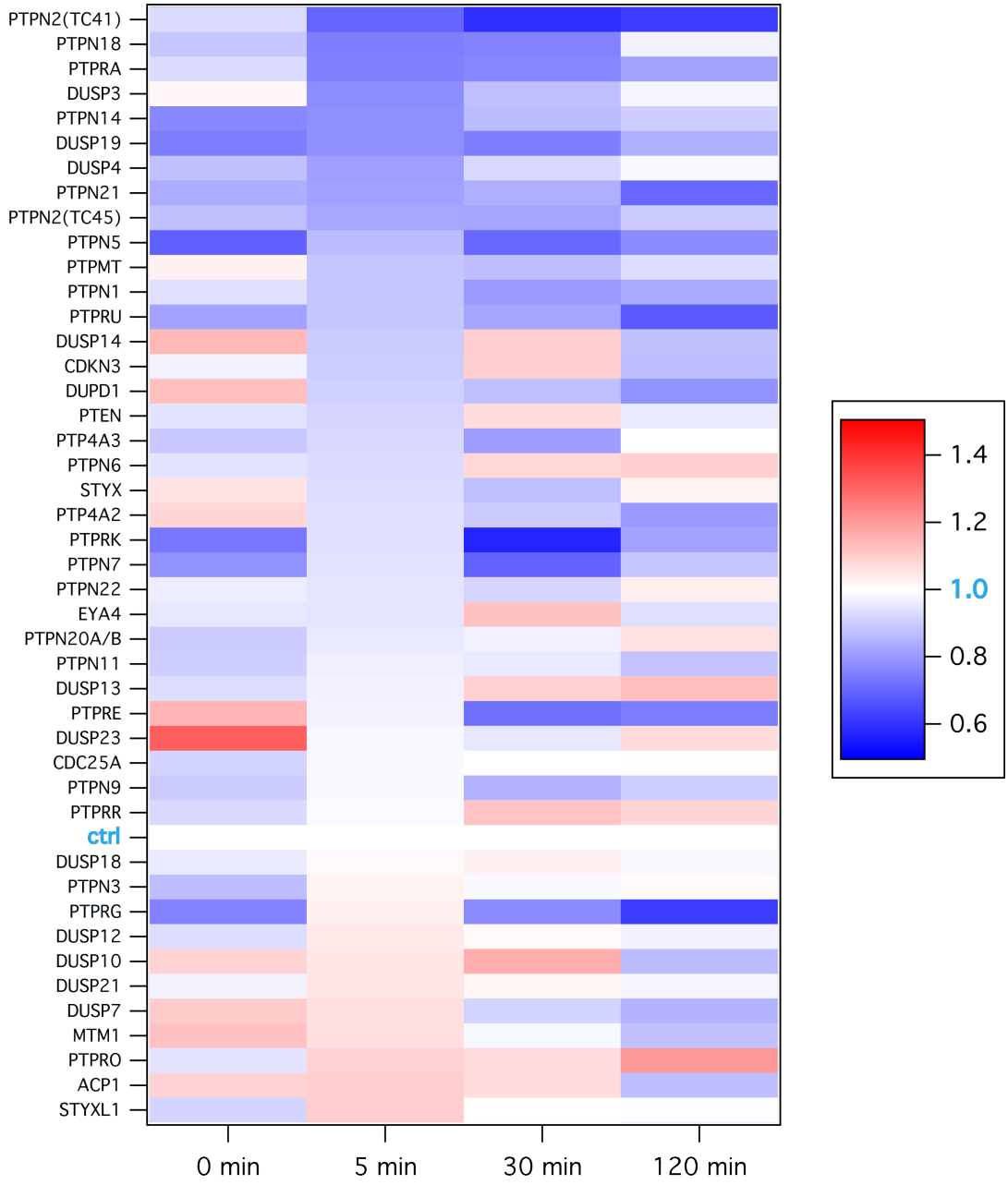

Figure 4.13 Time courses of the change in EGFR phosphorylation according different PTP expressions. The change in phosphorylation induced by a PTP at a distinct time point was normalized to the phosphorylated level under control conditions (score = PTP<cell-α>(x min) / Ctrl<cell-α>(x min)). PTPs are sorted by the change upon 5 min EGF. Scores ranged from 0.5 decreasing (blue) to 1.5 increasing (red). MCF7 cells growing on CAs were stimulated with 200 ng/ml EGF for the indicated time points. The data from both cDNA collections were combined in the presented graph (From the total of 51 cDNAs we excluded 7 candidates from the analysis due to a insufficient cell number).

To address the question whether different PTPs regulate the EGFR phosphorylation dynamics in a similar way we applied a novel classification method, which allowed us to group PTPs according to their regulatory function.

4.5.1 Classification of PTPs by the change of EGFR phosphorylation profiles

To classify PTPs according to their temporal activity, we assumed that similarities in the EGFR phosphorylation profiles obtained upon individual PTP perturbation indicate a comparable regulatory role of the corresponding phosphatases. To address this objective, we mapped the shape of the differently perturbed EGFR phosphorylation profiles by translating them into symbol sequences. In this way, PTPs that induce similar EGFR dynamics could be grouped together. This novel "response-based" clustering approach was based on the principle of ordinary patterns (Hempel et al., 2011) and was provided by A. Koseska **(Methods 3.9.4)**. To verify that the EGFR response profile obtained by averaging the phosphorylation values over large number of cells at different time points is a good representation of the phosphorylation profile as measured in single cells over time, we generated synthetic single-cell data based on the experimental EGFR response profiles, and use a permutation-based bootstrapping test to identify and compare the obtained symbol sequences with the corresponding results from the measurements **(Supplementary Figure 4.S7).** This computational analysis showed that the highest-ranking pattern derived from the synthetic data generally corresponds to the one obtained from the mean values per cells in the screening experiment. In order to account for cell-to-cell variance, which could affect the mapping of the patterns in this case, we additionally combined the patterns into groups of similar patterns according to their shape **(Supplementary Figure 4.S8)**. This allowed classification of PTPs into 5 distinct groups (I-V) according to their temporal regulatory function on EGFR phosphorylation **(Figure 4.14 a)**. As discussed in the beginning of this section, the cDNA screen was performed in two sequential rounds to guarantee a

sufficient number of cells for analysis. The clustering method described was applied to both PTP collections individually. We always included PTPN1 (PTP1B) and the third isoform of PTPN2 (TC41) in every screening experiment as controls because of their reliable negative regulation. To validate the robustness of the PTP classification obtained, we determined the significance that a given PTP is classified in one of the 5 groups by ranking the identified shapes over 5 different screening experiments for both PTP collections **(Figure 4.14 b, c).**

Approximately 38 % of the investigated PTPs were classified in group I, which showed a ***sustained*** phosphorylation profile with a shape similar to the unperturbed control profile. However, several PTPs within this group induced a reduction of the phosphorylation amplitude of EGFR while keeping the sustained shape of the profile. PTPN1 as well as PTPN9, PTPRA and the two isoforms of PTPN2 (TC45 and TC41) produce such a profile.

PTPN1 is located at the cytoplasmic surface of the ER and functions as a major negative regulator of RTKs, which dephosphorylates the INSR, PDGFR and EGFR (Elchebly et al., 1999; Haj et al., 2003). FRET measurements with a trapping mutant of PTPN1 have shown that PTP1B interact and dephosphorylates EGFR after 30 min EGF stimulation at specific sites at the surface of the ER (Haj et al., 2002). However, PTP1B dephosphorylates EGFR not only at this late time point but also immediately (2-5 min) after EGF stimulation when first endosomes are formed (Eden et al., 2010; Lammers et al., 1993), which is consistent with our result.

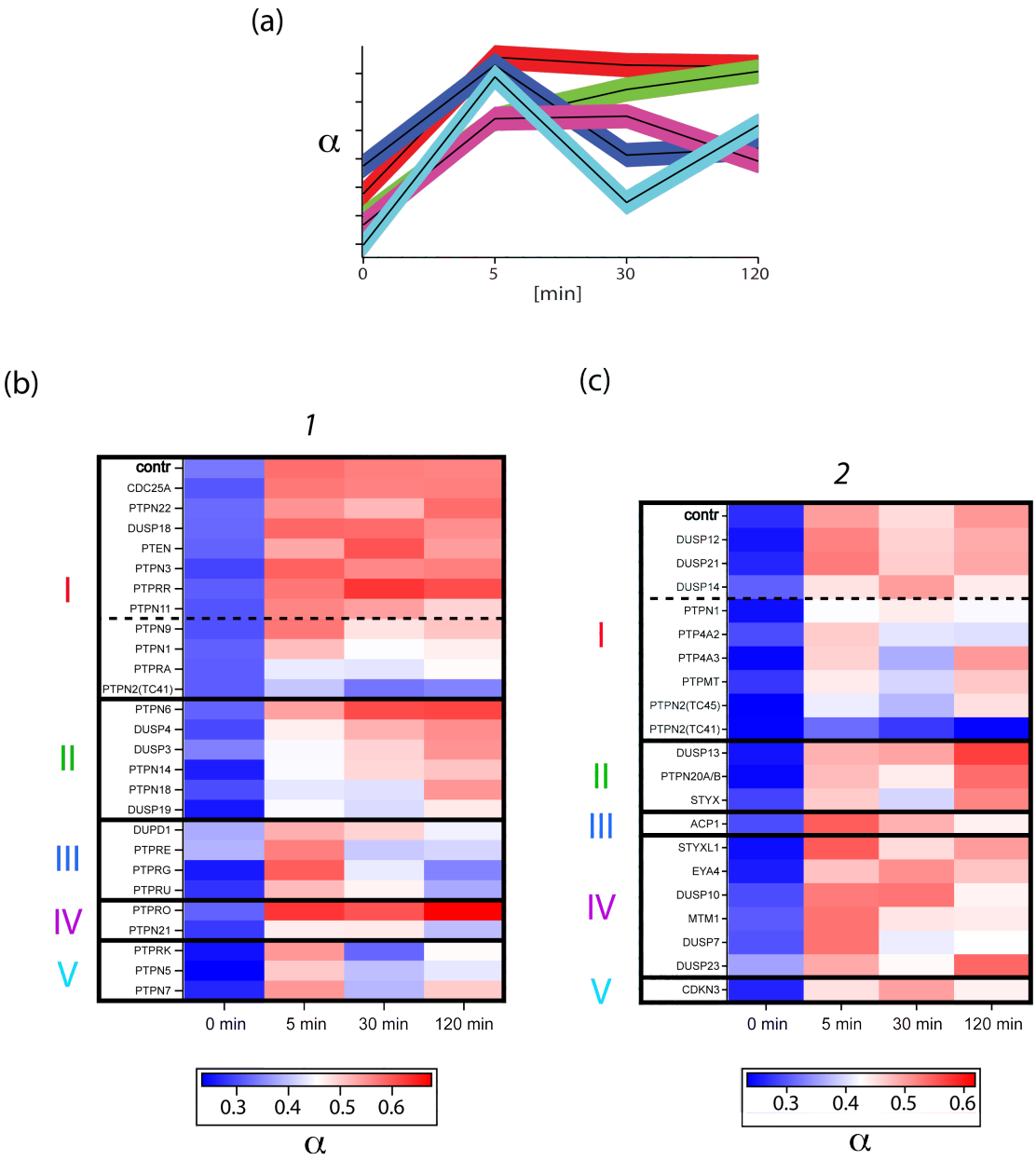

Figure 4.14 Response-based classification of PTPs. (a) Possible shapes of EGFR phosphorylation profiles obtained from single cell variation (5 shapes indicated in colors). Temporal α-profiles of EGFR upon corresponding PTP expression from the two cDNA collections 1 (b) and 2 (c). Resulting α-profiles were classified into the 5 shapes (I-V) indicated in the corresponding color in (a). Classification were performed on the bases of 5 individual screenings in each case. For each cDNA collection one representative data set of the 5 replicates is shown. Dotted line in group I divides PTPs that showed a change in the phosphorylation amplitude of EGFR. Response-based clustering of EGFR profiles was performed by A. Koseska.

In contrast to the ER localized PTPN1, **TC45** is localized in the nucleus and translocate to the cytoplasm upon EGF stimulation where it interacts with EGFR (Tiganis et al., 1998). This translocation was observed at 15 min after EGF

stimulation. Our data additionally indicate that the translocation of TC45 might occur immediately after stimulation because we observed an early reduction of EGFR phosphorylation after 5 min EGF. The C-terminus of TC45 contains the NLS that regulates its localization but also an autoregulatory site which modulates the activity of TC45 via a reversible intramolecular interaction with the catalytic domain (Hao et al., 1997). The same authors have shown that the removal of 20 C-terminal residues was sufficient to activate the enzyme. The sequence of this truncated mutant is almost equivalent to the third isoform of PTPN2 (**TC41**). In our screening we observed that TC41 expression nearly prevents EGFR phosphorylation after ligand stimulation. The lack of the NLS and its autoregulatory motive of TC41 might explain the strong negative function of this isoform when it is present in the cytoplasm where it can directly interact with EGFR without a ligand mediated translocation.

Furthermore, **PTPN9** (PTP-Meg2) was classified in group I and consistent with our data it has been shown previously that PTPN9 reduces EGFR phosphorylation immediately (5 min) but also after longer stimulation (30 min) with EGF (Yuan et al., 2010). According to the limited resolution in our screens, we detected PTPN9 as located generally in the cytoplasm (data not shown). However, biochemical analysis has been shown that PTPN9 is in particular localized in microsomes, transporting vesicles and partially at the PM (Yuan et al., 2010). This suggests that PTPN9 may interact with and/or dephosphorylate EGFR at the PM and in intracellular membrane compartments leading to the observed overall reduction of the phosphorylation amplitude of EGFR after EGF stimulation.

Furthermore, **PTPRA** (RPTPα) that was previously identified in our primary siRNA/cDNA screen **(Figure 4.10)** was also classified into group I. In addition, to these first experiments, we observed that PTPRA reduces EGFR phosphorylation also at later time points (30 and 120 min EGF). To investigate how PTPRA regulates EGFR phosphorylation at late time points, we examined the localization of PTPRA and EGFR after EGF stimulation. As described in the literature (Lacasa et al., 2005) we observed that PTPRA was predominately

present at the PM at normal growth conditions **(Supplementary Figure 4.S9)**. In contrast, to NRPTPs, PTPRA might not be able to access EGFR after internalized at late time points. Surprisingly, we observed only a small number of EGFR containing endosomes after 5 or 30 min stimulation in cells that ectopically express PTPRA **(Supplementary Figure 4.S10)**. This finding led us to hypothesize that PTPRA dephosphorylates the EGF-EGFR complexes at the PM in such a way that downstream signaling and ligand-induced internalization is inhibited. As discussed previously in **section 4.3.2,** PTPRA showed substrate specificity towards a peptide containing pY1068 of EGFR (Barr et al., 2009). This phosphotyrosine is one of the Grb2 binding sites involved in EGFR internalization (Jiang et al., 2003a). We therefore assume that the PTPRA mediated dephosphorylation results in an altered trafficking behavior upon EGF that might favor the recycling pathway.

In addition, we observed also a reduction in the phosphorylation amplitude of EGFR when two PRLs (**PTP4A2** and **PTP4A3**) were ectopically expressed **(Figure 4.14 c)**. PRLs were described in the past as potential oncogenes when overexpressed and as phosphatases that are involved in cancer development (Al-Aidaroos et al., 2013; Bessette et al., 2008; Hardy et al., 2010; Wang and Lazo, 2012). In particular, PTP4A3 has been described as potential cancer biomarker for assessing tumor aggressiveness because of PTP4A3 up-regulation in metastatic CRC (Saha et al., 2001). However, only little is known about physiological substrates of PRLs that could explain such effects. Recently, it has been shown that enhanced PTP4A3 expression in MDA-MB468 cells, that express high levels of endogenous EGFR, mediated a reduction of PTPN1 transcription and resulted in EGFR hyper-phosphorylation (Al-Aidaroos et al., 2013). This effect was observed in transient PTP4A3-transfected cells after 72 hours protein expression. Surprisingly, we observed in our screenings a negative effect on EGFR phosphorylation when PTP4A3 was ectopically expressed. Cells on CAs were incubated for 24 hours to guarantee PTP and EGFR expression and it might be possible that we could not detect transcriptional effects induced by a high PTP4A3 level. However, according to our data we rather suggest that PTPA2 and PTPA3 negatively regulate EGFR phosphorylation after EGF stimulation. A

unique structural feature of PRLs is that they are farnesylated and contain a polybasic region that both mediates their localization to the PM and endosomal structures (Rios et al., 2013) that would allow an association even with internalized EGFR.

In our second cDNA collection we identified **PTPMT** (PLIP) that belongs to the phospholipid specific PTEN-like phosphatases. In comparison to its direct relative PTEN that showed a substrate preference towards PtdIns(3,4,5)P_3, PTPMT exhibits a unique substrate specificity for the single phosphorylated PtdIns5P (Pagliarini et al., 2004). It has been reported that PTPMT is predominantly localized in mitochondria (Pagliarini et al., 2005), but we observed also a cytosolic fraction in cells that ectopically expressed PTPMT (data not shown). PtdIns5P has been shown to enhance the activity of various myotubularin phosphatases including MTM1, presumably through allosteric regulation (Schaletzky et al., 2003). We identified MTM1 as a potential positive regulator of EGFR phosphorylation in our first siRNA/cDNA screen and it can be assumed that PTPMT might regulate MTM1 activity by removing PtdIns5P from internal membranes.

The second defined group (group II) includes PTPs that act as early regulators, inducing a decrease in EGF-dependent EGFR phosphorylation only at the earliest time points. In this group, the amplitude of EGFR phosphorylation at 5 min was always lower compared to unperturbed cells, but increased over time to eventually reach the phosphorylation amplitude of unperturbed cells at late time points (***delayed sustained***). For example, we found PTPN6 (SHP-1) and DUSP3 (VHR) in this group that were described previously as negative regulators of EGFR (Keilhack et al., 1998; Wang et al., 2011). **PTPN6** is activated by binding to the phosphorylated EGFR via its SH2 domains resulting in dephosphorylation of the receptor after 5 - 10 min EGF (Keilhack et al., 1998; Vogel et al., 1993; You and Zhao, 1997) that is consistent with our data. However, this negative feedback mechanism might be limited to early time points. To explain the increase of EGFR phosphorylation over time it can be assumed that PTPN6 activates Src (Somani et al., 1997) that could in turn counteract against the

phosphatase activity, but Src also phosphorylates PTPN6 that results in an enhanced phosphatase activity (Frank et al., 2004). Moreover, PTPN6 can be inhibited by ROS (Singh et al., 2005) and a temporally delayed inhibition of the phosphatase activity might explain the measured increase of EGFR phosphorylation. PTPN6 requires pY1173 for binding and it might be that this particular site is not phosphorylated or accessible for PTPN6 at late time points (Keilhack et al., 1998).

In addition, three other cytosolic NRPTPs were classified in group II, such as PTPN14 (PEZ, PTPD2), PTPN18 (PTP-HSCF) and PTPN20B (TypPTP). According to its domain structure **PTPN14** is a direct relative of PTPN21 (PTPD1) both contain an N-terminal FERM (four point one, ezrin, radaxin, moesin) domain (Alonso et al., 2004). FERM domain facilitates the binding to phosphoinositides at the PM and FERM domain containing proteins have emerged as important players regulating the cytoskeleton by linking actin filaments to adhesion proteins (Hurley and Meyer, 2001). However, it can be assumed that the FERM domain of PTPN14 mediates the translocation to the PM in a phosphoinositide dependent manner that could allow the interaction and dephosphorylation of the EGFR immediately after EGF stimulation. In addition, PTPN14 contains a putative SH3-binding motif that could support the recruitment to ligand-induced EGFR signaling complexes (Sawada et al., 1994). The two other PTPs of this group, **PTPN18** and **PTPN20B** contain a proline-rich domain (Alonso et al., 2004). Proline-rich domains are known to mediate rapid protein-protein interactions such as the interaction of the SH3 domain of Grb2 and the proline-rich domain of Sos after RTK activation that results in the rapid activation of the MAPK cascade (Williamson, 1994). It has been shown that PTPN12 (PTP-PEST), which is not included in our cDNA library, also contains a proline-rich domain. PTPN12 interacts and dephosphorylates EGFR in breast cancer cells (Sun et al., 2011). Whether the proline-rich domain generally mediates recruitment of PTPs to EGFR needs to be further addressed.

Beside the 4 NRPTPs we found additionally 5 DSPs in group II including DUSP3 (VHR), DUSP4 (MKP-2), DUSP19 (SKRP1), DUSP13b (TMDP) and the

pseudophosphatase STYX. Many recently identified DSPs showed only little or no phosphatase activity against MAPKs, indicating that MAPK interaction is not the exclusive function of DSPs (Chen et al., 2002; Hood et al., 2002; Niwa et al., 2002; Wang et al., 2006). These DSPs are smaller in size and lack the MAPK-binding domain that classifies them as atypical DSPs (Alonso et al., 2004). It has been shown that **DUSP3** expression induced a lower phosphorylation at early time points after EGF stimulation, which then increases over time (Wang et al., 2011), which is consistent with our classification of DUSP3. The same authors found that DUSP3 interacts weakly with EGFR in absence of the ligand and the interaction was reduced after EGF stimulation that would explain the ineffective regulation of EGFR phosphorylation at late time points (Wang et al., 2011). To our knowledge, the other 3 atypical DSPs (**DUSP13b, DUSP19** and the pseudophosphatase **STYX**) were so far not associated with RTK regulation. It might be possible that DUSP19 and DUSP13b also dephosphorylate EGFR, comparable to DUSP3. However, DUSP19 displays only very low activity (Zama et al., 2002a) and is known as promoting scaffold protein in Jnk signaling (Zama et al., 2002a, b). Surprisingly, DUSP19 showed a high sequence similarity to the pseudophosphatase STYX (Nunes-Xavier et al., 2011). It has been described that pseudophosphatases might function as adaptor proteins, recruiting other "active" PTPs to their cellular targets (Alonso et al., 2004). Notably, STYX was recently identified as negative regulator of Erk (Reiterer et al., 2013). In particular, depletion of STYX has lead to an increased activity of Erk, whereas STYX overexpression has induced the opposite. According to our data we suggest an important function of such pseudophophatases that might act as scaffold proteins in early EGFR regulation.

Furthermore, we found PTPs whose ectopic expression changed the sustained EGFR phosphorylation profile to a ***transient*** profile (group III). These PTPs have only a limited negative effect on EGFR phosphorylation after 5 min of EGFR stimulation but the receptor phosphorylation decays over time. In this group we found several receptor-like PTPs e.g. **PTPRE** (RPTPε), **PTPRG** (RPTPγ) and **PTPRU** (RPTPλ). As described for PTPRA, it has been shown that PTPRE and PTPRG dephosphorylate a small phosphopeptide containing the pY1068 site of

EGFR *in vitro* (Barr et al., 2009). Therefore, a direct interaction of these RPTPs with EGFR might explain this result. In comparison to PTPRA, the RPTPs of group III were localized not explicitly at the PM but also at endosomal structures that would allow a late interaction with EGFR after EGF stimulation **(Supplementary Figure 4.S9)**. We have to note here that PTPRE exists as a trans-membrane receptor-like protein and in different soluble cytoplasmic isoforms (Elson and Leder, 1995; Gil-Henn et al., 2000; Nakamura et al., 1996). In our work we included only the transmembrane version. It has been shown that the EGFR phosphorylates PTPRE rapidly after EGF stimulation, which mediates the association of PTPRE and microtubuli. This interaction induces a reversible inactivation of PTPRE (Berman-Golan and Elson, 2007; Sines et al., 2007). The authors showed that the phosphorylated state of PTPRE is already recovered, 10 min after EGF stimulation probably by auto-dephosphorylation. Surprisingly, the same phosphorylation of PTPRE triggers the dephosphorylation and activation of Src (Berman-Golan and Elson, 2007). A combination of both mechanisms could explain the transient EGFR phosphorylation that is determined by the phosphorylated state of PTPRE. As discussed in **subsection 1.2.3.4**, a more general mechanism that leads to reversible PTP inhibition is mediated by the ligand-induced ROS production that might also support the EGFR phosphorylation early after EGF stimulation (Karisch et al., 2011). In addition to the identified RPTPs in group III, the atypical DSP named **DUPD1** (FMDSP, PTPN27b) induced a similar phosphorylation profile. In contrast to the atypical DSPs in group II that reduced the phosphorylation of EGFR at early time points, DUPD1 showed a late regulatory function. DUPD1 associates and dephosphorylates Erk1/2 and p38, but a function as RTK regulator has not been reported so far (Devi et al., 2011). Moreover, we identified **ACP1** (LMPTP) that belongs to the class II Cys-based PTPs **(section 1.2.1)**. It has been shown that ACP1 negatively regulates EGFR, FGFR and EphA2 signaling (Kikawa et al., 2002; Ramponi et al., 1989; Rigacci et al., 1999). ACP1 also activates Src as shown for Class I Cys-based PTPs and is also inhibited by RTK induced ROS production (Chiarugi et al., 2001; Zambuzzi et al., 2008). Both mechanisms could explain the measured transient phosphorylation profile of EGFR phosphorylation.

The next group of PTPs (group IV) showed a sustained profile from 5 to 30 min of stimulation compared to the control, but the profile eventually decreases after 2 hours (***limited sustained***). In this group we found 4 DSPs (DUSP7, STYXL1, DUSP10 and DUSP23), two classical PTPs (PTPRO and PTPN21) and one Asp-based PTP (EYA4). Notably, we observed in our screens that some PTPs (e.g. MTM1, DUSP7, DUSP10, PTPN21) of this group induced a stronger EGFR phosphorylation after 5 - 30 min EGF stimulation compared to unperturbed cells. But the positive effects of these candidates were not consistent over the 5 individual screens. However, both previously identified positive regulators MTM1 and DUSP7 (MKP-X) were found in this group. In addition it has been reported that PTPN21 (PTPD1) promotes Src activation and it can be assumed that this might lead to a higher EGFR phosphorylation (Cardone et al., 2004). Recent studies demonstrated that PTPN21 has an inert catalytic activity, which rather indicates a phosphatase activity independent function (Barr et al., 2009). Similar to MTM1, we observed that PTPN21 co-localized transiently with EGFR after EGF stimulation indicating a functional relevance in EGF signaling **(Supplementary figure 4.S11).**

Regardless whether certain PTPs potentially support EGFR phosphorylation, all candidates of group IV induced a limited sustained profile that suggests a late negative function. In particular, purified PTPRO showed a substrate specificity towards an EGFR phosphopeptide containing pY1068 (Barr et al., 2009). Furthermore, it has been shown that the direct relative of EGFR, ErbB2 and 4 other RTKs including TrkB, Ret, EphA4 and EphB2 are direct substrate of PTPRO (Gatto et al., 2013; Shintani et al., 2006; Yu et al., 2012). In particular, silencing of PTPRO induces up-regulation of ErbB2 phosphorylation strongest after 1 hour (Yu et al., 2012). We observed that ectopic PTPRO expression induced a late reduction of EGFR phosphorylation that is reciprocal to the result reported for ErbB2. Similar to other RPTPs, PTPRO is localized in endosomal structures that would allow a late interaction with internalized EGFR **(Supplementary Figure 4.S9)**.

PTPs of the last group V induce similar profiles to group III (i.e. a transient profile of EGFR phosphorylation) but the amplitude increases again at late time points. More specifically, EGFR phosphorylation is strongly reduced at 30 min after EGF but recovers at 2 hours (***transient-recovered***). In this group we found PTPRK (RPTPκ) that is a previously identified negative regulator of EGFR, two cytoplasmic MAPK specific NRPTPs termed PTPN5 (STEP) and PTPN7 (HePTP), and CDKN3 (KAP) that belong to the CDC14 subclass of DSPs.

It has previously been shown that that **PTPRK** dephosphorylates EGFR 5 – 30 min after EGF stimulation (Wang et al., 2005; Xu et al., 2005). However, as shown for group III candidates we measured a stronger regulatory potential at late time points. PTPRK also occupies vesicular structures near the PM **(Supplementary Figure 4.S9)** that would allow a late association with EGFR. PTPRK is known as an activator of Src and can be oxidized by ROS that both could mediate a lower dephosphorylation rate of EGFR after 5 min EGF (Karisch et al., 2011; Wang et al., 2005; Xu et al., 2006). Furthermore, both **PTPN5** and **PTPN7** contain a kinase interaction motive (KIM) that is in general a structural feature of MKPs. According their KIM, PTPN5 and PTPN7 are involved in negative regulation of Erk activity (Pettiford and Herbst, 2000; Pulido et al., 1998). However, purified PTPN5 showed a substrate specificity towards a small phosphopeptide containing the pY1068 site of EGFR (Barr et al., 2009). Together with our result it can be assumed that MAPK specific PTPs (MAPK-PTPs) have additional substrates beside MAPKs and might play also a direct role in RTK regulation. The activity of MAPK-PTPs is regulated by phosphorylation at multiple sites by PKA, PKC and Erk (Barr and Knapp, 2006). In particular, a serine phosphorylation within their KIM domain blocks the interaction of MAPKs with MAPK-PTPs thereby leading to phosphatase inactivity (Blanco-Aparicio et al., 1999; Braithwaite et al., 2006; Saxena et al., 1999). However, it has to be addressed whether the phosphorylated state of the KIM domain has consequences for the interaction with other targets such as RTKs. The last member of group V identified was **CDKN3** (KAP) that is one of the four CDC14 proteins (Alonso et al., 2004). CDC14s are involved in dephosphoryaltion of serine and threonine sites and are known to regulate cycline dependent kinases

during the cell cycle (Visintin et al., 1998). Surprisingly, we measured a late reduction of EGFR tyrosine phosphorylation when CDKN3 was ectopically expressed highlighting an additional indirect regulatory mechanism that controls cell proliferation.

With our novel classification method, we can determine the most probable pattern (shape) for each EGFR phosphorylation profile upon individual PTP expression by using the cell-to-cell variance and clustered them into 5 functional groups. We have shown that different PTPs either modulate the overall amplitude of the sustained response profile of EGFR or could even fundamentally change the shape of its temporal progress, leading to delayed or limited sustained EGFR phosphorylation. Moreover, the expression of some PTPs changes the sustained EGFR response to a transient response. We generally observed that PTPs within individual groups showed difference in their degree of EGFR regulation. This fact has led us to the next question of our aim. Whether individual PTPs possess differences in their regulatory potential or strength.

4.5.2 Determination of the regulatory influence of PTPs

To identify differences in the "strength" of PTPs that are involved in EGFR regulation we performed an amplitude-based clustering within each of the 5 groups (I-V) using affinity propagation **(Methods 3.9.5)**. The method of affinity propagation was provided by A.Koseska and can be described as a max-sum algorithm of a factor graph, that is used to search over configurations of the labels in the graph that maximize the net similarity. As a result, the PTPs in each group are separated into subgroups according to the magnitude to which they regulate EGFR phosphorylation. We have analyzed the data sets of both PTP collections (screen 1 and 2) to determine the differences in the regulatory strength of the corresponding PTPs. We note here that the amplitude of α of control cells was slightly different in both experiments. The results from affinity propagation of both cDNA collections (1 and 2) are presented in (**Figure 4.15)**

and **(Supplementary Figure 4.S12)** for one of the five individual screening repetitions.

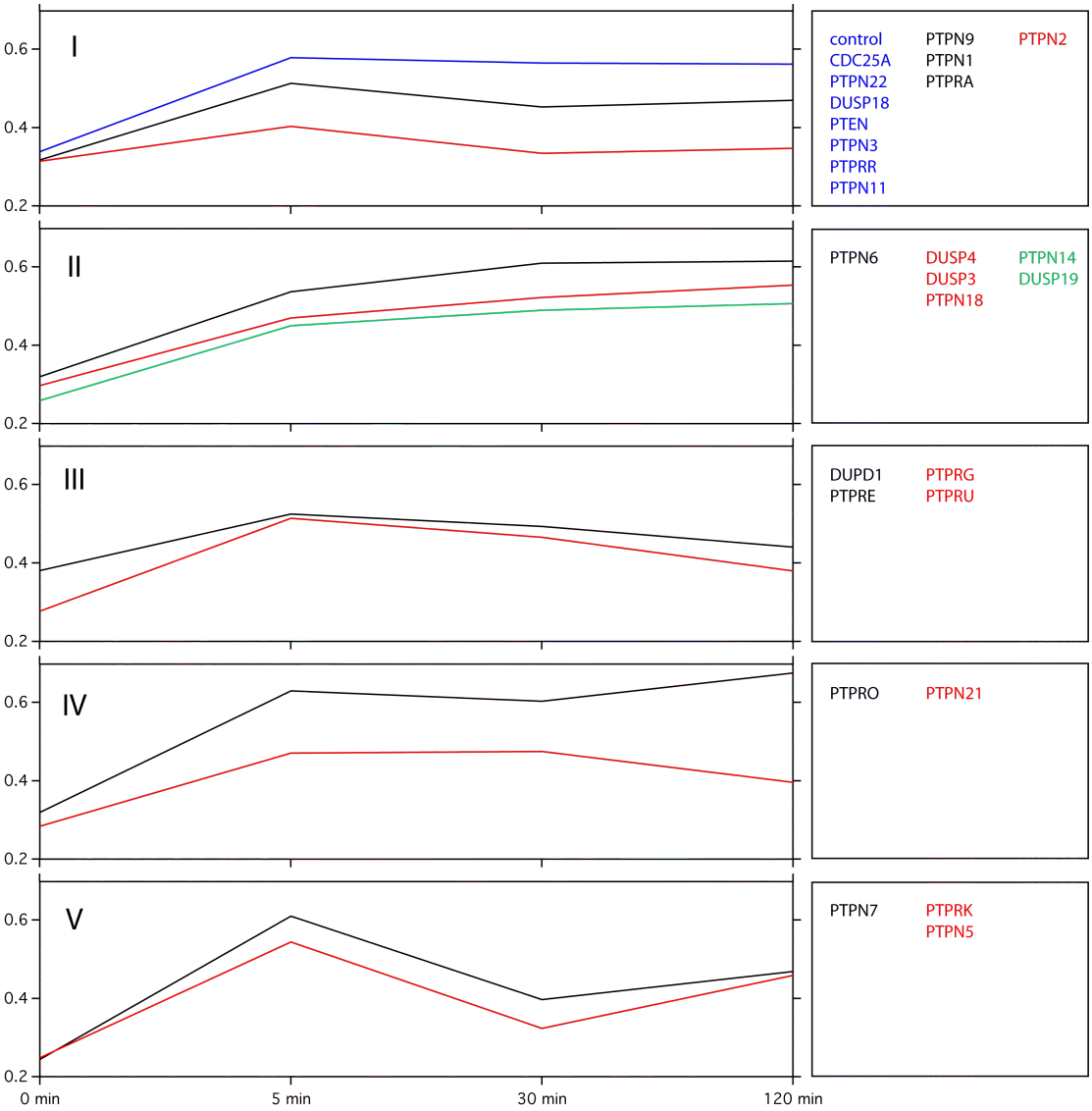

Figure 4.15 Amplitude clustering by affinity propagation. The 5 functional classes (I-V) derived by response-based classification are shown. Members of each class are divided into subgroups according to their change in amplitude. Control group in blue. Moderate regulators are shown in black and stronger regulators in red and green. A temporal profile is shown for each subgroup within a class. Profiles are representative for all members of a subgroup. Data presented here are from the first cDNA collection (screen 1). The clustering by affinity-propagation was provided by A. Koseska.

The members of group I do not induce a change in the shape of the response profile of EGFR, but we identified several PTPs in this group which have previously been found as negative regulators in the literature **(Table 1.1, Introduction)**. By using affinity propagation, we obtained 3 subgroups in group I representing significant differences in their influence on EGFR phosphorylation. In both cDNA collections (1 and 2), we identified several moderate (PTPN1, PTPRA and PTPN2 (TC45)) and one strong regulator (PTPN2 (TC41)). TC41 lacks any regulatory sequence and can be thought as a "hyperactive" cytosolic enzyme that completely abolish EGFR phosphorylation. As already described, PTPs of group II induce a delayed sustained profile of EGFR phosphorylation. Within this group, we also found 3 distinct subgroups. For example, the expression of PTPN6 induced a delayed but sustained phosphorylation profile of EGFR, while other PTPs (e.g DUSP3) induced a nearly linear increase over time. A third subgroup includes the FERM domain containing PTPN14 and the atypical DUSP19, which were both classified as the strongest regulators in group II. Furthermore, PTPs of class III, which induce a transient response of EGFR, could be divided into two subgroups, in which PTPRG and PTPRU had the strongest regulatory impact. We identified 3 different regulatory groups for class IV (screen 2) **(Supplementary Figure 4.S12)**, includeing the positive regulators MTM1 and DUSP7. However, while we could separate these groups into three subgroups we were not able to distinguish between these subgroups by their regulatory potential. The members of group V were divided into two regulatory subgroups and PTPRK and PTPN5 were identified as the strongest negative regulators in this group.

In summary, we have classified PTPs into 5 functional groups according to their induced changes in the EGFR phosphorylation profile. Moreover, affinity propagation clustering allowed us to distinguish between the regulatory influence of PTPs within their same functional group. In group III and IV, for example, we found in total 4 RPTPs that induce a transient phosphorylation profile of EGFR and three of them (PTPRU, PTPRK and PTPRG) also showed the strongest regulatory impact within their groups, suggesting that these RPTPs might play a major role in EGFR regulation. These differences guided us to our

next question. PTPs contain distinct localization sequences or binding domains that organize them into defined cellular regions and the EGFR encounters PTPs either at the PM or in endosomal compartments. We therefore asked whether the localization of PTPs correlates with their functional groups and thus, their regulatory influence.

4.5.3 Members of functional classes possess similar molecular features

The advantage of using fluorescent PTP-mCitrine fusion proteins is that the localization can be directly assessed. The observed localization of each PTP in our two collections was detected under normal growth conditions and verified by the UniProt and LOCATE databases. We then calculated the probability that a number of PTPs with a distinct localization (i.e. nucleus, cytosol or PM) belong to the same functional group by determining the hypergeometric distribution **(Methods 3.9.6) (Figure 4.16)**. By comparing the localization of PTPs within each group, we found a high diversity in most cases. However, we found out that all 9 PTPs of group II are localized in the nucleus, the cytoplasm or in both. In particular, the strongest identified regulators DUSP19 and PTPN14 are both localized exclusively at the cytoplasm. A similar relationship was observed for the short isoform of PTPN2 (TC41) of group I that was classified as the strongest negative regulator of EGFR in both PTP collections. This isoform is consistently located in the cytosol where it might encounter EGFR under basal conditions and upon stimulation. Moreover, the negative regulators found in group III such as PTPRE, PTPRG and PTPRU are all present at the PM and/or endosomal structures and therefore might share the same localization as EGFR. We obtained a p-value < 0.05 that the members of this group are not localized at random.

To summarize our temporally resolved screening experiments, we identified several known negative regulators including PTPN1, PTPN2 (TC45/41) and PTPN9 but also PTPRA that were identified in our primary siRNA/cDNA screen, which induced no change in the shape of the temporal profile but reduced the overall amplitude of EGFR phosphorylation. In addition

we found significant differences in the regulatory influence of these members by affinity propagation. The expression of group II PTPs that were predominantly localized at the cytosol and/or nucleus changed the EGFR profile from a sustained to a delayed response. The strongest regulators in this group were explicitly localized in the cytosol. Members of group III and V induce a transient EGFR response. Most candidates in group III were RPTPs including PTPRE and the two strong negative regulators PTPRG and PTPRU. We observed that the RPTPs of group III and IV are not restricted to the PM alone, which could support their late regulatory function. Furthermore, several members of group IV induced an increase of EGFR phosphorylation after 5 or 30 min of EGF stimulation. Supporting our observation, both positive regulators MTM1 and DUSP7 that where identified in our primary siRNA/cDNA screen were found in this group. However, we could not identify significant differences between these candidates by using affinity propagation. From class V we identified PTPRK and PTPN5 with the strongest regulatory potential.

In order to characterize the function of the newly identified candidates in more detail and to compare their regulatory role with known regulators of EGFR signaling, we used a different approach based on the cell-to-cell variance. In our cluster analysis, we used the cell-to-cell variance derived from single cell segmentation to determine the most probable response profile of EGFR phosphorylation upon a given PTP perturbation. Moreover, correlation analysis using cell variability has previously been described as a reliable method to identify causal protein connections, such as positive regulatory connections (Grecco et al., 2010). For an accurate correlation analysis a minimal number of sample replicates, which guarantees a sufficient number of cells is required. In our CA-FLIM experiments, we have used automated microscopy to investigate multiple PTPs with a limited number of replicates. However, automated microscopy is flexible and can be adjusted to address the function of a subset of PTPs using cell-to-cell variance with a high number of replicates.

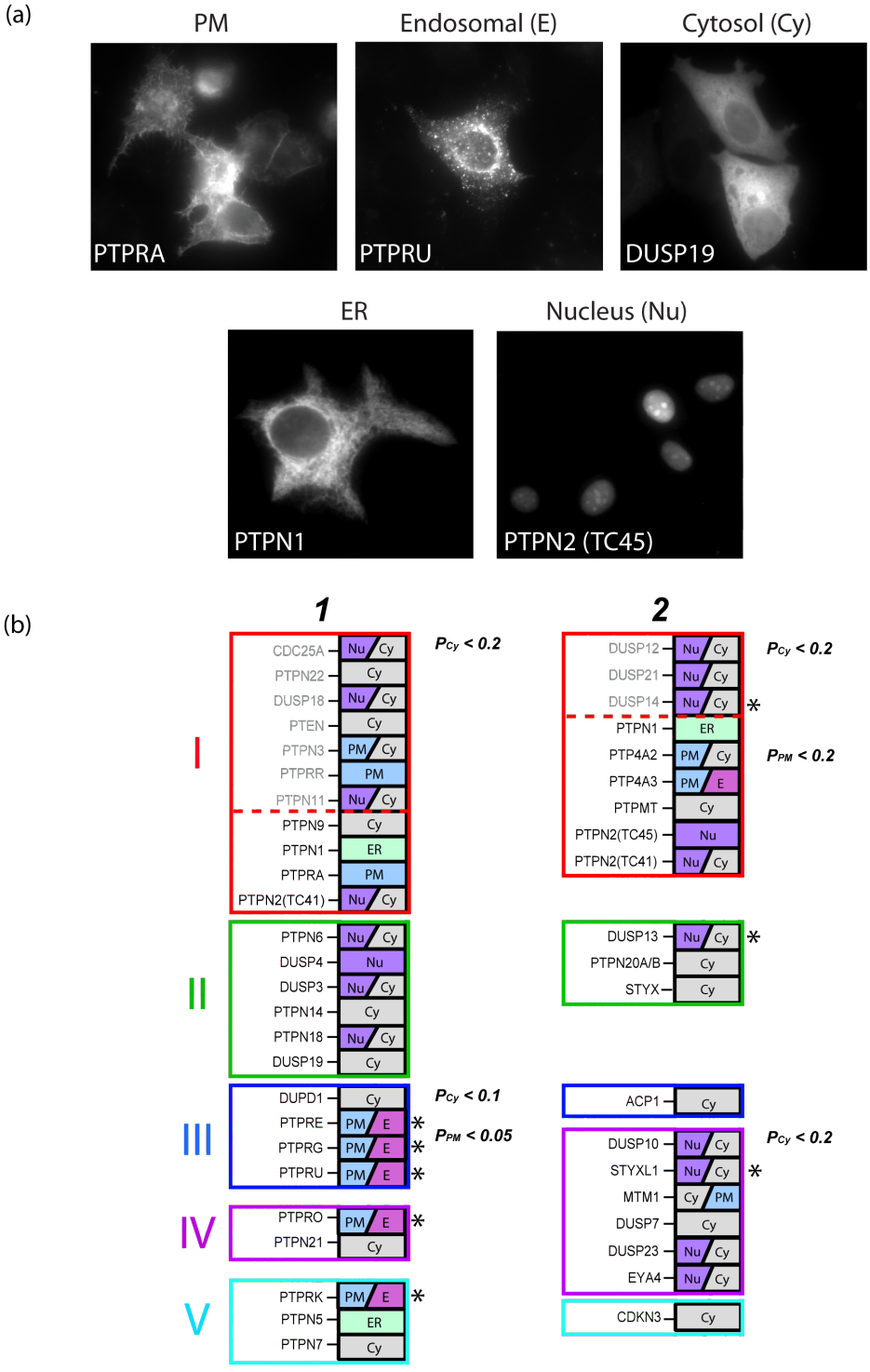

Figure 4.16 Comparison of functional groups with the localization of PTPs (a) Representative images of PTPs fused to mCitrine with a defined localization. (b) Group members defined by response-based clustering (I-V) are indicated for both cDNA collections (1 and 2). PTP names in grey indicate candidates that were not identified as EGFR regulators. Localization of each PTP at normal growth conditions is indicated on the right. Nu = nucleus, Cy = cytosol, PM = plasma membrane, ER = endoplasmic reticulum, E = endosomal structures. p-values calculated by hypergeometric distribution are indicated. Asterisks indicate additionally observed localizations, which could not be validated in UniProt- or LOCATE-databases.

4.6 Characterization of identified EGFR regulators by using the cell-to-cell variance

We focused our work on MTM1 (myotubularin), DUSP7 (MPK-X) and PTPRA (RPTPα), which were identified as novel regulators after 5 min EGF stimulation in our primary siRNA/cDNA screen **(Figure 4.10)**. Our first objective was to address whether the observed positive influence of MTM1 and DUSP7 occurs also at later time points after stimulation, because we were not able to detect increased EGFR phosphorylation dynamics in our previous experiments **(Supplementary Figure 4.S12)**. We included also PTPN21 (PTPD1), which has previously been shown to be a positive regulator of EGFR (Cardone et al., 2004; Carlucci et al., 2010). We found in our primary siRNA/cDNA screen that silencing of PTPN21 induced a lower phosphorylation of EGFR, but we could not observe a reciprocal effect when PTPN21 was ectopically expressed. However, we could observe that both PTPN21 and MTM1 co-localized with EGFR after EGF stimulation indicating a functional role in EGF signaling. We also included PTPRG (RPTPγ) as one of the "strong" regulators obtained by affinity propagation from group III. Beside the two identified negative regulators PTPRG and PTPRA we also included PTPN1 (PTP1B) and the hyperactive isoform of PTPN2 (TC41). MCF7 cells seeded in 8 well chambers were co-transfected with EGFR-mTFP as FRET-donor and one of the PTPs fused to mCitrine. Cells were stimulated for 6 different time points with EGF, fixed and used for automated FRET-FLIM measurements after incubating the FRET-acceptor (anti-pY-Cy3.5). FLIM-stacks at 50 positions per time point were acquired with a 40x objective. The phosphorylated fraction α was calculated by global analysis. Intensity images were used for single cell segmentation and average α values from single cells were calculated for each PTP and time point. Consistent with the results obtained in previous experiments, expression of PTPN1, PTPN2, PTPRA or PTPRG showed a reduced phosphorylation level of EGFR compared to cells expressing only EGFR (control) **(Figure 17a)**. On the other hand, MTM1, DUSP7 and PTPN21 showed a general increase in EGFR phosphorylation at early time points.

To characterize potentially positive or negative functions of PTPs in our subset, we performed single cell correlation analysis. We have plotted the average intensity of mCitrine as a measure of the PTP expression against the phosphorylated fraction of EGFR (α) in each cell. An positive correlation between these two parameters can, for example, indicate a promoting connection, whereas a negative correlation highlights an inhibitory connection. A positive correlation between the EGFR phosphorylation (α) and MTM1 expression could be found at all different time points after EGF stimulation **(Figure 17b).** This effect was also visible under basal conditions. Furthermore, we observed a steeper slope after 30 – 60 min of EGF stimulation. Moreover, positive correlations were also obtained for DUSP7 at early stimulation time points (2 - 5 min after EGF). PTPN1, on the other hand, showed a negative correlation at all time points. This finding indicates that the ER anchored PTPN1 has a stronger effect after the internalization of EGFR. Expression of the cytosolic PTPN2 isoform TC41 induced a negative correlation at all measured time points including basal conditions. This indicates that TC41 associates with EGFR independent of EGF stimulation, resulting in a constitutive dephosphorylation of the receptor.

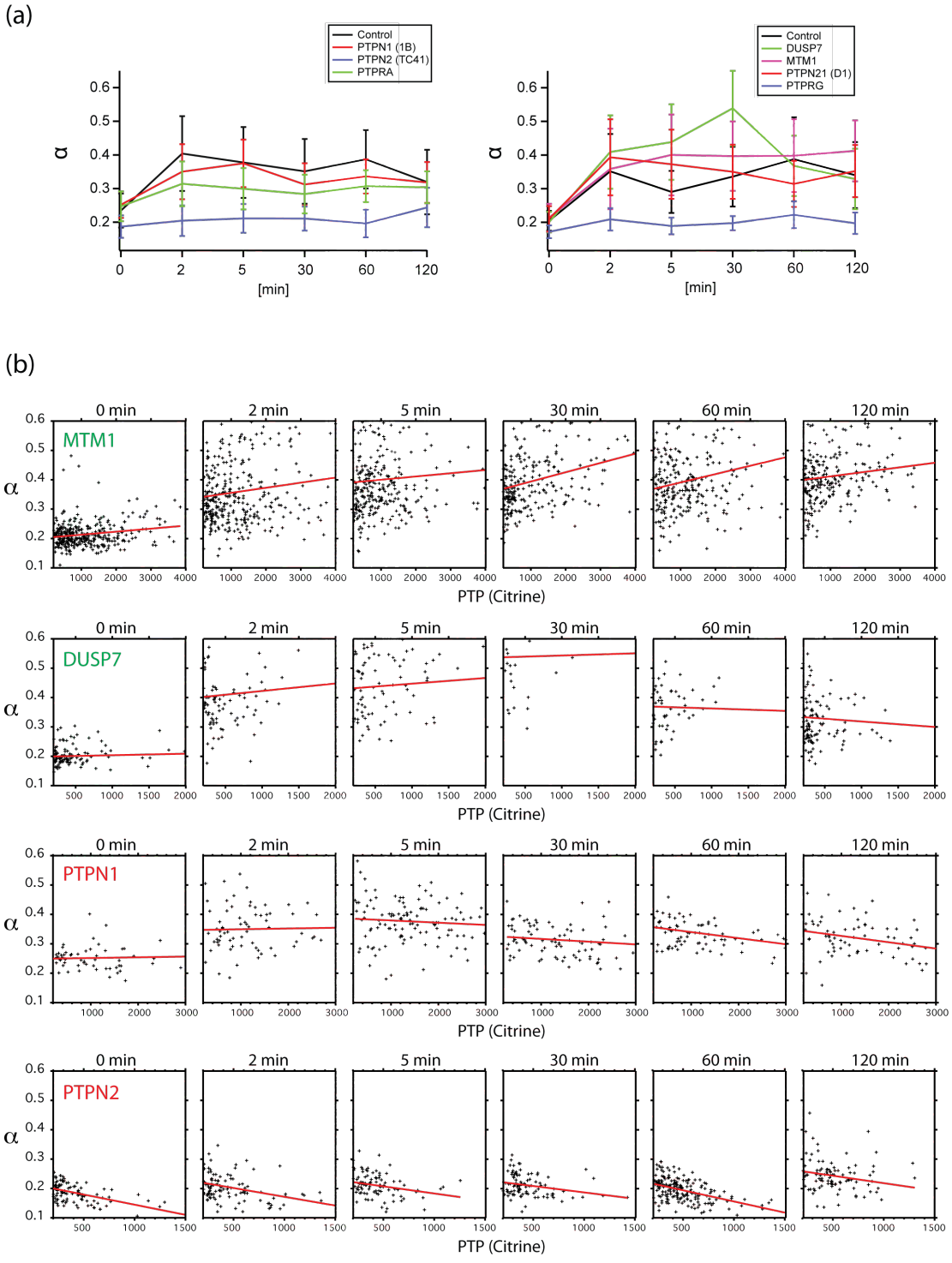

Figure 4.17 Identification of positive and negative regulators by single cell analysis. (a) Phosphorylation profiles of EGFR upon different PTP expression measured by automated microscopy. Error bars indicate the standard deviation. (b) Single cell correlation of EGFR α against PTP-mCitrine intensity. Linear fits are indicated in red.

Notably, we observed that the average α values of EGFR phosphorylation in **(Figure 4.17a)** showed a relatively high standard deviation of +/-0.1. The standard deviation of EGFR phosphorylation might result from differences in the EGFR and PTP expression levels in each cell within the sample. However, even a relatively high cell-to-cell variance can be an advantage. For example, it has been demonstrated that variance can be used to identify positive feedback between proteins belonging to the same signaling network (Stewart-Ornstein et al., 2012). In general, we observed that expression of positive regulators (MTM1 or DUSP7) induced a higher variance in EGFR phosphorylation compared to cells expressing a negative regulator such as PTPN2 **(Figure 4.17a, b)**. Thus, the observed variability of EGFR α upon PTP perturbation can be used to validate our findings quantitatively. Stochasticity is an inherent property of biochemical systems that generally arises due to infrequent molecular events. In the context of our study, this is manifested as variability in the levels of the expressed proteins or active protein states. The variance of a given protein-state differs between cells according to the given regulatory interactions in which the protein is embedded. For example, measuring the fraction of phosphorylated EGFR in different cells when positive regulatory PTPs are expressed results in a higher variance of EGFR phosphorylation values, in contrast to the case where negative regulators are expressed. As an appropriate measure of the relative size of the variance observed in EGFR phosphorylation upon expression of PTPs, we have calculated the Fano-factor (Fa) of each EGFR α-distribution **(Methods 3.9.7)**, which is defined as the ratio of the variance and the mean value (**Figure 18**).

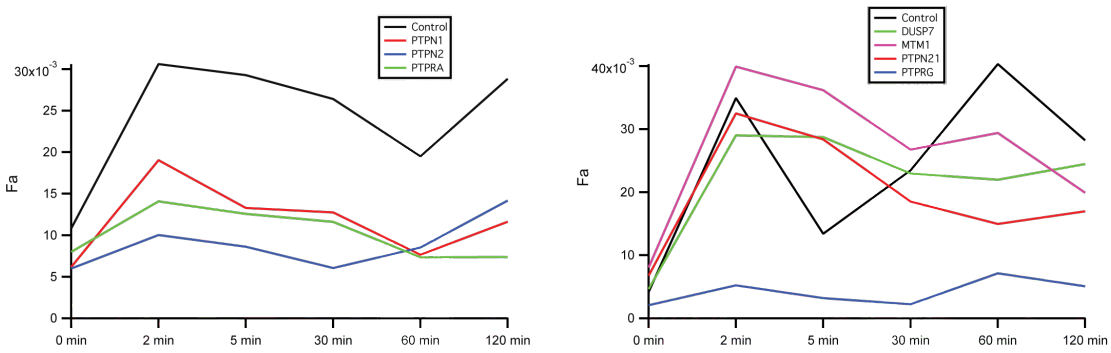

Figure 4.18 Fano-factor (Fa) that reflects the level of cell-to-cell variance of EGFR α is shown for each time for different PTP expressions.

The Fano-factor of EGFR phosphorylation in case of PTPN1, PTPN2, PTPRA or PTPRG expression was lower compared to the control or positive regulators. This result validates our finding that both PTPRA and PTPRG regulate EGFR phosphorylation negatively and are comparable in function to the better characterized PTPN1 and PTPN2. We observed that the variance of EGFR phosphorylaiton was lowest upon expression of PTPN2 (TC41) and, in general, higher when PTPRA or PTPN1 was expressed. A similar graduation was observed in our affinity propagation analysis **(Figure 4.15)**. These results let us conclude that PTPRA has a comparable regulatory influence to the ER localized PTPN1, but is lower than TC41. The variance of cells expressing PTPN1, PTPN2 or PTPRA showed almost no differences over longer time points, supporting our previous classification of these PTPs in group I. PTPRG was previously classified in group III because of its induction of a rather transient EGFR phosphorylation. Here we observed an overall reduction of the EGFR phosphorylation amplitude. PTPRG was classified as one of the *"strongest"* negative regulators within group III, which is characterized by a relatively low peak after 5 min EGF stimulation **(Figure 4.15).**

On the other hand, the Fano-factor of cells expressing either MTM1, DUSP7 or PTPN21 showed a higher variance of EGFR phosphorylation at early time points compared to control cells. This data supports our initial findings in the first siRNA/cDNA screen **(Figure 4.10)** in which MTM1 and DUSP7 were identified as positive regulators of EGFR after 5 min of EGF stimulation. The predominantly higher cell-to-cell variance in EGFR phosphorylation induced by the expression of a positive regulator might explain why we measured no significant effects for these proteins with our clustering approach **(section 4.5)**. Compared to our CA screens, our measurements in 8 well chambers provided us with a 10-times higher number of cells for analysis. By calculating the EGFR phosphorylation of approximately 100 single cells expressing the same PTP, we could not only validate the positive function of MTM1 and DUSP7, we also identified a similar function for PTPN21. All three candidates were previously classified in group IV **(Figure 4.14),** which is characterized by a late reduction of EGFR phosphorylation. With our analysis based on single cell variance, we

conclude that MTM1, DUSP7 and PTPN21 support EGFR phosphorylation at early time points ranging from 2 – 30 min after EGF stimulation, depending on the PTP expressed. Consistent with our previous classification into group IV, we observed that the cell-to-cell variance of EGFR phosphorylation decreased over time for all 3 candidates. In particular, this result suggested that there exists a distinct window of time when these positive regulators may promote EGFR phosphorylation. As already discussed, MTM1 expression supports EGFR stability and might induce a temporal accumulation of EGF-EGFR in early endosomes that could lead to the enhanced EGFR phosphorylation because of the high receptor density in such compartments. Similarly, PTPN21 silencing promotes rapid degradation of EGFR after EGF stimulation (Carlucci et al., 2010). PTPN21 interacts with KIF16B, a component of the endocytic pathway, at endosomes. KIF16B belongs to the kinesin family motor proteins that transport early endosomes to the plus end of microtubules and KIF16B overexpression relocated early endosomes to the cell periphery and inhibited the transport to the degradative pathway. (Hoepfner et al., 2005). This implies that PTPN21 may have a synergistic role with KIF16B in favoring recycling of internalized EGFR through the endocytic pathway (Carlucci et al., 2010). In this way, PTPN21 induced a similar EGFR phosphorylation as discussed for MTM1 expression by regulating EGFR trafficking with different mechanism.

In summary, automated microscopy provides the phosphorylated fraction of EGFR in a large cell population perturbed by PTP expression. The cell-to-cell variance within this cell population was used to identify positive and negative regulators of EGFR phosphorylation. After the characterization of positive and negative regulators of EGFR, we wanted to address the question where PTPs regulate EGFR phosphorylation and how these interactions alter the trafficking behavior of EGFR.

4.7 PTPs regulate the spatial-temporal phosphorylation pattern of EGFR

Quantitative microscopy provides us with the phosphorylated fraction of EGFR in each pixel of the cell. In our previous screens we have used average values calculated from single cells to determine the phosphorylation dynamics of EGFR. However, to address the question how PTPs regulate the spatial phosphorylation of EGFR we developed a method to segment cells into spatial regions. Such a segmentation is essential to compare the spatial phosphorylation between differently perturbed cells **(Figure 4.20) (Methods 3.9.8)**.

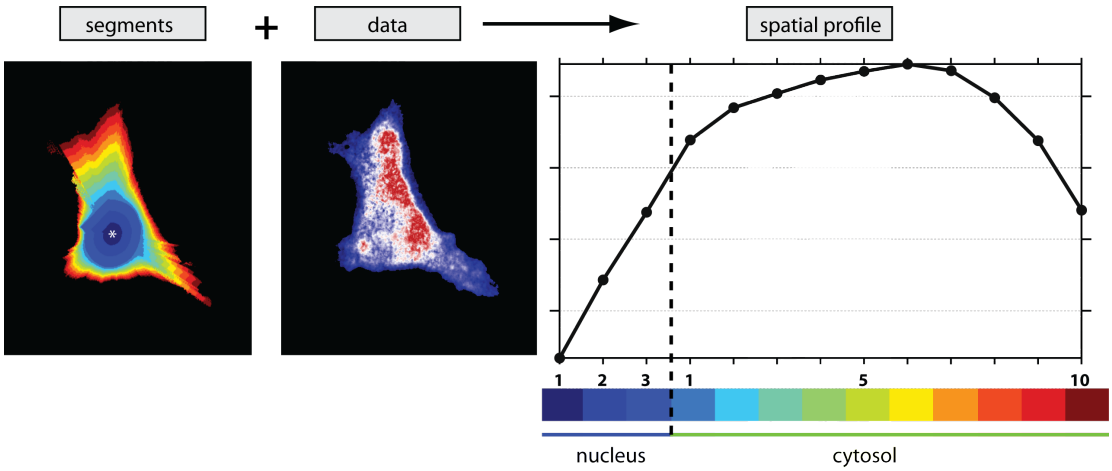

Figure 4.20 Schematic of radial segmentation. Cells were segmented into 13 spatial regions between the center of the nucleus and the PM (left). The center of the cell was defined by the center of the nucleus (white asterisk). The width of each region varies according to the relative distance between the center of the nucleus at a given angel. The average α of each segment can be calculated by using the α image of the corresponding cell. In this way, a spatial profile of the average a of every spatial segment between the nucleus and the PM can be generated for each cell (right). Radial segmentation analysis was developed and provided by Hernan Grecco.

Each cell was divided into 13 radial regions between the PM and the center of the nucleus. The average of EGFR phosphorylation (α) was calculated for each radial region. We excluded cells that were too small or showed an incomplete masking of the cytosol to guarantee a certain amount of pixels per radial region. A detailed description used for automated cell filtering is provided in **(Methods 3.9.8)** EGFR α values derived from spatial-segments were

calculated from single cells stimulated with EGF for 0, 5, 30 or 120 min. Spatial-segments from single cells were combined for each stimulation time point respectively, resulting in a spatial-temporal phosphorylation profile of EGFR **(Supplementary Figure 4.S13)**. After calculating the spatial-temporal profile of EGFR α, we recognized that the pattern generated was not comparable with the spatial-temporal phosphorylation observed by microscopy **(Figure 4.12)**. EGFR undergoes rapid autophosphorylation at the PM where the majority of the receptor becomes internalized within the first 5 min after EGF stimulation and propagates deeper inside the cell. In contrast to these observations, we could not detect any temporal or spatial differences in our generated profiles. We next calculated the intensity-weighted α of EGFR (EGFRp), which represents the total amount of phosphorylated receptor in each pixel **(Methods 3.9.8)**. In comparison to the fraction of phosphorylation EGFR (α), we could reconstruct the spatial-temporal phosphorylation pattern of EGFR as observed with microscopy by using the amount of phosphorylated receptor (EGFRp) (**Figure 4.12)** and **(Figure 4.21a)**.

The generated spatial-temporal profile of EGFR followed a distinct time dependent propagation **(Figure 4.21a)**. Five min after stimulation, the phosphorylated receptor is limited to areas close to the PM. This activated fraction propagates gradually deeper into the cytoplasm until it reaches the periphery of the nucleus. After developing a method to obtain the spatial-temporal phosphorylation profile of EGFR from different cell populations, we wanted to know whether the expression of PTPs have an effect on this profile. We focused our work on the three positive (MTM1, DUSP7 and PTPN21) and the four negative (PTPN1, PTPN2, PTPRA and PTPRG) regulators that were already characterized in **section 4.6**. By using the spatial segmentation method, we also calculated the average fluorescence intensity of each expressed PTP for all radial regions. In general, we observed that the spatial-temporal phosphorylation of EGFR followed different patterns according to the expressed PTP **(Figure 4.21b,c)**.

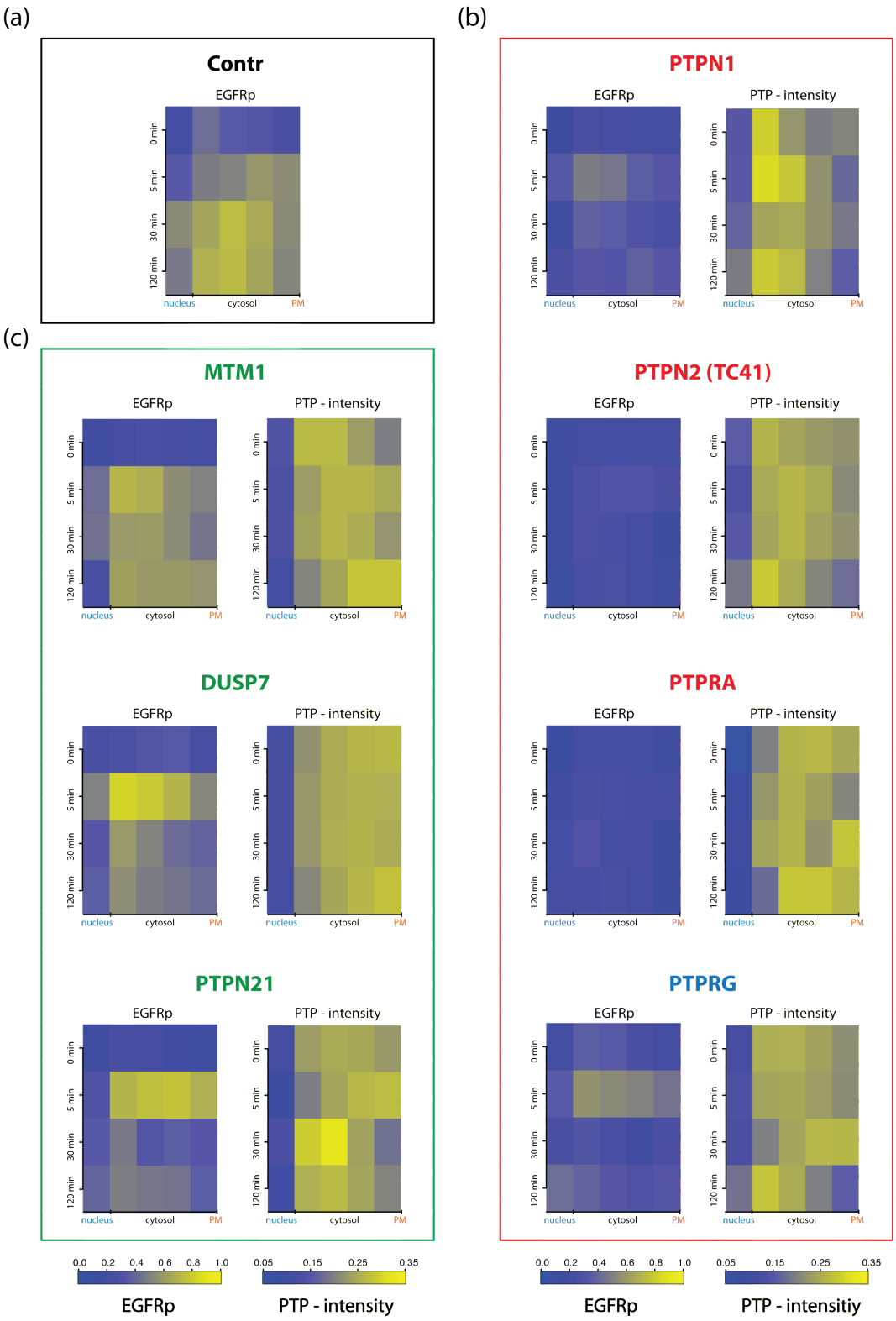

Figure 4.21 Spatial-temporal phosphorylation profiles of EGFR upon PTP expression. Profiles generated by radial segmentation. The area between the cell center (defined by the center of the nucleus) and the PM was divided into 4 cytosolic and 1 nuclear segments. Averages of the intensity weighted EGFR α (EGFRp) derived from each radial-region (one nuclear segment and four cytosolic segments) are presented for all four EGF stimulations (0, 5, 30, 120 min). (a) Spatial-temporal profile of EGFRp from cells expressing EGFR-mTFP alone (Control). (b, c)

Spatial-temporal profiles of EGFRp from cells transfected with EGFR-mTFP and different PTPs as indicated. Corresponding spatial-temporal profiles of the PTP-intensities are shown on the left respectively (The sum of intensity of all segments was normalized to 1). Colors indicate previous classification of PTPs: Positive regulators of group IV are shown in green, negative regulators of group I in red and the negative regulator PTPRG classified in group III is highlighted in blue. Each profile was calculated from approximately 10 acquired cells per time point.

The ER anchored PTPN1, the cytosolic version of PTPN2 (TC41) and the receptor-like PTPRA were previously classified in group I. These PTPs induced an overall reduction of the EGFR phosphorylation amplitude but maintained a sustained profile. Consistent with our result from the temporal profiles, we observed an near complete loss of EGFR phosphorylation when one of these three PTPs was co-expressed **(Figure 4.21b)**. The spatial-temporal profile of cells expressing PTPN1 demonstrated an initial phosphorylation and internalization of the EGFR population after 5 min EGF stimulation. Consistent with the known localization of PTPN1 at the ER, we detected an enriched localization of PTPN1 at perinuclear regions. Notably, PTPN1 and EGFR shared the same spatial-temporal region after 5 min EGF stimulation highlighting possible interactions between the ER and EGF-EGFR loaded endosomes. The phosphorylation of EGFR is already reduced at this time point. EGFR phosphorylation continued to decrease leading to an almost full dephosphorylation of the receptor after 30 or 120 min of EGF stimulation. Moreover, expression of the hyperactive version of PTPN2 (TC41) abolished the early and late phosphorylation of EGFR, consistent with its stronger regulatory potential compared to PTPN1. PTPN2 was detected in the cytosol and we assume that this enzyme keeps the population of ligand-bound EGFRs in a dephosphorylated state. We suggested that such a severe dephosphorylation might result in a reduced EGF dependent internalization.

A similar spatial-temporal profile of EGFR was observed upon PTPRA expression. We demonstrate that PTPRA reduced the number of endosomes loaded with EGF-EGFR complexes after stimulation (**Supplementary Figure 4.S10)**. Consistent with this result, we show here that PTPRA also nearly abolished the phosphorylation of EGFR after activation. We assume that PTPRA activity towards EGFR autophosphorylation might change the trafficking

behavior. The strong regulation by PTPRA might induce recycling of EGF-EGFR complexes instead of degradation. From localization analysis, we concluded that PTPRA is predominantly localized at the PM **(Supplementary Figure 4.S9)**. In contrast to this observation, the spatial-temporal profile generated for PTPRA intensity suggested a cytosolic fraction **(Figure 4.21b)**. Our screening is based on widefield imaging in which stray light coming from the PM above or below the focal plane cannot be excluded from the intensity obtained in cytosolic areas. Due to this imaging limitation, fluorescence of the PM cannot be avoided in cytosolic segments resulting in a rather undefined spatial-temporal intensity profile for PM localized proteins.

Furthermore, PTPRG was previously classified in group III because its expression induces a rather transient phosphorylation profile of EGFR. The spatial-temporal profile of EGFR phosphorylation confirmed this observation. We observed that the phosphorylation of EGFR was limited to 5 min after EGF stimulation but, similar to PTPN1, the level of phosphorylation was already reduced at this time point. We observed that the phosphorylated EGFR and PTPRG shared the same spatial regions after 5 min of EGF stimulation. High EGFR phosphorylation was associated with a higher level of PTPRG. In comparison to the first 5 min after stimulation, the phosphorylation of EGFR was almost abolished at later time points. Our previous image analysis showed that PTPRG was not only restricted to the PM but also present in endosomal compartments **(Supplementary Figure 4.S9)**. The spatial temporal phosphorylation profile indicates that PTPRG interacts with EGFR in cytosolic compartments and exhibits its strongest effects on EGFR dephosphorylation at later time points.

In addition, we then generated spatial-temporal phosphorylation profiles of EGFR when different positive regulators including MTM1, DUSP7 or PTPN21 were expressed **(Figure 4.21c)**. All three phosphatases were previously classified in group IV and induced a limited sustained temporal profile. In **section 4.6**, we validated that all three enzymes promote EGFR phosphorylation early after EGF stimulation. We observed that MTM1 co-localizes with EGFR at

membrane regions 5 min after EGF simulation. Consistent with this observation, the spatial-temporal PTP-intensity profile indicated an enrichment of MTM1 at the PM at this time point. In addition, the phosphorylation of internalized EGFR was enhanced in parallel. Altogether, we observed a rather stable EGFR phosphorylation over the whole period of 2 hours. DUSP7 was evenly distributed in the cytosol and we detected a strongly enhanced phosphorylation of the internalized EGFR after 5 min EGF. PTPN21 showed a similar spatial-temporal profile of EGFR phosphorylation. But more similar to MTM1, we detected PTPN21 enrichment at the PM after 5 min of EGF stimulation. This result was consistent with the observed co-localization of PTPN21 and EGFR after stimulation (**Supplementary Figure 4.S11)**. It has been shown that MTM1 and PTPN21 increase receptor stability by regulating EGFR trafficking (Carlucci et al., 2010; Tsujita et al., 2004). When MTM1 or PTPN21 are ectopically expressed, we assume that internalized, ligand-bound EGF receptors are "trapped" in early endosomal compartments, which mature only slow towards receptor degradation. However, our data indicate that the positive function of PTPN21 is rather limited to early time points in contrast to MTM1. A similar temporal effect was observed for DUSP7, which might enhance EGFR phosphorylation by regulating a feedback mechanism in which Erk activity mediates dephosphorylation of EGFR (Prahallad et al., 2012).

In our last results section we presented a novel method to generate spatial-temporal profiles of EGFR phosphorylation from single cell populations. This method allowed us to address the questions where and when PTPs regulate EGFR phosphorylation. Our data indicate that ER-anchored PTPN1 dephosphorylates EGFR after internalization, while the cytosolic version of PTPN2 and the PM localized PTPRA are able to abolish ligand-induced phosphorylation of EGFR already at the PM. PTPRG allows EGFR phosphorylation and internalization but its activity becomes stronger over time. The positive regulators MTM1, PTPN21 and DUSP7 enhanced the phosphorylation of EGFR in early endosomal compartments by probably different underlying mechanisms. Our method allowed a direct comparison of the EGFR phosphorylation profile with the associated PTP-intensity pattern,

which indicates the amount and localization of the co-expressed PTP at every time point. Consistent with our pervious observations, we observed an enrichment of MTM1 and PTPN21 at the PM after EGF stimulation.

4.8 Supplementary data

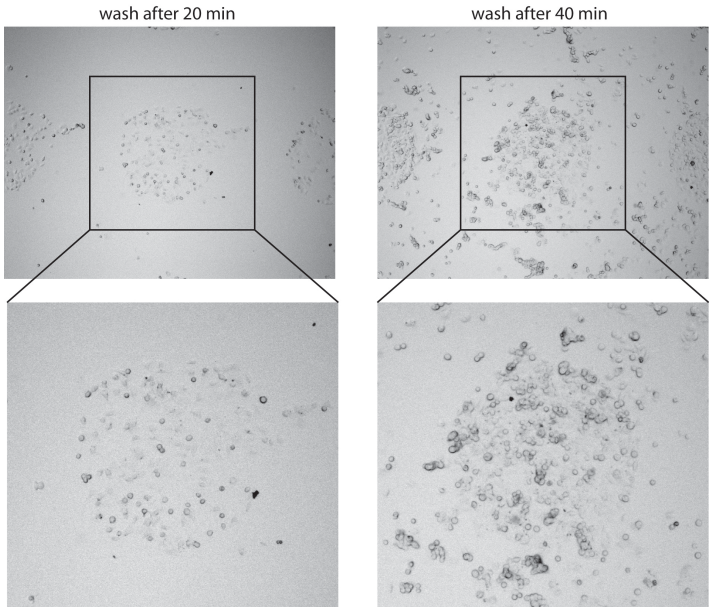

Supplementary Figure 4.S1 Effect of washing on cell seeding. HeLa cells seeded on arrays were washed 20 min or 40 min after seeding and immediately imaged under the microscope. Cell adherence on spots and the surrounding glass surface is compared. Magnification of spots acquired with 4x objective are shown (lower panel). Figure adapted from (Fengler et al., 2012)

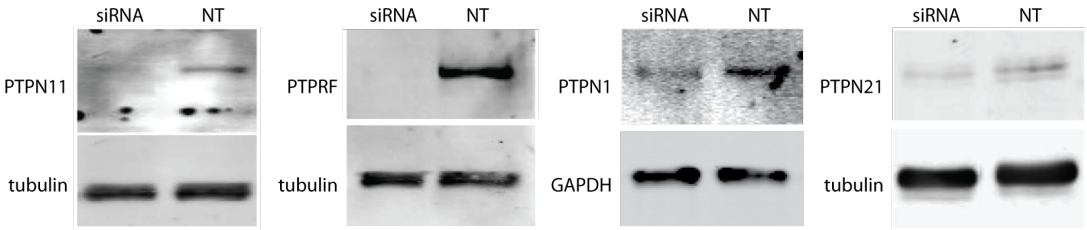

Supplementary Figure 4.S2 (a) Western blot analysis of PTP down modulation by siRNA transfection (Dharmacon, On-Target-Plus pool). MCF7 cells were transfected with siRNAs targeting PTPN11, PTPRF, PTPN1 or PTPN21. Lysates of targeting siRNA were always compared with a control lysate derived from non-targeting (NT) siRNA transfected cells. Cells were incubated for 48 hours and cell lysates were used for westernblot analysis. Specific antibodies for PTPs and house keeping genes (tubulin or GAPDH) were used for detection.

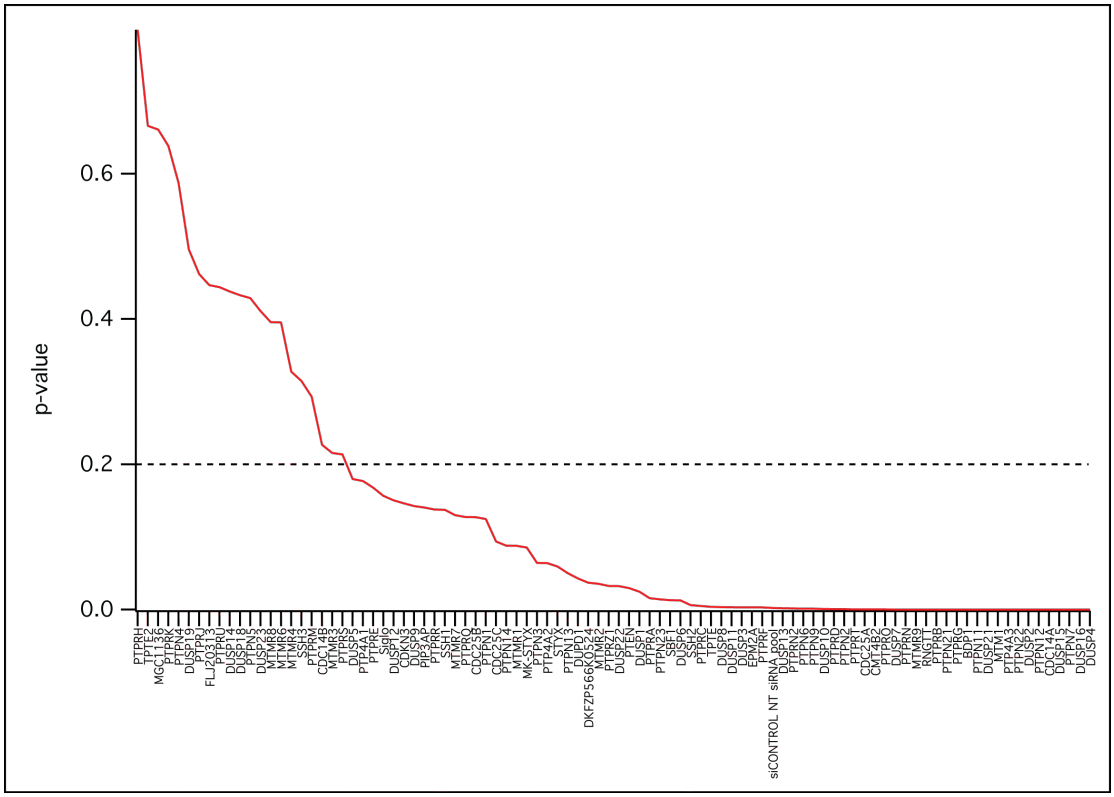

Supplementary Figure 4.S3 Two-tailed Kolmogorov-Smirnov-test of siRNA screening data. The α-distribution of each PTP obtained from single cell measurements was tested for being not identical to the control distribution (NT siRNA). p-values for every PTP is indicated.

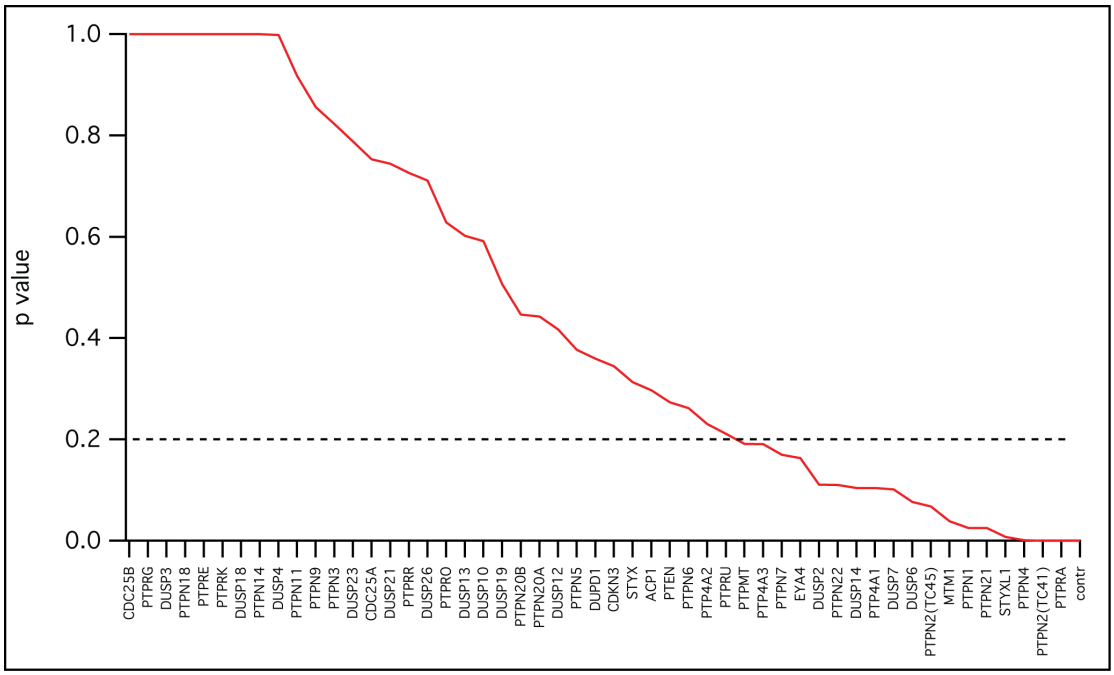

Supplementary Figure 4.S4 Two-tailed Kolmogorov-Smirnov-test of cDNA screening data. The α-distribution of each PTP obtained from single cell measurements was tested for being not identical to the control distribution. p-values for every PTP is indicated

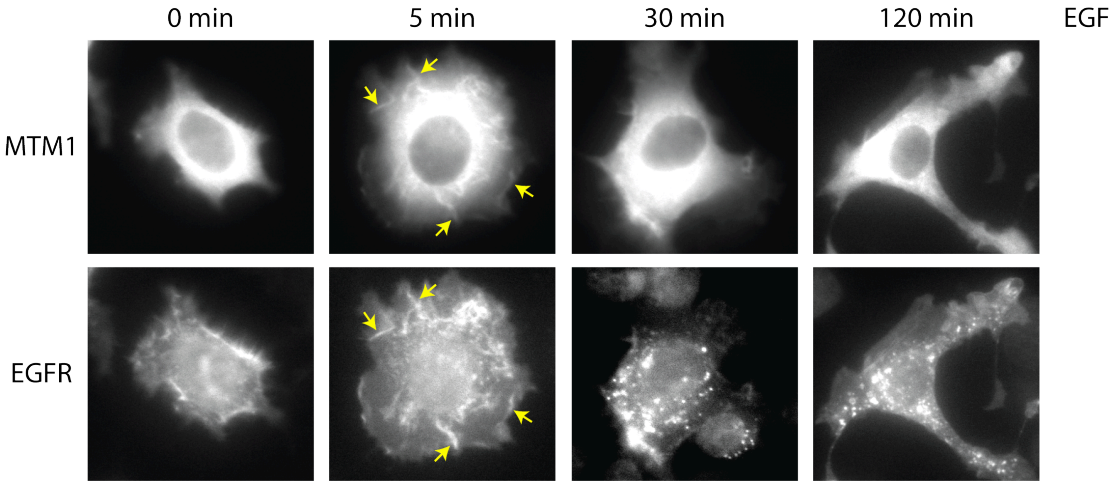

Supplementary Figure 4.S5 Transient co-localization of MTM1 and EGFR after EGF stimulation. MCF7 cells co-transfected with MTM1-mCitrine and EGFR-mTFP were stimulated with 200 ng/ml EGF for indicated time points. Yellow arrows show co-localization sites of EGFR and MTM1.

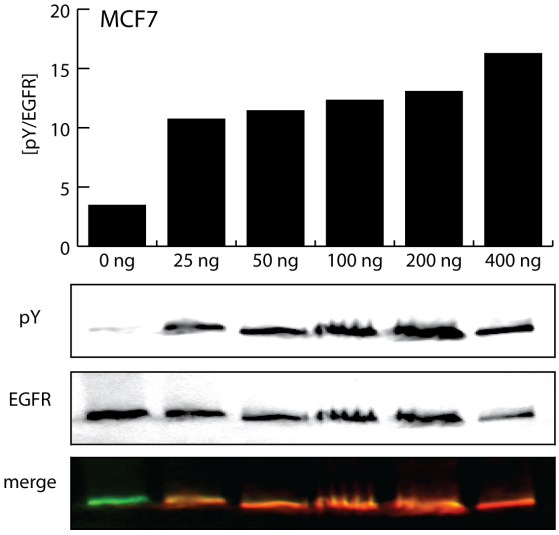

Supplementary Figure 4.S6 Dose response of EGFR analyzed by western blot. MCF7 cells were transient transfected with EGFR-mCitrine and stimulated for 5 min EGF with different concentrations ranging from 25 - 400 ng/ml. Intensity based ratios of phosphorylated (pY) and total EGFR are shown on top.

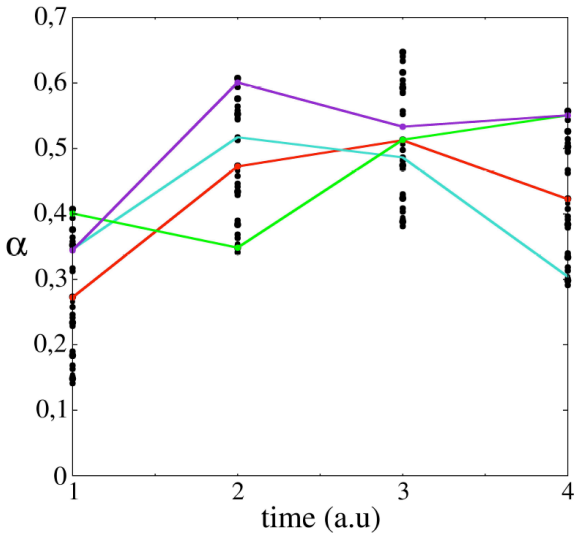

Supplementary Figure 4.S7 EGFR (α) calculated for single cells. Different temporal profiles using a permutation-based bootstrapping test by drawing 1000 random profiles. Figure provided by A. Koseska.

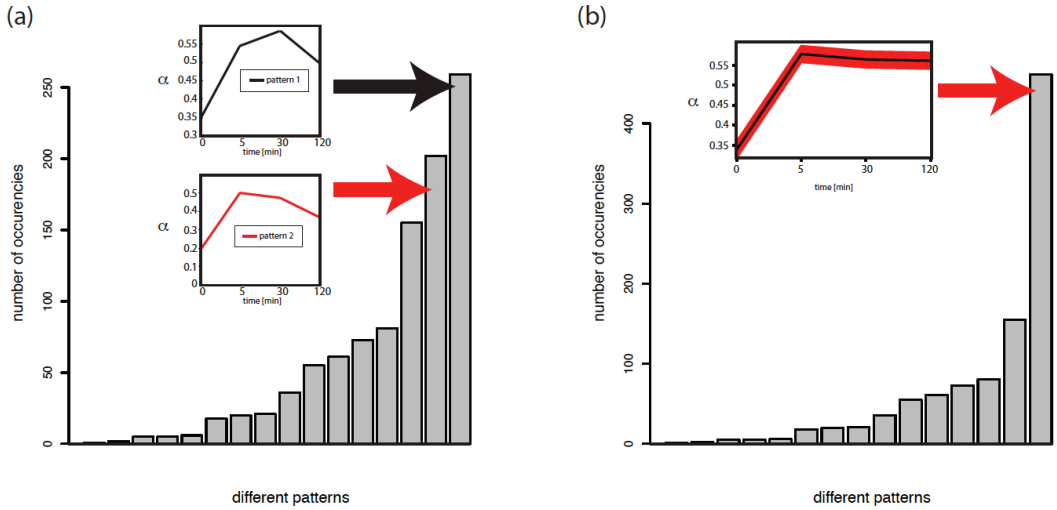

Supplementary Figure 4.S8 (a) The different patterns obtained by bootstrapping and the numbers of their occurrences are shown. (b) By combining the 2 top ranking patterns according to similarities in their shape, we determine a group of patterns, which in turn defines one of the 5 functional groups. Figure provided by A. Koseska.

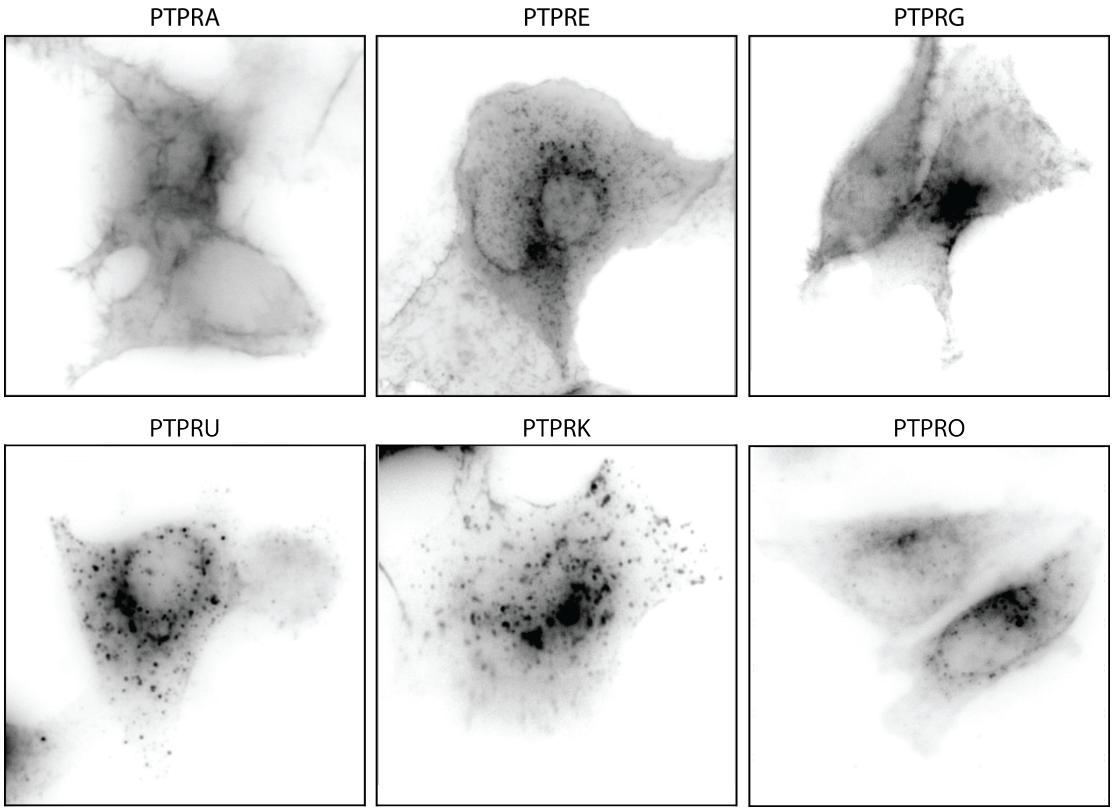

Supplementary Figure 4.S9 Localization of RPTPs in MCF7 cells. Different RPTPs mCitrine fusion proteins were transfected as indicated. Localization is shown under normal growth conditions. Fluorescence intensity inverted.

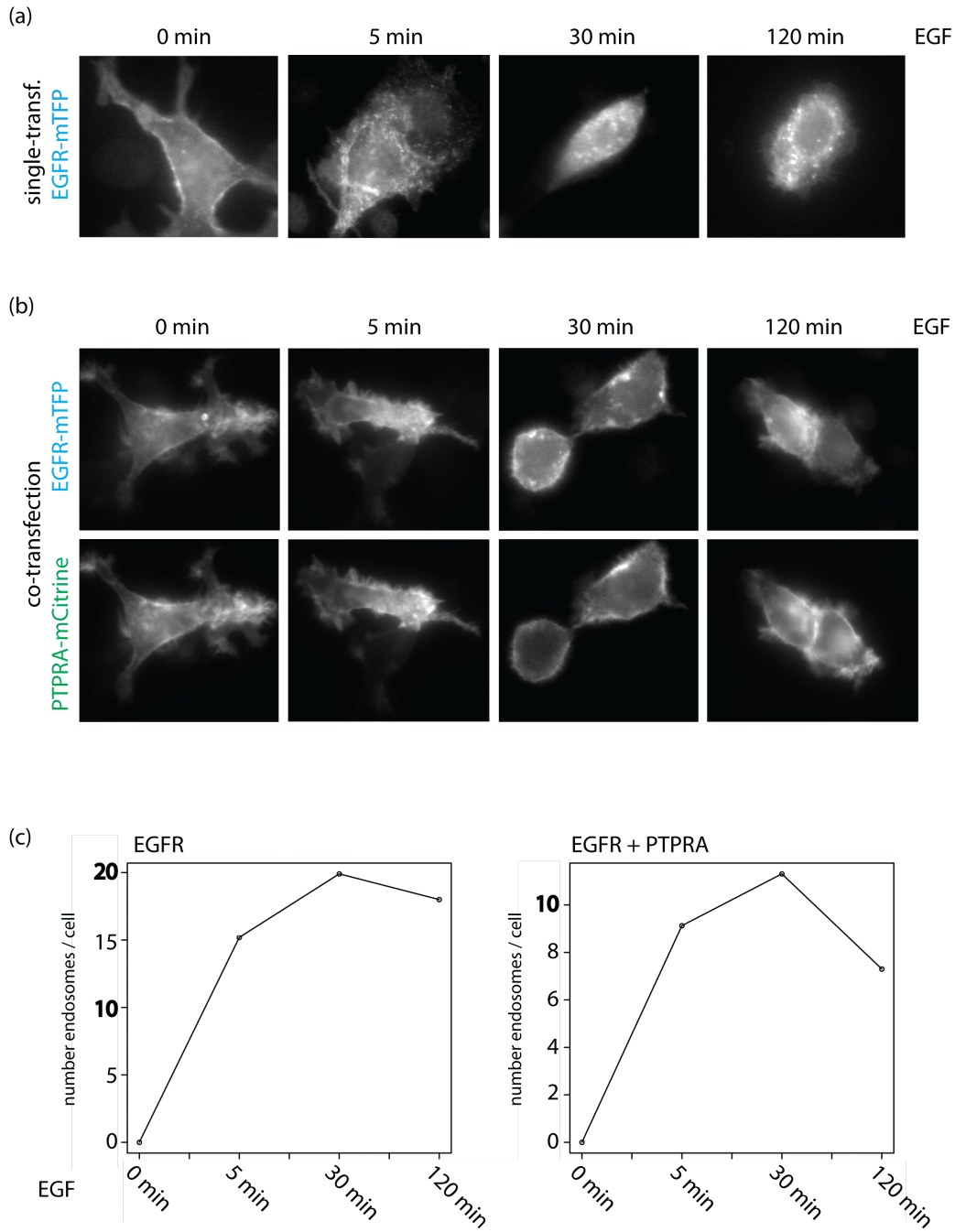

Supplementary Figure 4.S10 PTPRA co-localizes with EGFR at the PM and reduces endocytosis after EGF stimulation. MCF7 cells expressing EGFR-mTFP alone (a) or EGFR-mTFP together with PTPRA-mCitrine (b). Images of fixed cells after 5, 30 and 120 min EGF (200 ng/ml) are shown. (c) Single or co-transfected cells were stimulated with EGF-Alexa647 and fixed after indicated time points. The average-number of endosomes per cell was calculated by using the EGF-Alexa fluorescence. Endosomes were identified with cell profiler software. Averages of 10 -20 cells per time point are shown.

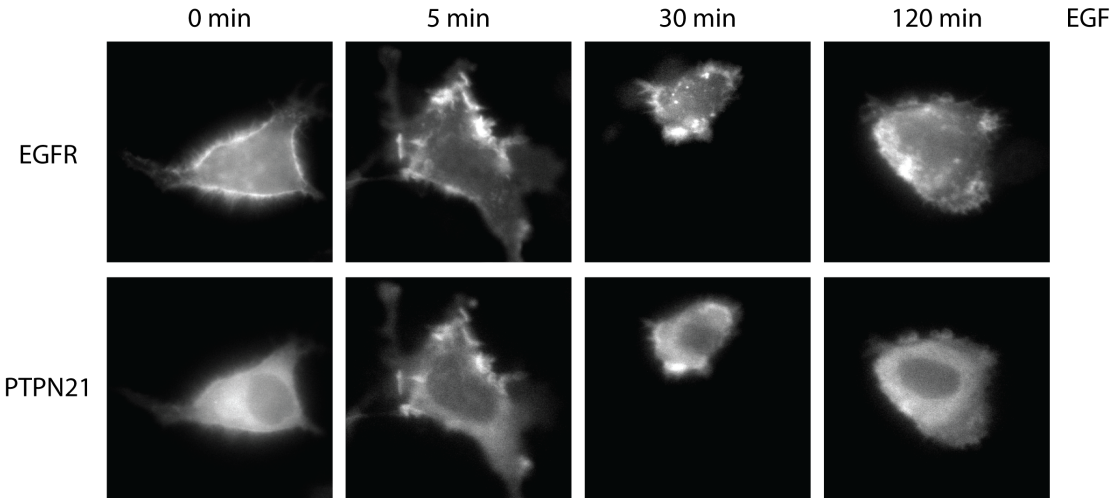

Supplementary Figure 4.S11 Transient co-localization of PTPN21 and EGFR after EGF stimulation. MCF7 cells co-transfected with PTPN21-mCitrine and EGFR-mTFP were stimulated with 200 ng/ml EGF for indicated time points.

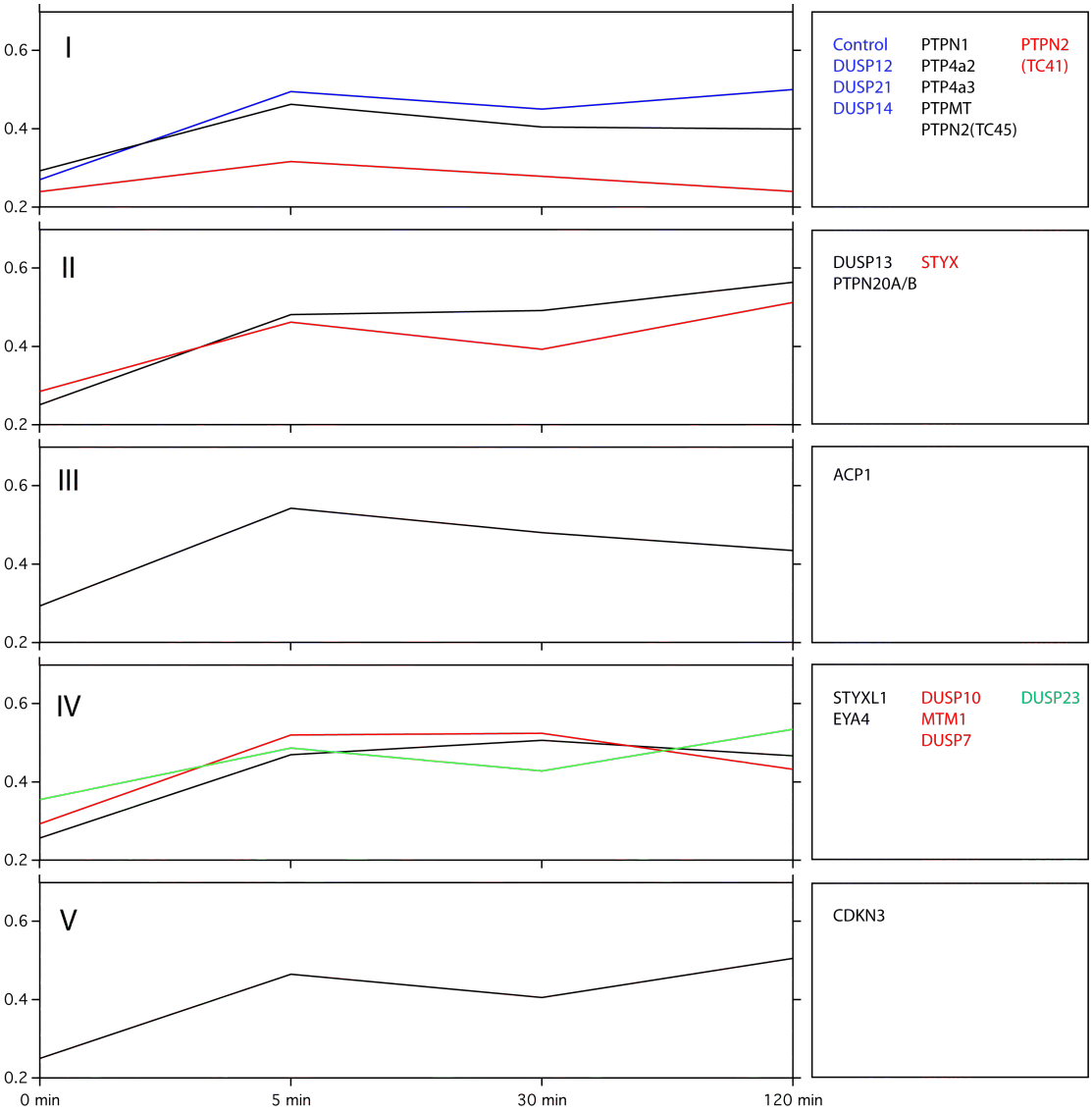

Supplementary Figure 4.S12 Amplitude clustering by affinity propagation. The 5 functional classes (I-V) derived by response-based classification are shown. Members of each class are divided into subgroups according to their change in amplitude. Control group in blue. Moderate regulators are shown in black and stronger regulators in red and green. A temporal profile is shown for each subgroup within a class. Profiles are representative for all members of a subgroup. Data presented here are from the second cDNA collection (screen 2). The clustering by affinity-propagation was provided by A. Koseska. Group III and IV contained only one candidate and makes the clustering unnecessary.

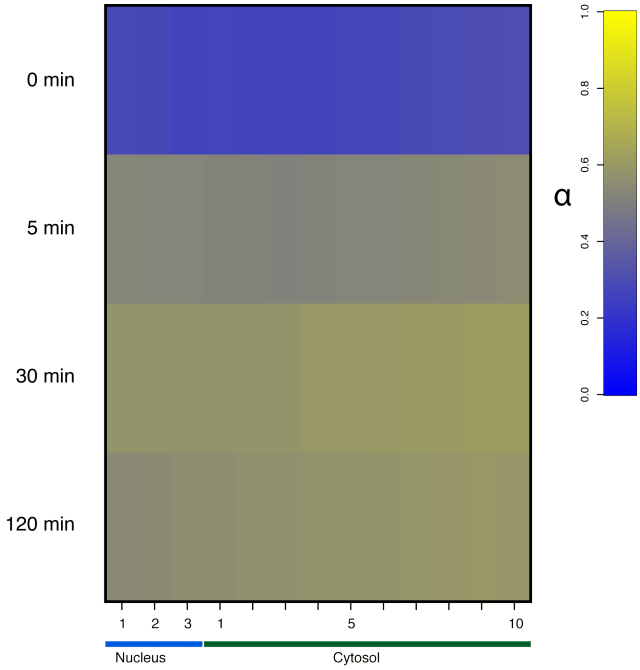

Supplementary Figure 4.S13 Spatial-temporal phosphorylation profile of EGFR. Profiles generated by radial segmentation. The area between the cell center (defined by the center of the nucleus) and the PM was divided into 10 cytosolic and 3 nuclear segments by binning. Averages of the EGFR α of each radial-bin and time point is shown as heatmap.

V DISCUSSION

It was long believed that PTPs recognize their substrates unspecific and that the regulation of growth factor signaling is dominated by the activity of protein kinases alone. Research of the last years however has shown that PTPs, equally to RTKs exert major influence in signal propagation. It has been shown that the activity of RTKs and PTPs are coupled (Reynolds et al., 2003). PTPs on the one hand, dephosphorylate specific phosphotyrosines, thus inhibiting the autocatalytic activity of RTKs. On the other hand, phosphorylated RTKs induce the local production of ROS by activating PI3K/Rac-dependent NADPH-oxidase complexes leading to reversible PTP inhibition. Due to the coupling of RTK-activation with PTP-inhibition by ligand induced ROS production, the system is bistable and responds in a switch-like manner (Reynolds et al., 2003).

Similar to other RTKs, EGFR can be activated in absence of a ligand because of its autocatalytic activity and PTPs are required to prevent such spurious receptor signals through their dephosphorylation activity. PTPs interact with EGFR during recycling, which keeps its phosphorylation level in check. RPTPs for example are able to access EGFR directly at the PM, while intracellular PTPs might interact with EGFR at the recycling endosomes. EGF binding on the other hand favors asymmetric dimer formation, resulting in increased activation and robust *trans*-phosphorylation of EGFR at the PM (Zhang et al., 2006). When a certain EGF concentration is reached, sufficient to overcome the constant dephosphorylation activity of PTPs by ROS production, the whole EGFR population at the PM undergoes a rapid self-amplifying phosphorylation wave that propagates through the cell (Verveer et al., 2000b). However, differences in the coupling of EGFR and PTP activities have direct consequences on the global phosphorylation profile of the receptor. In contrast to the double negative feedback that leads to the described lateral propagation, a negative feedback between EGFR and PTPs induces phosphorylation hot spots instead (Grecco et al., 2011b). Because of the robust phosphorylation status of EGF-EGFR complexes and recruitment of proteins required for internalization and degradation, most of the receptors exit the recycling path and become internalized (G. Xouri, unpublished data, Sabet et al., submitted). Thus, the interactions between particular PTPs and EGFR occur at specific time and

specific regions within the cell and regulate the signal duration of EGFR. Moreover, the trafficking of EGFR is also regulated by these spatially dependent interactions. In particular, dephosphorylation of specific phosphotyrosines required for EGFR degradation might rescue the receptor from degradation by supporting the recycling process.

The result of our first siRNA/cDNA screen highlighted that the regulation of EGFR by PTPs is not always associated with receptor dephosphorylation. Approximately one third of all candidates promote EGFR phosphorylation after 5 min EGF exposure **(Figure 4.10)**. We have discussed that several PTPs dephosphorylate the inhibitory phosphotyrosine of SFKs resulting in activation and phosphorylation of EGFR **(section 1.3.4)**. This mechanism is only one example how PTPs might promote EGFR phosphorylation. Possible network motives between EGFR and PTPs are shown in **(Figure 5.1)**.

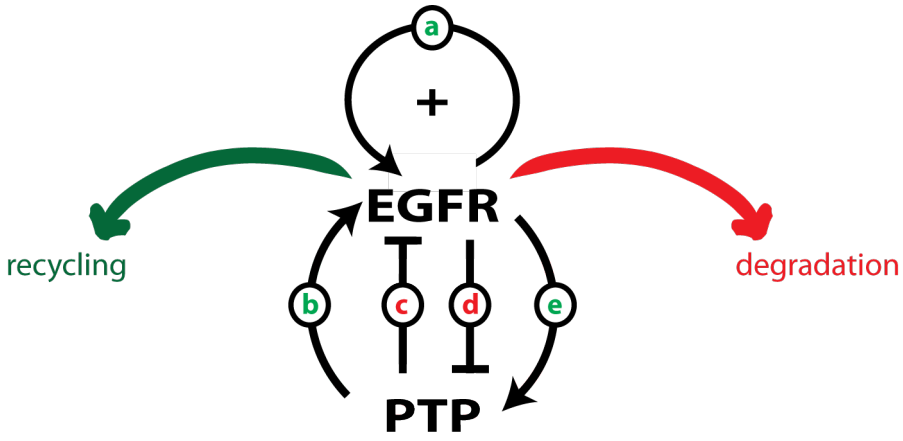

Figure 5.1 Possible coupling between EGFR and PTPs. Both PTPs and EGFR can promote or inhibit each other dependent on the given molecular context. PTPs can dephosphorylate EGFR (c) or promote receptor phosphorylation by dephosphorylating inhibitory sites of cytosolic PTKs (such as SRC) that themselves phosphorylate EGFR (b). Activation of EGFR leads to ROS production that inhibits PTPs transiently (d). SH2 domain mediated binding to phosphorylated tyrosines at the C-terminal tail of EGFR or at adaptor proteins can result in PTP activation (e). The autocatalytic activity of EGFR is indicated by the positive feedback (a). The specific phosphorylation pattern of the receptor determines whether EGFR undergoes recycling or degradation after ligand binding.

In summary, EGFR phosphorylation induced by 5 min EGF stimulation is the product of its autocatalytic property and the suppressing activity of PTPs. However, several PTPs supported EGFR phosphorylation instead. We noted that a number of PTPs do not show symmetric effects upon opposite perturbations **(Figure 4.10)**. The reasons can be manifold: *i)* if the expression levels of the endogenous proteins are low, siRNA might not induce significant differences in EGFR phosphorylation; *ii)* similar when the endogenous expression is very high, ectopic expression might not induce detectable differences in EGFR phosphorylation because the relative increase of PTPs might be too low; *iii)* quantifying the amount of PTP down-modulation necessary to induce significant effects is not possible, and *iv)* regulation of EGFR phosphorylation might be threshold dependent: only specific PTP expression levels can significantly modulate the EGFR phosphorylation pattern. Additionally, the spatial PTP localization might not contribute to early (5 min after EGF) modulation of EGFR phosphorylation. We therefore performed quantitative measurements of EGFR phosphorylation over a longer time span.

5.1 Five functional groups of PTPs regulate EGFR dynamics

Differences in the temporal phosphorylation pattern of RTKs are associated with different changes in downstream-protein dynamics that encode distinct cellular responses (Nagashima et al., 2007). Several studies have shown that perturbations of PTPs, which in particular regulate the phosphorylation level of RTKs, result in changes of the cellular responses induced upon receptor stimulation (Prahallad et al., 2012; Sun et al., 2011; Tarcic et al., 2009; Yuan et al., 2010). It has also been shown that EGFR undergoes transient phosphorylation upon EGF stimulation in most tissue culture cells containing normal protein levels of EGFR (Marshall, 1995; Nagashima et al., 2007). Ectopic expression of fluorescent EGFR fusion proteins in MCF7 cells that allow the measurement of its phosphorylated fraction by FRET-FLIM, mimics the EGF-induced sustained phosphorylation of EGFR observed in epithelial cancer cells that express unusually high levels of the receptor (Hyatt and Ceresa, 2008; Sturani et al., 1988). Consistent with the literature, MCF7 cells ectopically expressing EGFR showed a sustained phosphorylation profile of EGFR over the duration of 2 hours (Hsu et al., 2011; Wouters and Bastiaens, 1999). In particular, studies in which EGFR was overexpressed in PC12 cells showed that the RTK activity directly influences the duration of Erk activity and thereby controls the cellular response. EGFR overexpressing PC12 cells showed a more sustained Erk activity upon EGF stimulation (Traverse et al., 1994) and undergo differentiation instead of proliferation. Computational analysis showed that the duration of Erk activity was more prolonged upon by increasing EGFR density in comparison to physiological concentrations of EGFR that caused transient Erk phosphorylation (Schoeberl et al., 2002).

In comparison to previous screens that were based on measurements of fold-changes in phosphorylation under perturbed conditions (Tarcic et al., 2009; Yuan et al., 2010), we have addressed how PTP expression changes the temporal phosphorylation profile of EGFR. Moreover, we categorized PTPs according their influence on EGFR phosphorylation dynamics (**Figure 4.14)**. In summary, we have identified five distinct functional groups of PTPs that induce distinct

phosphorylation profiles ranging from a reduced overall amplitude (I), as well as a delayed (II), transient (III), limited sustained (IV) or an oscillation-like shape (V). A schematic overview of all five functional groups is provided in **(Table 5.1)**. The majority of the PTPs identified as EGFR regulators are localized in the cytosol or share the nuclear/cytosolic compartment. In particular, a cytosolic localization allows the access to EGFR before and during stimulation. Most PTPs of group I, II and IV showed a cytosolic localization including those that showed an early regulatory function, regardless whether they function as a supporter or suppressor of EGFR phosphorylation. For example, in group I we measured a stronger regulation of EGFR by the cytosolic isoform of PTPN2 (TC41) as compared to the nuclear isoform TC45, which translocates to the cytosol in an EGF-induced manner (Tiganis et al., 1999). The ectopic expression of group I PTPs resulted in a lower phosphorylation amplitude of EGFR probably due to a consistent dephosphorylation activity on EGF-EGFR complexes. In contrast to group I PTPs, the candidates of group II permit a higher EGFR phosphorylation amplitude over time. For example, it has been shown that DUSP3 associates with EGFR under basal conditions but dissociates upon EGF stimulation. Due to this decrease in association after stimulation, it can be assumed that the ligand bound EGFR reaches higher phosphorylation levels due to its autocatalytic properties. Notably, both positive regulators (MTM1 and DUSP7) that were identified in our primary siRNA/cDNA screen were classified into group IV. We later validated their supporting function by using automated microscopy with 8 well chambers. Using the same method we also identified a similar function for PTPN21. Positive regulators induce a higher variance in EGFR phosphorylation, adding to the difficulty in identifying such regulators. To overcome this technical problem, we utilized and quantified the differences in the cell-to-variance to validate the positive regulatory function of MTM1, DUSP7 and PTPN21 **(Figure 4.18)**. In contrast to the other 4 groups (I, II, III and V) of negative regulators, positive regulators are only found in group IV, which might suggest that these PTPs induce a similar response pattern of EGFR phosphorylation.

Gene	Protein	Regulators at 5 min EGF [result siRNA/cDNA screen]	Cluster [result over 5 screens]	regulatory strengh	Localization
PTPN1	PTP1B	significant neg. effects	I	moderate	ER
PTPN2 (TC45)	TCPTP, iso2	significant neg. effects	I	-	Nu, (Cy)
PTPN2 (TC41)	TCPTP, iso3	significant neg. effects	I	strong	Nu, Cy
PTPN9	MEG2	-	I	moderate	(Cy)
PTPRA	RPTPα	significant neg. effects	I	moderate	PM
PTPMT	PLIP	-	I	-	Cy
PTP4A2	PRL2	-	I	-	PM, Cy
PTP4A3	PRL3	-	I	-	PM, E
PTPN6	SHP1	neg. effects	II	-	Nu, Cy
DUSP3	VHR	neg. effects	II	moderate	Nu, Cy
PTPN14	MEG1	-	II	strong	Cy
PTPN18	BDP1	-	II	moderate	Nu, Cy
PTPN20A/B	TypPTP	-	II	-	Cy
DUSP4	MKP2	-	II	moderate	Nu
DUSP13	TMDP	-	II	-	Nu, Cy
DUSP19	SKRP1	-	II	strong	Cy
STYX	STYX	neg. effects	II	moderate	Cy
ACP1	LMPTP	-	III	-	Cy
PTPRE	RPTPε	-	III	-	PM, E
PTPRG	RPTPγ	neg. effects	III	moderate	PM, E
PTPRU	RPTPλ	-	III	moderate	PM, E
DUPD1	FMDSP	-	III	-	Cy
PTPN21	PTPD1	-	IV	(/)	Cy
PTPRO	GLEPP1	pos. effects	IV	-	PM, E
DUSP7	MKPx	segnificant pos.effects	IV	(/)	Cy
DUSP10	MKP5	pos. effects	IV	(/)	Nu, Cy
DUSP23	MOSP	-	IV	(/)	Nu, Cy
MTM1	myotubularin	segnificant pos.effects	IV	(/)	Cy, PM
STYXL1	MK-STYX	-	IV	-	Nu, Cy
EYA4	EYA4	-	IV	-	Nu, Cy
PTPRK	RPTPκ	-	V	moderate	PM, E
PTPN5	STEP	-	V	moderate	ER
PTPN7	HePTP	pos. effects	V	-	Cy
CDKN3	KAP	-	V	-	Cy

Table 5.1 Overview of identified phosphatases modulating temporal EGFR phosphorylation profile. PTPs are colour-coded according to their classification (I-V). PTP names in bold letters indicate a previously identified regulatory function in EGFR phosphorylation (see text for details). PTPs that showed reciprocal effects after 5 min EGF stimulation in the siRNA/cDNA screenings are indicated in red (negative function) or green (positive function). Significant effects are indicated that showed a p-value < 0.1 in both siRNA and cDNA experiments using a KS-test. Regulatory strength determined by affinity propagation is shown for PTPs that have induced moderate or strong changes of EGFR phosphorylation. Localization of PTPs is indicated in the last column: Nu: nucleus, Cy: cytosol, PM: plasma membrane, E: endosomes, ER: endoplasmic reticulum.

The localization of RPTPs at the PM would suggest their involvement in early regulation of EGFR. Notably, several receptor-like PTPs predominantly induced a transient response in EGFR phosphorylation and were therefore classified into group III and V. We observed that these RPTPs were, in fact, not explicitly localized at the PM and also occupy endosomal structures, which might permit a direct interaction with EGFR after internalization. It is possible that

most of these RPTPs also have the potential to regulate EGFR at early time points, but their activity might be inhibited at this time. For example, it has been shown that PTPRE associates with microtubules immediately after EGF stimulation resulting in a transient phosphatase inhibition (Sines et al., 2007). Several RPTPs are also known to be Src activators, which could explain their supporting function in EGFR phosphorylation **(section 1.3.5)**. In addition, recent studies have provided novel insights about how and which PTPs are regulated by ROS, in what can be thought of as a general mechanism to explain the transient inhibition of RPTPs (Karisch et al., 2011; Tonks, 2006). However, exactly why RPTPs of group III and IV are more prone for ROS-mediated oxidation than others, i.e. PTPs of group I and II, remains to be addressed. Due to the local ROS production at the PM, it could be assumed that the localization of RPTPs might favor their reversible oxidation in contrast to more distal cytosolic PTPs. Surprisingly, PTPRA which was classified to group I, induced an overall reduction of EGFR phosphorylation amplitude and, according to our results, is not transiently inhibiting EGFR after EGF stimulation. Moreover, PTPRA was also not localized in endosomal structures and therefore should not be able to interact with EGFR after internalization. We found that this RPTP suppresses EGFR endocytosis to trap EGF-EGFR complexes at the PM, which might instead induce constant receptor dephosphorylation. A schematic overview about all 5 functional groups is provided in **Figure 5.2**.

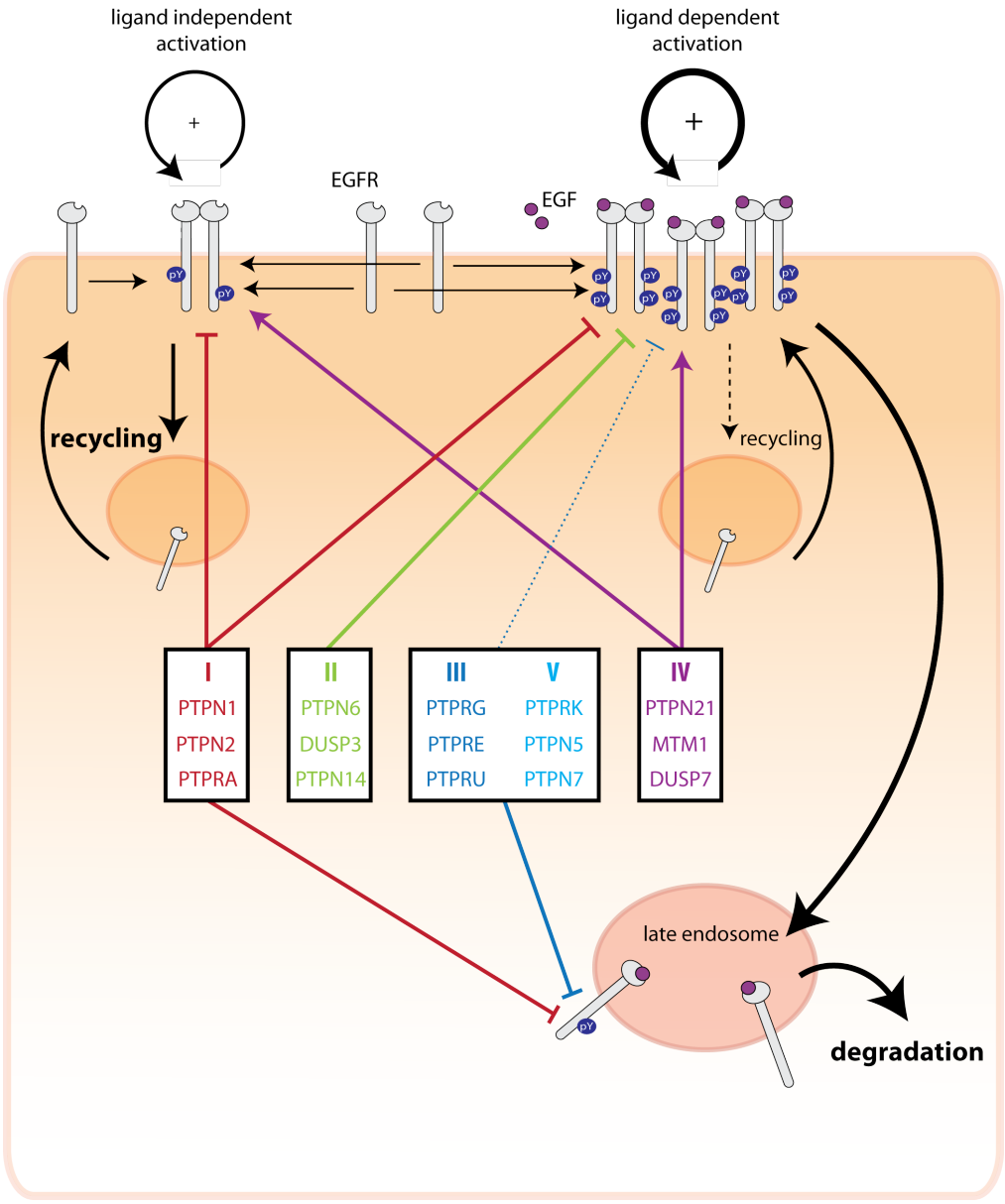

Figure 5.2 Spatial-temporal regulation of EGFR phosphorylation by PTPs in presence and absence of EGF. Inhibitory and supporting functions are indicated for each group (I-V) of PTPs. Examples of PTPs in each group are shown. PTPs in group I reduced the overall amplitude of EGFR phosphorylation after EGF binding. Single cell correlation analysis have also highlighted that such PTPs also reduce the basal phosphorylation state of EGFR. In contrast, PTPs in group II reduced the EGFR phosphorylation immediately after EGF stimulation (5 min EGF). We summarized group III and V because of their similar regulatory functions. Both groups permit a transient response of EGFR phosphorylation. Most members of these two groups reduced the EGFR phosphorylation immediately after stimulation, but in general showed a stronger regulatory potential at late time points (e.g. 30 min EGF). Several candidates of group IV provided a supporting function of EGFR phosphorylation immediately after EGF stimulation. PTPN21 and MTM1 especially showed also a positive effect under basal conditions. As discussed in the text, we note that not all PTPs classified in group IV demonstrate a supporting function.

5.2 Tonic suppression and EGFR density

It has been shown that ectopic EGFR expression in HEK293 or CHO cells is sufficient to induce activation and phosphorylation of the EGFR population in absence of ligand (Lammers et al., 1993; Vogel et al., 1993; Xu et al., 2005). Moreover, recent work from *Endres* and colleagues (2013) showed that EGFR density correlates exponentially with the phosphorylation of EGFR in COS-7 cells in the absence of ligand. In order to measure EGFR phosphorylation in our experiments, we exogenously expressed a fluorescent EGFR version (as FRET-donor) in MCF7 cells, which in turn enhances the concentration of the receptor in our analyzed cells. In a similar experiment, it has been shown that the phosphorylated fraction (α) of expressed EGFR-YFP positively correlated with its YFP intensity in MCF7 cells treated with unspecific phosphatase inhibitor pervanadate (Grecco et al., 2010). The correlation between phosphorylation response and expression provides an indicator for the autocatalytic property of EGFR (Grecco et al., 2010). To clarify weather the ectopic EGFR expression in MCF7 cells influences the phosphorylated fraction of the receptor in absence or after EGF stimulation we revisited our single cell data. Similar to the work from *Grecco* and colleagues (2010), we observed positive correlations between EGFR phosphorylation and its protein level **(Figure 5.3).** However, in comparison to unstimulated cells, we observed higher slopes when cells were stimulated with EGF. In absence of EGF, only a small fraction of cells showed comparable phosphorylation amplitudes as measured in EGF stimulated samples. The range of EGFR-mTFP fluorescence intensity was generally constant over the different samples (0, 5, 30, and 120 min) and we could exclude the possibility that cells in the unstimulated samples had a lower amount of EGFR as compared to stimulated cells.

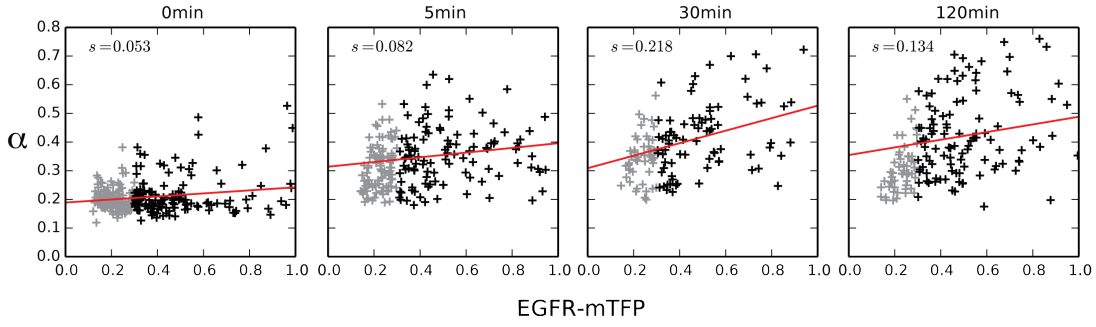

Figure 5.3 Single cell correlation of EGFR phosphorylation (α) vs EGFR intensity (mTFP) in MCF7 cells. FLIM measurements were done by using EGFR-mTFP (FRET-donor) and Cy3.5 (FRET-acceptor) conjugated anti-pY antibody. Times of EGF stimulations (200 ng/ml EGF) are indicated. Cells with a lower intensity than 0.3 were excluded from the fit.

In contrast to the findings in HEK293 or CHO cells in which ectopic EGFR expression resulted in spontaneous EGFR activation (Lammers et al., 1993; Vogel et al., 1993; Xu et al., 2005), EGFR expression in MCF7 cells did not lead to spontaneous receptor activation and was only detected in a few cells of the population. We observed a low but positive correlation in the absence of EGF, indicating a slightly higher basal phosphorylation of cells that express higher EGFR amounts. However, the phosphorylated fraction of such cells was generally low in comparison to stimulated cells. Because of the positive slope, it can be assumed that the probability of spontaneous activation might be favored with higher EGFR levels. MCF7 cells have a relatively low level of endogenous EGFR in comparison to other cell lines (Coticchia et al., 2009) and it might be that the level of exogenously expressed EGFR is still not sufficient to reach a receptor concentration at the PM that is required for spontaneous activation. In contrast to our generic anti-phosphotyrosine antibody, the work of *Endres* and colleagues was (2013) based on quantitative intensity measurements of antibodies detecting specific phosphorylation sites of EGFR (pY1068 and pY1173). However, similar to our findings, the authors showed higher EGFR phosphorylation levels and steeper slopes when cells were stimulated with EGF in comparison to basal conditions (Endres et al., 2013).

Several PTPs were previously identified as negative regulators under basal conditions **(section 1.3.4)**. In these studies, EGFR was ectopically expressed in HEK293 or CHO cells resulting in expression-induced EGFR phosphorylation. After co-transfection of PTPN1, PTPN2 or PTPN6 the expression-induced receptor phosphorylation was reduced (Lammers et al., 1993; Vogel et al., 1993). Recent data have shown that ligand independent activation of EGFR induced a lower phosphorylation of pY1045 in comparison to EGF stimulated cells (G. Xouri, unpublished data). As mentioned, pY1045 is required for Cbl binding and ubiquitylation that targets the receptor for degradation. This finding shows that ligand-independent receptor activation does not result in receptor degradation. Instead, EGFRs that are not phosphorylated at pY1045 might undergo recycling. According to the work from *Lammers* (1993) and *Vogel* (1993), it can be assumed that PTPN1, PTPN2 and PTPN6 dephosphorylate active EGFR during recycling.

In our screening results with MCF7 cells that are not prone to expression-induced activation, few negative regulators classified in group III and V have indicated a potential to decrease the basal phosphorylation level of EGFR, including PTPRG, PTPRU, PTPRK, PTPN5 and PTPN7 **(Figure 4.14)**. On the other hand, we detected an enhanced EGFR phosphorylation when MTM1, DUPS7 or DUSP10 that where classified in group IV were co-expressed. These changes in EGFR phosphorylation were not consistent over the 5 performed screens, but we validated some of these findings in our follow up experiments in 8 well chambers by performing single cell correlation analysis **(Figure 4.17)**. We observed a negative correlation of EGFR phosphorylation and the expression level of PTPN2 (TC41), clearly indicating its function as negative regulator at basal conditions. In contrast, MTM1 expression indicated a supporting role of EGFR phosphorylation in absence of ligand. Moreover, quantification of single cell experiments also indicated a lower variance in EGFR phosphorylation of PTPN1, PTPN2, PTPRA and PTPRG expressing cells. Opposing effects were observed for MTM1 and PTPN21 that showed a slightly higher variance compared to control cells. In summary, we conclude that this set of PTPs influences the phosphorylation level of EGFR population under basal conditions **(Figure 5.2)**. Whether the different

level of basal phosphorylation influences the activation threshold for ligand-dependent activation has to be addressed. In contrast, we could not detect an increased variance of EGFR phosphorylation when DUSP7 was expressed and it can be assumed that its positive function is dependent on EGF stimulation. More studies have to be performed to identify other PTPs that are involved in the regulation of the basal phosphorylation level of EGFR.

5.3 PTPs regulate phosphorylation and trafficking of EGFR

We have presented a novel method that allows the transformation of high throughput microscopy data into spatial-temporal profiles. This method provides us with a tool to quantify when and where PTPs regulate EGFR phosphorylation. The resulting spatial-temporal phosphorylation profile of EGFR upon ectopic expression of different PTPs yielded different patterns of signaling propagation.

Phosphatases including MTM1, PTPN21 and DUSP7 induced a larger increase in EGFR phosphorylation immediately after EGF stimulation. It can be speculated that MTM1 and PTPN21 enhance the stability of internalized EGF-EGFR complexes in early endosomes by either modifying the lipid content at endosomal membranes (Tsujita et al., 2004) or by regulating proteins involved in vesicular trafficking (Carlucci et al., 2010), respectively. Both mechanisms might reduce the flux of activated EGFR towards late endosomes or lysosomes. We assume that the resulting high density of accumulating EGF-EGFR complexes in endosomal compartments explains the overall enhancement of EGFR phosphorylation after internalization. In contrast to MTM1 and PTPN21, which regulate EGFR trafficking, DUSP7 might instead regulate the activity of Erk and thereby modulate the negative feedback loop in which Erk-activated CDC25 dephosphorylates EGFR (Prahallad et al., 2012).

On the other hand, negative regulators including PTPN1, PTPN2 and PTPRA strongly reduced EGFR phosphorylation. Our data suggest that ectopic expression of such PTPs can abolish the axial phosphorylation signal after EGF stimulation. As discussed, we could observe that PTPRA reduces the number of endosomal structures after EGF stimulation, highlighting its negative effect on receptor internalization. We could show that PTPRG allows ligand-induced EGFR phosphorylation to a certain extent, but its dephosphorylating activity becomes stronger over time. Studies on clathrin-dependent endocytosis have shown that the internalization of EGFR requires its phosphorylation at specific binding sites. In particular, mutations of Y1068 and Y1086 phosphorylation sites at the C-

terminus resulted in a decrease of internalization (Jiang et al., 2003b). Moreover, pY1045, pY1068 and pY1086 are required for the interaction with the ubiquitin ligase Cbl that regulates receptor degradation by ubiquitylation (Jiang et al., 2003b; Levkowitz et al., 1999; Waterman et al., 2002). Recently, it has been reported that ubiquitylation of EGFR is determined by the cooperative recruitment of Cbl, in complex with Grb2 resulting in a threshold response (Sigismund et al., 2013). The same authors found that this interaction is dependent on the simultaneous presence of two phosphotyrosines, pY1045 and either one of pY1068 or pY1086, on the same EGFR moiety. Studies with an EGFR Y1045F mutant demonstrated decreased degradation of the EGFR, as well as efficient recycling of EGFR to the PM (Grovdal et al., 2004). Several PTPs dephosphorylate Cbl binding sites **(Table 1.1)** and it can be assumed that such interactions directly influence the degradation of ligand-bound EGFR. In particular, it has been shown that PTPN1, PTPN2, PTPRA but also PTPRG dephosphorylate pY1068 *in vivo* (Barr et al., 2009). In summary, such negative regulatory PTPs reduce both the downstream signaling and the degradation rate of ligand-bound EGFR. According to our result, PTPN1, PTPN2 (TC41) and PTPRA might induce a decelerated translocation of EGFR to late endosomes, and those receptors that eventually reach the endocytic compartment have only a limited number of phosphotyrosine docking sites. In particular, the negative regulation of PTPRG became stronger after EGFR internalization highlighting a second level of system control after ligand-induced EGFR phosphorylation. As discussed before, PTPRG might undergo transient inhibition and allow transient activation of downstream pathways, but might also function as a late suppressor of receptor degradation. Notably, the report from *Barr* and colleagues (2009) showed that all four negative regulators PTPN1, PTPN2, PTPRA and also PTPRG dephosphorylate a small peptide containing the pY674 site of Cbl, which could explain their collective inhibitory role in EGFR degradation. **Figure 5.4** shows a possible model of how different PTPs might affect EGFR trafficking.

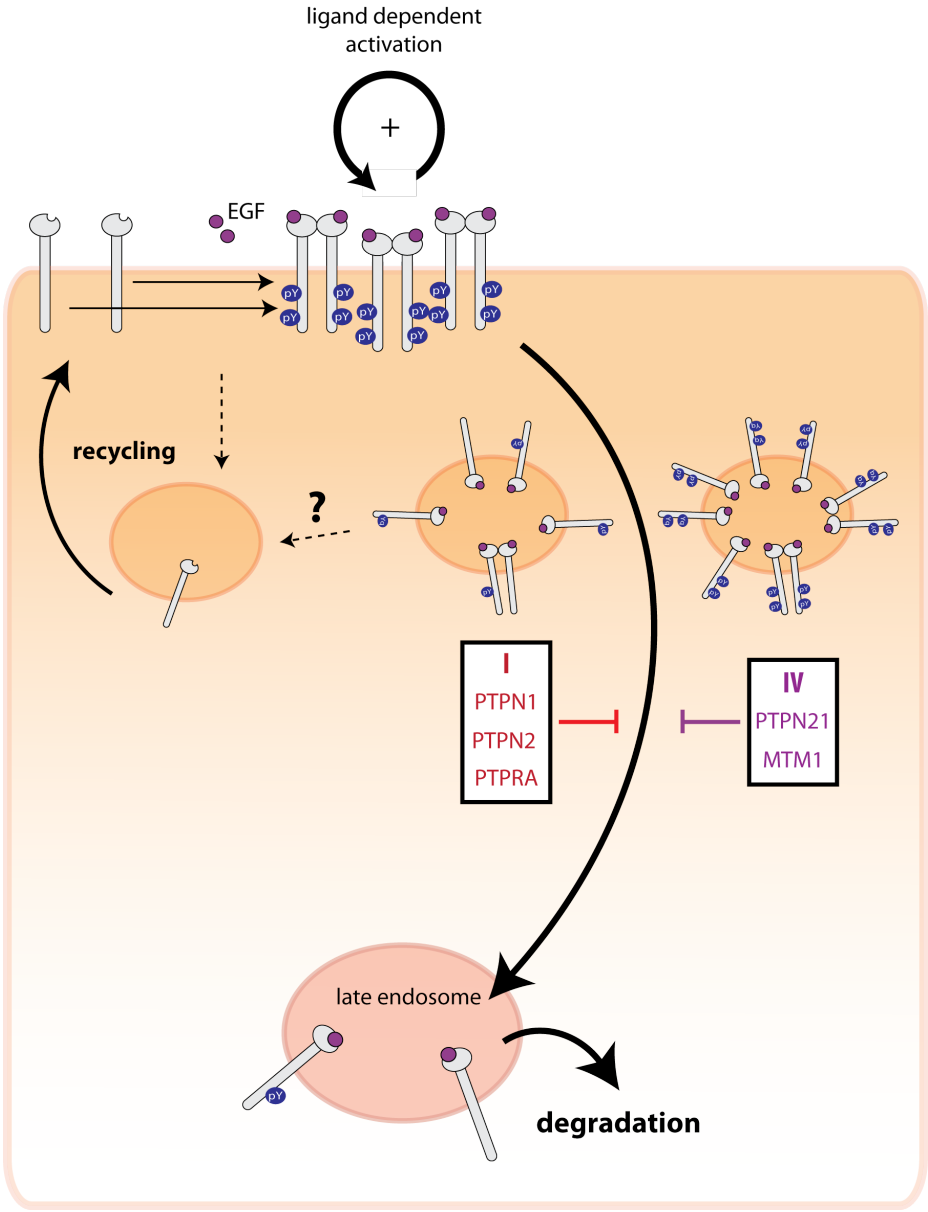

Figure 5.4 A model representing the effect of PTPs on EGFR trafficking. Expression of group I PTPs reduced or nearly abolished EGFR phosphorylation early after EGF-induced endocytosis. Early dephosphorylation activity of PTPs towards Cbl binding sites (pY1045, pY1068 or pY1086) might result in reduced ubiquitylation and decelerates receptor degradation. Consequently, these PTPs have the potential to abolish EGFR downstream signaling and might support EGFR recycling. In contrast, PTPN21 and MTM1 (group IV) could inhibit EGFR degradation by regulating the trafficking machinery. Both phosphatases enhanced EGFR phosphorylation early after EGF stimulation. An accelerated internalization, but an inhibited degradation might lead to an accumulation of ligand-bound EGFR in endosomal structures. The high receptor density in those compartments might enhance the overall phosphorylation of EGFR.

5.4 The sustained phosphorylation of ectopically expressed EGFR is mediated by a saturated degradation machinery

As already discussed, our biochemical analysis **(Figure 4.11)** indicated a sustained phosphorylation profile of EGFR at high levels of EGFR. Moreover, ectopically expressed EGFR was not degraded after EGF stimulation, even after 2 hours of stimulation. We assume that the high level of EGFR present in these cells might saturate the degradation machinery. The overload of internalized EGFR after cell stimulation might lead to a much slower degradation rate compared to normal EGFR expression levels. This could also explain the sustained phosphorylation profile that has been previously described (Hsu et al., 2011; Wouters and Bastiaens, 1999). It has been reported that 1 hour after EGF stimulation ectopically expressed EGFR-GFP co-localizes with lysosomal markers (Offterdinger and Bastiaens, 2008). In contrast, expression of an EGFR-GFP Y1045F mutant showed no co-localization with lysosomal compartments, even after 2 hours stimulation (Offterdinger and Bastiaens, 2008). To further clarify why ectopic EGFR expression induces a sustained EGFR phosphorylation profile, we performed a co-transfection experiment with Cbl. Consistent with our hypothesis, we observed a rapid reduction of EGFR phosphorylation when Cbl was co-transfected in MCF7 cells **(Figure 5.5)**. The expression of Cbl changed the phosphorylation profile of EGFR from a sustained **(Figure 4.21 a)** to transient profile.

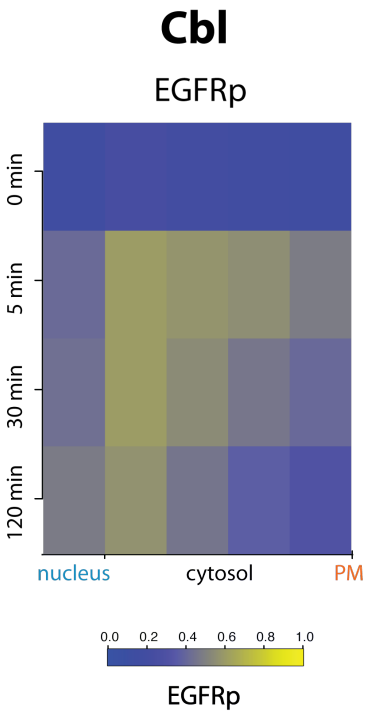

Figure 5.5 Spatial-temporal phosphorylation profile of EGFR in MCF7 cells co-expressing Cbl. Profile was generated similar as described in **section 4.7**. For comparison, see the spatial-temporal phosphorylation profile of EGFR expressing MCF7 cells (contr.) in **(Figure 4.21 a)**.

5.5 Closing remarks

The understanding of how distinct cell responses can be induced by different external growth factors using shared signaling protein modules remains one of the major challenges of systems biology. Insights into this issue came from studies with PC12 cells, a model for neuronal differentiation (Greene and Tischler, 1976). Stimulation of PC12 cells with NGF resulted in a sustained Erk activity and cell differentiation, whereas EGF stimulation induced a transient Erk activity and cell proliferation (Marshall, 1995). The observation that the signaling duration of the MAPK Erk determines the response of a cell was later extended to other cellular models and other growth factors (Murphy et al., 2002; Nagashima et al., 2007; Neve et al., 2002; Thottassery et al., 2004). On the level of RTK regulation, differences of receptor degradation upon ligand binding were associated with differences in the cellular response. Primary studies have shown that both NGF and EGF are internalized by PC12 cells, but at different rates and to different extents (Chandler and Herschman, 1983). While sequestration happens rapidly and nearly quantitatively for bound EGF, NGF sequestration was slower due to counteracting dissociation reactions. The same authors showed that EGF and NGF are degraded, but internalized EGF was degraded to a greater extent than NGF (Chandler and Herschman, 1983). As mentioned before EGF bound EGFR undergoes ubiquitylation mediated by Cbl, which targets the receptor for rapid degradation in lysosomal compartments. In contrast, NGF bound TrkA showed a significantly higher recycling rate compared to EGF-EGFR complexes (Chen et al., 2005). A rapid internalization and degradation as observed for EGFR would therefore lead to a transient phosphorylation signal inducing cell proliferation, whereas the low degradation rate of NGF-TrkA complexes would generate a sustained Erk signal that results in cell differentiation in PC12 cells (Chen et al., 2005). Similar to PC12 cells, different growth factor ligands induce distinct kinetics of Erk activity in MCF7 cells (Neve et al., 2002; Thottassery et al., 2004). Different ErbB ligands, EGF and heregulin (HRG), induce dose-dependent transient and sustained Erk activity, which was then associated with proliferation and differentiation of MCF7 cells respectively (Nagashima et al., 2007). Accordingly, EGF and HRG treatments resulted also in

different phosphorylation dynamics of ErbB receptors. As mentioned, EGF induced a transient response of EGFR phosphorylation in MCF7 cells, whereas HRG induced a sustained phosphorylation of EGFR and ErbB2 (Nagashima et al., 2007).

Considering that PTPs are able to control the signal duration of activated EGFR by regulating the phosphorylation state and the degradation velocity of the receptor, we postulate that PTPs are fundamentally involved in encoding growth factor stimulation into cellular responses. We have identified several PTPs that have the potential to reduce or even prevent EGF signaling (group I PTPs), but also candidates that changed the signal duration of EGF-EGFR complexes (group III/IV) in MCF7 cells. Our classification allowed us to distinguish the functional role of PTPs.

The ectopic expression of EGFR induces a sustained phosphorylation profile in MCF7 cells due to decelerated receptor degradation. Co-transfection of certain PTPs (group III and IV etc.) or Cbl resulted in a transient response of EGFR phosphorylation comparable to cells expressing normal amounts of the receptor. Based on our data we would suggest further experiments to determine whether cellular responses of MCF7 cells can be manipulated by PTP expression or silencing. For example, HRG stimulated MCF7 cells ectopically expressing a PTP candidate of group III/IV might switch the sustained phosphorylation profile of EGFR to a transient one, resulting in reduced cell differentiation. Another important question is whether EGF could induce differentiation of MCF7 cells that ectopically express EGFR and whether this cellular response can be reversed by PTP co-expression.

In general, knowledge of how PTPs regulate the duration of EGFR phosphorylation could be used to modulate the cellular response of other cell lines such as PC12 cells. Notably, ectopic expression of EGFR in PC12 cells induced a sustained Erk activity resulting in cell differentiation (Traverse et al., 1994). We assume a decelerated degradation and a prolonged phosphorylation of EGFR according to the high amount of receptors present in these cells. Ectopic

expression of specific PTPs that induce a transient phosphorylation profile of EGFR might reverse the observed phenotype towards proliferation in PC12 cells. In conclusion, our results afford comprehensive insights about when and where PTPs regulate EGFR phosphorylation, providing fundamental details about how spatiotemporal differences in PTP activity ultimately shape the cellular response to growth factor stimulation. Finally, this knowledge opens new ideas for therapeutic approaches to modulate pathophysiological responses to growth factors in diseases like cancer.

“ The days of phosphatases as housekeeping enzymes are over! ”

Nicholas K. Tonks

APPENDIX

6.1 Materials and Equipment

6.1.1 Chemicals

Acrylamide 30 % /Bis solution	Bio-Rad Laboratories, Inc.
Ammonium persulfate (APS)	SERVA Electrophoresis GmbH
beta-glycerophosphate	Sigma-Aldrich
Bicine	Sigma-Aldrich
Bromophenolblue	Sigma-Aldrich
Dimethyl sulfoxide (DMSO)	SERVA Electrophoresis GmbH
Disodium hydrogen phosphate (Na2HPO4)	Merck KG
Dithiothreitol (DTT)	Fluka Analytical
DMF	SERVA Electrophoresis GmbH
EDTA	Fluka Analytical
EDTA free protease inhibitor tap	Roche
EGTA	Sigma-Aldrich
Ethidium bromide (10 mg/ml)	Fisher Scientic
Ethylenediaminetetraacetic acid (EDTA)	Fluka Analytical
Gelatine	Sigma-Aldrich
Glycerol	GERBU Biotechnik GmbH
Glycine	Carl Roth GmbH
Hoechst 33342, trihydrochloride, trihydrate	Molecular Probes
IGEPAL	Sigma-Aldrich
Methanol	AppliChem GmbH
N,N,N',N'-Tetramethylene-diamine (TEMED)	Sigma-Aldrich
NaCl	Fluka Analytical
NaOH	J.T. Baker
Paraformaldehyde (PFA)	Sigma-Aldrich
Phosphatase Inhibitor Cocktail 1	Sigma-Aldrich
Phosphatase Inhibitor Cocktail 2	Sigma-Aldrich
PMSF	Sigma-Aldrich
Potassium chloride (KCl)	J.T.Baker
Sodium acetate (NaOAc)	Merck KG
Sodium chloride (NaCl)	Fluka Analytical
Sodium-deoxicolate	Sigma-Aldrich
Sodium-pyrophosphate	Sigma-Aldrich
Sucrose	Sigma-Aldrich
Tris-base	Carl Roth GmbH
Tris-HCl	J.T. Baker
Triton X-100	SERVA Electrophoresis GmbH
Tween 20	SERVA Electrophoresis GmbH
UltraPureTM Agarose	Life Technologies
β-Mercapto-ethanol	SERVA Electrophoresis GmbH

6.1.2 Biological regents and kits

2-log DNA ladder	New England Biolabs Inc.
Ampicillin sodium salt	SERVA Electrophoresis GmbH
Anti-EGFR antibody, # 4267	Cell Signaling
Anti-GFP antibody - IRDye 800	Rockland
Anti-LAR antibody, #AF3004	R&DSystems
Anti-phosphotyrosine (pY72) antibody	Invivo bioscience
Anti-PTPD1 antibody, #B50270	Stratagen
Anti-PTPN1 antibody, FG6-1G	Calbiochem (EMD Mililore)
Anti-SHP2 antibody, #2752	Cell Signaling
BigDye® Terminator v3.1 Cycle Sequencing kit	Life Technologies
Bradford reagent #B6916	Sigma-Aldrich
BSA	Sigma-Aldrich
chicken anti-rabbit Alexa647 #A21443	Invitrogen
ClaI	New England Biolabs Inc.
Complete Mini EDTA-free protease inhibitor tablets	Roche Applied Science
Cy3 reactive dye	GE Healthcare
Cy3.5 reactive dye	GE Healthcare
DharmaFECT	ThermoScientific
dNTP mix	Life Technologies
DPBS	PAN Biotech GmbH
DpnI	Stratagen
Dulbecco's Modied Eagle's Medium (DMEM)	PAN Biotech GmbH
DyeEX® 2.0 Spin kit	Qiagen
Epidermal Growth Factor (Human EGF)	Cell Signaling Technology
Fetal calf serum (FCS)	PAN Biotech GmbH
Fibronectin, bovine	Sigma-Aldrich
Fugene ® 6 transfection reagent	Roche Applied Science
FuGENE®	Promega
Gel Orange pearls	Carl Roth GmbH
Gelatin	Sigma-Aldrich
HindIII	New England Biolabs Inc.
HiPerFect	Qiagen
Hoechst solution	Sigma-Aldrich
IRDye ® 680 goat anti-mouse IgG	LI-COR Biosciences
IRDye ® 680 goat anti-rabbit IgG	LI-COR Biosciences
IRDye ® 800 goat anti-mouse IgG	LI-COR Biosciences
Kanamycine sulfate	GERBU Biotechnik GmbH
KpnI	New England Biolabs Inc.
L-Glutamine	PAN Biotech GmbH
Lipofectamin2000	Invitrogen
NcoI	New England Biolabs Inc.
non-essential amino acids	PAN Biotech GmbH
Nucleo Bond® Xtra Midi Plus EF® kit	Macherey-Nagel GmbH & Co.KG.
Nucleo Bound® Finalizer	Macherey-Nagel GmbH & Co.KG.
Odyssey Infrared Imaging System - blocking buffer	Li-Cor R Biosciences
OptiMEM	GIBCO /Invitrogen Life Technologies
Penicillin/Streptomycin	GIBCO /Invitrogen Life Technologies
Pfu-Ultra-HF	Stratagen
PureYield™ Plasmid Midiprep System	Promega
QIAprep ® Spin Miniprep kit	Qiagen
QIAquick ® PCR Purification kit	Qiagen
Quick LigationTM Kit	New England Biolabs Inc.
QuikChange XL Site-Directed Mutagenesis kit	Stratagene

SphI	New England Biolabs Inc.
Super-stay24color® #450 fire garnet	Maybelline New York
Trypsin/EDTA	PAN Biotech GmbH
UltraPureTM Agarose	Life Technologies
Zymoclean Gel DNA recovery kit	Zymoresearch

6.1.3 Consumables

1-well LabTek chambered coverglass	Nalge Nunc International
384-well low volume plates	Nalge Nunc International
6 well plates	Nalge Nunc International
8-well LabTek chambered coverglass	Nalge Nunc International
96-well cell culture plates	Cell star
Amicon Ultra-15 centrifugal filter unit (30K)	Millipore
Cell scraper	BD Falcon
Desalting spin column # 89849	Thermo scientific
PVDF membrane	Millipore
Reservoir	Nalge Nunc International
SDS Gel system	Bio Rad
Silica Gel Orange	Carl Roth GmbH
Spin Gel columns	ThermoScientific
Sterile filter, 0.45 µm	Millipore
T75 tissue culture fask	BD Falcon
Tissue culture plate (6 well)	BD Falcon
UV-Cuvettes (1 ml)	Sarstedt Aktiengesellschaft & Co.

6.1.4 Prepared buffers and solutions

1x PBS (pH 7.4)	137 mM NaCl, 10 mM Na2HPO4, 2.6 mM KCl, 1.8 mM KH2PO4
1x TBS (pH7.4)	100 mM Tris-HCl (pH 7.4), 150 mM NaCl
1x TBST	TBS + 0.1 % Tween 20
5x SDS sample buffer	60 mM Tris-HCl (pH 6.8), 25 % glycerol, 2 % SDS, 14.4 mM 2-mercapto-ethanol, 0.1 % brom-phenolblue
LB agar plates	LB medium with 1.5 % agar
LB medium	10 g/l Bacto-Trypton, 5 g/l bacto-yeast extract, 10 g/l NaCl
SDS running buffer	25 mM Tris-base, 192 mM glycine, 0.1 % SDS
Separation buffer	1.5 M Tris-HCl (pH 8.8)
SOC medium	20 g/l Bacto-Trypton, 5 g/l bacto-yeast extract, 0.5 g/l NaCl, 2.5 mM KCl, 10 mM $MgCl_2$, 20 mM glucose
Stacking gel buffer	0.5 M Tris-HCl (pH 6.8)
Transfer buffer	25 mM Tris-base, 192 mM glycine, 0.1 % SDS, 20 % methanol

6.1.5 Bacterial strains

SCS110	Stratagen
XL10 Gold	Stratagen

6.1.6 Mammalian cell lines

A431D: Derivative of A431 cells that do not express a classical cadherin but do express α –actinin. A431 are derived from epidermoid carcinoma, skin/epidermis.	Kindly provided by Prof. Alpha Yap, Institute for Molecular Bioscience, University of Queensland, Australia
HeLa: Human adenocarcinoma, derived from cervix.	ATCC
MCF7: Human adenocarcinoma, mammary gland/breast, derived from metastatic site: pleural effusion.	ATCC

6.1.7 Laboratory equipment

Centrifuge 5415R	Eppendorf
Centrifuge 5810 R	Eppendorf
Concentrator 5301	Eppendorf
DU 800 fluorescent spectrometer	Beckman Coulter
Gel Imaging Station	Bio-Rad
Microlab Star Line Liquid Handling Workstation	Hamilton
Nanodrop ® ND-1000 spectrophotometer	Peqlab Biotechnologie GmbH
Odyssey Infrared Imager	LI-COR Biosciences
PCR-Cycler\Mastercycler	Eppendorf
Plate Centrifuge 5430	Eppendorf
Robot spotter Qarray2	Genetix / Molecular devices
Semi-dry western blot system	Bio-Rad
Solid microarray pins 300 nm diameter	Array-It corporation
Solid microarray pins, 500 nm diameter	Array-It corporation
Vi-Cell-XR Cell counter	Beckman Coulter

6.1.8 Microscope equipment

10x objective (UPSLAPO 10×)	Olympus
20× objective (UPSLAPO 20×)	Olympus
40x objective (UPSLAPO 40×)	Olympus
4x objective (UPSLAPO 4×)	Olympus
Acousto-optic modulator (SWM-804AE1-1)	IntraAction
Acousto-optic tunable filter (AOTFnC-VIS-TN)	AA
Acousto-optic tunable filter Controller (AA,MDS8C-D66-22-80.153)	AA
Computer controlled stage (SCAN IM 120 × 100)	Märzhäuser
Dichroic filter (530LP)	Chroma
Emission filter (538/25)	Chroma
Fast photodiode (DET10A)	Thorlabs
Fiber (#46688-03)	Schäfter & Kirchhoff GmbH
FluoView 1000 Spectral	Olympus
Fully motorized microscope, IX81	Olympus

High frequency oscilloscope (TDS 820)	Tektronix
Intensified CCD and controller (Picostar HRI 12)	LaVision
Iris diaphragm (ID25/M)	Thorlabs
Laser (Innova 305)	Coherent
Mirrors and mirror holders (KM100-E02)	Thorlabs
Mode scrambler	(home built)
RF Amplifier	IntraAction
Rotation mount (PR01)	Thorlabs
Two signal generators (2023A)	Aeroflex
U-MNUA2	Olympus
U-MRFPHQ	Olympus
U-MYFPHQ	Olympus

6.1.9 Software

Adobe Acrobat Pro	Adobe Systems Inc.
Adobe Illustrator	Adobe Systems Inc.
Cell profiler 2.0	Carpenter, Jones, Kamentsky 2003
EndNote X4.0.2	Thomson Reuters
IgorPro v.6.12	WaveMatrics
ImageJ 1.47b /Fiji	Wayne Rasband, National Institutes of Health, USA
Labview	National Instruments
Lasergene 10	DNASTAR, Inc.
MATLAP R2012b	Math Works
Microsoft Excel 2011	Microsoft Corporation
Microsoft word 2011	Microsoft Corporation
Python	Python Software Foundation

6.2 On-Target-Plus-pool siRNA library

RODPC Custom Plate Maps

OTP™ siARRAY®

DHARMACON – RNA TECHNOLOGIES

Pool Number	Gene Name	Gene ID	Accession	GI Number	Sequence
L-009385-00	PTPN18	26469	NM_014369	18375654	GAUGGCCUGUCGAGAGAUA
L-009385-00	PTPN18	26469	NM_014369	18375654	GAGGAAGAACCGCUACAAA
L-009385-00	PTPN18	26469	NM_014369	18375654	CCAGGCACUUCUCGCCAUA
L-009385-00	PTPN18	26469	NM_014369	18375654	GGACCCGGGUGUAAGUCUA
L-008067-00	PTPRC	5788	NM_080921	18641361	GGUAAAAGCUCUACGCAAA
L-008067-00	PTPRC	5788	NM_080921	18641361	CAGCAAAGCUAAAUGUUAA
L-008067-00	PTPRC	5788	NM_080921	18641361	AGAAAUGAGUCGCAUAAGA
L-008067-00	PTPRC	5788	NM_080921	18641361	GAUAAUAGUAUGCAUGUCA
L-008476-00	PTPRJ	5795	NM_002843	18860899	UGACGGUGCUUCCGAGUAU
L-008476-00	PTPRJ	5795	NM_002843	18860899	GAACGGAAGUCACGUAUUU
L-008476-00	PTPRJ	5795	NM_002843	18860899	CAUCAACCAUGGUGUAACA
L-008476-00	PTPRJ	5795	NM_002843	18860899	CAGCAACGCAACACAAGUA
L-008500-00	PTPRO	5800	NM_030668	13677215	GCCAAAGACUCUGACUAUA
L-008500-00	PTPRO	5800	NM_030668	13677215	GGUCAUACCGGAUGUCUAU
L-008500-00	PTPRO	5800	NM_030668	13677215	UCAGUGAUGUCAUAUACGA
L-008500-00	PTPRO	5800	NM_030668	13677215	CAAACAUCCUACCAUAUGA
L-009417-00	PTPN23	25930	NM_015466	24308072	GUGCACAGGUGGUAGAUUA
L-009417-00	PTPN23	25930	NM_015466	24308072	GCAAACAGCGGAUGAGCAA
L-009417-00	PTPN23	25930	NM_015466	24308072	GCAUGAAGGUCUCCUGUAC
L-009417-00	PTPN23	25930	NM_015466	24308072	GUAGUGUCCUCCGCAAGUA
L-008394-00	PTPN7	5778	NM_080589	18375661	GCACAGCCGUUGACCUUGU
L-008394-00	PTPN7	5778	NM_080589	18375661	GAAGUGUCCCUCAUUGUCA
L-008394-00	PTPN7	5778	NM_080589	18375661	GGACGGAGAUUACAUCAAU
L-008394-00	PTPN7	5778	NM_080589	18375661	UGAAAGAGUGCCCAGAAUA
L-009315-00	PTPRN	5798	NM_002846	18860905	GCCCACGGCUGUCUAUUUG
L-009315-00	PTPRN	5798	NM_002846	18860905	GUAAAUGUUGGAGCUGAUA
L-009315-00	PTPRN	5798	NM_002846	18860905	GGACAGGUCUGGCUUGGCA
L-009315-00	PTPRN	5798	NM_002846	18860905	CAACAAGCAGGGCUGGUGA
L-008070-00	PTPRN2	5799	NM_130843	19743913	GCAGUGACCUUCAAAGUGA
L-008070-00	PTPRN2	5799	NM_130843	19743913	UCACGUGGCAGGAUGACUA
L-008070-00	PTPRN2	5799	NM_130843	19743913	CAAGAGGUCCAUCGUCUGA
L-008070-00	PTPRN2	5799	NM_130843	19743913	GAUGGAGCACGGAUUCAUA
L-008375-00	PTPRF	5792	NM_130440	18860895	CGAAUUGACCCGUGUGUGU
L-008375-00	PTPRF	5792	NM_130440	18860895	GAGCGGAUCAUCAUGUAUG
L-008375-00	PTPRF	5792	NM_130440	18860895	AGUCAGCUGUGCCCUUUAA
L-008375-00	PTPRF	5792	NM_130440	18860895	GAACCUGUAUGUGCGAGUG
L-008066-00	PTPN22	26191	NM_012411	15619017	CCUCAGCUGUGAAGGUAAA
L-008066-00	PTPN22	26191	NM_012411	15619017	GGAGUCAGCUGUACUAGCA
L-008066-00	PTPN22	26191	NM_012411	15619017	GAAUAUAGUGUCCUUAUCA
L-008066-00	PTPN22	26191	NM_012411	15619017	ACACAGAGGCCUUCAUUAG
L-009489-00	PTPN4	5775	NM_002830	18104987	GCACGGAAAUUAAUGGAUU
L-009489-00	PTPN4	5775	NM_002830	18104987	ACAGAGAUAUUUCGCCUUA
L-009489-00	PTPN4	5775	NM_002830	18104987	GGAAGAUGACCCUAUUUAA
L-009489-00	PTPN4	5775	NM_002830	18104987	GAACAGGGUACGAAUGAAU
L-008832-00	PTPN9	5780	NM_002833	18375663	GAAAACAACGCUAGAAAUU
L-008832-00	PTPN9	5780	NM_002833	18375663	GGACAGUUCAGUACAAUGU
L-008832-00	PTPN9	5780	NM_002833	18375663	GUCAGUAACUCUCCUACGA
L-008832-00	PTPN9	5780	NM_002833	18375663	AAAUUGAUCUCGCCACUUG
L-004017-00	PTPRR	5801	NM_130846	19743916	GCACCUACAUUAAUGCUAA
L-004017-00	PTPRR	5801	NM_130846	19743916	GAAGGUAGCAAUGGAGUAU
L-004017-00	PTPRR	5801	NM_130846	19743916	GUGCUAUACUGGCCGGAAA
L-004017-00	PTPRR	5801	NM_130846	19743916	CCAAAGGUACUGAAUGUUG
L-008064-00	PTPN12	5782	NM_002835	18375651	GGAAUUAAGUUCAGAUCUA
L-008064-00	PTPN12	5782	NM_002835	18375651	GUAAUGGCCUGCCGAGAAU
L-008064-00	PTPN12	5782	NM_002835	18375651	GGACACUCUUACUUGAAUU
L-008064-00	PTPN12	5782	NM_002835	18375651	CGGGAGGUAUUCACUAUGA
L-004204-00	PTPRK	5796	NM_002844	18860901	GAAGUAGAGUACCGAAUGA
L-004204-00	PTPRK	5796	NM_002844	18860901	CAACAUAACUUUAGUCCAA
L-004204-00	PTPRK	5796	NM_002844	18860901	GGAGAUUAGUGUAUGAUUA
L-004204-00	PTPRK	5796	NM_002844	18860901	UCUCCUAGUUGUCAUAUUA
L-008065-00	PTPN13	5783	NM_080684	18375647	GGAAAGAAGAGUUCGUUUA
L-008065-00	PTPN13	5783	NM_080684	18375647	GCUAUCAAGUCAUCCUUUA
L-008065-00	PTPN13	5783	NM_080684	18375647	UAACAAAGGGCUUAGUAAA
L-008065-00	PTPN13	5783	NM_080684	18375647	CUAGUUCGAUGGAUAAGUA
L-003529-00	PTPN1	5770	NM_002827	18104977	GGAGAAAGGUUCGUUAAAA
L-003529-00	PTPN1	5770	NM_002827	18104977	CUACCUGGCUGUGAUCGAA
L-003529-00	PTPN1	5770	NM_002827	18104977	GCCCAAAGGAGUUACAUUC
L-003529-00	PTPN1	5770	NM_002827	18104977	GACCAUAGUCGGAUUAAAC
L-009379-00	PTPN21	11099	NM_007039	18375656	GAGAAGAGCUUUAGGUACU
L-009379-00	PTPN21	11099	NM_007039	18375656	GAGCGUGUCUUGAAGGUAU

L-009379-00	PTPN21	11099	NM_007039	18375656	GCACCAACUCCUUAAAUAA
L-009379-00	PTPN21	11099	NM_007039	18375656	GUUCGACGCCAUACAAAUA
L-004519-00	PTPRA	5786	NM_080841	18450370	GAGAAUGGCAGACGACAAU
L-004519-00	PTPRA	5786	NM_080841	18450370	GCAUUACAAUUUCACCAAA
L-004519-00	PTPRA	5786	NM_080841	18450370	GAUUAGAGGAGGAGUUUAA
L-004519-00	PTPRA	5786	NM_080841	18450370	CGGCAGAACCAGUUAAAGA
L-004994-00	PTPRB	5787	NM_002837	18491009	GAACAAUUCCGGUCGUAAU
L-004994-00	PTPRB	5787	NM_002837	18491009	GAGAAUACAUUGUCACUCA
L-004994-00	PTPRB	5787	NM_002837	18491009	UCACAGAGAUCCAGUCUAU
L-004994-00	PTPRB	5787	NM_002837	18491009	GCAACCGAGUAUCGAUUUA
L-008509-00	PTPN14	5784	NM_005401	34328898	GAAGACAAGCGGUAAUAUA
L-008509-00	PTPN14	5784	NM_005401	34328898	CAUAACAAGUCGACCAUUC
L-008509-00	PTPN14	5784	NM_005401	34328898	GCUAAUGAGCCUUUGCUUU
L-008509-00	PTPN14	5784	NM_005401	34328898	GGUGAGCACUACUCGGAAA
L-008527-00	PTPRD	5789	NM_130393	18860893	GAAUGGAGCUCGAAUUUAA
L-008527-00	PTPRD	5789	NM_130393	18860893	UCAGAGAUUUGAGGUAAUA
L-008527-00	PTPRD	5789	NM_130393	18860893	GAUGAUAUGCCAAUAGGAA
L-008527-00	PTPRD	5789	NM_130393	18860893	UUAAGGAGAUAUCUAGGAA
L-008068-00	PTPRE	5791	NM_130435	40805848	GCGAACAGGUACAUUCAUA
L-008068-00	PTPRE	5791	NM_130435	40805848	CCAUUGGGAUGCUGAAGUU
L-008068-00	PTPRE	5791	NM_130435	40805848	CAUCAACGCAUCCUUCAUA
L-008068-00	PTPRE	5791	NM_130435	40805848	GCAAGCAGUUUCGGGAGGA
L-008069-00	PTPRG	5793	NM_002841	18860897	CGACAUGACAGACUUCUUA
L-008069-00	PTPRG	5793	NM_002841	18860897	UCGGUGAGCUCUAUUCUAA
L-008069-00	PTPRG	5793	NM_002841	18860897	GAACCGUGUUGGUGGAUUU
L-008069-00	PTPRG	5793	NM_002841	18860897	CCACAUACUACGAAAGAUU
L-009372-00	PTPN3	5774	NM_002829	18104985	GGGAUCAAAUCGUGUUAAU
L-009372-00	PTPN3	5774	NM_002829	18104985	CAUCAAGCCAGUACAAGUU
L-009372-00	PTPN3	5774	NM_002829	18104985	GUUGACGACUCUCACAGAA
L-009372-00	PTPN3	5774	NM_002829	18104985	UAACAAAAGUCGAAUCUCU
L-006326-00	PTPRM	5797	NM_002845	18860903	GGACUUGCCUGGCGACUUU
L-006326-00	PTPRM	5797	NM_002845	18860903	GCAAUUAUAUCGAUGGUUA
L-006326-00	PTPRM	5797	NM_002845	18860903	GAACGUCCUCGAAGAACUA
L-006326-00	PTPRM	5797	NM_002845	18860903	GAGUGAGGCUGCAGACAAU
L-008072-00	PTPRT	11122	NM_007050	48762923	GGAGGCUGGUGUUCGAUUA
L-008072-00	PTPRT	11122	NM_007050	48762923	GGUCUGGUGUGUCCAACUA
L-008072-00	PTPRT	11122	NM_007050	48762923	CCAACUACAUUGACGGAUA
L-008072-00	PTPRT	11122	NM_007050	48762923	GAAGAUGGCUGGCGUGAUC
L-027185-00	PTPRQ	374462	XM_926134	89035630	UAUCAAAGCUCCAGCACGA
L-027185-00	PTPRQ	374462	XM_926134	89035630	GGAUAUAUAUGGACUAGUA
L-027185-00	PTPRQ	374462	XM_926134	89035630	GGAUAAGACCUGACACUAU
L-027185-00	PTPRQ	374462	XM_926134	89035630	GGACAUACAUACAAUAUCA
L-009328-00	PTPRU	10076	NM_133178	19743932	GCAUUGAUCCUCAGAGUAA
L-009328-00	PTPRU	10076	NM_133178	19743932	CAUCAGACCCGGCAGUGAA
L-009328-00	PTPRU	10076	NM_133178	19743932	GGCGGCUGGUCUACGAUUA
L-009328-00	PTPRU	10076	NM_133178	19743932	CGAGAAUGAUACCCACUGU
L-009662-00	PTPRS	5802	NM_130853	19743920	CAGGUCACGUUGCUAGAUA
L-009662-00	PTPRS	5802	NM_130853	19743920	GCCAAGUGCAUAAGACUAA
L-009662-00	PTPRS	5802	NM_130853	19743920	CAGUAUGGCGGCUUCGAUA
L-009662-00	PTPRS	5802	NM_130853	19743920	CAGAUCCUGUGUCCUAUUA
L-013909-00	DKFZP566K0524	26095	NM_015605	45243553	CGAAGGAGCAGUAUCACUU
L-013909-00	DKFZP566K0524	26095	NM_015605	45243553	CAGAGCCUGUAAACGAUUA
L-013909-00	DKFZP566K0524	26095	NM_015605	45243553	CAGAUUCGGCCAUUAAUAU
L-013909-00	DKFZP566K0524	26095	NM_015605	45243553	GCAGGAAUUUAUGGCUUUA
L-009685-00	PTPRZ1	5803	NM_002851	4506328	GAGAUUGGCUGGUCCUAUA
L-009685-00	PTPRZ1	5803	NM_002851	4506328	GAACAUAUCCCAAGGGUAU
L-009685-00	PTPRZ1	5803	NM_002851	4506328	GAGCUGUACUGUUGACUUA
L-009685-00	PTPRZ1	5803	NM_002851	4506328	GUUCUUAGAUCUCCACAUA
L-009448-00	PTPRH	5794	NM_002842	67190343	GGAAUGACGUAGCCAGUUC
L-009448-00	PTPRH	5794	NM_002842	67190343	GCACAACAGAGACUCGAAA
L-009448-00	PTPRH	5794	NM_002842	67190343	GGUCAUUGCCGGAGCCUUU
L-009448-00	PTPRH	5794	NM_002842	67190343	ACUCUCAGUUGUACGUAUA
L-009778-00	PTPN6	5777	NM_080548	34328901	GGAACAAAUGCGUCCCAUA
L-009778-00	PTPN6	5777	NM_080548	34328901	AUACAAACUCCGUACCUUA
L-009778-00	PTPN6	5777	NM_080548	34328901	UAUGAGAACCUGCACACUA
L-009778-00	PTPN6	5777	NM_080548	34328901	GCUCCGAUCCCACUAGUGA
L-003947-00	PTPN11	5781	NM_002834	33356176	GAACAUCACGGGCAAUUAA
L-003947-00	PTPN11	5781	NM_002834	33356176	GAAGCACAGUACCGAUUUA
L-003947-00	PTPN11	5781	NM_002834	33356176	GGAGAUGGUUUCACCCAAA
L-003947-00	PTPN11	5781	NM_002834	33356176	GGACGUUCAUUGUGAUUGA
L-003600-00	PTPN5	84867	NM_032781	22095374	CGAGAAAUGCACCGAGUAU

L-003600-00	PTPN5	84867	NM_032781	22095374	GACAUGUGCUGCAGUGAGA
L-003600-00	PTPN5	84867	NM_032781	22095374	AGCGAGGCCUGAAGCAUUA
L-003600-00	PTPN5	84867	NM_032781	22095374	GAGGAGGGCUUUGGCUAUC
L-008969-00	PTPN2	5771	NM_080423	18104981	GAUGUGAAGUCGUAUUAUA
L-008969-00	PTPN2	5771	NM_080423	18104981	GAUGUAAGCCCAUAUGAUC
L-008969-00	PTPN2	5771	NM_080423	18104981	AUACAAUGGGAACAGAAUA
L-008969-00	PTPN2	5771	NM_080423	18104981	ACAAAGGAGUUACAUCUUA
L-003469-00	CDC14A	8556	NM_033313	15451932	GGACAUUGAUAGCCUGUUA
L-003469-00	CDC14A	8556	NM_033313	15451932	CUUGUGAGUUCAUGAAAGA
L-003469-00	CDC14A	8556	NM_033313	15451932	GCACAGUAAAUACCCACUA
L-003469-00	CDC14A	8556	NM_033313	15451932	GAACAUUAUGAGCGAGUUG
L-003470-00	CDC14B	8555	NM_003671	15451934	GCUACAUCAUGAAGCAUUA
L-003470-00	CDC14B	8555	NM_003671	15451934	CGAAAUCAAUGGAGUGACA
L-003470-00	CDC14B	8555	NM_003671	15451934	GUACAUUAUUUCAGCAUAG
L-003470-00	CDC14B	8555	NM_003671	15451934	GUUGAUGACAUUUCCAUAA
L-003226-00	CDC25A	993	NM_201567	42490759	GGGCAGUGAUUAUGAGCAA
L-003226-00	CDC25A	993	NM_201567	42490759	UCAGGUUUCUGUCUAGAUU
L-003226-00	CDC25A	993	NM_201567	42490759	GCAAGCGUGUCAUUGUUGU
L-003226-00	CDC25A	993	NM_201567	42490759	CAUGACAUCUUUCAGCUCA
L-003227-00	CDC25B	994	NM_212530	47078254	GAGAUUACUCUAAGGCCUU
L-003227-00	CDC25B	994	NM_212530	47078254	GCAGAUACCCCUAUGAAUA
L-003227-00	CDC25B	994	NM_212530	47078254	UGGAUAAGUUUGUGAUUGU
L-003227-00	CDC25B	994	NM_212530	47078254	AGAGUGACUUAAAGGAUGA
L-003228-00	CDC25C	995	NM_022809	12408657	GAAACUUGGUGGACAGUGA
L-003228-00	CDC25C	995	NM_022809	12408657	AGGAAGGGCUUAUGUUUAA
L-003228-00	CDC25C	995	NM_022809	12408657	GAGAGAGACACUUCCUUUA
L-003228-00	CDC25C	995	NM_022809	12408657	GGGCAAAUUUCUUGGUGAU
L-026458-00	DUPD1	338599	NM_001003892	51491913	CCUCAAGAAUGCCUACUCA
L-026458-00	DUPD1	338599	NM_001003892	51491913	CUUCAUCGACAGAGCGCUA
L-026458-00	DUPD1	338599	NM_001003892	51491913	CCAAGAGGCUGUCGCCGAA
L-026458-00	DUPD1	338599	NM_001003892	51491913	CGACGACCACAGUAAGAUC
L-003484-00	DUSP1	1843	NM_004417	7108342	CCAAUUGUCCCAACCAUUU
L-003484-00	DUSP1	1843	NM_004417	7108342	GCAUAACUGCCUUGAUCAA
L-003484-00	DUSP1	1843	NM_004417	7108342	GCGCAAGUCUUCUUCCUCA
L-003484-00	DUSP1	1843	NM_004417	7108342	GAAGGGUGUUUGUCCACUG
L-003565-00	DUSP2	1844	NM_004418	12707563	GGAGAUCAGUGCCUGGUUC
L-003565-00	DUSP2	1844	NM_004418	12707563	GUCCCGAUCUGUGCUCUGA
L-003565-00	DUSP2	1844	NM_004418	12707563	UCACAGCCGUCCUCAACGU
L-003565-00	DUSP2	1844	NM_004418	12707563	CGAGGCCUUUGACUUCGUU
L-007894-00	DUSP3	1845	NM_004090	37655179	UCACAUACCUGGGCAUCAA
L-007894-00	DUSP3	1845	NM_004090	37655179	UGAAAGGGCUGCCGACUUC
L-007894-00	DUSP3	1845	NM_004090	37655179	CAACACCAAUGCCAACUUC
L-007894-00	DUSP3	1845	NM_004090	37655179	GCUCUUAGUUCUUCAAGUA
L-003963-00	DUSP4	1846	NM_001394	58331238	GUACAUCGAUGCCGUGAAG
L-003963-00	DUSP4	1846	NM_001394	58331238	CAUCACGGCUCUGUUGAAU
L-003963-00	DUSP4	1846	NM_001394	58331238	GAAGGACACUAUCAGUACA
L-003963-00	DUSP4	1846	NM_001394	58331238	GGACUGCCCAAACCACUUU
L-003566-00	DUSP5	1847	NM_004419	62865889	GAGACUUUCUACUCGGAAU
L-003566-00	DUSP5	1847	NM_004419	62865889	UCACCUCGCUACUCGCUUG
L-003566-00	DUSP5	1847	NM_004419	62865889	AAACUGGGAUGGAGGAAUC
L-003566-00	DUSP5	1847	NM_004419	62865889	CCACUUUCAAGAAGCAAUA
L-003964-00	DUSP6	1848	NM_022652	42764686	GAACUGUGGUGUCUUGGUA
L-003964-00	DUSP6	1848	NM_022652	42764686	GACUGUGGCUUACCUUAUG
L-003964-00	DUSP6	1848	NM_022652	42764686	GGCAUUAGCCGCUCAGUCA
L-003964-00	DUSP6	1848	NM_022652	42764686	GAAAUGGCGAUCAGCAAGA
L-003567-00	DUSP7	1849	NM_001947	38348231	CAAGGUGGUUUCAACAAGU
L-003567-00	DUSP7	1849	NM_001947	38348231	GGACGUGCUCGGCAAGUAU
L-003567-00	DUSP7	1849	NM_001947	38348231	CAACGACGCCUACGACUUU
L-003567-00	DUSP7	1849	NM_001947	38348231	CUAAGCAGCCCGUGCGACA
L-003568-00	DUSP8	1850	NM_004420	4758211	CGACGACGCCUACAGGUUC
L-003568-00	DUSP8	1850	NM_004420	4758211	AACGACAACUACUGUGAAA
L-003568-00	DUSP8	1850	NM_004420	4758211	AAACAAGGAUCUGAUGACG
L-003568-00	DUSP8	1850	NM_004420	4758211	GUUCAUCGAUAAAGCCAAG
L-003569-00	DUSP9	1852	NM_001395	4503420	CGACUGCUCUGAUGCGGAA
L-003569-00	DUSP9	1852	NM_001395	4503420	CGAGAAGAAUGGUGACUUU
L-003569-00	DUSP9	1852	NM_001395	4503420	CAGGGAGGCUUCAGCAGAU
L-003569-00	DUSP9	1852	NM_001395	4503420	CCACCUCUCUCUCAACGAU
L-003965-00	DUSP10	11221	NM_144729	21536332	CAAAGGCAAACGACCAAUU
L-003965-00	DUSP10	11221	NM_144729	21536332	UGGAGACGGUUGUGUGACA
L-003965-00	DUSP10	11221	NM_144729	21536332	CGAGAAUCCUUACACCAAA
L-003965-00	DUSP10	11221	NM_144729	21536332	CAUGACUGAUGCUUAUAAA

L-008038-00	MTMR2	8898	NM_016156	41350313	UGUCACGAAUUAUAGGUUA
L-008039-00	MTMR3	8897	NM_153051	23510388	GACCAAACGUGGACAGUUC
L-008039-00	MTMR3	8897	NM_153051	23510388	GGGCAGGCAUUGAGAUACA
L-008039-00	MTMR3	8897	NM_153051	23510388	GCAAAGUUAUCAGGUGUCA
L-008039-00	MTMR3	8897	NM_153051	23510388	UGAAUGCCGAGAUAUAUUU
L-008040-00	MTMR4	9110	NM_004687	31377795	CAGCAUAGGUUACGGCAAA
L-008040-00	MTMR4	9110	NM_004687	31377795	UAACAAGUGUGAUGGAGUU
L-008040-00	MTMR4	9110	NM_004687	31377795	GAGAGAAGGUGUGAAGUCA
L-008040-00	MTMR4	9110	NM_004687	31377795	UAUAGACACUUGCGCAAUG
L-021405-00	SBF1	6305	NM_002972	37574611	GCGCCGAGCUCUUCCGUAA
L-021405-00	SBF1	6305	NM_002972	37574611	CUACGGACCUGUUCGAUGA
L-021405-00	SBF1	6305	NM_002972	37574611	GCGGAGCCUUCACAGGAAA
L-021405-00	SBF1	6305	NM_002972	37574611	GAUACAGCUUCACCUAUGU
L-008309-00	MTMR6	9107	NM_004685	37537693	UCUCACAGAUUUACAGUUU
L-008309-00	MTMR6	9107	NM_004685	37537693	CCUAGGCAGUCUGUAUUUA
L-008309-00	MTMR6	9107	NM_004685	37537693	AAACUUGCUUUGACUACUU
L-008309-00	MTMR6	9107	NM_004685	37537693	UAAAGCCAAUCCAGUCAAU
L-008041-00	MTMR7	9108	NM_004686	56118316	UGCAAGAACUUUCAGAUAA
L-008041-00	MTMR7	9108	NM_004686	56118316	GCUGAUCGAUCUUAGUGAA
L-008041-00	MTMR7	9108	NM_004686	56118316	GACAGUCAGUUACAGAUUA
L-008041-00	MTMR7	9108	NM_004686	56118316	GGAUGGGCCUCCCUAAUCA
L-008042-00	MTMR8	55613	NM_017677	21361758	GACUGUAUCUGGCAAUUAA
L-008042-00	MTMR8	55613	NM_017677	21361758	CAACCCACCUGAUCUAUGU
L-008042-00	MTMR8	55613	NM_017677	21361758	GCCAUGAGGUUUAUAUUUC
L-008042-00	MTMR8	55613	NM_017677	21361758	GAUCUAAGAGUCUAUGAGA
L-019244-00	MTMR9	66036	NM_015458	33598962	GAACUCUAUUCUUCAGCUA
L-019244-00	MTMR9	66036	NM_015458	33598962	GUAGCUACAUUUCGACAUG
L-019244-00	MTMR9	66036	NM_015458	33598962	GCAGAUCCUUCGUCAGUUU
L-019244-00	MTMR9	66036	NM_015458	33598962	GAAGAAAUGGUUAACAUCA
L-020758-01	FLJ20313	54893	NM_017762	8923296	CUGAAGCAGCUAUGCGUUA
L-020758-01	FLJ20313	54893	NM_017762	8923296	GCAGUGCUCUUGUGCGAAU
L-020758-01	FLJ20313	54893	NM_017762	8923296	UGACCUAGGGAGCGGGAAA
L-020758-01	FLJ20313	54893	NM_017762	8923296	GGAUAUCAGUUUCUAGACA
L-018883-01	CRA	10903	NM_181873	89111940	GGGACUGGGAUUUACGUUA
L-018883-01	CRA	10903	NM_181873	89111940	CAGGAGUUAUUACGGAAAU
L-018883-01	CRA	10903	NM_181873	89111940	CAACGAGAGGUUCGACGUA
L-018883-01	CRA	10903	NM_181873	89111940	GAUUAGAGGCUGUGAGCGG
L-021326-00	PIP3AP	54545	NM_019061	27477131	CUAAACUGCUUAAACGAUU
L-021326-00	PIP3AP	54545	NM_019061	27477131	GGUCAUGGCAUACCAAUAU
L-021326-00	PIP3AP	54545	NM_019061	27477131	CAAGAACCAUACCGUAAUG
L-021326-00	PIP3AP	54545	NM_019061	27477131	GCCCAGCGCUACCUACGUU
L-014684-01	CMT4B2	81846	NM_030962	29788754	CCAGAAAGUUCCACGGCCA
L-014684-01	CMT4B2	81846	NM_030962	29788754	CAACAUUGCCGCAGCAUUA
L-014684-01	CMT4B2	81846	NM_030962	29788754	GCUCUAAAGCCCAAUGUAA
L-014684-01	CMT4B2	81846	NM_030962	29788754	GGGCAAUAUUAGACCAUCA
L-003023-00	PTEN	5728	NM_000314	73765543	GAUCAGCAUACACAAAUUA
L-003023-00	PTEN	5728	NM_000314	73765543	GACUUAGACUUGACCUAUA
L-003023-00	PTEN	5728	NM_000314	73765543	GAUCUUGACCAAUGGCUAA
L-003023-00	PTEN	5728	NM_000314	73765543	CGAUAGCAUUUGCAGUAUA
L-006333-00	PTP4A1	7803	NM_003463	62865860	GAUUGUUGAUGACUGGUUA
L-006333-00	PTP4A1	7803	NM_003463	62865860	CCAAUGCGACCUUAAACAA
L-006333-00	PTP4A1	7803	NM_003463	62865860	GCAAGCAACUUCUGUAUUU
L-006333-00	PTP4A1	7803	NM_003463	62865860	GAAAGAAGGUAUCCAUGUU
L-009078-00	PTP4A2	8073	NM_080392	18104972	CCUAUGAGAACAUGCGUUU
L-009078-00	PTP4A2	8073	NM_080392	18104972	AGUAUGGAGUGACGACUUU
L-009078-00	PTP4A2	8073	NM_080392	18104972	GAAAUACCGACCUAAGAUG
L-009078-00	PTP4A2	8073	NM_080392	18104972	CCAAUGCUACUCUCAACAA
L-006859-00	PTP4A3	11156	NM_007079	14589853	AAACAGAGGCUGCGGUUCA
L-006859-00	PTP4A3	11156	NM_007079	14589853	GAGGUGAGCUACAAACACA
L-006859-00	PTP4A3	11156	NM_007079	14589853	GGACUGGCCGUUUGACGAU
L-006859-00	PTP4A3	11156	NM_007079	14589853	GAAGUGACCUAUGACAAAA
L-029988-00	LOC114971	114971	XM_374879	51470940	UCGCCAAGAUCCGGUCAUA
L-029988-00	LOC114971	114971	XM_374879	51470940	CCAGAAGGGAGUCCAAUUU
L-029988-00	LOC114971	114971	XM_374879	51470940	GGAUGGGACUUUUGUCAUU
L-029988-00	LOC114971	114971	XM_374879	51470940	GGUGGCAGCAUACCUGAUU
L-009782-00	RNGTT	8732	NM_003800	4506562	AUACAAACCUGGUCGAUGU
L-009782-00	RNGTT	8732	NM_003800	4506562	UAUAAGUCCUCGACACGAA
L-009782-00	RNGTT	8732	NM_003800	4506562	CUACAAGGGUGAUUAUUUG
L-009782-00	RNGTT	8732	NM_003800	4506562	GAAUUUCCAUUUCGUAAAG
L-008083-00	SSH1	54434	NM_018984	40254883	CGAAGAAGAUCGAAAAUUA
L-008083-00	SSH1	54434	NM_018984	40254883	ACAAUGAGAUGCUACUUAU

L-008083-00	SSH1	54434	NM_018984	40254883	CAUGGAGGAUGAUGCUAUA
L-008083-00	SSH1	54434	NM_018984	40254883	CAACCCAGCUCGAUCAAAA
L-008084-00	SSH2	85464	NM_033389	37674209	CCACAUAGCUCUAGUAGUG
L-008084-00	SSH2	85464	NM_033389	37674209	GAAUGUCACUCGAGAGAUA
L-008084-00	SSH2	85464	NM_033389	37674209	GGACUUGAAUUGACUAGUU
L-008084-00	SSH2	85464	NM_033389	37674209	GGGUAGAAAUCAUUGAAUA
L-008937-00	SSH3	54961	NM_018276	24586672	GAGACGCACCGCUUCAUUG
L-008937-00	SSH3	54961	NM_018276	24586672	CCUAUGCCAUGAAGCAGUA
L-008937-00	SSH3	54961	NM_018276	24586672	GAACGCAGCAAACCUGGAG
L-008937-00	SSH3	54961	NM_018276	24586672	UCAAUGAGUGGACGGCUAU
L-009571-00	STYX	6815	NM_145251	34222188	GUUCUUAGGCCCAUAUUCA
L-009571-00	STYX	6815	NM_145251	34222188	CAGCCUUUGUUAUUGCAUA
L-009571-00	STYX	6815	NM_145251	34222188	UGUCACCACUCCAGAUAGA
L-009571-00	STYX	6815	NM_145251	34222188	GACGAGAGAUGCAGGAAAU
L-008107-00	TPTE2	93492	NM_199255	40549426	CCGAGGAAAGCCUAUAUUA
L-008107-00	TPTE2	93492	NM_199255	40549426	GAUUCGUGGUGAUGUAUGU
L-008107-00	TPTE2	93492	NM_199255	40549426	GAAAGUCCACAGACAAACG
L-008107-00	TPTE2	93492	NM_199255	40549426	GGAGAAAGGCGAACCAAUA
L-008745-00	TPTE	7179	NM_199261	40549436	UUUAUUCGAUUCCUCGUUA
L-008745-00	TPTE	7179	NM_199261	40549436	UCAAGGAAGUUGUGCGGUU
L-008745-00	TPTE	7179	NM_199261	40549436	GAAAUAUGUUCAACUGCAA
L-008745-00	TPTE	7179	NM_199261	40549436	UAAAGGAGGCACAGAUAGA
D-001810-04	OTP siCONTROL non-targeting siRNA #4				
D-001810-10	OTP siCONTROL non-targeting siRNA pool				

APPENDIX 6.3

cDNA library of mCitrine fusion proteins

Class	type	Gene Name	Synonyms	Localization	Ref Sequence	Mass kDA	Isoform	plasmid backbone	DPF cloning F-Primer	DPF cloning R-Primer
Class I Cys-Based	NRPTP	PTPN1	PTP1B	ER	NM_002827	50.0	1	pmCitrine - C1	-	-
Class I Cys-Based	NRPTP	PTPN11	SHP2	Cy	BC008692	52.8	3	p2150 pOPIN (c)mCitrine	AGGAGATATACCATGACATCGCGGAGATGGTTTCACC	AACAGAACTTCCAGAAACCTGCAGTGCACCACGACC
Class I Cys-Based	NRPTP	PTPN14	PEZ, PTPD2	Cy	BC101754	135.3	1	p2150 pOPIN (c)mCitrine	AGGAGATATACCATGCCTTTTGGTCTGAAGCTCCGCC	CAGAACTTCCAGAAAGCTAATGAGTCTGGAGTTTTGGAGGAACTG
Class I Cys-Based	NRPTP	PTPN18	BDP1	Nu, Cy	NM_014369	50.5	1	p2297 pOPIN (n)mCitrine	GAAGTTCTGTTTCAGGGTAGCCGCAGCCTGGACTC	CTGGTCTAGAAAGCTTTACACCCGGGTCCACTCAGC
Class I Cys-Based	NRPTP	PTPN2 (TC41)	TCPTP (variant3)	Nu, Cy	BC016727	41.0	3	p2297 pOPIN (n)mCitrine	GAAGTTCTGTTTCAGGGTCCCACCACCATCGAGCGG	CTGGTCTAGAAAGCTTTAGGTGTCTGTCAATCTTGGCCTCTCA
Class I Cys-Based	NRPTP	PTPN2 (TC45)	TCPTP (TC45, variant2)	Nu	BC008244	45.2	2	p2297 pOPIN (n)mCitrine	GAAGTTCTGTTTCAGGGTCCCACCACCATCGAGCGG	CTGGTCTAGAAAGCTTTAGGTGTCTGTCAATCTTGGCCTTTTTCTT
Class I Cys-Based	NRPTP	PTPN20A	PTPN20	Cy	BC093750	25.9	7	p2150 pOPIN (c)mCitrine	AGGAGATATACCATGTCTTCACCTAGGGACTTTAGAGCAGAG	CAGAACTTCCAGAAAGCTAGCACAATATCGTAACAAAAGTGATACTGCTC
Class I Cys-Based	NRPTP	PTPN20B	PTPN20	Cy	BC141460	25.9	7	p2150 pOPIN (c)mCitrine	AGGAGATATACCATGTCTTCACCTAGGGACTTTAGAGCAGAG	AACAGAACTTCCAGAAAAGCACAATATCGTAACAAAAGTGATACTGCTC
Class I Cys-Based	NRPTP	PTPN21	PTPD1	Cy	NM_007039	133.3	1	pmCitrine - N1	-	-
Class I Cys-Based	NRPTP	PTPN22	LYP, PTPN8	Cy	BC017785	20.9	5	p2150 pOPIN (c)mCitrine	AGGAGATATACCATGGACCAAAGAGAAATTCTGCAGAAGTTCCT	CAGAACTTCCAGAAAGCTGAAATGAGCTGGAGTTATTTGACTGAACAGATTC
Class I Cys-Based	NRPTP	PTPN3	PTPH1	PM, Cy	BC126117	104.0	1	p2150 pOPIN (c)mCitrine	AGGAGATATACCATGACCTCCCGGTTACGTGCG	AACAGAACTTCCAGAAAACTAGGATCCAGCATTTGGACTAAACCT
Class I Cys-Based	NRPTP	PTPN4	MEG	Cy	BC010674	105.9	1	p2297 pOPIN (n)mCitrine	GAAGTTCTGTTTCAGGGTACCTCACGTTTCCGATTGCCTG	CTGGTCTAGAAAGCTTTATTTATTTGTTGATGTTGTTAAGGGTTTAACAAAGCC
Class I Cys-Based	NRPTP	PTPN5	STEP	ER	BC064807	63.6	1	p2297 pOPIN (n)mCitrine	GAAGTTCTGTTTCAGGGTAATTATGAGGGAGCCAGGAGTGAGA	CTGGTCTAGAAAGCTTTATTCTGGGGACTGGTGGGACA
Class I Cys-Based	NRPTP	PTPN6	SHP1	Nu, Cy	BC002523	67.7	2	p2297 pOPIN (n)mCitrine	GAAGTTCTGTTTCAGGGTCTGTCCCGTGGGTGGTTTCA	CTGGTCTAGAAAGCTTTACTTCCTCTTGAGGGAACCCTTGC
Class I Cys-Based	NRPTP	PTPN7	HePTP	Cy	BC001746	45.0	2	p2150 pOPIN (c)mCitrine	AGGAGATATACCATGGGAGCCTCCTTCTGGCCAATC	CAGAACTTCCAGAAAGCTGGGGCTGGGTTCCTCAGG
Class I Cys-Based	NRPTP	PTPN9	MEG2	Cy	BT007405	68.0	1	p2150 pOPIN (c)mCitrine	AGGAGATATACCATGGAGCCCGCGACCGCG	CAGAACTTCCAGAAAGCTCTGACTCTCCACGGCCAGC
Class I Cys-Based	RPTP	PTPRA	PTPα	PM	DQ891155	89.7	4	p2150 pOPIN (c)mCitrine	AGGAGATATACCATGGATTCCTGGTTCATTCTTGTTCTGCTCG	AACAGAACTTCCAGAAACTTGAAGTTGGCATAATCTGAGAATGCATCAATATACT
Class I Cys-Based	RPTP	PTPRE	PTPε	PM	BC050062	80.7	1	p2150 pOPIN (c)mCitrine	AGGAGATATACCATGGAGCCCTTGTGTCCACTCCTG	CAGAACTTCCAGAAAGCTTTTGAAATTAGCATAATCAGAAAATATATCAATAAAATCTTGTACCACTT
Class I Cys-Based	RPTP	PTPRG	PTPγ	PM	BC140904	162.0	1	p2150 pOPIN (c)mCitrine	AGGAGATATACCATGCGGAGGTTACTGGAACCGTGTTG	AACAGAACTTCCAGAAACACTAGGGACTCCATGCTCTCAGC
Class I Cys-Based	RPTP	PTPRK	PTPκ	PM	BC140775	163.1	3	p2150 pOPIN (c)mCitrine	AGGAGATATACCATGGATACGACTGCGGCGGCG	AACAGAACTTCCAGAAAAGATGATTCCAGGTACTCCAAAGCTACA
Class I Cys-Based	RPTP	PTPRO	GLEPP1	PM	BC126201	138.4	1	p2150 pOPIN (c)mCitrine	AGGAGATATACCATGGGGCACCTGCCCACGG	AACAGAACTTCCAGAAAGGACTTGCTAACATTCTCGTATATGACATCAC
Class I Cys-Based	RPTP	PTPRR	PCPTP1	PM	BC110900	46.6	3	p2150 pOPIN (c)mCitrine	AGGAGATATACCATGATTCTTTACAGATTAAAAGAAAGATTTCAGCTTTCCTTAAGA	CAGAACTTCCAGAAAGCTCTGGACAGTCTCTGCTGAAAGTCTG
Class I Cys-Based	RPTP	PTPRU	PTPλ	PM, E	BC146655	160.8	3	p2150 pOPIN (c)mCitrine	AGGAGATATACCATGGCCCGTGCCCAGGCG	AACAGAACTTCCAGAAATCTTGACTCCAGCCCCTCCAA
Class I Cys-Based	atypical DUSP	DUPD1	FMDSP, DUSP27	Cy	BC137322	25.3	1	p2297 pOPIN (n)mCitrine	GAAGTTCTGTTTCAGGGTACATCTGGAGAAGTGAAGACAAGCC	CTGGTCTAGAAAGCTTTACAGCTCCCTGCCATCCTCCTC
Class I Cys-Based	atypical DUSP	DUSP12	YVH1	Nu, Cy	BT006633	37.7	1	p2150 pOPIN (c)mCitrine	AGGAGATATACCATGTTGGAGGCTCCGGGCC	CAGAACTTCCAGAAAGCTTATTTTTCCTGTTTGTGATCCCAAAACAGGC
Class I Cys-Based	atypical DUSP	DUSP13b	TMDP, SKRP4	non	DQ892732	22.2	1	p2297 pOPIN (n)mCitrine	GAAGTTCTGTTTCAGGGTGACTCACTGCAGAAGCAGGACC	CTGGTCTAGAAAGCTTTAGAACCGCCCCGTCTCCC
Class I Cys-Based	atypical DUSP	DUSP14	MKP6	non	DQ891379	22.3	1	p2150 pOPIN (c)mCitrine	AGGAGATATACCATGAGCTCCAGAGGTCACAGCAC	CAGAACTTCCAGAAAGCTAATCCCCCAGTAAGGCATCAGGT
Class I Cys-Based	atypical DUSP	DUSP18	LMW-DSP20, DUSP20	Nu, Cy	BC030987	21.1	1	p2297 pOPIN (n)mCitrine	GAAGTTCTGTTTCAGGGTACAGCACCCTCGTGTGCC	CTGGTCTAGAAAGCTTTACAGTGGAATCATCAAACGGACTTCCTTC
Class I Cys-Based	atypical DUSP	DUSP19	SKRP1, DUSP17	Cy	DQ891206	24.2	1	p2150 pOPIN (c)mCitrine	AGGAGATATACCATGTACTCCCTTAACCAGGAAATTAAAGCATTCTC	CAGAACTTCCAGAAAGCTTGAACTGTTCTCCTGTATTCTGTCACACTTAT
Class I Cys-Based	atypical DUSP	DUSP21	LMW-DSP21	Nu, Cy	BC119755	21.5	1	p2150 pOPIN (c)mCitrine	AGGAGATATACCATGACAGCATCCGCGTCCTCC	CAGAACTTCCAGAAAGCTCATTGATATCATCATACGTAGGTCCTTCTCATAGATG
Class I Cys-Based	atypical DUSP	DUSP23	VHZ	Nu, Cy	BC001140	16.6	1	p2297 pOPIN (n)mCitrine	GAAGTTCTGTTTCAGGGTGGCGTGCAGCCCCCC	CTGGTCTAGAAAGCTTTATTTCGTTCGCTGGTAGAACTGGA
Class I Cys-Based	atypical DUSP	DUSP26	MKP8	Nu, Cy	BC067804	24.0	1	p2297 pOPIN (n)mCitrine	GAAGTTCTGTTTCAGGGTTGCCCTGGTAACTGGCTTTGG	CTGGTCTAGAAAGCTTTATGCTTCCAGACCCTGCCG
Class I Cys-Based	atypical DUSP	DUSP3	VHR	Nu, Cy	DQ893122	20.5	1	p2150 pOPIN (c)mCitrine	AGGAGATATACCATGTCGGGCTCGTTCGAGCTCT	CAGAACTTCCAGAAAGCTGGGTTTCAACTTCCCCTCCTTGG
Class I Cys-Based	atypical DUSP	STYX	STYX	Cy	BC020265	25.5	1	p2297 pOPIN (n)mCitrine	GAAGTTCTGTTTCAGGGTGAGGACGTGAAGCTGGAGTTCC	CTGGTCTAGAAAGCTTTAGCCATTCTGTGCAGTCGCCAC
Class I Cys-Based	MKP	DUSP10	MKP5	Nu, Cy	EU176242	52.7	1	p2297 pOPIN (n)mCitrine	GAAGTTCTGTTTCAGGGTCCTCCGTCTCCTTTAGACGACAGG	CTGGTCTAGAAAGCTTTACACAACCGTCTCCACGCCC
Class I Cys-Based	MKP	DUSP2	PAC1	Nu	EU832639	34.4	1	p2297 pOPIN (n)mCitrine	GAAGTTCTGTTTCAGGGTGGGCTGGAGGCGGCG	CTGGTCTAGAAAGCTTTAGTGACACAGCACCTGGGTCTC
Class I Cys-Based	MKP	DUSP4	MKP2	Nu	BC014565	43.0	1	p2150 pOPIN (c)mCitrine	AGGAGATATACCATGGTGACGATGGAGGAGCTGCG	AACAGAACTTCCAGAAAACAGCTGGGAGAGGTGGTGA
Class I Cys-Based	MKP	DUSP6	MKP3	Cy	BC037236	42.3	1	p2297 pOPIN (n)mCitrine	GAAGTTCTGTTTCAGGGTATAGATACGCTCAGACCCGTGCC	CTGGTCTAGAAAGCTTTACGTAGATTGCAGAGAGTCCACCTG
Class I Cys-Based	MKP	DUSP7	PYST2	Cy	BC104880	40.6	2	p2150 pOPIN (c)mCitrine	AGGAGATATACCATGCCCTGCAAGAGCGCCGA	CAGAACTTCCAGAAAGCTCGTGGACTCCAGCGTATTGAGTG
Class I Cys-Based	MKP	STYXL1	DUSP24, MK-STYXL	Cy	DQ893420	35.8	1	p2297 pOPIN (n)mCitrine	GAAGTTCTGTTTCAGGGTCCTGGTTTGCTTTTATGTGAACCGAC	CTGGTCTAGAAAGCTTTAGTAGAGCGGATCCATGATGTTTGTGATGG
Class I Cys-Based	PRL	PTP4A1	PRL1	PM, ER, E	DQ890715	19.8	1	p2297 pOPIN (n)mCitrine	GAAGTTCTGTTTCAGGGTGCTCGAATGAACCGCCCAGC	CTGGTCTAGAAAGCTTTATTGAATGCAACAGTTGTTTCTATGACCGT
Class I Cys-Based	PRL	PTP4A2	PRL2	Cy, PM	NM_080391.2	19.1	1	p2297 pOPIN (n)mCitrine	GAAGTTCTGTTTCAGGGTAACCGTCCAGCCCCTGTG	CTGGTCTAGAAAGCTTTACTGAACACAGCAATGCCCATTGGTATC
Class I Cys-Based	PRL	PTP4A3	PRL3	PM, E	BT007303	16.8	2	p2297 pOPIN (n)mCitrine	GAAGTTCTGTTTCAGGGTGCCCGGATGAACCGCCC	CTGGTCTAGAAAGCTTTACATAACGCAGCACCGGGTCT
Class I Cys-Based	CDC14	CDKN3	KAP1	Cy	NM_005192	23.8	1	p2297 pOPIN (n)mCitrine	GAAGTTCTGTTTCAGGGTAAGCCGCCCAGTTCAATACAAACA	CTGGTCTAGAAAGCTTTATCTTGATACAGATCTTGATTGTGAATCTCTTGATGATAGA
Class I Cys-Based	PTEN-like	PTEN	MMAC1	Cy	DQ892604	47.2	1	p2297 pOPIN (n)mCitrine	GAAGTTCTGTTTCAGGGTACAGCCATCATCAAAGAGATCGTTAGC	CTGGTCTAGAAAGCTTTAGACTTTTGTAATTTGTGTATGCTGATCTTCATCAAAAGG
Class I Cys-Based	PTEN-like	PTPMT	PTPMT, PLIP	Cy, Mito	BC020242	22.9	1	p2150 pOPIN (c)mCitrine	AGGAGATATACCATGGCGGCCACCGCGC	CAGAACTTCCAGAAAGCTTGTCTTTGAAATGACAAAAGTCCCATCCTTT
Class I Cys-Based	Myotubularins	MTM1	CG2	Cy, PM	NM_000252	70.0	1	p2297 pOPIN (n)mCitrine	GAAGTTCTGTTTCAGGGTGCTTCTGCATCAACTTCTAAATATAATTCACACTC	CTGGTCTAGAAAGCTTTAGAAGTGAGTTTGCACATGGGGCATC
Class II Cys-Based	LMPTP	ACP1	LMW-PTP	Cy	BT007136	18.0	2	p2150 pOPIN (c)mCitrine	AGGAGATATACCATGGCGGAACAGGCTACCAAGTCC	CAGAACTTCCAGAAAGCTGTGGGCCTTCTCCAAGAACGC
Class III Cys-based	CDC25	CDC25A	CDC25A	Nu, Cy	DQ892919	59.1	1	p2297 pOPIN (n)mCitrine	GAAGTTCTGTTTCAGGGTGAACTGGGCCCGGAGCC	CTGGTCTAGAAAGCTTTAGAGCTTCTTCAGACGACTGTACATCTC
Class III Cys-based	CDC25	CDC25B	CDC25B	Cy	BC009953	65.0	3	p2150 pOPIN (c)mCitrine	AGGAGATATACCATGGAGGTGCCCCAGCCGG	AACAGAACTTCCAGAAACTGGTCCTGCAGCCGGC
Asp-Based	EyA	EYA4	EYA4	Nu, Cy	BC041063	67.1	2	p2150 pOPIN (c)mCitrine	AGGAGATATACCATGGAAGACTCCCAGGATTTAAATGAACAATCAGTAA	CAGAACTTCCAGAAAGCTCAAATACTCTAATTCCAGTGCTTGGTGGAG

BIBLIOGRAPHY

Abram, C.L., and Courtneidge, S.A. (2000). Src family tyrosine kinases and growth factor signaling. Exp Cell Res *254*, 1-13.

Agazie, Y.M., and Hayman, M.J. (2003a). Development of an efficient "substrate-trapping" mutant of Src homology phosphotyrosine phosphatase 2 and identification of the epidermal growth factor receptor, Gab1, and three other proteins as target substrates. J Biol Chem *278*, 13952-13958.

Agazie, Y.M., and Hayman, M.J. (2003b). Molecular mechanism for a role of SHP2 in epidermal growth factor receptor signaling. Mol Cell Biol *23*, 7875-7886.

Al-Aidaroos, A.Q., Yuen, H.F., Guo, K., Zhang, S.D., Chung, T.H., Chng, W.J., and Zeng, Q. (2013). Metastasis-associated PRL-3 induces EGFR activation and addiction in cancer cells. J Clin Invest *123*, 3459-3471.

Alon, U. (2007). Network motifs: theory and experimental approaches. Nat Rev Genet *8*, 450-461.

Alonso, A., Sasin, J., Bottini, N., Friedberg, I., Osterman, A., Godzik, A., Hunter, T., Dixon, J., and Mustelin, T. (2004). Protein tyrosine phosphatases in the human genome. Cell *117*, 699-711.

Andersen, J.N., Jansen, P.G., Echwald, S.M., Mortensen, O.H., Fukada, T., Del Vecchio, R., Tonks, N.K., and Moller, N.P. (2004). A genomic perspective on protein tyrosine phosphatases: gene structure, pseudogenes, and genetic disease linkage. Faseb J *18*, 8-30.

Andersen, J.N., Mortensen, O.H., Peters, G.H., Drake, P.G., Iversen, L.F., Olsen, O.H., Jansen, P.G., Andersen, H.S., Tonks, N.K., and Moller, N.P. (2001). Structural and evolutionary relationships among protein tyrosine phosphatase domains. Mol Cell Biol *21*, 7117-7136.

Arkhipov, A., Shan, Y., Das, R., Endres, N.F., Eastwood, M.P., Wemmer, D.E., Kuriyan, J., and Shaw, D.E. (2013). Architecture and membrane interactions of the EGF receptor. Cell *152*, 557-569.

Backer, J.M. (2000). Phosphoinositide 3-kinases and the regulation of vesicular trafficking. Mol Cell Biol Res Commun *3*, 193-204.

Bae, Y.S., Kang, S.W., Seo, M.S., Baines, I.C., Tekle, E., Chock, P.B., and Rhee, S.G. (1997). Epidermal growth factor (EGF)-induced generation of hydrogen peroxide. Role in EGF receptor-mediated tyrosine phosphorylation. J Biol Chem *272*, 217-221.

Baghdoyan, S., Roupioz, Y., Pitaval, A., Castel, D., Khomyakova, E., Papine, A., Soussaline, F., and Gidrol, X. (2004). Quantitative analysis of highly parallel transfection in cell microarrays. Nucleic acids research *32*, e77.

Barr, A.J., and Knapp, S. (2006). MAPK-specific tyrosine phosphatases: new targets for drug discovery? Trends Pharmacol Sci *27*, 525-530.

Barr, A.J., Ugochukwu, E., Lee, W.H., King, O.N.F., Filippakopoulos, P., Alfano, I., Savitsky, P., Burgess-Brown, N.A., Muller, S., and Knapp, S. (2009). Large-Scale Structural Analysis of the Classical Human Protein Tyrosine Phosphatome. Cell *136*, 352-363.

Bastiaens, P.I., and Squire, A. (1999). Fluorescence lifetime imaging microscopy: spatial resolution of biochemical processes in the cell. Trends Cell Biol *9*, 48-52.

Batzer, A.G., Rotin, D., Urena, J.M., Skolnik, E.Y., and Schlessinger, J. (1994). Hierarchy of binding sites for Grb2 and Shc on the epidermal growth factor receptor. Mol Cell Biol *14*, 5192-5201.

Becskei, A., and Serrano, L. (2000). Engineering stability in gene networks by autoregulation. Nature *405*, 590-593.

Berman-Golan, D., and Elson, A. (2007). Neu-mediated phosphorylation of protein tyrosine phosphatase epsilon is critical for activation of Src in mammary tumor cells. Oncogene *26*, 7028-7037.

Berrow, N.S., Alderton, D., Sainsbury, S., Nettleship, J., Assenberg, R., Rahman, N., Stuart, D.I., and Owens, R.J. (2007). A versatile ligation-independent cloning method suitable for high-throughput expression screening applications. Nucleic acids research *35*, e45.

Bessette, D.C., Qiu, D.X., and Pallen, C.J. (2008). PRL PTPs: mediators and markers of cancer progression. Cancer Metast Rev *27*, 231-252.

Bilwes, A.M., den Hertog, J., Hunter, T., and Noel, J.P. (1996). Structural basis for inhibition of receptor protein-tyrosine phosphatase-alpha by dimerization. Nature *382*, 555-559.

Birtwistle, M.R., and Kholodenko, B.N. (2009). Endocytosis and signalling: a meeting with mathematics. Mol Oncol *3*, 308-320.

Biscardi, J.S., Maa, M.C., Tice, D.A., Cox, M.E., Leu, T.H., and Parsons, S.J. (1999). c-Src-mediated phosphorylation of the epidermal growth factor receptor on Tyr845 and Tyr1101 is associated with modulation of receptor function. J Biol Chem *274*, 8335-8343.

Bjorge, J.D., Pang, A., and Fujita, D.J. (2000). Identification of protein-tyrosine phosphatase 1B as the major tyrosine phosphatase activity capable of dephosphorylating and activating c-Src in several human breast cancer cell lines. Journal of Biological Chemistry *275*, 41439-41446.

Blanco-Aparicio, C., Torres, J., and Pulido, R. (1999). A novel regulatory mechanism of MAP kinases activation and nuclear translocation mediated by PKA and the PTP-SL tyrosine phosphatase. Journal of Cell Biology *147*, 1129-1135.

Blume-Jensen, P., and Hunter, T. (2001). Oncogenic kinase signalling. Nature *411*, 355-365.

Bonifacino, J.S., and Lippincott-Schwartz, J. (2003). Coat proteins: shaping membrane transport. Nat Rev Mol Cell Biol *4*, 409-414.

Braithwaite, S.P., Paul, S., Nairn, A.C., and Lombroso, P.J. (2006). Synaptic plasticity: one STEP at a time. Trends Neurosci *29*, 452-458.

Brondello, J.M., Pouyssegur, J., and McKenzie, F.R. (1999). Reduced MAP kinase phosphatase-1 degradation after p42/p44(MAPK)-dependent phosphorylation. Science *286*, 2514-2517.

Burgess, A.W., Cho, H.S., Eigenbrot, C., Ferguson, K.M., Garrett, T.P., Leahy, D.J., Lemmon, M.A., Sliwkowski, M.X., Ward, C.W., and Yokoyama, S. (2003). An open-and-shut case? Recent insights into the activation of EGF/ErbB receptors. Mol Cell *12*, 541-552.

Cao, C., Laporte, J., Backer, J.M., Wandinger-Ness, A., and Stein, M.P. (2007). Myotubularin lipid phosphatase binds the hVPS15/hVPS34 lipid kinase complex on endosomes. Traffic *8*, 1052-1067.

Cardone, L., Carlucci, A., Affaitati, A., Livigni, A., DeCristofaro, T., Garbi, C., Varrone, S., Ullrich, A., Gottesman, M.E., Avvedimento, E.V.*, et al.* (2004). Mitochondrial AKAP121 binds and targets protein tyrosine phosphatase D1, a novel positive regulator of src signaling. Mol Cell Biol *24*, 4613-4626.

Carlucci, A., Porpora, M., Garbi, C., Galgani, M., Santoriello, M., Mascolo, M., di Lorenzo, D., Altieri, V., Quarto, M., Terracciano, L.*, et al.* (2010). PTPD1 supports receptor stability and mitogenic signaling in bladder cancer cells. J Biol Chem *285*, 39260-39270.

Carpentier, J.L., White, M.F., Orci, L., and Kahn, R.C. (1987). Direct visualization of the phosphorylated epidermal growth factor receptor during its internalization in A-431 cells. J Cell Biol *105*, 2751-2762.

Chandler, C.E., and Herschman, H.R. (1983). Binding, Sequestration, and Processing of Epidermal Growth-Factor and Nerve Growth-Factor by Pc12-Cells. Journal of Cellular Physiology *114*, 321-327.

Chen, A.J., Zhou, G.S., Juan, T., Colicos, S.M., Cannon, J.P., Cabriera-Hansen, M., Meyer, C.F., Jurecic, R., Copeland, N.G., Gilbert, D.J.*, et al.* (2002). The dual specificity JKAP specifically activates the c-Jun N-terminal kinase pathway. Journal of Biological Chemistry *277*, 36592-36601.

Chen, Z.Y., Ieraci, A., Tanowitz, M., and Lee, F.S. (2005). A novel endocytic recycling signal distinguishes biological responses of Trk neurotrophin receptors. Mol Biol Cell *16*, 5761-5772.

Chiarugi, P., Fiaschi, T., Taddei, M.L., Talini, D., Giannoni, E., Raugei, G., and Ramponi, G. (2001). Two vicinal cysteines confer a peculiar redox regulation to

low molecular weight protein tyrosine phosphatase in response to platelet-derived growth factor receptor stimulation. Journal of Biological Chemistry *276*, 33478-33487.

Chinkers, M., McKanna, J.A., and Cohen, S. (1979). Rapid induction of morphological changes in human carcinoma cells A-431 by epidermal growth factors. J Cell Biol *83*, 260-265.

Chung, I., Akita, R., Vandlen, R., Toomre, D., Schlessinger, J., and Mellman, I. (2010). Spatial control of EGF receptor activation by reversible dimerization on living cells. Nature *464*, 783-787.

Citri, A., and Yarden, Y. (2006). EGF-ERBB signalling: towards the systems level. Nat Rev Mol Cell Biol *7*, 505-516.

Clayton, A.H., Hanley, Q.S., and Verveer, P.J. (2004). Graphical representation and multicomponent analysis of single-frequency fluorescence lifetime imaging microscopy data. J Microsc *213*, 1-5.

Cool, D.E., Tonks, N.K., Charbonneau, H., Walsh, K.A., Fischer, E.H., and Krebs, E.G. (1989). cDNA isolated from a human T-cell library encodes a member of the protein-tyrosine-phosphatase family. P Natl Acad Sci USA *86*, 5257-5261.

Coticchia, C.M., Revankar, C.M., Deb, T.B., Dickson, R.B., and Johnson, M.D. (2009). Calmodulin modulates Akt activity in human breast cancer cell lines. Breast Cancer Res Treat *115*, 545-560.

den Hertog, J., Ostman, A., and Bohmer, F.D. (2008). Protein tyrosine phosphatases: regulatory mechanisms. Febs J *275*, 831-847.

den Hertog, J., Sap, J., Pals, C.E., Schlessinger, J., and Kruijer, W. (1995). Stimulation of receptor protein-tyrosine phosphatase alpha activity and phosphorylation by phorbol ester. Cell Growth Differ *6*, 303-307.

Denu, J.M., and Tanner, K.G. (1998). Specific and reversible inactivation of protein tyrosine phosphatases by hydrogen peroxide: evidence for a sulfenic acid intermediate and implications for redox regulation. Biochemistry *37*, 5633-5642.

Devi, Y.S., Seibold, A.M., Shehu, A., Maizels, E., Halperin, J., Le, J., Binart, N., Bao, L., and Gibori, G. (2011). Inhibition of MAPK by Prolactin Signaling through the Short Form of Its Receptor in the Ovary and Decidua INVOLVEMENT OF A NOVEL PHOSPHATASE. Journal of Biological Chemistry *286*, 7609-7618.

Dowd, S., Sneddon, A.A., and Keyse, S.M. (1998). Isolation of the human genes encoding the Pyst1 and Pyst2 phosphatases: Characterisation of Pyst2 as a cytosolic dual-specificity MAP kinase phosphatase and its catalytic activation by both MAP and SAP kinases. J Cell Sci *111*, 3389-3399.

Dunn, W.A., and Hubbard, A.L. (1984). Receptor-mediated endocytosis of epidermal growth factor by hepatocytes in the perfused rat liver: ligand and receptor dynamics. J Cell Biol *98*, 2148-2159.

Eden, E.R., White, I.J., Tsapara, A., and Futter, C.E. (2010). Membrane contacts between endosomes and ER provide sites for PTP1B-epidermal growth factor receptor interaction. Nat Cell Biol *12*, 267-272.

Efron, B. (1981). Nonparametric Estimates of Standard Error - the Jackknife, the Bootstrap and Other Methods. Biometrika *68*, 589-599.

Elchebly, M., Payette, P., Michaliszyn, E., Cromlish, W., Collins, S., Loy, A.L., Normandin, D., Cheng, A., Himms-Hagen, J., Chan, C.C.*, et al.* (1999). Increased insulin sensitivity and obesity resistance in mice lacking the protein tyrosine phosphatase-1B gene. Science *283*, 1544-1548.

Elson, A., and Leder, P. (1995). Identification of a cytoplasmic, phorbol ester-inducible isoform of protein tyrosine phosphatase epsilon. P Natl Acad Sci USA *92*, 12235-12239.

Endres, N.F., Das, R., Smith, A.W., Arkhipov, A., Kovacs, E., Huang, Y., Pelton, J.G., Shan, Y., Shaw, D.E., Wemmer, D.E.*, et al.* (2013). Conformational coupling across the plasma membrane in activation of the EGF receptor. Cell *152*, 543-556.

Erfle, H., Neumann, B., Liebel, U., Rogers, P., Held, M., Walter, T., Ellenberg, J., and Pepperkok, R. (2007). Reverse transfection on cell arrays for high content screening microscopy. Nature protocols *2*, 392-399.

Erfle, H., Simpson, J.C., Bastiaens, P.I.H., and Pepperkok, R. (2004). siRNA cell arrays for high-content screening microscopy. Biotechniques *37*, 454-+.

Fang, K.S., Sabe, H., Saito, H., and Hanafusa, H. (1994). Comparative study of three protein-tyrosine phosphatases. Chicken protein-tyrosine phosphatase lambda dephosphorylates c-Src tyrosine 527. J Biol Chem *269*, 20194-20200.

Fano, U. (1947). Ionization Yield of Radiations .2. The Fluctuations of the Number of Ions. Phys Rev *72*, 26-29.

Fengler, S., Bastiaens, P.I., Grecco, H.E., and Roda-Navarro, P. (2012). Optimizing cell arrays for accurate functional genomics. BMC Res Notes *5*, 358.

Ferguson, K.M., Berger, M.B., Mendrola, J.M., Cho, H.S., Leahy, D.J., and Lemmon, M.A. (2003). EGF activates its receptor by removing interactions that autoinhibit ectodomain dimerization. Mol Cell *11*, 507-517.

Fili, N., Calleja, V., Woscholski, R., Parker, P.J., and Larijani, B. (2006). Compartmental signal modulation: Endosomal phosphatidylinositol 3-phosphate controls endosome morphology and selective cargo sorting. P Natl Acad Sci USA *103*, 15473-15478.

Finkel, T. (2006). Intracellular redox regulation by the family of small GTPases. Antioxid Redox Signal *8*, 1857-1863.

Fischer, E.H., Charbonneau, H., and Tonks, N.K. (1991). Protein tyrosine phosphatases: a diverse family of intracellular and transmembrane enzymes. Science *253*, 401-406.

Fjeldbo, C.S., Misund, K., Gunther, C.C., Langaas, M., Steigedal, T.S., Thommesen, L., Laegreid, A., and Bruland, T. (2008). Functional studies on transfected cell microarray analysed by linear regression modelling. Nucleic acids research *36*, e97.

Flint, A.J., Tiganis, T., Barford, D., and Tonks, N.K. (1997). Development of "substrate-trapping" mutants to identify physiological substrates of protein tyrosine phosphatases. P Natl Acad Sci USA *94*, 1680-1685.

Förster, T. (1948). "Zwischenmolekulare Energiewanderung und Fluoreszenz" [Intermolecular energy migration and fluorescence]. Annalen der Physik (in German) 437: 55–75.

Frangioni, J.V., Beahm, P.H., Shifrin, V., Jost, C.A., and Neel, B.G. (1992). The nontransmembrane tyrosine phosphatase PTP-1B localizes to the endoplasmic reticulum via its 35 amino acid C-terminal sequence. Cell *68*, 545-560.

Frangioni, J.V., Oda, A., Smith, M., Salzman, E.W., and Neel, B.G. (1993). Calpain-catalyzed cleavage and subcellular relocation of protein phosphotyrosine phosphatase 1B (PTP-1B) in human platelets. Embo J *12*, 4843-4856.

Frank, C., Burkhardt, C., Imhof, D., Ringel, J., Zschornig, O., Wieligmann, K., Zacharias, M., and Bohmer, F.D. (2004). Effective dephosphorylation of Src substrates by SHP-1. J Biol Chem *279*, 11375-11383.

Frey, B.J., and Dueck, D. (2007). Clustering by passing messages between data points. Science *315*, 972-976.

Gadella, T.W.J., Jovin, T. M., & Clegg, R. M. (1993). Fluorescence lifetime imaging microscopy (FLIM): spatial resolution of microstructures on the nanosecond time scale. Biophysical Chemistry, 48(2), 221-239.

Garrett, T.P., McKern, N.M., Lou, M., Elleman, T.C., Adams, T.E., Lovrecz, G.O., Zhu, H.J., Walker, F., Frenkel, M.J., Hoyne, P.A.*, et al.* (2002). Crystal structure of a truncated epidermal growth factor receptor extracellular domain bound to transforming growth factor alpha. Cell *110*, 763-773.

Gatto, G., Dudanova, I., Suetterlin, P., Davies, A.M., Drescher, U., Bixby, J.L., and Klein, R. (2013). Protein Tyrosine Phosphatase Receptor Type O Inhibits Trigeminal Axon Growth and Branching by Repressing TrkB and Ret Signaling. Journal of Neuroscience *33*, 5399-5410.

Gil-Henn, H., and Elson, A. (2003). Tyrosine phosphatase-epsilon activates Src and supports the transformed phenotype of Neu-induced mammary tumor cells. Journal of Biological Chemistry *278*, 15579-15586.

Gil-Henn, H., Volohonsky, G., Toledano-Katchalski, H., Gandre, S., and Elson, A. (2000). Generation of novel cytoplasmic forms of protein tyrosine phosphatase epsilon by proteolytic processing and translational control. Oncogene *19*, 4375-4384.

Goldbeter, A., and Koshland, D.E., Jr. (1981). An amplified sensitivity arising from covalent modification in biological systems. P Natl Acad Sci USA *78*, 6840-6844.

Gotoh, N., Tojo, A., Hino, M., Yazaki, Y., and Shibuya, M. (1992). A highly conserved tyrosine residue at codon 845 within the kinase domain is not required for the transforming activity of human epidermal growth factor receptor. Biochem Biophys Res Commun *186*, 768-774.

Grecco, H.E., Roda-Navarro, P., Fengler, S., and Bastiaens, P.I. (2011a). High-throughput quantification of posttranslational modifications in situ by CA-FLIM. Methods in enzymology *500*, 37-58.

Grecco, H.E., Roda-Navarro, P., Girod, A., Hou, J., Frahm, T., Truxius, D.C., Pepperkok, R., Squire, A., and Bastiaens, P.I. (2010). In situ analysis of tyrosine phosphorylation networks by FLIM on cell arrays. Nature methods *7*, 467-472.

Grecco, H.E., Roda-Navarro, P., and Verveer, P.J. (2009). Global analysis of time correlated single photon counting FRET-FLIM data. Opt Express *17*, 6493-6508.

Grecco, H.E., Schmick, M., and Bastiaens, P.I. (2011b). Signaling from the living plasma membrane. Cell *144*, 897-909.

Greene, L.A., and Tischler, A.S. (1976). Establishment of a noradrenergic clonal line of rat adrenal pheochromocytoma cells which respond to nerve growth factor. P Natl Acad Sci USA *73*, 2424-2428.

Griesbeck, O., Baird, G.S., Campbell, R.E., Zacharias, D.A., and Tsien, R.Y. (2001). Reducing the environmental sensitivity of yellow fluorescent protein. Mechanism and applications. J Biol Chem *276*, 29188-29194.

Groen, A., Lemeer, S., van der Wijk, T., Overvoorde, J., Heck, A.J.R., Ostman, A., Barford, D., Slijper, M., and den Hertog, J. (2005). Differential oxidation of protein-tyrosine phosphatases. Journal of Biological Chemistry *280*, 10298-10304.

Groenen, L.C., Nice, E.C., and Burgess, A.W. (1994). Structure-function relationships for the EGF/TGF-alpha family of mitogens. Growth Factors *11*, 235-257.

Grovdal, L.M., Stang, E., Sorkin, A., and Madshus, I.H. (2004). Direct interaction of Cbl with pTyr 1045 of the EGF receptor (EGFR) is required to sort the EGFR to lysosomes for degradation. Exp Cell Res *300*, 388-395.

Haigler, H.T., McKanna, J.A., and Cohen, S. (1979). Direct visualization of the binding and internalization of a ferritin conjugate of epidermal growth factor in human carcinoma cells A-431. J Cell Biol *81*, 382-395.

Haj, F.G., Markova, B., Klaman, L.D., Bohmer, F.D., and Neel, B.G. (2003). Regulation of receptor tyrosine kinase signaling by protein tyrosine phosphatase-1B. Journal of Biological Chemistry *278*, 739-744.

Haj, F.G., Verveer, P.J., Squire, A., Neel, B.G., and Bastiaens, P.I. (2002). Imaging sites of receptor dephosphorylation by PTP1B on the surface of the endoplasmic reticulum. Science *295*, 1708-1711.

Hao, L., Tiganis, T., Tonks, N.K., and Charbonneau, H. (1997). The noncatalytic C-terminal segment of the T cell protein tyrosine phosphatase regulates activity via an intramolecular mechanism. J Biol Chem *272*, 29322-29329.

Hardy, S., Wong, N.N., Muller, W.J., Park, M., and Tremblay, M.L. (2010). Overexpression of the Protein Tyrosine Phosphatase PRL-2 Correlates with Breast Tumor Formation and Progression. Cancer Research *70*, 8959-8967.

Harris, R.C., Chung, E., and Coffey, R.J. (2003). EGF receptor ligands. Exp Cell Res *284*, 2-13.

He, D., Song, X., Liu, L., Burk, D.H., and Zhou, G.W. (2005). EGF-stimulation activates the nuclear localization signal of SHP-1. Journal of cellular biochemistry *94*, 944-953.

Helin, K., and Beguinot, L. (1991). Internalization and down-regulation of the human epidermal growth factor receptor are regulated by the carboxyl-terminal tyrosines. J Biol Chem *266*, 8363-8368.

Hempel, S., Koseska, A., Nikoloski, Z., and Kurths, J. (2011). Unraveling gene regulatory networks from time-resolved gene expression data - a measures comparison study. BMC Bioinformatics *12*, 292.

Hennipman, A., Vanoirschot, B.A., Smits, J., Rijksen, G., and Staal, G.E.J. (1989). Tyrosine Kinase-Activity in Breast-Cancer, Benign Breast Disease, and Normal Breast-Tissue. Cancer Research *49*, 516-521.

Hoepfner, S., Severin, F., Cabezas, A., Habermann, B., Runge, A., Giilooly, D., Stenmark, H., and Zerial, M. (2005). Modulation of receptor recycling and degradation by the endosomal kinesin KIF16B. Cell *121*, 437-450.

Hof, P., Pluskey, S., Dhe-Paganon, S., Eck, M.J., and Shoelson, S.E. (1998). Crystal structure of the tyrosine phosphatase SHP-2. Cell *92*, 441-450.

Hood, K.L., Tobin, J.F., and Yoon, C. (2002). Identification and characterization of two novel low-molecular-weight dual specificity phosphatases. Biochem Biophys Res Commun *298*, 545-551.

Hsu, J.M., Chen, C.T., Chou, C.K., Kuo, H.P., Li, L.Y., Lin, C.Y., Lee, H.J., Wang, Y.N., Liu, M., Liao, H.W*., et al.* (2011). Crosstalk between Arg 1175 methylation and Tyr 1173 phosphorylation negatively modulates EGFR-mediated ERK activation. Nat Cell Biol *13*, 174-181.

Hsuan, J.J., Totty, N., and Waterfield, M.D. (1989). Identification of a novel autophosphorylation site (P4) on the epidermal growth factor receptor. Biochem J *262*, 659-663.

Huang, F., Goh, L.K., and Sorkin, A. (2007). EGF receptor ubiquitination is not necessary for its internalization. P Natl Acad Sci USA *104*, 16904-16909.

Huang, F., Kirkpatrick, D., Jiang, X., Gygi, S., and Sorkin, A. (2006). Differential regulation of EGF receptor internalization and degradation by multiubiquitination within the kinase domain. Mol Cell *21*, 737-748.

Hurley, J.H., and Meyer, T. (2001). Subcellular targeting by membrane lipids. Curr Opin Cell Biol *13*, 146-152.

Hyatt, D.C., and Ceresa, B.P. (2008). Cellular localization of the activated EGFR determines its effect on cell growth in MDA-MB-468 cells. Exp Cell Res *314*, 3415-3425.

Hyun, S.W., Anglin, I.E., Liu, A., Yang, S., Sorkin, J.D., Lillehoj, E., Tonks, N.K., Passaniti, A., and Goldblum, S.E. (2011). Diverse injurious stimuli reduce protein tyrosine phosphatase-mu expression and enhance epidermal growth factor receptor signaling in human airway epithelia. Exp Lung Res *37*, 327-343.

Jiang, X., Huang, F., Marusyk, A., and Sorkin, A. (2003a). Grb2 regulates internalization of EGF receptors through clathrin-coated pits. Mol Biol Cell *14*, 858-870.

Jiang, X.J., Huang, F.T., Marusyk, A., and Sorkin, A. (2003b). Grb2 regulates internalization of EGF receptors through clathrin-coated pits. Mol Biol Cell *14*, 858-870.

Julien, S.G., Dube, N., Hardy, S., and Tremblay, M.L. (2011). Inside the human cancer tyrosine phosphatome. Nat Rev Cancer *11*, 35-49.

Jura, N., Endres, N.F., Engel, K., Deindl, S., Das, R., Lamers, M.H., Wemmer, D.E., Zhang, X., and Kuriyan, J. (2009). Mechanism for activation of the EGF receptor catalytic domain by the juxtamembrane segment. Cell *137*, 1293-1307.

Kamentsky, L., Jones, T.R., Fraser, A., Bray, M.A., Logan, D.J., Madden, K.L., Ljosa, V., Rueden, C., Eliceiri, K.W., and Carpenter, A.E. (2011). Improved structure, function and compatibility for CellProfiler: modular high-throughput image analysis software. Bioinformatics *27*, 1179-1180.

Kao, S.C., Jaiswal, R.K., Kolch, W., and Landreth, G.E. (2001). Identification of the mechanisms regulating the differential activation of the MAPK cascade by epidermal growth factor and nerve growth factor in PC12 cells. Journal of Biological Chemistry *276*, 18169-18177.

Karisch, R., Fernandez, M., Taylor, P., Virtanen, C., St-Germain, J.R., Jin, L.L., Harris, I.S., Mori, J., Mak, T.W., Senis, Y.A.*, et al.* (2011). Global proteomic assessment of the classical protein-tyrosine phosphatome and "Redoxome". Cell *146*, 826-840.

Keilhack, H., Tenev, T., Nyakatura, E., Godovac-Zimmermann, J., Nielsen, L., Seedorf, K., and Bohmer, F.D. (1998). Phosphotyrosine 1173 mediates binding of the protein-tyrosine phosphatase SHP-1 to the epidermal growth factor receptor and attenuation of receptor signaling. J Biol Chem *273*, 24839-24846.

Keyse, S.M. (2008). Dual-specificity MAP kinase phosphatases (MKPs) and cancer. Cancer Metast Rev *27*, 253-261.

Kholodenko, B.N., Kiyatkin, A., Bruggeman, F.J., Sontag, E., Westerhoff, H.V., and Hoek, J.B. (2002). Untangling the wires: a strategy to trace functional interactions in signaling and gene networks. P Natl Acad Sci USA *99*, 12841-12846.

Kikawa, K.D., Vidale, D.R., Van Etten, R.L., and Kinch, M.S. (2002). Regulation of the EphA2 kinase by the low molecular weight tyrosine phosphatase induces transformation. Journal of Biological Chemistry *277*, 39274-39279.

Kim, L.C., Song, L.X., and Haura, E.B. (2009). Src kinases as therapeutic targets for cancer. Nat Rev Clin Oncol *6*, 587-595.

Kirchhausen, T. (2000). Clathrin. Annu Rev Biochem *69*, 699-727.

Knowles, P.P., Murray-Rust, J., Kjaer, S., Scott, R.P., Hanrahan, S., Santoro, M., Ibanez, C.F., and McDonald, N.Q. (2006). Structure and chemical inhibition of the RET tyrosine kinase domain. J Biol Chem *281*, 33577-33587.

Koshio, O., Akanuma, Y., and Kasuga, M. (1988). Hydrogen peroxide stimulates tyrosine phosphorylation of the insulin receptor and its tyrosine kinase activity in intact cells. Biochem J *250*, 95-101.

Krieger-Brauer, H.I., Medda, P.K., and Kather, H. (1997). Insulin-induced activation of NADPH-dependent H2O2 generation in human adipocyte plasma membranes is mediated by Galphai2. J Biol Chem *272*, 10135-10143.

Kulas, D.T., Goldstein, B.J., and Mooney, R.A. (1996). The transmembrane protein-tyrosine phosphatase LAR modulates signaling by multiple receptor tyrosine kinases. J Biol Chem *271*, 748-754.

Kumar, R., Conklin, D.S., and Mittal, V. (2003). High-throughput selection of effective RNAi probes for gene silencing. Genome research *13*, 2333-2340.

Lacasa, D., Boute, N., and Issad, T. (2005). Interaction of the insulin receptor with the receptor-like protein tyrosine phosphatases PTPalpha and PTPepsilon in living cells. Mol Pharmacol *67*, 1206-1213.

Lakowicz, J. (2008). Principles of Fluorescence Spectroscopy. 3rd edn. Spring Street, New York, NY, USA.

Lam, M.H., Michell, B.J., Fodero-Tavoletti, M.T., Kemp, B.E., Tonks, N.K., and Tiganis, T. (2001). Cellular stress regulates the nucleocytoplasmic distribution of the protein-tyrosine phosphatase TCPTP. J Biol Chem *276*, 37700-37707.

Lambeth, J.D. (2004). NOX enzymes and the biology of reactive oxygen. Nat Rev Immunol *4*, 181-189.

Lammers, R., Bossenmaier, B., Cool, D.E., Tonks, N.K., Schlessinger, J., Fischer, E.H., and Ullrich, A. (1993). Differential activities of protein tyrosine phosphatases in intact cells. J Biol Chem *268*, 22456-22462.

Lammers, R., Moller, N.P.H., and Ullrich, A. (1997). The transmembrane protein tyrosine phosphatase alpha dephosphorylates the insulin receptor in intact cells. FEBS Lett *404*, 37-40.

Landau, M., and Ben-Tal, N. (2008). Dynamic equilibrium between multiple active and inactive conformations explains regulation and oncogenic mutations in ErbB receptors. Biochimica et biophysica acta *1785*, 12-31.

Le Roy, C., and Wrana, J.L. (2005). Clathrin- and non-clathrin-mediated endocytic regulation of cell signalling. Nat Rev Mol Cell Bio *6*, 112-126.

Lemmon, M.A., and Schlessinger, J. (2010). Cell signaling by receptor tyrosine kinases. Cell *141*, 1117-1134.

Levkowitz, G., Waterman, H., Ettenberg, S.A., Katz, M., Tsygankov, A.Y., Alroy, I., Lavi, S., Iwai, K., Reiss, Y., Ciechanover, A.*, et al.* (1999). Ubiquitin ligase activity and tyrosine phosphorylation underlie suppression of growth factor signaling by c-Cbl/Sli-1. Mol Cell *4*, 1029-1040.

Li, M.Z., and Elledge, S.J. (2007). Harnessing homologous recombination in vitro to generate recombinant DNA via SLIC. Nature methods *4*, 251-256.

Li, Q., Harraz, M.M., Zhou, W., Zhang, L.N., Ding, W., Zhang, Y., Eggleston, T., Yeaman, C., Banfi, B., and Engelhardt, J.F. (2006). Nox2 and Rac1 regulate H2O2-dependent recruitment of TRAF6 to endosomal interleukin-1 receptor complexes. Mol Cell Biol *26*, 140-154.

Liu, F., and Chernoff, J. (1997). Protein tyrosine phosphatase 1B interacts with and is tyrosine phosphorylated by the epidermal growth factor receptor. Biochem J *327 (Pt 1)*, 139-145.

Lombardo, C.R., Consler, T.G., and Kassel, D.B. (1995). In vitro phosphorylation of the epidermal growth factor receptor autophosphorylation domain by c-src: Identification of phosphorylation sites and c-src SH2 domain binding sites. Biochemistry *34*, 16456-16466.

Low-Nam, S.T., Lidke, K.A., Cutler, P.J., Roovers, R.C., van Bergen en Henegouwen, P.M., Wilson, B.S., and Lidke, D.S. (2011). ErbB1 dimerization is promoted by domain co-confinement and stabilized by ligand binding. Nat Struct Mol Biol *18*, 1244-1249.

Ma, H.W., and Zeng, A.P. (2003). The connectivity structure, giant strong component and centrality of metabolic networks. Bioinformatics *19*, 1423-1430.

Mangan, S., Zaslaver, A., and Alon, U. (2003). The coherent feedforward loop serves as a sign-sensitive delay element in transcription networks. J Mol Biol *334*, 197-204.

Mannherz, O., Mertens, D., Hahn, M., and Lichter, P. (2006). Functional screening for proapoptotic genes by reverse transfection cell array technology. Genomics *87*, 665-672.

Margolis, B.L., Lax, I., Kris, R., Dombalagian, M., Honegger, A.M., Howk, R., Givol, D., Ullrich, A., and Schlessinger, J. (1989). All autophosphorylation sites of epidermal growth factor (EGF) receptor and HER2/neu are located in their carboxyl-terminal tails. Identification of a novel site in EGF receptor. J Biol Chem *264*, 10667-10671.

Marshall, C.J. (1995). Specificity of receptor tyrosine kinase signaling: transient versus sustained extracellular signal-regulated kinase activation. Cell *80*, 179-185.

Matozaki, T., Murata, Y., Mori, M., Kotani, T., Okazawa, H., and Ohnishi, H. (2010). Expression, localization, and biological function of the R3 subtype of receptor-type protein tyrosine phosphatases in mammals. Cell Signal *22*, 1811-1817.

Mattila, E., Pellinen, T., Nevo, J., Vuoriluoto, K., Arjonen, A., and Ivaska, J. (2005). Negative regulation of EGFR signalling through integrin-alpha(1)beta(1)-mediated activation of protein tyrosine phosphatase TCPTP. Nat Cell Biol *7*, 78-+.

Mauro, L.J., and Dixon, J.E. (1994). 'Zip codes' direct intracellular protein tyrosine phosphatases to the correct cellular 'address'. Trends Biochem Sci *19*, 151-155.

McKanna, J.A., Haigler, H.T., and Cohen, S. (1979). Hormone receptor topology and dynamics: morphological analysis using ferritin-labeled epidermal growth factor. P Natl Acad Sci USA *76*, 5689-5693.

Meng, K., Rodriguez-Pena, A., Dimitrov, T., Chen, W., Yamin, M., Noda, M., and Deuel, T.F. (2000). Pleiotrophin signals increased tyrosine phosphorylation of beta beta-catenin through inactivation of the intrinsic catalytic activity of the receptor-type protein tyrosine phosphatase beta/zeta. P Natl Acad Sci USA *97*, 2603-2608.

Meng, T.C., Fukada, T., and Tonks, N.K. (2002). Reversible oxidation and inactivation of protein tyrosine phosphatases in vivo. Mol Cell *9*, 387-399.

Miaczynska, M., Pelkmans, L., and Zerial, M. (2004). Not just a sink: endosomes in control of signal transduction. Curr Opin Cell Biol *16*, 400-406.

Michell, R.H., Heath, V.L., Lemmon, M.A., and Dove, S.K. (2006). Phosphatidylinositol 3,5-bisphosphate: metabolism and cellular functions. Trends Biochem Sci *31*, 52-63.

Miller, K., Beardmore, J., Kanety, H., Schlessinger, J., and Hopkins, C.R. (1986). Localization of the epidermal growth factor (EGF) receptor within the endosome of EGF-stimulated epidermoid carcinoma (A431) cells. J Cell Biol *102*, 500-509.

Morandell, S., Stasyk, T., Skvortsov, S., Ascher, S., and Huber, L.A. (2008). Quantitative proteomics and phosphoproteomics reveal novel insights into complexity and dynamics of the EGFR signaling network. Proteomics *8*, 4383-4401.

Mori, M., Murata, Y., Kotani, T., Kusakari, S., Ohnishi, H., Saito, Y., Okazawa, H., Ishizuka, T., Mori, M., and Matozaki, T. (2010). Promotion of Cell Spreading and Migration by Vascular Endothelial-Protein Tyrosine Phosphatase (VE-PTP) in Cooperation With Integrins. Journal of Cellular Physiology *224*, 195-204.

Mousses, S., Caplen, N.J., Cornelison, R., Weaver, D., Basik, M., Hautaniemi, S., Elkahloun, A.G., Lotufo, R.A., Choudary, A., Dougherty, E.R.*, et al.* (2003). RNAi microarray analysis in cultured mammalian cells. Genome research *13*, 2341-2347.

Murphy, L.O., Smith, S., Chen, R.H., Fingar, D.C., and Blenis, J. (2002). Molecular interpretation of ERK signal duration by immediate early gene products. Nat Cell Biol *4*, 556-564.

Myers, M.P., Andersen, J.N., Cheng, A., Tremblay, M.L., Horvath, C.M., Parisien, J.P., Salmeen, A., Barford, D., and Tonks, N.K. (2001). TYK2 and JAK2 are substrates of protein-tyrosine phosphatase 1B. J Biol Chem *276*, 47771-47774.

Nagashima, T., Shimodaira, H., Ide, K., Nakakuki, T., Tani, Y., Takahashi, K., Yumoto, N., and Hatakeyama, M. (2007). Quantitative transcriptional control of ErbB receptor signaling undergoes graded to biphasic response for cell differentiation. Journal of Biological Chemistry *282*, 4045-4056.

Nagy, P., Claus, J., Jovin, T.M., and Arndt-Jovin, D.J. (2010). Distribution of resting and ligand-bound ErbB1 and ErbB2 receptor tyrosine kinases in living cells using number and brightness analysis. P Natl Acad Sci USA *107*, 16524-16529.

Nakakuki, T., Birtwistle, M.R., Saeki, Y., Yumoto, N., Ide, K., Nagashima, T., Brusch, L., Ogunnaike, B.A., Okada-Hatakeyama, M., and Kholodenko, B.N. (2010). Ligand-Specific c-Fos Expression Emerges from the Spatiotemporal Control of ErbB Network Dynamics. Cell *141*, 884-896.

Nakamura, K., Mizuno, Y., and Kikuchi, K. (1996). Molecular cloning of a novel cytoplasmic protein tyrosine phosphatase PTP epsilon. Biochem Biophys Res Commun *218*, 726-732.

Neel, B.G., Gu, H., and Pao, L. (2003). The 'Shp'ing news: SH2 domain-containing tyrosine phosphatases in cell signaling. Trends Biochem Sci *28*, 284-293.

Neve, R.M., Chin, K., Fridlyand, J., Yeh, J., Baehner, F.L., Fevr, T., Clark, L., Bayani, N., Coppe, J.P., Tong, F.*, et al.* (2006). A collection of breast cancer cell lines for the study of functionally distinct cancer subtypes. Cancer Cell *10*, 515-527.

Neve, R.M., Holbro, T., and Hynes, N.E. (2002). Distinct roles for phosphoinositide 3-kinase, mitogen-activated protein kinase and p38 MAPK in mediating cell cycle progression of breast cancer cells. Oncogene *21*, 4567-4576.

Niwa, R., Nagata-Ohashi, K., Takeichi, M., Mizuno, K., and Uemura, T. (2002). Control of actin reorganization by Slingshot, a family of phosphatases that dephosphorylate ADF/cofilin. Cell *108*, 233-246.

Nunes-Xavier, C., Roma-Mateo, C., Rios, P., Tarrega, C., Cejudo-Marin, R., Tabernero, L., and Pulido, R. (2011). Dual-Specificity MAP Kinase Phosphatases as Targets of Cancer Treatment. Anti-Cancer Agent Me *11*, 109-132.

Nunes-Xavier, C.E., Martin-Perez, J., Elson, A., and Pulido, R. (2013). Protein tyrosine phosphatases as novel targets in breast cancer therapy. Bba-Rev Cancer *1836*, 211-226.

Offterdinger, M., and Bastiaens, P.I. (2008). Prolonged EGFR signaling by ERBB2-mediated sequestration at the plasma membrane. Traffic *9*, 147-155.

Ogiso, H., Ishitani, R., Nureki, O., Fukai, S., Yamanaka, M., Kim, J.H., Saito, K., Sakamoto, A., Inoue, M., Shirouzu, M., *et al.* (2002). Crystal structure of the complex of human epidermal growth factor and receptor extracellular domains. Cell *110*, 775-787.

Oliner, J.D., Kinzler, K.W., and Vogelstein, B. (1993). In vivo cloning of PCR products in E. coli. Nucleic acids research *21*, 5192-5197.

Ostman, A., and Bohmer, F.D. (2001). Regulation of receptor tyrosine kinase signaling by protein tyrosine phosphatases. Trends Cell Biol *11*, 258-266.

Ostman, A., Hellberg, C., and Bohmer, F.D. (2006). Protein-tyrosine phosphatases and cancer. Nature Reviews Cancer *6*, 307-320.

Owens, D.M., and Keyse, S.M. (2007). Differential regulation of MAP kinase signalling by dual-specificity protein phosphatases. Oncogene *26*, 3203-3213.

Pagliarini, D.J., Wiley, S.E., Kimple, M.E., Dixon, J.R., Kelly, P., Worby, C.A., Casey, P.J., and Dixon, J.E. (2005). Involvement of a mitochondrial phosphatase in the regulation of ATP production and insulin secretion in pancreatic beta cells. Mol Cell *19*, 197-207.

Pagliarini, D.J., Worby, C.A., and Dixon, J.E. (2004). A PTEN-like phosphatase with a novel substrate specificity. Journal of Biological Chemistry *279*, 38590-38596.

Pallen, C.J. (2003). Protein tyrosine phosphatase alpha (PTP alpha): A src family kinase activator and mediator of multiple biological effects. Curr Top Med Chem *3*, 821-835.

Pao, L.I., Badour, K., Siminovitch, K.A., and Neel, B.G. (2007). Nonreceptor protein-tyrosine phosphatases in immune cell signaling. Annu Rev Immunol *25*, 473-523.

Pawson, T. (2004). Specificity in signal transduction: from phosphotyrosine-SH2 domain interactions to complex cellular systems. Cell *116*, 191-203.

Persson, C., Sjoblom, T., Groen, A., Kappert, K., Engstrom, U., Hellman, U., Heldin, C.H., den Hertog, J., and Ostman, A. (2004). Preferential oxidation of the second phosphatase domain of receptor-like PTP-alpha revealed by an antibody against oxidized protein tyrosine phosphatases. P Natl Acad Sci USA *101*, 1886-1891.

Pettiford, S.M., and Herbst, R. (2000). The MAP-kinase ERK2 is a specific substrate of the protein tyrosine phosphatase HePTP. Oncogene *19*, 858-869.

Prahallad, A., Sun, C., Huang, S., Di Nicolantonio, F., Salazar, R., Zecchin, D., Beijersbergen, R.L., Bardelli, A., and Bernards, R. (2012). Unresponsiveness of colon cancer to BRAF(V600E) inhibition through feedback activation of EGFR. Nature *483*, 100-103.

Pulido, R., Zuniga, A., and Ullrich, A. (1998). PTP-SL and STEP protein tyrosine phosphatases regulate the activation of the extracellular signal-regulated kinases ERK1 and ERK2 by association through a kinase interaction motif. Embo Journal *17*, 7337-7350.

Qian, H., and Beard, D.A. (2006). Metabolic futile cycles and their functions: a systems analysis of energy and control. Syst Biol (Stevenage) *153*, 192-200.

Qiu, C., Tarrant, M.K., Boronina, T., Longo, P.A., Kavran, J.M., Cole, R.N., Cole, P.A., and Leahy, D.J. (2009). In vitro enzymatic characterization of near full length EGFR in activated and inhibited states. Biochemistry *48*, 6624-6632.

Ramponi, G., Manao, G., Camici, G., Cappugi, G., Ruggiero, M., and Bottaro, D.P. (1989). The 18 Kda Cytosolic Acid-Phosphatase from Bovine Liver Has Phosphotyrosine Phosphatase-Activity on the Autophosphorylated Epidermal Growth-Factor Receptor. FEBS Lett *250*, 469-473.

Rantala, J.K., Makela, R., Aaltola, A.R., Laasola, P., Mpindi, J.P., Nees, M., Saviranta, P., and Kallioniemi, O. (2011). A cell spot microarray method for production of high density siRNA transfection microarrays. BMC Genomics *12*, 162.

Reiterer, V., Fey, D., Kolch, W., Kholodenko, B.N., and Farhan, H. (2013). Pseudophosphatase STYX modulates cell-fate decisions and cell migration by spatiotemporal regulation of ERK1/2. P Natl Acad Sci USA *110*, E2934-2943.

Ren, L., Chen, X., Luechapanichkul, R., Selner, N.G., Meyer, T.M., Wavreille, A.S., Chan, R., Iorio, C., Zhou, X., Neel, B.G.*, et al.* (2011). Substrate specificity of protein tyrosine phosphatases 1B, RPTPalpha, SHP-1, and SHP-2. Biochemistry *50*, 2339-2356.

Reynolds, A.R., Tischer, C., Verveer, P.J., Rocks, O., and Bastiaens, P.I. (2003). EGFR activation coupled to inhibition of tyrosine phosphatases causes lateral signal propagation. Nat Cell Biol *5*, 447-453.

Rhee, S.G. (2006). Cell signaling. H2O2, a necessary evil for cell signaling. Science *312*, 1882-1883.

Rigacci, S., Rovida, E., Bagnoli, S., Dello Sbarba, P., and Berti, A. (1999). Low M(r) phosphotyrosine protein phosphatase activity on fibroblast growth factor receptor is not associated with enzyme translocation. FEBS Lett *459*, 191-194.

Rios, P., Li, X., and Kohn, M. (2013). Molecular mechanisms of the PRL phosphatases. Febs Journal *280*, 505-524.

Roskoski, R. (2005). Src kinase regulation by phosphorylation and dephosphorylation. Biochem Biophys Res Commun *331*, 1-14.

Sacco, F., Gherardini, P.F., Paoluzi, S., Saez-Rodriguez, J., Helmer-Citterich, M., Ragnini-Wilson, A., Castagnoli, L., and Cesareni, G. (2012). Mapping the human phosphatome on growth pathways. Mol Syst Biol *8*, 603.

Saha, S., Bardelli, A., Buckhaults, P., Velculescu, V.E., Rago, C., St Croix, B., Romans, K.E., Choti, M.A., Lengauer, C., Kinzler, K.W*., et al.* (2001). A phosphatase associated with metastasis of colorectal cancer. Science *294*, 1343-1346.

Salmeen, A., Andersen, J.N., Myers, M.P., Tonks, N.K., and Barford, D. (2000). Molecular basis for the dephosphorylation of the activation segment of the insulin receptor by protein tyrosine phosphatase 1B. Mol Cell *6*, 1401-1412.

Salmeen, A., and Barford, D. (2005). Functions and mechanisms of redox regulation of cysteine-based phosphatases. Antioxid Redox Signal *7*, 560-577.

Santos, S.D., Verveer, P.J., and Bastiaens, P.I. (2007). Growth factor-induced MAPK network topology shapes Erk response determining PC-12 cell fate. Nat Cell Biol *9*, 324-330.

Sasagawa, S., Ozaki, Y., Fujita, K., and Kuroda, S. (2005). Prediction and validation of the distinct dynamics of transient and sustained ERK activation. Nat Cell Biol *7*, 365-U331.

Sato, K., Nagao, T., Kakumoto, M., Kimoto, M., Otsuki, T., Iwasaki, T., Tokmakov, A.A., Owada, K., and Fukami, Y. (2002). Adaptor protein Shc is an isoform-specific direct activator of the tyrosine kinase c-Src. Journal of Biological Chemistry *277*, 29568-29576.

Sattler, M., Winkler, T., Verma, S., Byrne, C.H., Shrikhande, G., Salgia, R., and Griffin, J.D. (1999). Hematopoietic growth factors signal through the formation of reactive oxygen species. Blood *93*, 2928-2935.

Sawada, M., Ogata, M., Fujino, Y., and Hamaoka, T. (1994). Cdna Cloning of a Novel Protein-Tyrosine-Phosphatase with Homology to Cytoskeletal Protein-4.1 and Its Expression in T-Lineage Cells. Biochem Biophys Res Commun *203*, 479-484.

Sawano, A., Takayama, S., Matsuda, M., and Miyawaki, A. (2002). Lateral propagation of EGF signaling after local stimulation is dependent on receptor density. Dev Cell *3*, 245-257.

Saxena, M., Williams, S., Tasken, K., and Mustelin, T. (1999). Crosstalk between cAMP-dependent kinase and MAP kinase through a protein tyrosine phosphatase. Nat Cell Biol *1*, 305-311.

Schaletzky, J., Dove, S.K., Short, B., Lorenzo, O., Clague, M.J., and Barr, F.A. (2003). Phosphatidylinositol-5-phosphate activation and conserved substrate specificity of the myotubularin phosphatidylinositol 3-phosphatases. Current Biology *13*, 504-509.

Schlessinger, J. (2002). Ligand-induced, receptor-mediated dimerization and activation of EGF receptor. Cell *110*, 669-672.

Schlessinger, J., and Lemmon, M.A. (2003). SH2 and PTB domains in tyrosine kinase signaling. Sci STKE *2003*, RE12.

Schoeberl, B., Eichler-Jonsson, C., Gilles, E.D., and Muller, G. (2002). Computational modeling of the dynamics of the MAP kinase cascade activated by surface and internalized EGF receptors. Nat Biotechnol *20*, 370-375.

Schulze, W.X., Deng, L., and Mann, M. (2005). Phosphotyrosine interactome of the ErbB-receptor kinase family. Mol Syst Biol *1*, 2005 0008.

Shan, Y., Eastwood, M.P., Zhang, X., Kim, E.T., Arkhipov, A., Dror, R.O., Jumper, J., Kuriyan, J., and Shaw, D.E. (2012). Oncogenic mutations counteract intrinsic disorder in the EGFR kinase and promote receptor dimerization. Cell *149*, 860-870.

Shintani, T., Ihara, M., Sakuta, H., Takahashi, H., Watakabe, I., and Noda, M. (2006). Eph receptors are negatively controlled by protein tyrosine phosphatase receptor type O. Nat Neurosci *9*, 761-769.

Shu, S.T., Sugimoto, Y., Liu, S., Chang, H.L., Ye, W., Wang, L.S., Huang, Y.W., Yan, P., and Lin, Y.C. (2010). Function and regulatory mechanisms of the candidate tumor suppressor receptor protein tyrosine phosphatase gamma (PTPRG) in breast cancer cells. Anticancer Res *30*, 1937-1946.

Sigismund, S., Algisi, V., Nappo, G., Conte, A., Pascolutti, R., Cuomo, A., Bonaldi, T., Argenzio, E., Verhoef, L.G.G.C., Maspero, E.*, et al.* (2013). Threshold-controlled ubiquitination of the EGFR directs receptor fate. Embo Journal *32*, 2140-2157.

Sigismund, S., Argenzio, E., Tosoni, D., Cavallaro, E., Polo, S., and Di Fiore, P.P. (2008). Clathrin-mediated internalization is essential for sustained EGFR signaling but dispensable for degradation. Dev Cell *15*, 209-219.

Sines, T., Granot-Attas, S., Weisman-Welcher, S., and Elson, A. (2007). Association of tyrosine phosphatase epsilon with microtubules inhibits phosphatase activity

and is regulated by the epidermal growth factor receptor. Mol Cell Biol *27*, 7102-7112.

Singh, D.K., Kumar, D., Siddiqui, Z., Basu, S.K., Kumar, V., and Rao, K.V.S. (2005). The strength of receptor signaling is centrally controlled through a cooperative loop between Ca2+ and an oxidant signal. Cell *121*, 281-293.

Somani, A.K., Bignon, J.S., Mills, G.B., Siminovitch, K.A., and Branch, D.R. (1997). Src kinase activity is regulated by the SHP-1 protein-tyrosine phosphatase. Journal of Biological Chemistry *272*, 21113-21119.

Sorkin, A., and Goh, L.K. (2008). Endocytosis and intracellular trafficking of ErbBs. Exp Cell Res *314*, 3093-3106.

Sorkin, A., Krolenko, S., Kudrjavtceva, N., Lazebnik, J., Teslenko, L., Soderquist, A.M., and Nikolsky, N. (1991). Recycling of epidermal growth factor-receptor complexes in A431 cells: identification of dual pathways. J Cell Biol *112*, 55-63.

Stewart-Ornstein, J., Weissman, J.S., and El-Samad, H. (2012). Cellular noise regulons underlie fluctuations in Saccharomyces cerevisiae. Mol Cell *45*, 483-493.

Stover, D.R., Becker, M., Liebetanz, J., and Lydon, N.B. (1995). Src Phosphorylation of the Epidermal Growth-Factor Receptor at Novel Sites Mediates Receptor Interaction with Src and P85-Alpha. Journal of Biological Chemistry *270*, 15591-15597.

Sturani, E., Zippel, R., Toschi, L., Morello, L., Comoglio, P.M., and Alberghina, L. (1988). Kinetics and regulation of the tyrosine phosphorylation of epidermal growth factor receptor in intact A431 cells. Mol Cell Biol *8*, 1345-1351.

Suarez Pestana, E., Tenev, T., Gross, S., Stoyanov, B., Ogata, M., and Bohmer, F.D. (1999). The transmembrane protein tyrosine phosphatase RPTPsigma modulates signaling of the epidermal growth factor receptor in A431 cells. Oncogene *18*, 4069-4079.

Sun, T., Aceto, N., Meerbrey, K.L., Kessler, J.D., Zhou, C., Migliaccio, I., Nguyen, D.X., Pavlova, N.N., Botero, M., Huang, J.*, et al.* (2011). Activation of multiple proto-oncogenic tyrosine kinases in breast cancer via loss of the PTPN12 phosphatase. Cell *144*, 703-718.

Sundaresan, M., Yu, Z.X., Ferrans, V.J., Irani, K., and Finkel, T. (1995). Requirement for generation of H2O2 for platelet-derived growth factor signal transduction. Science *270*, 296-299.

Tarcic, G., Boguslavsky, S.K., Wakim, J., Kiuchi, T., Liu, A., Reinitz, F., Nathanson, D., Takahashi, T., Mischel, P.S., Ng, T.*, et al.* (2009). An unbiased screen identifies DEP-1 tumor suppressor as a phosphatase controlling EGFR endocytosis. Curr Biol *19*, 1788-1798.

Theodosiou, A., and Ashworth, A. (2002). MAP kinase phosphatases. Genome Biol *3*.

Thien, C.B., and Langdon, W.Y. (2005). c-Cbl and Cbl-b ubiquitin ligases: substrate diversity and the negative regulation of signalling responses. Biochem J *391*, 153-166.

Thottassery, J.V., Sun, Y.J., Westbrook, L., Rentz, S.S., Manuvakhova, M., Qu, Z.C., Samuel, S., Upshaw, R., Cunningham, A., and Kern, F.G. (2004). Prolonged extracellular signal-regulated kinase 1/2 activation during fibroblast growth factor 1- or heregulin beta 1-induced antiestrogen-resistant growth of breast cancer cells is resistant to mitogen-activated protein/extracellular regulated kinase kinase inhibitors. Cancer Research *64*, 4637-4647.

Tiganis, T., Bennett, A.M., Ravichandran, K.S., and Tonks, N.K. (1998). Epidermal growth factor receptor and the adaptor protein p52Shc are specific substrates of T-cell protein tyrosine phosphatase. Mol Cell Biol *18*, 1622-1634.

Tiganis, T., Kemp, B.E., and Tonks, N.K. (1999). The protein-tyrosine phosphatase TCPTP regulates epidermal growth factor receptor-mediated and phosphatidylinositol 3-kinase-dependent signaling. J Biol Chem *274*, 27768-27775.

Tischer, C., and Bastiaens, P.I. (2003). Lateral phosphorylation propagation: an aspect of feedback signalling? Nat Rev Mol Cell Biol *4*, 971-974.

Tonks, N.K. (2006). Protein tyrosine phosphatases: from genes, to function, to disease. Nat Rev Mol Cell Biol *7*, 833-846.

Tonks, N.K. (2013). Protein tyrosine phosphatases--from housekeeping enzymes to master regulators of signal transduction. Febs J *280*, 346-378.

Tonks, N.K., and Neel, B.G. (2001). Combinatorial control of the specificity of protein tyrosine phosphatases. Curr Opin Cell Biol *13*, 182-195.

Tracy, S., van der Geer, P., and Hunter, T. (1995). The receptor-like protein-tyrosine phosphatase, RPTP alpha, is phosphorylated by protein kinase C on two serines close to the inner face of the plasma membrane. J Biol Chem *270*, 10587-10594.

Tran, K.T., Rusu, S.D., Satish, L., and Wells, A. (2003). Aging-related attenuation of EGF receptor signaling is mediated in part by increased protein tyrosine phosphatase activity. Exp Cell Res *289*, 359-367.

Traverse, S., Seedorf, K., Paterson, H., Marshall, C.J., Cohen, P., and Ullrich, A. (1994). Egf Triggers Neuronal Differentiation of Pc12 Cells That Overexpress the Egf Receptor. Current Biology *4*, 694-701.

Tsujita, K., Itoh, T., Ijuin, T., Yamamoto, A., Shisheva, A., Laporte, J., and Takenawa, T. (2004). Myotubularin regulates the function of the late endosome through the

gram domain-phosphatidylinositol 3,5-bisphosphate interaction. J Biol Chem *279*, 13817-13824.

Uchida, T., Matozaki, T., Noguchi, T., Yamao, T., Horita, K., Suzuki, T., Fujioka, Y., Sakamoto, C., and Kasuga, M. (1994). Insulin stimulates the phosphorylation of Tyr538 and the catalytic activity of PTP1C, a protein tyrosine phosphatase with Src homology-2 domains. J Biol Chem *269*, 12220-12228.

Ullrich, A., and Schlessinger, J. (1990). Signal transduction by receptors with tyrosine kinase activity. Cell *61*, 203-212.

Umebayashi, K., Stenmark, H., and Yoshimori, T. (2008). Ubc4/5 and c-Cbl continue to ubiquitinate EGF receptor after internalization to facilitate polyubiquitination and degradation. Mol Biol Cell *19*, 3454-3462.

van der Wijk, T., Overvoorde, J., and den Hertog, J. (2004). H2O2-induced intermolecular disulfide bond formation between receptor protein-tyrosine phosphatases. J Biol Chem *279*, 44355-44361.

van Munster, E.B., and Gadella, T.W., Jr. (2004). Suppression of photobleaching-induced artifacts in frequency-domain FLIM by permutation of the recording order. Cytometry A *58*, 185-194.

Verveer, P.J., and Bastiaens, P.I. (2003). Evaluation of global analysis algorithms for single frequency fluorescence lifetime imaging microscopy data. J Microsc *209*, 1-7.

Verveer, P.J., and Bastiaens, P.I. (2008). Quantitative microscopy and systems biology: seeing the whole picture. Histochemistry and cell biology *130*, 833-843.

Verveer, P.J., Squire, A., and Bastiaens, P.I. (2000a). Global analysis of fluorescence lifetime imaging microscopy data. Biophys J *78*, 2127-2137.

Verveer, P.J., Wouters, F.S., Reynolds, A.R., and Bastiaens, P.I. (2000b). Quantitative imaging of lateral ErbB1 receptor signal propagation in the plasma membrane. Science *290*, 1567-1570.

Visintin, R., Craig, K., Hwang, E.S., Prinz, S., Tyers, M., and Amon, A. (1998). The phosphatase Cdc14 triggers mitotic exit by reversal of Cdk-dependent phosphorylation. Mol Cell *2*, 709-718.

Vogel, W., Lammers, R., Huang, J.T., and Ullrich, A. (1993). Activation of a Phosphotyrosine Phosphatase by Tyrosine Phosphorylation. Science *259*, 1611-1614.

Walton, G.M., Chen, W.S., Rosenfeld, M.G., and Gill, G.N. (1990). Analysis of deletions of the carboxyl terminus of the epidermal growth factor receptor reveals self-phosphorylation at tyrosine 992 and enhanced in vivo tyrosine phosphorylation of cell substrates. J Biol Chem *265*, 1750-1754.

Wang, J.Y., Lin, C.H., Yang, C.H., Tan, T.H., and Chen, Y.R. (2006). Biochemical and biological characterization of a neuroendocrine-associated phosphatase. J Neurochem *98*, 89-101.

Wang, J.Y., Yeh, C.L., Chou, H.C., Yang, C.H., Fu, Y.N., Chen, Y.T., Cheng, H.W., Huang, C.Y., Liu, H.P., Huang, S.F.*, et al.* (2011). Vaccinia H1-related phosphatase is a phosphatase of ErbB receptors and is down-regulated in non-small cell lung cancer. J Biol Chem *286*, 10177-10184.

Wang, R., He, G., Nelman-Gonzalez, M., Ashorn, C.L., Gallick, G.E., Stukenberg, P.T., Kirschner, M.W., and Kuang, J. (2007). Regulation of Cdc25C by ERK-MAP kinases during the G2/M transition. Cell *128*, 1119-1132.

Wang, S.E., Wu, F.Y., Shin, I., Qu, S.M., and Arteaga, C.L. (2005). Transforming growth factor beta (TGF-beta)-Smad target gene protein tyrosine phosphatase receptor type kappa is required for TGF-beta function. Mol Cell Biol *25*, 4703-4715.

Wang, Y., and Lazo, J.S. (2012). Metastasis-associated phosphatase PRL-2 regulates tumor cell migration and invasion. Oncogene *31*, 818-827.

Wang, Z., Wang, M., Lazo, J.S., and Carr, B.I. (2002). Identification of epidermal growth factor receptor as a target of Cdc25A protein phosphatase. J Biol Chem *277*, 19470-19475.

Waterman, H., Katz, M., Rubin, C., Shtiegman, K., Lavi, S., Elson, A., Jovin, T., and Yarden, Y. (2002). A mutant EGF-receptor defective in ubiquitylation and endocytosis unveils a role for Grb2 in negative signaling (vol 21, pg 303, 2002). Embo Journal *21*, 3917-3917.

Wiley, H.S. (2003). Trafficking of the ErbB receptors and its influence on signaling. Exp Cell Res *284*, 78-88.

Wiley, H.S., Herbst, J.J., Walsh, B.J., Lauffenburger, D.A., Rosenfeld, M.G., and Gill, G.N. (1991). The role of tyrosine kinase activity in endocytosis, compartmentation, and down-regulation of the epidermal growth factor receptor. J Biol Chem *266*, 11083-11094.

Williamson, M.P. (1994). The Structure and Function of Proline-Rich Regions in Proteins. Biochemical Journal *297*, 249-260.

Wishart, M.J., and Dixon, J.E. (2002). PTEN and myotubularin phosphatases: from 3-phosphoinositide dephosphorylation to disease. Trends Cell Biol *12*, 579-585.

Wouters, F.S., and Bastiaens, P.I. (1999). Fluorescence lifetime imaging of receptor tyrosine kinase activity in cells. Curr Biol *9*, 1127-1130.

Wu, W.D., Graves, L.M., Gill, G.N., Parsons, S.J., and Samet, J.M. (2002). Src-dependent phosphorylation of the epidermal growth factor receptor on tyrosine 845 is required for zinc-induced Ras activation. Journal of Biological Chemistry *277*, 24252-24257.

Xu, Y., Tan, L.J., Grachtchouk, V., Voorhees, J.J., and Fisher, G.J. (2005). Receptor-type protein-tyrosine phosphatase-kappa regulates epidermal growth factor receptor function. J Biol Chem *280*, 42694-42700.

Xu, Y.R., Shao, Y., Voorhees, J.J., and Fisher, G.J. (2006). Oxidative inhibition of receptor-type protein-tyrosine phosphatase kappa by ultraviolet irradiation activates epidermal growth factor receptor in human keratinocytes. Journal of Biological Chemistry *281*, 27389-27397.

Yarden, Y., and Sliwkowski, M.X. (2001). Untangling the ErbB signalling network. Nat Rev Mol Cell Biol *2*, 127-137.

Yoshikawa, T., Uchimura, E., Kishi, M., Funeriu, D.P., Miyake, M., and Miyake, J. (2004). Transfection microarray of human mesenchymal stem cells and on-chip siRNA gene knockdown. Journal of controlled release : official journal of the Controlled Release Society *96*, 227-232.

You, M., and Zhao, Z.Z. (1997). Positive effects of SH2 domain-containing tyrosine phosphatase SHP-1 on epidermal growth factor- and interferon-gamma-stimulated activation of STAT transcription factors in HeLa cells. Journal of Biological Chemistry *272*, 23376-23381.

Yu, M., Lin, G., Arshadi, N., Kalatskaya, I., Xue, B., Haider, S., Nguyen, F., Boutros, P.C., Elson, A., Muthuswamy, L.B.*, et al.* (2012). Expression Profiling during Mammary Epithelial Cell Three-Dimensional Morphogenesis Identifies PTPRO as a Novel Regulator of Morphogenesis and ErbB2-Mediated Transformation. Mol Cell Biol *32*, 3913-3924.

Yuan, T., Wang, Y., Zhao, Z.J., and Gu, H. (2010). Protein-tyrosine phosphatase PTPN9 negatively regulates ErbB2 and epidermal growth factor receptor signaling in breast cancer cells. J Biol Chem *285*, 14861-14870.

Zama, T., Aoki, R., Kamimoto, T., Inoue, K., Ikeda, Y., and Hagiwara, M. (2002a). A novel dual specificity phosphatase SKRP1 interacts with the MAPK kinase MKK7 and inactivates the JNK MAPK pathway. Journal of Biological Chemistry *277*, 23909-23918.

Zama, T., Aoki, R., Kamimoto, T., Inoue, K., Ikeda, Y., and Hagiwara, M. (2002b). Scaffold role of a mitogen-activated protein kinase phosphatase, SKRP1, for the JNK signaling pathway. Journal of Biological Chemistry *277*, 23919-23926.

Zambuzzi, W.F., Granjeiro, J.M., Parikh, K., Yuvaraj, S., Peppelenbosch, M.P., and Ferreira, C.V. (2008). Modulation of Src Activity by Low Molecular Weight Protein Tyrosine Phosphatase During Osteoblast Differentiation. Cellular Physiology and Biochemistry *22*, 497-506.

Zhang, X., Gureasko, J., Shen, K., Cole, P.A., and Kuriyan, J. (2006). An allosteric mechanism for activation of the kinase domain of epidermal growth factor receptor. Cell *125*, 1137-1149.

Zheng, X.M., Wang, Y., and Pallen, C.J. (1992). Cell transformation and activation of pp60c-src by overexpression of a protein tyrosine phosphatase. Nature *359*, 336-339.

Ziauddin, J., and Sabatini, D.M. (2001). Microarrays of cells expressing defined cDNAs. Nature *411*, 107-110.

ACKNOWLEDGEMENTS

I would like to thank Prof. Philippe I. H. Bastiaens for giving me the opportunity and guidance to carry out my thesis in his laboratory. My deepest thanks goes to Prof. Hernán E. Grecco and Pedro Roda-Navaro for their excellent supervision, outstanding support and encouragement during my entire study. I would like to extent my sincerest thanks and appreciation to Anetta Koseska, Klaus. C. Schuermann and Amit Mhamane. This project would not be successful without such a great team. A very special thanks goes to Zeta Xouri, Astrid Krämer, Wayne Stallaert and Ola Sabet for their helpful discussions and comments on this manuscript. Many thanks to Lisaweta Rosmannek and Jutta Luig for the organization and cloning of the cDNA library in cooperation with the DPF. Furthermore, I would like to thank all cell culture members (Anette Langerak, Petra Glitz and Michael Richl) for keeping this project running without complications. I would like to thank all members of department II, especially and in no particular order; Rahul Ravindran, Thies Klüssendorf, Eulashini Chuntharpursat, Lisa Karajannis, Christina Maria Hecker, Manuela Grygier, Gabi Betz, Johann Jarzombek, Ivonne Radon, Maja Sinn, Hendrike Schütz, Martin Baumdick, Rabea Stockert, Jana Mallah, Björn Papke, Dina Truxius, Sven Müller, Jian Hou, Martin Masip, Justine Mondry, Jenny Ibach, Marton Gelleri, Angel Stanoev, Sheriff Rahuman, Tanja Forck, Lale Azar, Jens Christmann and Jan Hübinger. It was a great pleasure to work in such a nice group. I would like to express my deepest gratitude to my parents, my brother and Kim for their love and constant support, which kept me always grounded and confident during my study. Finally, I want to express my heartfelt thanks to Elke den Brave for giving me mental balance and calmness.

Von ganzem Herzen danke!

Curriculum Vitae

Sven Fengler
born 22. October 1982, Leverkusen, Germany

Permanent address: Fasanenweg 4-6, 51381 Leverkusen, Germany
E-mail: svenfengler@googlemail.com

EDUCATION

September 2008 Diploma in Biology, University of Cologne, Germany. Thesis: Analysis of the NF-κB signalling pathway by advanced fluorescent microscopy. Department of Mouse Genetics and Inflammation, University of Cologne, Germany.

PROFESSIONAL EXPERIENCE

January 2009 – July 2014 Graduate Student, Department of Systemic Cell Biology, Max Planck Institute of Molecular Physiology, Dortmund, Germany

December 2007 – September 2008 Undergraduate Research Assistant, Department of Mouse Genetics and Inflammation, University of Cologne, Germany

July 2006 – September 2006 Undergraduate research, Summer school program (SPUR/UREKA), Department of Physiology and Medical Physics, Royal College of Surgeons Research Centre, Dublin, Ireland

January 2006 – March 2006 Undergraduate research, Internship, Research and Development of Insecticide, Bayer Crop Science AG, Monheim, Germany

WORKSHOPS

Project management, CoachING 2012, Technical University Dortmund, Germany

Scientific writing, Herbstakademie 2011, University of Duisburg-Essen, Germany

Project management basics, Herbstakademie 2011, University of Duisburg-Essen, Germany

Principles of fluorescence techniques, Fluorescence Foundation 2008, Department of Physics, University of Genoa, Italy

PUBLICATIONS

Sven Fengler, Hernán E. Grecco, Anetta Koseska, Pedro Roda-Navaro, Klaus. C. Schuermann, Amit Mhamane, Lisaweta Rosmannek, Jutta Luig and Philippe I. H. Bastiaens. Spatial-temporal regulation of EGFR by protein tyrosine phosphatases. **(in preparation)**

Sven Fengler, Philippe I. H. Bastiaens, Hernán E. Grecco, Pedro Roda-Navarro (2012). Optimizing cell arrays for accute functional genomics. BMC Res Notes. 2012 Jul 17;5(1):358

Hernán E. Grecco, Pedro Roda-Navarro, **Sven Fengler**, Philippe I. H. Bastiaens (2011). High throughput quantification of posttranslational modifications *in situ* by CA-FLIM. Methods Enzymol., 2011;500:37-58.

Rossana De Lorenzi, Ralph Gareus, **Sven Fengler**, and Manolis Pasparakis (2008). GFP-p65 knock-in mice as a tool to study NF-κB dynamics in vivo. Genesis, 2009 Mar 4; 47(5):323-329.

MEETING CONTRIBUTION

Pedro Roda-Navarro, Hernan E. Grecco, **Sven Fengler** (presenter), Philippe Bastiaens (2010): Analysing tyrosine phosphorylation networks by CA-FLIM. EMBO Heidelberg, Germany. From Functional Genomics to Systems Biology 11/2010: Abstract No. 55 (Poster)

Sven Fengler, Hernán E. Grecco, Pedro Roda-Navarro, Jian Hou, Eulashini Chuntharpursat, Philippe I. H. Bastiaens (2010): High throughput quantification of post translational modifications in situ by CA-FLIM. University of Bochum, Germany. Annual Meeting of the German Biophysical Society 10/2010: Abstract No. P6.4. (Poster)

Sven Fengler, Carla O'Connor, Jochen H. M. Prehn, Markus Rehm (2006): Caspase-3 Inhibitor XIAP regulates Death Receptor mediated Apoptosis upstream of Caspase-3 Inhibition: a Single Cell Analysis. Royal College of Surgeons Dublin, Ireland. SPUR symposium 09/2006: Abstract No. PP03 (Poster)